RESOURCE RECOVERY FROM WASTEWATER

NOVEL TREATMENT TECHNOLOGIES FOR NUTRIENTS RECOVERY AND BIOSOLIDS MANAGEMENT

By Hui Guo, B.ENG., M.ENG.

A Thesis Submitted to the School of Graduate Studies in Partial Fulfillment of the

Requirements for the Degree of Doctor of Philosophy

McMaster University DOCTOR OF PHILOSOPHY (2021)

Hamilton, Ontario (Civil Engineering)

TITLE: Novel treatment technologies for nutrients recovery and biosolids management

AUTHOR: Hui Guo, B.ENG., M.ENG.

SUPERVISOR: Dr. Younggy Kim

NUMBER OF PAGES: xxviii, 230

Lay Abstract

High energy consumption is a main challenge in wastewater treatment. However, a large amount of energy in wastewater can be recovered and reused. The recovery of energy from wastewater can reduce energy costs, save resources, and protect the environment. This research aims to develop novel wastewater treatment technologies to save energy by recovering nutrients and producing biogas from wastewater. Bioelectrochemical systems are used to produce hydrogen gas and recover heavy metals from municipal or industrial wastewater. Electrodialysis systems are applied in ammonia recovery and fertilizer production. Anaerobic digestion systems are employed to produce methane gas as a renewable energy source from wasted sludge. These technologies reduce energy consumption in wastewater treatment and help to establish a new green circular economy for resource recovery.

Abstract

High energy consumption in conventional wastewater treatment contributes to a large amount of greenhouse emissions and causes environmental problems such as acid rain and climate change. Many technologies, microbial electrolysis cells (MECs), electrodialysis (ED), and anaerobic digestion (AD), were developed to make wastewater treatment more efficient and economical. This thesis investigated novel MECs and ED to decrease energy consumption in wastewater treatment and recover resources from wastewater. In addition, inhibition of ammonia and acetic acid on high-solid AD was examined in this research.

The multi-electrode stack design was applied in MECs to treat municipal wastewater. Rapid organic removal and minimized biosolids production were observed in the stacked MECs. In addition to municipal wastewater treatment, MECs can also recover/remove heavy metals from industrial wastewater. Various removal/recovery mechanisms of toxic heavy metals were discussed in this thesis. ED with bipolar membranes (BPMs) was examined to produce high-purity ammonium sulfate from real wastewater steams. This examination indicates valuable nutrients resources (e.g., ammonium sulfate) can be recovered from wastewater and used as land fertilizers for food production. Membrane scaling problems were also evaluated in ED systems since the formation of inorganic scalants can affect the efficiency of nutrients recovery significantly. In addition, the inhibition of ammonia and acetic acid on AD performance was incorporated in a modified anaerobic digestion model (ADM) for reliable simulation of individual biological reactions in high-solid AD.

This research contributes to the body of knowledge by developing wastewater treatment technologies with less energy consumption and biosolids production. The reduction of energy consumption and biosolids production can reduce fossil fuel combustion and waste disposal. Resources, such as ammonia and heavy metals, can be recovered and reused by using the investigatory technologies. Therefore, with these developed technologies, wastewater treatment meets the goal of sustainable development and helps to establish a new green circular economy.

Preface

This thesis has been prepared in accordance with the guidelines of the sandwich thesis format from the School of Graduate Studies at McMaster University. Six papers are included in this thesis as listed below.

- Guo, H., & Kim, Y. (2018). Scalable multi-electrode microbial electrolysis cells for high electric current and rapid organic removal. *Journal of Power Sources*, *391*, 67-72.
- Guo, H., & Kim, Y. (2019). Stacked multi-electrode design of microbial electrolysis cells for rapid and low-sludge treatment of municipal wastewater. *Biotechnology for biofuels*, *12*(1), 1-10.
- Guo, H., & Kim, Y. (2020). Mechanisms of Heavy Metal Separation in Bioelectrochemical Systems and Relative Significance of Precipitation. *Microbial Electrochemical Technologies*, 128.
- Guo, H., Yuan, P., Pavlovic, V., Barber, J., & Kim, Y. (2021). Ammonium sulfate production from wastewater and low-grade sulfuric acid using bipolar-and cation-exchange membranes. *Journal of Cleaner Production*, *285*, 124888.
- Guo, H., & Kim, Y. (under review). Membrane Scaling in Electrodialysis for Nutrients Separation from High-strength Wastewater. *Environmental Engineering Science.*
- Guo, H., Fernandes, S., and Kim, Y. Modeling Ammonia and Acetic Acid Inhibition on Mesophilic Anaerobic Digestion Fed with Thickened Waste Activated Sludge. In preparation.

The first manuscript is presented in Chapter 2. The work was started in June 2016. The manuscript was submitted in February 2018 and accepted in April 2018. The work was conducted under the supervision of Dr. Younggy Kim. The manuscript is included in this thesis as it provided a novel wastewater treatment technology to save energy. My contributions include:

- Designed and built reactors
- Performed experiments
- Collected and analyzed experimental data
- Wrote the manuscript

The second manuscript is presented in Chapter 3. The work was started in September 2016. The manuscript was submitted in September 2018 and accepted in January 2019. The work was conducted under the supervision of Dr. Younggy Kim. The manuscript is included in this thesis as it demonstrated the great wastewater treatability of stack-designed microbial electrolysis cells. My contributions include:

- Designed and built reactors
- Performed experiments
- Collected and analyzed experimental data
- Wrote the manuscript

The third manuscript is presented in Chapter 4. The work was started in October 2017. The manuscript was submitted in March 2018 and accepted in March 2019. The work was conducted under the supervision of Dr. Younggy Kim. The manuscript is included in this

thesis as it provides a novel technology for heavy metal recovery/removal from wastewater. My contributions include:

- Reviewed previous studies
- Summarized the mechanisms
- Wrote the manuscript

The fourth manuscript is presented in Chapter 5. The work was started in January 2019. The manuscript was submitted in June 2020 and accepted in October 2020. The work was conducted under the supervision of Dr. Younggy Kim. The manuscript is included in this thesis as it provides a novel technology for nutrients recovery from wastewater. My contributions include:

- Designed reactors
- Performed experiments
- Collected and analyzed experimental data
- Wrote the manuscript

The fifth manuscript is presented in Chapter 6. The work was started in September 2019. The manuscript was submitted in January 2021. The work was conducted under the supervision of Dr. Younggy Kim. The manuscript is included in this thesis as it provides a better understanding of membrane scaling problems. My contributions include:

- Designed and built reactors
- Performed experiments
- Collected and analyzed experimental data
- Wrote the manuscript

The sixth manuscript is presented in Chapter 7. The work was started in July 2020. The work was conducted under the supervision of Dr. Younggy Kim. The manuscript is included in this thesis as it modified the anaerobic digestion model with inhibition functions. My contributions include:

- Modified anaerobic digestion model and validated the model with experimental results
- Wrote the manuscript

Copyright Permission

I have secured permission to include copyright material in this Ph.D. thesis from the copyright holder. The permission includes a grant of an irrevocable, non-exclusive license to McMaster University and to Library and Archives Canada to reproduce the material as part of the thesis.

Acknowledgments

I would like to express my sincere gratitude to my supervisor Dr. Younggy Kim. My Ph.D. study is enjoyable and memorable with your professional and patient guidance. Thank you for sharing your academic and life experience with me. I cannot achieve this milestone without your help.

I would like to thank my supervisory committee members, Dr. Brian Baetz and Dr. Yiping Guo, for your insightful comments and advice on my research. I always enjoyed talking with you in my committee meetings.

Thanks to Mr. Yongseck Hong, Dr. John Barber, Dr. Vladimir Pavlovic, and Mr. Pengyi Yuan, for your technical supports and research suggestions.

Thanks to my colleagues and friends in offices 330, 331, and 228. I will always remember the time with you at McMaster.

Thanks to Ms. Monica Han for the technical supports and it is fantastic to have bubble teas with you.

Special thanks to Dr. Shuming Du for your company and encouragement.

Thanks to my family and friends for their supports, and encouragement when I pursued my goals. Your love has been my greatest motivation.

CONTENTS

Lists of Figures and Tables

List of Figures

List of Tables

List of Abbreviations and Acronyms

ACC: amorphous calcium carbonate

AD: anaerobic digestion

ADM: anaerobic digestion model

ADM1: Anaerobic Digestion Model No.1

AEMs: anion-exchange membranes

BES: bioelectrochemical systems

BMED: bipolar membrane electrodialysis

BMP: biochemical methane potential

BOD: biochemical oxygen demand

BPMs: bipolar membranes

CE: coulombic efficiency

CEMs: cation-exchange membranes

CIP: clean-in-place

COD: chemical oxygen demand

ED: electrodialysis

FAN: free ammonia

FW: food waste

HRT: hydraulic residence time

MECs: microbial electrolysis cells

MEC-1: MEC with 1 electrode pair

MEC-5: MEC with 5 electrode pairs

MEC-10: MEC with 10 electrode pairs

MFCs: microbial fuel cells

MW: municipal waste

ICP-OES: inductive coupled plasma-optical emission spectrometry

IEMs: ion-exchange membranes

OLR: organic loading rates

SEM-EDS: scanning electron microscopy and energy-dispersive X-ray spectroscopy

SCOD: Soluble Chemical Oxygen Demand

TAN: total ammonia

TCD-GC: thermal conductivity detector – gas chromatograph

TCOD: Total Chemical Oxygen Demand

TSS: total suspended solids

TVFAs: total volatile fatty acids

TWAS: thickened waste activated sludge

VFAs: volatile fatty acids

VS: Volatile solids

VSS: volatile suspended solid

Declaration of Academic Achievement

Hui Guo was the main contributor to six manuscripts presented in this thesis. The contributions from the co-authors are detailed at the beginning of each Chapter.

1 Introduction

1.1 Overview

High-energy consumption is one of the main challenges in wastewater treatment. Around 38% of the energy (electricity and natural gas) used by municipalities is consumed by water and wastewater systems in Ontario, Canada (Environmental Commissioner of Ontario, 2017). In the United States, electricity consumption in wastewater treatment accounts for around 3.4% of the total energy produced in the country (Panepinto et al., 2016). The worldwide wastewater treatment utilized about 1% of the total world energy consumption (International Energy Agency, 2018). The high energy consumption of wastewater treatment contributes to a large amount of greenhouse emissions and further results in climate change. Therefore, novel wastewater treatment technologies with low energy consumption are needed.

Management and final disposal of wastewater sludge is another key challenge in wastewater treatment. Stabilization of sludge including thickening, anaerobic digestion, and dewatering makes wastewater treatment expensive and inefficient. In addition, the disposal of wastewater sludge including landfilling and incineration can cause land and air pollution. Thus, efficient sludge treatment or low sludge production is essential to minimize the adverse environmental effects of sludge disposal.

Excessive nutrients such as nitrogen and phosphorus in treated wastewater can cause eutrophication in natural water systems. Conventional methods such as chemical precipitation and nitrification-denitrification consume a large amount of energy and

increase the cost of wastewater treatment (Huang et al., 2016; Kuai and Verstraete, 1998). Recently, the demand for ammonium and phosphate that used in fertilizer is increased with the increasing population (Ye et al., 2020). Considering the high concentration of nutrients in wastewater, wastewater can be a valuable source to produce land fertilizers to be used in the agricultural industry.

1.2 Microbial electrolysis cells for municipal wastewater treatment

Microbial electrolysis cells (MECs) can be used to treat wastewater and simultaneously produce hydrogen gas (Liu et al., 2005; Call and Logan, 2008; Wanger et al., 2009). In a MEC, organic substrates are oxidized at the bioanode by exoelectrogenic bacteria while water is reduced to hydrogen gas at the cathode. A small voltage (0.13-1.23 V) needs to be applied in MECs to drive electrode reactions (Logan et al., 2008). The magnitude of electric current induced in the MECs represents the rate of electrode reactions (i.e., organics removal and hydrogen gas production). The electric current generation in MECs fed with acetate is generally high since acetate is used as the primary substrate for exoelectrogenic microorganisms (Rozendal et al., 2007; Hu et al., 2008; Cheng and Logan., 2007). However, electric current in MECs fed with real wastewater is low because of the low conductivity of wastewater (Cusick et al., 2010; Escapa et al., 2012). The low electric current generation in MECs represents the low rates in both organic removal and hydrogen gas production, indicating the low wastewater treatment efficiency. Therefore, a modified design is necessary to improve electric current generation in MECs.

The electric current generation is governed by many factors, such as electrode materials, electrode size, electrode catalyst, inter-electrode distance, and solution

conductivity. For instance, the sandwiched electrode assembly MECs minimized the inter-electrode distance and significantly decreased the internal resistance of MECs (Ghangrekar et al., 2007; Ahn et al., 2014). The large surface area of electrodes contributed to the high electric current generation (Lee and Rittmann, 2010; Tartakovsky et al., 2009). The application of catalytic cathodes or biocathodes is also an effective way to modify the electric current generation in MECs (Jeremiasse et al., 2010; Yang et al., 2017). Therefore, a new design of stacked electrodes was proposed and examined in MECs to increase the electric current and organic removal rates. The repeated stack provided large surface areas for bacterial growth and the narrow inter-electrode distance contributed to the low resistance.

In conventional wastewater treatment plants, activated sludge systems produce a large amount of sludge that needs to be treated. The sludge treatment processes consume a large amount of energy and make wastewater treatment complicated and inefficient. MECs are expected to produce a much smaller amount of waste sludge than conventional activated sludge because of the small yield coefficient (0.02 g-VSS/g-COD) of exoelectrogenic microorganisms (Wilson and Kim, 2016; Brown et al., 2015). However, there were limited studies that reported the sludge production or reduction in MECs fed with real wastewater. Thus, the biosolids production or reduction was estimated in the newly designed MEC reactors.

1.3 Heavy metal removal/recovery from industrial wastewater

Heavy metal removal/recovery from wastewater has attracted increasing attention since the accumulation of heavy metal in the environment can cause serious health and

environmental problems (Galanis et al., 2009; Wu et al., 2012;). For instance, arsenic and chromium (VI) are carcinogens and can cause death with long-term exposure (Martin and Griswold, 2009). Due to the potentially toxic and carcinogenic effects of heavy metals, United States Environmental Protection Agency (US EPA) listed 12 heavy metals as the priority pollutants. Stringent discharge standards were published for various heavy metals in wastewater. On the one hand, heavy metals in wastewater need to be removed to avoid environmental pollution. On the other hand, some heavy metals, such as silver, gold, copper, and zinc, which have high market values should be recovered from wastewater. U.S Water Environment Research Foundation reported that $9 thousand – $4 million worth of silver can be recovered from the daily wastewater (Huang and Ren, 2014).

Many methods, which include membrane filtration, ion exchange, adsorption, chemical precipitation, photocatalysis, and biosorption, have been developed to remove/recover heavy metals (Ritchie et al., 2001; Fu and Wang 2011; Kurniawan et al. 2006; He and Chen 2014). Bioelectrochemical systems (BES) have emerged as a novel technology for heavy metal removal/recovery because of the low energy consumption (Nancharaiah et al., 2015; Wang and Ren, 2014; Dominguez-Benetton et al., 2018). In BES, the electrons produced from the substrates are transferred to the anode and then flow to the cathode. The oxidized heavy metal ions can gain electrons and be reduced to metallic metals. The reduction potential of heavy metal ions represents the spontaneity of the reaction. In addition, the precipitation of heavy metal is also possible in BES due to the high pH near the cathode. To summarize the development of BES in heavy metal recovery/removal, a comprehensive review that focused on mechanisms of heavy metal

separation in BES was prepared.

1.4 Electrodialysis systems for ammonia recovery

Ammonia is the main source to cause algal blooms in water systems. The high concentration of ammonia in water is posing a threat to human health due to toxic fish and contaminated water. US EPA recommends a chronic criterion magnitude of 1.9 mg TAN/L at pH 7 and 20°C for a 30-day average duration (US EPA 2013). Canadian Council of Ministers of the Environment (CCME) requires that the free ammonia concentration in the freshwater should be lower than 19 μg/L (CCME 2001). To meet the standards of ammonia, many methods, such as filtration, sedimentation, chemical precipitation, adsorption, aerobic, and anaerobic have been developed to remove ammonia from wastewater (Karri et al., 2018).

In conventional wastewater treatment plants, dewatering centrate (i.e., down-stream wastewater from the dewatering process of digested sludge) that contains high concentrations of ammonia (~1000 g-N/L) is sent back to the mainstream wastewater treatment processes (Holloway et al., 2007) and mixed with raw wastewater. The recycled dewatering centrate contributes to 15-20% of nitrogen load in the influent and further results in high operating costs. However, dewatering centrate can also be a valuable source to produce fertilizer (e.g., ammonium sulfate) because of the high concentration of ammonia. Therefore, an efficient method is needed to recover ammonia from dewatering centrate.

Electrodialysis (ED) is a type of membrane technology that consists of a series of cation- and anion-exchange membranes (CEMs and AEMs) between two electrodes

(Strathmann, 2010; Xu and Huang, 2008). In an ED reactor, anions and cations are transferred through the ion exchange membranes under an electric field. ED has been used for more than 50 years to produce potable water from brackish water sources (Strathmann, 2010; AI-Amshawee et al., 2020; Patel et al., 2020; Nguyen et al., 2019). Nowadays, ED with bipolar membranes (BPMs) has been widely used in the chemical process industry, wastewater treatment, and food industry (Tian et al., 2019; Lei et al., 2020; Shi et al., 2018). A conventional ED stack with CEMs and AEMs can separate ammonium from dilute cells to concentrate cells. However, anions that are concentrated through AEMs affect the purity of the final products. Thus, an electrodialysis reactor with BPMs and CEMs was proposed to exclude the effects of anions and produce high purity ammonia sulfate from wastewater (i.e., dewatering centrate).

A BPM is manufactured by attaching a CEM and an AEM (Strathmann, 2010). Water is dissociated into protons and hydroxide ions in the interface between CEM and AEM. The protons and hydroxide ions produced in the interface are separated by CEM and AEM, thus ED with BPMs (BMED) is widely used to produce an acid and a base from a relative salt (Herrero-Gonzalez et al., 2020; Achoh et al., 2019; Sun et al., 2017). The application of BMED in ammonia recovery was also reported (Li et al., 2016). The typical structure of BMED that consists of CEMs, AEMs, and BPMs (Huang and Xu 2006; Pourcelly 2002) resulted in high energy consumption. Considering the purity of the final products and energy consumption of the system, a BMED reactor excluded AEMs were built to recover ammonia from wastewater.

1.5 Ion-exchange membrane scaling problems

Ion-exchange membrane (IEM) scaling problems (i.e., inorganic salt precipitated deposited on IEM surfaces) can limit the broad application of the ED technology since the inorganic scalants decrease membrane permeability and reduce membrane life span (Guo et al., 2012; Brewster et al., 2017). IEM scaling occurs when the ionic product of salts is higher than the solubility product of salts (Schorr, 2011). In an ED system, concentrated divalent cations, such as Ca^{2+} and Mg^{2+}, can combine with CO_3^{2-} and OH^- to form scalants. Various scalants including gypsum, calcium carbonate, and magnesium hydroxide were observed in ED reactors fed with synthetic wastewater (Asraf-Snir et al., 2016, Andreeva et al., 2018, Casademont et al., 2007). Serious scaling problems were also detected in the ED systems for nutrients recovery from wastewater since the concentrations of Ca^{2+} and Mg^{2+} in the wastewater were relatively high (Ward et al., 2018).

Although many studies reported the formation of scalants in ED systems, limited studies investigated the membrane damage due to the shape of scalants. For example, needle-shaped aragonite and struvite (Asraf-Snir et al., 2016; Andritsos et al., 1997; Le Corre et al., 2005) may pierce the membrane and cause irreversible damage. Therefore, the shape of scalants especially for magnesium and calcium precipitates should be investigated to have a better understanding of scaling formation in ED systems. In addition, high-strength wastewater, such as liquid digestate of municipal and food waste, which commonly have high concentrations of nutrients is an ideal source for nutrients recovery. Thus, we also investigated the scaling formation in ED fed with various high-strength wastewater.

1.6 Inhibition in anaerobic digestion

Anaerobic digestion (AD) is an essential wastewater treatment method for energy recovery and sludge management. In AD processes, organic materials were converted to methane and carbon dioxide with multiple biological reactions (Mata-Alvarez et al., 2000). The formation of methane by methanogens (i.e., methanogenesis) is an important indicator of AD stability (Rajagopal et al., 2013). Many factors, such as pH, inorganic nitrogen, hydrogen gas, ammonia, and VFAs, govern the performance of methanogenesis in AD (Chen et al., 2008; Yenigün and Demirel, 2013; Rajagopal et al., 2013). Although many studies reported the toxicity of ammonia on methanogens, there is still limited understanding of the inhibition of ammonia on AD especially the inhibition of ammonia on hydrogenotrophic methanogenesis. In addition, the inhibition of acetic acid on methanogenesis needs to be investigated since the accumulation of acetic acid can change pH and affect the methanogenic activity.

Ammonia is an essential nutrient for bacterial growth. Generally, low ammonia concentration (less than 0.2 g-N/L) is beneficial to AD processes (Liu and Sung, 2002). The inhibition of ammonia on methane production has been reported in many studies. For instance, around 50% of methane reduction was observed in the AD when the total ammonia (TAN) concentration ranged from 1.7 to 14 g-N/L (Bujoczek et al., 2000; Hansen et al., 1998; Chen et al., 2008). The wide range of TAN concentration can be explained by the different operation conditions, sludge retention time, and the different properties of substrates (Chen et al., 2008; Angelidaki and Ahiring, 1994).

Ammonium ion (NH_4^+) and free ammonia (FAN) (i.e., un-ionized ammonia) are two forms of inorganic ammonia in water systems. FAN has been regarded as the main inhibitor for AD because of the high permeability of FAN to bacterial cell membranes (Müller et al., 2006). The mechanism of ammonia toxicity in methanogens is currently not clear. However, ammonia may inhibit the activity of methanogens in two ways: (1) ammonium ions inhibit the methane production enzymes directly; (2) FAN molecule diffuses passively into bacterial cells, resulting in the imbalance of proton or insufficiency of potassium (Gallert et al., 1998, Rajagopal et al., 2013).

The high concentration of volatile fatty acids (VFAs) especially the high concentration of acetate is the most noticeable result of an unstable AD process. The accumulation of acetate can decrease pH significantly and further inhibit the activity of methanogens (Xiao et al., 2013; Wilson et al., 2012; Xu et al., 2014; Fezzani et al., 2010). However, low VFAs concentrations can also inhibit methane production since VFAs including butyric acid, propionic acid, valeric acid, and acetic acid contribute to more than 70% of methane production. Among the pathways of methane production, methane production from acetate (i.e., acetoclastic methanogenesis) is an important step in AD processes.

Anaerobic digestion model 1 (ADM1) was developed by the International Water Association (IWA) task group to simulate the AD process (Batstone et al., 2002). The inhibitions of hydrogen gas, pH, and inorganic nitrogen (as substrate) were expressed by various functions (non-competitive inhibition, substrate limitation, Empirical). Although the inhibition of ammonia on acetoclastic methanogens was presented by a non-

competitive inhibition function in ADM1, the ammonia inhibition on hydrogenotrophic methanogens was not considered. In addition, the ammonia inhibition of acetic acid (as inhibitor) and acetate (as substrate) also should be implemented in ADM1.

1.7 Research objectives

The research presented in this thesis aims to provide novel wastewater treatment methods for nutrients recovery and biosolids management with low energy consumption. Many methods, such as BES, ED, and AD were developed and discussed in this thesis. The following specific objectives were set to be achieved:

- Chapter 2: to design a stacked electrodes MEC to improve the electric current generation; to investigate the start-up of the stacked electrodes MEC; to evaluate the performance of the newly designed MEC under different operating conditions; to examine two stackable cathode materials.
- Chapter 3: to demonstrate high electric current generation in MECs fed with real wastewater by using sandwiched electrode stacks; to investigate the effects of reactor designs and operating conditions on electric current generation; to examine the wastewater treatability (organic removal rate and biosolids reduction); to study the energy consumption in stacked electrode MECs.
- Chapter 4: to summarize the previous studies that focus on the heavy metal separation in BES; to report the fundamentals for separating heavy metal in BES; to discuss the mechanisms of heavy metal separation in BES.
- Chapter 5: to produce highly concentrated ammonium sulfate from dewatering centrate by using BMED; to investigate the effects of applied voltage and flow rate

on the ammonia recovery efficiency; to examine the scaling formation in membrane stack; evaluate the energy consumption in BMED.

- Chapter 6: to investigate the formation of scalants in ED for nutrient recovery; to study the effects of electric current density on membrane scaling; to examine the scalants formation in ED fed with municipal and food waste liquid digestate; to observe the morphology of scalants on IEMs.
- Chapter 7: to analyze the inhibition of ammonia and acetic acid on methane production; to investigate the effects of high pH on the ammonia and acetic acid inhibition; to modify the ADM1 by adding ammonia and acetic acid inhibition functions; to analyze the sensitivity of inhibition parameters in the model simulation.

References

Achoh, A., Zabolotsky, V., & Melnikov, S. (2019). Conversion of water-organic solution of sodium naphtenates into naphtenic acids and alkali by electrodialysis with bipolar membranes. Separation and purification technology, 212, 929-940.

Ahn, Y., Hatzell, M. C., Zhang, F., & Logan, B. E. (2014). Different electrode configurations to optimize performance of multi-electrode microbial fuel cells for generating power or treating domestic wastewater. Journal of Power Sources, 249, 440-445.

Al-Amshawee, S., Yunus, M. Y. B. M., Azoddein, A. A. M., Hassell, D. G., Dakhil, I. H., & Hasan, H. A. (2020). Electrodialysis desalination for water and wastewater: A review. Chemical Engineering Journal, 380, 122231.

Andreeva, M. A., Gil, V. V., Pismenskaya, N. D., Dammak, L., Kononenko, N. A., Larchet, C., ... & Nikonenko, V. V. (2018). Mitigation of membrane scaling in electrodialysis by electroconvection enhancement, pH adjustment and pulsed electric field application. Journal of Membrane Science, 549, 129-140.

Andritsos, N., Karabelas, A. J., & Koutsoukos, P. G. (1997). Morphology and structure of CaCO3 scale layers formed under isothermal flow conditions. Langmuir, 13(10), 2873-2879.

Angelidaki, I., & Ahring, B. K. (1994). Anaerobic thermophilic digestion of manure at different ammonia loads: effect of temperature. Water research, 28(3), 727-731.

Asraf-Snir, M., Gilron, J., & Oren, Y. (2016). Gypsum scaling of anion exchange membranes in electrodialysis. Journal of Membrane Science, 520, 176-186.

Batstone, D. J., Keller, J., Angelidaki, I., Kalyuzhnyi, S. V., Pavlostathis, S. G., Rozzi, A., ... & Vavilin, V. A. (2002). The IWA anaerobic digestion model no 1 (ADM1). Water Science and technology, 45(10), 65-73.

Brewster, E. T., Ward, A. J., Mehta, C. M., Radjenovic, J., & Batstone, D. J. (2017). Predicting scale formation during electrodialytic nutrient recovery. Water research, 110, 202-210.

Brown, R. K., Harnisch, F., Dockhorn, T., & Schröder, U. (2015). Examining sludge production in bioelectrochemical systems treating domestic wastewater. Bioresource technology, 198, 913-917.

Bujoczek, G., Oleszkiewicz, J., Sparling, R., & Cenkowski, S. (2000). High solid anaerobic digestion of chicken manure. Journal of Agricultural Engineering Research, 76(1), 51-60.

Call, D., & Logan, B. E. (2008). Hydrogen production in a single chamber microbial electrolysis cell lacking a membrane. Environmental science & technology, 42(9), 3401-3406.

Casademont, C., Pourcelly, G., & Bazinet, L. (2007). Effect of magnesium/calcium ratio in solutions subjected to electrodialysis: Characterization of cation-exchange membrane fouling. Journal of colloid and interface science, 315(2), 544-554.

CCME (20001). Water quality guidelines for the protection of aquatic life.

Chen, Y., Cheng, J. J., & Creamer, K. S. (2008). Inhibition of anaerobic digestion process: a review. Bioresource technology, 99(10), 4044-4064.

Cheng, S., & Logan, B. E. (2007). Sustainable and efficient biohydrogen production via electrohydrogenesis. Proceedings of the National Academy of Sciences, 104(47), 18871-18873.

Cusick, R. D., Kiely, P. D., & Logan, B. E. (2010). A monetary comparison of energy recovered from microbial fuel cells and microbial electrolysis cells fed winery or domestic wastewaters. International Journal of hydrogen energy, 35(17), 8855-8861.

Dominguez-Benetton, X., Varia, J. C., Pozo, G., Modin, O., Ter Heijne, A., Fransaer, J., & Rabaey, K. (2018). Metal recovery by microbial electro-metallurgy. Progress in Materials Science, 94, 435-461.

Environmental commissioner of Ontario (2017). Every Drop Counts: Reducing the Energy and Climate Footprint of Ontario's Water Use. Environmental commissioner of Ontario: Toronto, Canada.

Escapa, A., Gil-Carrera, L., García, V., & Morán, A. (2012). Performance of a continuous flow microbial electrolysis cell (MEC) fed with domestic wastewater. Bioresource technology, 117, 55-62.

Fezzani, B., & Cheikh, R. B. (2010). Two-phase anaerobic co-digestion of olive mill wastes in semi-continuous digesters at mesophilic temperature. Bioresource technology, 101(6), 1628-1634

Fu, F., & Wang, Q. (2011). Removal of heavy metal ions from wastewaters: a review. Journal of environmental management, *92*(3), 407-418.

Galanis, A., Karapetsas, A., & Sandaltzopoulos, R. (2009). Metal-induced carcinogenesis, oxidative stress and hypoxia signalling. Mutation research/Genetic toxicology and environmental mutagenesis, 674(1-2), 31-35.

Gallert, C., Bauer, S., & Winter, J. J. A. M. (1998). Effect of ammonia on the anaerobic degradation of protein by a mesophilic and thermophilic biowaste population. Applied microbiology and biotechnology, 50(4), 495-501.

Galvagno, G., Eskicioglu, C., & Abel-Denee, M. (2016). Biodegradation and chemical precipitation of dissolved nutrients in anaerobically digested sludge dewatering centrate. Water research, 96, 84-93.

Ghangrekar, M. M., & Shinde, V. B. (2007). Performance of membrane-less microbial fuel cell treating wastewater and effect of electrode distance and area on electricity production. Bioresource Technology, 98(15), 2879-2885.

Guo, W., Ngo, H. H., & Li, J. (2012). A mini-review on membrane fouling. Bioresource technology, 122, 27-34

Hansen, K. H., Angelidaki, I., & Ahring, B. K. (1998). Anaerobic digestion of swine manure: inhibition by ammonia. Water research, 32(1), 5-12.

He, J., & Chen, J. P. (2014). A comprehensive review on biosorption of heavy metals by algal biomass: materials, performances, chemistry, and modeling simulation tools. Bioresource technology, 160, 67-78.

Herrero-Gonzalez, M., Diaz-Guridi, P., Dominguez-Ramos, A., Irabien, A., & Ibañez, R. (2020). Highly concentrated HCl and NaOH from brines using electrodialysis with bipolar membranes. Separation and Purification Technology, 242, 116785.

Hindatu, Y., Annuar, M. S. M., & Gumel, A. M. (2017). Mini-review: Anode modification for improved performance of microbial fuel cell. Renewable and Sustainable Energy Reviews, 73, 236-248.

Holloway, R. W., Childress, A. E., Dennett, K. E., & Cath, T. Y. (2007). Forward osmosis for concentration of anaerobic digester centrate. Water research, 41(17), 4005-4014.

Huang, H., Zhang, P., Zhang, Z., Liu, J., Xiao, J., & Gao, F. (2016). Simultaneous removal of ammonia nitrogen and recovery of phosphate from swine wastewater by

struvite electrochemical precipitation and recycling technology. Journal of cleaner production, 127, 302-310.

Huang, C., & Xu, T. (2006). Electrodialysis with bipolar membranes for sustainable development. Environmental science & technology, 40(17), 5233-5243.

Hua, T., Li, S., Li, F., Zhou, Q., & Ondon, B. S. (2019). Microbial electrolysis cell as an emerging versatile technology: a review on its potential application, advance and challenge. Journal of Chemical Technology & Biotechnology, 94(6), 1697-1711.

Hu, H., Fan, Y., & Liu, H. (2008). Hydrogen production using single-chamber membrane-free microbial electrolysis cells. Water research, 42(15), 4172-4178.

International Energy Agency. World Energy Outlook 2018; International Energy Agency: Paris, France, 2018; pp. 23–28.

Jeremiasse, A. W., Hamelers, H. V., & Buisman, C. J. (2010). Microbial electrolysis cell with a microbial biocathode. Bioelectrochemistry, 78(1), 39-43.

Kuai, L., & Verstraete, W. (1998). Ammonium removal by the oxygen-limited autotrophic nitrification-denitrification system. Applied and environmental microbiology, 64(11), 4500-4506.

Kumar, R., Singh, L., Zularisam, A. W., & Hai, F. I. (2018). Microbial fuel cell is emerging as a versatile technology: a review on its possible applications, challenges and strategies to improve the performances. International Journal of Energy Research, 42(2), 369-394.

Kurniawan, T. A., Chan, G. Y., Lo, W. H., & Babel, S. (2006). Physico–chemical treatment techniques for wastewater laden with heavy metals. Chemical engineering journal, 118(1-2), 83-98.

Le Corre, K. S., Valsami-Jones, E., Hobbs, P., & Parsons, S. A. (2005). Impact of calcium on struvite crystal size, shape and purity. Journal of crystal growth, 283(3-4), 514-522.

Lee, H. S., & Rittmann, B. E. (2010). Significance of biological hydrogen oxidation in a continuous single-chamber microbial electrolysis cell. Environmental science & technology, 44(3), 948-954.

Lei, C., Li, Z., Gao, Q., Fu, R., Wang, W., Li, Q., & Liu, Z. (2020). Comparative study on the production of gluconic acid by electrodialysis and bipolar membrane electrodialysis: Effects of cell configurations. Journal of Membrane Science, 608, 118192.

Liu, T., & Sung, S. (2002). Ammonia inhibition on thermophilic aceticlastic methanogens. Water Science and Technology, 45(10), 113-120.

Liu, H., Grot, S., & Logan, B. E. (2005). Electrochemically assisted microbial production of hydrogen from acetate. Environmental science & technology, 39(11), 4317-4320.

Logan, B. E., Call, D., Cheng, S., Hamelers, H. V., Sleutels, T. H., Jeremiasse, A. W., & Rozendal, R. A. (2008). Microbial electrolysis cells for high yield hydrogen gas production from organic matter. Environmental science & technology, 42(23), 8630-8640.

Martin, S., & Griswold, W. (2009). Human health effects of heavy metals. Environmental Science and Technology briefs for citizens, 15, 1-6.

Mata-Alvarez, J., Macé, S., & Llabres, P. (2000). Anaerobic digestion of organic solid wastes. An overview of research achievements and perspectives. Bioresource technology, 74(1), 3-16.

Müller, T., Walter, B., Wirtz, A., & Burkovski, A. (2006). Ammonium toxicity in bacteria. Current microbiology, 52(5), 400-406.

Nancharaiah, Y. V., Mohan, S. V., & Lens, P. N. L. (2015). Metals removal and recovery in bioelectrochemical systems: a review. Bioresource Technology, 195, 102-114.

Nguyen, L. D., Gassara, S., Bui, M. Q., Zaviska, F., Sistat, P., & Deratani, A. (2019). Desalination and removal of pesticides from surface water in Mekong Delta by coupling electrodialysis and nanofiltration. Environmental Science and Pollution Research, 26(32), 32687-32697.

Patel, S. K., Qin, M., Walker, W. S., & Elimelech, M. (2020). Energy efficiency of electro-driven brackish water desalination: electrodialysis significantly outperforms membrane capacitive deionization. Environmental science & technology, 54(6), 3663-3677.

Palanisamy, G., Jung, H. Y., Sadhasivam, T., Kurkuri, M. D., Kim, S. C., & Roh, S. H. (2019). A comprehensive review on microbial fuel cell technologies: Processes, utilization, and advanced developments in electrodes and membranes. Journal of cleaner production, 221, 598-621.

Panepinto, D., Fiore, S., Zappone, M., Genon, G., & Meucci, L. (2016). Evaluation of the energy efficiency of a large wastewater treatment plant in Italy. Applied Energy, 161, 404-411.

Pourcelly, G. (2002). Electrodialysis with bipolar membranes: principles, optimization, and applications. Russian Journal of Electrochemistry, 38(8), 919-926.

Ritchie, S. M., Kissick, K. E., Bachas, L. G., Sikdar, S. K., Parikh, C., & Bhattacharyya, D. (2001). Polycysteine and other polyamino acid functionalized microfiltration membranes for heavy metal capture. Environmental science & technology, 35(15), 3252-3258.

Rajagopal, R., Massé, D. I., & Singh, G. (2013). A critical review on inhibition of anaerobic digestion process by excess ammonia. Bioresource technology, 143, 632-641.

Rozendal, R. A., Hamelers, H. V., Molenkamp, R. J., & Buisman, C. J. (2007). Performance of single chamber biocatalyzed electrolysis with different types of ion exchange membranes. Water research, 41(9), 1984-1994.

Schorr, M. (Ed.). (2011). Desalination: Trends and Technologies. BoD–Books on Demand.

Shi, L., Hu, Y., Xie, S., Wu, G., Hu, Z., & Zhan, X. (2018). Recovery of nutrients and volatile fatty acids from pig manure hydrolysate using two-stage bipolar membrane electrodialysis. Chemical Engineering Journal, 334, 134-142.

Strathmann, H. (2010). Electrodialysis, a mature technology with a multitude of new applications. Desalination, 264(3), 268-288.

Sun, X., Lu, H., & Wang, J. (2017). Recovery of citric acid from fermented liquid by bipolar membrane electrodialysis. Journal of Cleaner Production, 143, 250-256.

Tartakovsky, B., Manuel, M. F., Wang, H., & Guiot, S. R. (2009). High rate membrane-less microbial electrolysis cell for continuous hydrogen production. International Journal of Hydrogen Energy, 34(2), 672-677.

Tian, W., Wang, X., Fan, C., & Cui, Z. (2019). Optimal treatment of hypersaline industrial wastewater via bipolar membrane electrodialysis. ACS Sustainable Chemistry & Engineering, 7(14), 12358-12368.

US EPA (2013). Aquatic Life Ambient Water Quality Criteria for Ammonia – Freshwater.

Wagner, R. C., Regan, J. M., Oh, S. E., Zuo, Y., & Logan, B. E. (2009). Hydrogen and methane production from swine wastewater using microbial electrolysis cells. water research, 43(5), 1480-1488.

Wang, H., & Ren, Z. J. (2014). Bioelectrochemical metal recovery from wastewater: a review. Water research, 66, 219-232.

Ward, A. J., Arola, K., Brewster, E. T., Mehta, C. M., & Batstone, D. J. (2018). Nutrient recovery from wastewater through pilot scale electrodialysis. Water research, 135, 57-65.

Wilson, E. L., & Kim, Y. (2016). The yield and decay coefficients of exoelectrogenic bacteria in bioelectrochemical systems. Water research, 94, 233-239.

Wilson, C. A., Novak, J., Takacs, I., Wett, B., & Murthy, S. (2012). The kinetics of process dependent ammonia inhibition of methanogenesis from acetic acid. Water research, 46(19), 6247-6256.

Wu, G., Wu, J. Y., & Shao, H. B. (2012). Hazardous heavy metal distribution in Dahuofang catchment, Fushun, Liaoning, an important industry city in China: a case study. CLEAN–Soil, Air, Water, 40(12), 1372-1375.

Xiao, K. K., Guo, C. H., Zhou, Y., Maspolim, Y., Wang, J. Y., & Ng, W. J. (2013). Acetic acid inhibition on methanogens in a two-phase anaerobic process. Biochemical engineering journal, 75, 1-7.

Xu, T., & Huang, C. (2008). Electrodialysis ‐ based separation technologies: a critical review. AIChE journal, 54(12), 3147-3159.

Xu, Z., Zhao, M., Miao, H., Huang, Z., Gao, S., & Ruan, W. (2014). In situ volatile fatty acids influence biogas generation from kitchen wastes by anaerobic digestion. Bioresource technology, 163, 186-192.

Yang, Y., Ren, H., Ben-Tzvi, P., Yang, X., & He, Z. (2017). Optimal interval of periodic polarity reversal under automated control for maximizing hydrogen production in microbial electrolysis cells. international journal of hydrogen energy, 42(31), 20260-20268.

Yenigün, O., & Demirel, B. (2013). Ammonia inhibition in anaerobic digestion: a review. Process Biochemistry, 48(5-6), 901-911.

Ye, Y., Ngo, H. H., Guo, W., Chang, S. W., Nguyen, D. D., Zhang, X., ... & Liang, S. (2020). Nutrient recovery from wastewater: From technology to economy. Bioresource Technology Reports, 100425.

2 Scalable Multi-electrode Microbial Electrolysis Cells for High Electric Current and Rapid Organic Removal

Microbial electrolysis cells (MECs) have been regarded as an environmentally friendly technology for wastewater treatment since MECs can remove organic materials and produce hydrogen gas simultaneously. Electric current which represents hydrogen gas production rate and organic removal rate was low in MECs. Therefore, a multi-electrode stack design was proposed in MECs to enhance the electric current generation. Many factors, such as the number of electrode pairs, cathode materials, applied voltage, and flow rate, were examined in this study to maximize the electric current generation.

The following published journal article is included in this chapter.

- Guo, H., & Kim, Y. (2018). Scalable multi-electrode microbial electrolysis cells for high electric current and rapid organic removal. *Journal of Power Sources*, *391*, 67-72.

The co-author's contributions include:

- Funding acquisition
- Supervision and technical support
- Manuscript review and revision

Abstract

Microbial electrolysis cells (MECs) can be used to produce hydrogen gas from wastewater. A novel multi-electrode stack design was proposed and examined under various operating conditions to maximize electric current in MECs without precious metal catalysts. For the cathode in the electrode stack, stainless steel mesh generated higher electric current than activated carbon cloth. The electric current density increased in proportion to the number of electrode pairs as the maximum current density was 520 A m^{-3} in MEC-10 (10 electrode pairs), 270 A m^{-3} in MEC-5 (5 electrode pairs), and 45 A m^{-3} with a single electrode pair. The stacked MEC was not ideal for fed-batch operation due to the short inter-electrode distance (~2 mm); consequently, continuous-recycle and -flow operation resulted in the high electric current generation. During continuous-flow operation, individual electrodes in MEC-10 and MEC-5 showed a variation in electric current capacity (0.9-2.7 mA for 0.6 mL min^{-1}). The COD (chemical oxygen demand) removal rate increased from 45.7 to 128.8 mg-COD L^{-1} h^{-1} with increasing flow rate from 0.1 to 0.6 mL min^{-1}. These findings indicate that the stacked multi-electrode design can magnify the current generation and COD removal rate in MECs.

Keywords

Bioelectrochemical system; electrode stack; multi-electrode design; COD removal rate; cathode materials; MEC start-up

2.1 Introduction

Microbial electrolysis cells (MECs) are an emerging technology to treat wastewater and simultaneously produce hydrogen gas [1]. A MEC reactor consists of an anode and a cathode. Organic substrates are oxidized by exoelectrogenic bacteria to release electrons to the anode while water is reduced at the cathode to hydrogen gas. To drive the electrode reactions, a small voltage (0.13 to 1.23 V) needs to be applied to the MEC; as a result, the energy recovered as H_2 gas is usually much greater than the energy consumed for the applied voltage [2-3]. In MEC operation, the rate of organic removal and hydrogen gas production is represented by the magnitude of electric current. There are many factors that govern the electric current generation in MECs, such as electrode materials, electrode size, electrode catalysts, inter-electrode distance, and material transport near electrodes, which is often determined by hydrodynamic conditions. The inter-electrode distance has been minimized in previous studies by developing the sandwiched electrode assembly that significantly decreases the internal resistance of bioelectrochemical systems (BES) [4-6]. The separators such as carbon cloth [6-7], glass fiber [8-9], and spacers [10] are commonly used in the sandwiched electrode assembly design. In addition, the specific surface area of electrodes (electrode surface area per volume of the reactor) also affects the electric current generation. For instance, a recent study employed bundles of 73,000 graphite fibers in a 0.125 L MEC (specific anode surface area was 2530 m^2 m^{-3}) and demonstrated substantially high electric current generation at 1470 A m^{-3} [11]. However, the bundled electrode design can hardly be scaled up for practical applications of MECs. In another study, high current generation (2.82 A m^{-3}) was demonstrated in a relatively large-scale

MEC reactor (6.6 L) with a specific anode surface area of 6.1 m^2 m^{-3} [2]. A maximum current density of 180 A m^{-3} was demonstrated by increasing the specific anode surface area to 100 m^2 m^{-3} using carbon felt in MECs [12]. Carbon cloth was also utilized in MEC construction to maximize the specific electrode surface area and the resulting current density was also relatively high at 65.3 A m^{-3} and this current density was higher than that produced in another MEC with the same electrode materials but reduced specific surface area from 12 to 6 m^2 m^{-3} [2,13]. The multi-electrode design is an effective way to increase the specific surface area of electrodes. A multi-electrode MEC with 8 separate electrode pairs produced a maximum current density of 74 A m^{-3} [14]. However, this MEC design used graphite fiber brushes as the anodes and thus required a certain reactor space for the brushes. As a result, the specific surface area was limited to 64 m^2 m^{-3}. Therefore, in this study, we proposed and examined a new MEC electrode design that satisfies the three key requirements: high specific surface area; low internal resistance; and easy scalability. Various anode materials have been examined in the BES, including graphite brushes [14-15], graphite granules [16], carbon cloth [1,13], and carbon felt [12,17-18]. Graphite brushes can provide a large specific surface area for the growth of exoelectrogenic bacteria. Graphite granules also provide a large surface area and relatively high electric current generation (66 ± 2 to 156 ± 1 A m^{-3}) [16]. Unlike graphite brushes or granules, carbon cloth or carbon felt can substantially decrease the inter-electrode distance without electric short-circuiting problems. By decreasing the inter-electrode distance, the internal resistance dropped from 580 to 220 Ω by using carbon cloth [19]. Porous anode materials were also examined for BES scale-up [20-21]. However, the highly porous activated carbon materials were found to

be non-ideal for stacked electrode design compared to carbon cloth materials because of the potential limitation of substrate transport in the activated carbon pores.

The catalytic capability of the cathode is also an important factor that governs the MEC operation efficiency. For MEC cathode preparation, biocathodes or biocatalysts [22-23] are an alternative way to eliminate the use of expensive Pt catalysts [24]. The concept of biocathode was proposed based on the utilization of a large variety of microorganisms that can produce hydrogen gas [25]. The biocathode application resulted in a substantially higher current generation (3.3 A m^{-2}) than that in the control MEC (0.3 A m^{-2}; cathode without biofilms) in a previous study [23]. Thus, we examined the biocatalytic effect in our newly designed MEC reactors.

In this study, a new design of stacked electrodes was proposed and examined in MECs to improve the electric current generation and organic removal rate. The repeated stack with narrow inter-electrode distance allowed significantly large specific electrode areas and low resistance. The stack of multiple electrode pairs can result in slow transport of reactants and products of the MEC electrode reactions, making the MEC performance limited by mass transfer. The mass transfer limitation can be reduced by employing continuous flow operation at a high flow rate. Continuous flow operation is usually designed for practical applications in wastewater treatment and energy production while fed-batch operation is widely used for lab-scale MEC studies.

We also examined various MEC operating conditions, such as fed-batch, continuous flow with effluent recycle, and continuous flow without effluent recycle to optimize the electric current generation and reactor operation for the stacked MEC design. For

continuous flow operation, an increased flow rate can reduce the mass transport limitation for a high electric current generation. At a high flow rate, however, the exoelectrogenic microorganisms growing on the anode can be washed away. In addition, individual electrodes in a stacked design can perform differently depending on their location and other operating conditions, such as flow rate. Since there are no previous studies on the performance of individual electrodes under continuous flow conditions, we focused on providing a clear understanding of individual electrode performance in stacked-electrode MECs. Other specific objectives of this study are to: investigate the start-up of the stacked electrode MECs; evaluate the performance of the MECs under fed-batch, continuous-recycle, and continuous-flow operation conditions; examine two stackable cathode materials (carbon cloth and stainless steel mesh); maximize the electric current generation and organic removal rate in 3 stacked MECs (1, 5, and 10 electrode pairs); and study the performance of individual electrodes on electric current generation

2.2 Material and methods

2.2.1 Stacked MEC construction

A polypropylene block with a cylindrical hole (7 cm^2 in cross-section) was used to build each MEC reactor. Four MEC reactors were built in this study: one MEC with 10 electrode pairs (MEC-10 as shown in Figures 2.1A and 2.1B); one with 5 electrode pairs (MEC-5); and two MECs with a single electrode pair. Activated carbon cloth (ACC100, Evertech Envisafe Ecology, Taiwan) was used as the anode after treating in a surfactant solution [26]. The stainless steel mesh (304 stainless steel, 200 × 200 mesh, McMaster Carr, USA) was used as the cathode without any precious metal catalysts in MEC-10, MEC-5,

and one of the MECs with a single electrode pair. For the other MEC with a single electrode pair, the cathode was the same material as the anode (activated carbon cloth). Two rubber gaskets and one plastic mesh were sandwiched between the anode and cathode to avoid potential electric short circuits between the electrodes as previously described [27]. The mean distance between the electrodes as well as between the electrode pairs was 2.8 mm spaced by the two rubber gaskets. Each electrode pair was operated and monitored independently.

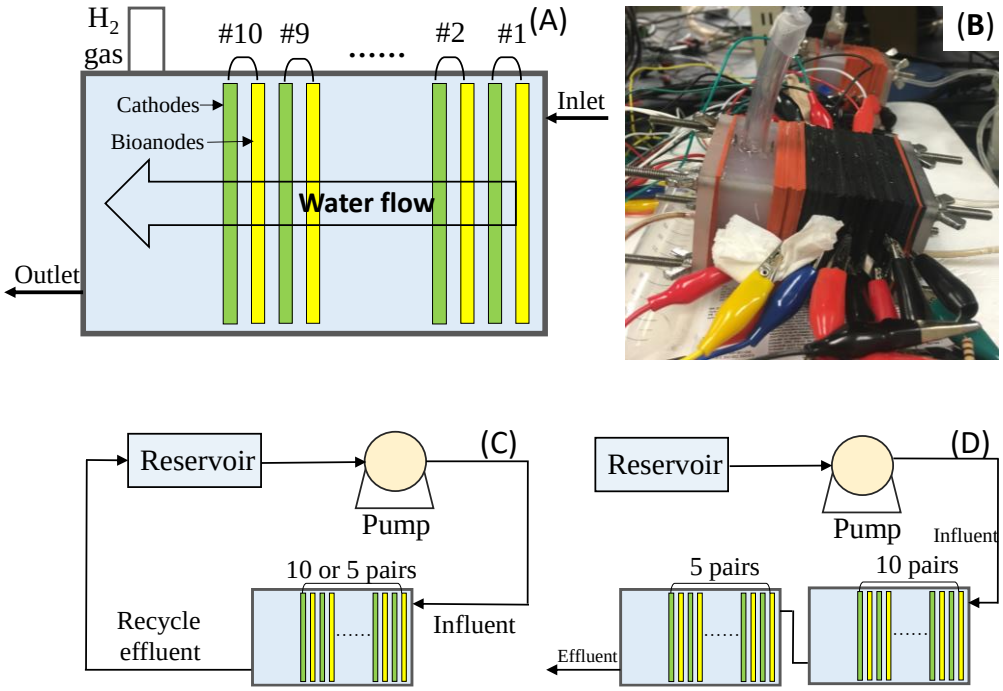

Figure 2.1. (A) Schematic diagram of MEC-10 design; (B) Photograph of MEC-10; (C) Schematic diagram of continuous recycle operation; (D) Schematics for continuous flow operation.

The effective volume of MEC-10 and MEC-5 were 40 and 35 mL, respectively. The volume of the MECs with a single pair of electrodes was 28 mL. The upper and lower parts of each electrode were cut off by 0.3 cm from the edge to allow water and gas flow, resulting in 5.42 cm^2 of the surface area per electrode. Therefore, the specific surface area for MEC-10 (10 electrode pairs) was 136 m^2 m^{-3} and 77 m^2 m^{-3} for MEC-5 (5 electrode pairs).

2.2.2 Reactor operation

Effluent from existing lab-scale MECs that were originally started with primary clarifier effluent from a local wastewater treatment plant was used to inoculate the constructed MECs during the start-up period. Thus, the experiments were conducted with mixed-culture MECs. The feed solution was prepared with sodium acetate (1 or 2 g L^{-1} $NaCH_3COO$) in 25 mM phosphate buffer solution (4.33 g L^{-1} Na_2HPO_4-$7H_2O$; 1.07 g L^{-1} NaH_2PO_4; 0.16 g L^{-1} NH_4Cl; 0.065 g L^{-1} KCl) with trace minerals and vitamins [28]. The MECs were operated in three different modes: fed batch; continuous recycle; and continuous flow. For the fed-batch mode, the sodium acetate concentration was 2 g L^{-1} and the applied voltage (E_{ap}) was 0.6 V using an external power supplier (GPS-1850D; GW Instek, Taiwan). Each fed-batch cycle lasted approximately 5 days and the fed-batch operation was repeated over 10 cycles or more for MEC-10 and MEC-5. After the fed-batch study, each of MEC-10 and MEC-5 was operated in the continuous recycle mode (Figure 2.1C). The feed solution of 1 g L^{-1} sodium acetate was stored in an external reservoir (250 mL for MEC-10 and 150 mL for MEC-5) and continuously pumped to the MEC using a peristaltic pump at 2 mL min^{-1}. In the continuous recycle operation, the feed

solution was continuously recirculated between the reservoir and MEC reactor. Each of the continuous recycles operation lasted around 3 days and the operation was repeated 4 times with various E_{ap} conditions (0.8, 0.9, 1.0, and 1.1 V). Note that the various voltage conditions were examined during continuous recycle operation since electric current generation during fed-batch operation is limited by mass transfer due to the very short inter-electrode distance. For the continuous flow operation, MEC-10 and MEC-5 were arranged in series where the feed solution (1 g L^{-1} sodium acetate) was introduced to MEC-10 and then into MEC-5 (Figure 2.1D). The serial MEC system was operated at three different flow rate conditions (0.1, 0.3, 0.6 mL min^{-1}) and E_{ap} was consistently 1.1 V. During the continuous-recycle and –flow operation, the external reservoir was kept in an ice cooler to minimize microbial activities in the reservoir. Between the reservoir and MEC, a 30-cm long copper tube was immersed in water to maintain the influent temperature at 22.9 ± 0.3°C.

2.2.3 Experimental measurement

A 10-Ω resistor was connected to each electrode pair and the voltage drop across the resistor was monitored every 20 min using a digital multimeter and data acquisition system (Model 2700, Keithley Instruments, USA). The electric current for all individual electrode pairs was added and normalized by the effective volume of the MEC reactor to obtain the volume-based current density.

The COD (chemical oxygen demand) test tubes were used to measure the COD of the experimental samples (Hach Company, USA). The influent and effluent were analyzed for pH and conductivity (SevenMulti, Mettler-Toledo International Inc., USA). The influent

pH was 7.0 and the effluent was also neutral between 7.1 and 7.6. There were no significant changes in conductivity (4.5 mS cm^{-1}) during the MEC operation.

2.2.4 Coulombic efficiency and organic removal rate

The Coulombic efficiency (*CE*) is the ratio between the number of electrons generated in the electric current and the total amount of electrons released from COD removal [3]:

$$CE = \frac{8\sum_n I}{QF\Delta COD} \quad \text{(Eq 2.1)}$$

I is the electric current from an individual electrode pair, n is the number of electrode pairs in the MEC, *F* is the Faraday's constant (96485 C mol^{-1}), and ΔCOD is the COD change between the influent and effluent, and *Q* is the flow rate of feed solution.

The COD removal rate during the continuous flow operation was calculated by ΔCOD divided by hydrolytic retention time (τ):

$$\text{COD removal rate} = \frac{\Delta\text{COD}}{\tau} \quad \text{(Eq 2.2)}$$

2.3 Results and discussion

2.3.1 MEC start-up and cathode materials

The reactor start-up for the MEC with a single electrode pair was faster than that for multi-electrode MECs. It took 40-50 days until the consistent peak current was obtained in MEC-5 and MEC-10 (Figures 2.2A and 2.2B) while the single-paired electrode MEC reached the consistent peak current shortly after 20 days. The slower start-up for the multi-electrode MECs can be explained by the longer time required for exoelectrogenic microorganisms to grow on the large surface areas of the multiple anodes. Even though the start-up was relatively slow, the peak current density in MEC-10 and MEC-5 during the

start-up period was usually 40 A m^{-3} (Figures 2.2A and 2.2B), which was higher than the maximum current density of the MEC with single pair after the full enrichment (24 A m^{-3}) (see Appendix, Figure A1A).

Thin electrode materials, such as mesh and cloth, are necessary for the electrode stack design. For the stacked cathode, stainless steel mesh was found to be more effective for high electric current generation than activated carbon cloth. The maximum current density was only 18 A m^{-3} when activated carbon cloth was used as the cathode (Appendix, Figure A1B) while it was 24 A m^{-3} with stainless steel mesh as the cathode (Appendix, Figure A1A). The stainless steel metal alloy containing nickel is thought to enhance the current generation as demonstrated in previous studies [29]. The MEC with the activated carbon cloth cathode showed a rapid drop in the electric current shortly after reaching the peak current (Appendix, Figure A1B). This trend can be explained by the slow release of H_2 gas and OH^- ions from the cloth structure of the cathode. Activated carbon materials are commonly used for biocathodes in bioelectrochemical systems [22-23,25,30-32]. However, for the electrode stack design where the electrodes are compactly sandwiched in a small space, the biocatalytic effect can be compromised by the slow H_2 gas removal from the cathode. Thus, stainless steel mesh is recommended as the cathode for the stacked electrode design so that H_2 gas can be produced at catalytic sites of stainless steel (e.g., nickel).

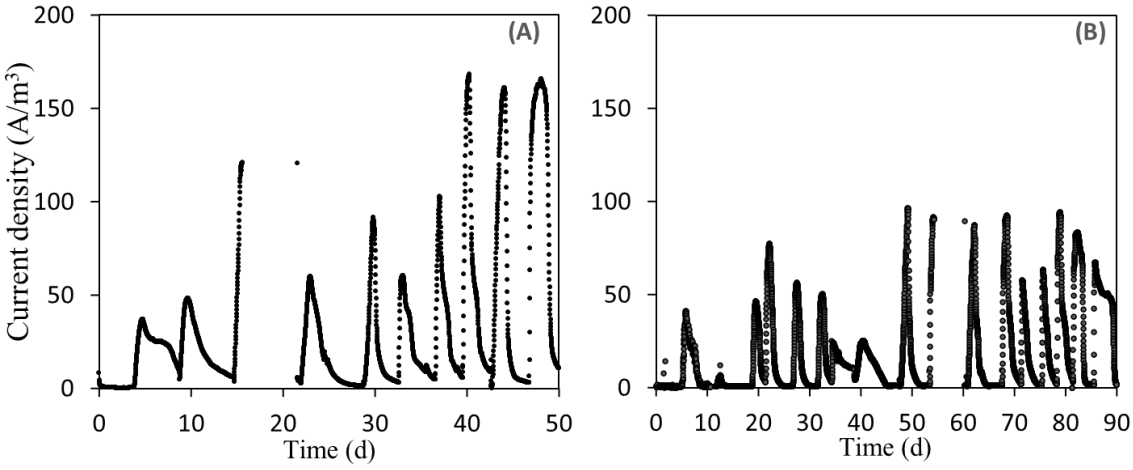

Figure 2.2. Electric current generation during fed-batch operation at Eap of 0.6 V: (A) MEC-10; (B) MEC-5; The MEC reactors were inoculated at time 0.

2.3.2 Fed-batch MEC operation

The total electric current density showed an almost linear increase with the number of electrode pairs during the fed-batch operation. The maximum current density was 170 A m^{-3} in MEC-10 (Figure 2.2A) and 92 A m^{-3} in MEC-5 (Figure 2.2B). Considering the relatively low applied voltage (Eap = 0.6 V) and the absence of Pt catalysts on the cathode, the sandwiched electrode stack design substantially enhanced the current generation in MECs. The high current generation and the linear increase in the current density can be explained by the increased electrode surface area. The total anode or cathode area was 54.2 cm^2 for MEC-10, 27.1 cm^2 for MEC-5, and 5.42 cm^2 for MEC with the single paired electrode MEC.

Comparing electric current generation from individual electrode pairs, the electric current in electrode pair #10 (the 10th electrode pair from the inlet) in MEC-10 (Appendix, Figure A2). Electrode pair #10 in MEC-10 generated electric current higher than 1.3 mA

while the other electrode pairs produced electric current less than 1.2 mA (Appendix, Figure A2). Consistent results were observed for MEC-5 with 1.2 mA for electrode pair #5 and less than 1 mA for the other electrode pairs (Appendix, Figure A3). These results can be explained by the large volume of solution (~24 mL) next to electrode pair #10 in MEC-10 and #5 in MEC-5. This mass transfer limitation can be reduced by flowing the feed solution continuously through the multi-electrode stack. Thus, the stacked electrode MECs can produce even higher electric current under continuous recycle or continuous flow operations.

2.3.3 Continuous recycle operation

The electric current generation was greatly improved for continuous recycle operation (Figure 2.3). As the feed solution flows through the electrode stack, the organic substrate (acetate) was easily supplied to the bioanode, allowing the higher current. For the given flow rate (2 mL min^{-1}), the mean hydraulic residence time was around 1 min per electrode pair. The higher current densities with the reduced hydraulic residence time compared to fed-batch operation imply faster COD removal with reduced mass transfer limitation. The electric current generation was also sensitively governed by the applied voltage regardless of the stack size (Figure 2.3). The maximum current density in MEC-10 increased by 33% from 390 A m^{-3} to 520 A m^{-3} for the increasing applied voltage from 0.8 V to 1.1 V (Figure 2.3A). For MEC-5, the increase was much greater by 93% from 145 A m^{-3} to 280 A m^{-3} (Figure 2.3B). Thus, the current generation in MEC-10 was less sensitive to the applied voltage than that in MEC-5. This comparison indicates that increasing the number of

electrode pairs in MECs is a more effective way to enhance the current generation than increasing the applied voltage, allowing energy-efficient operation of MECs.

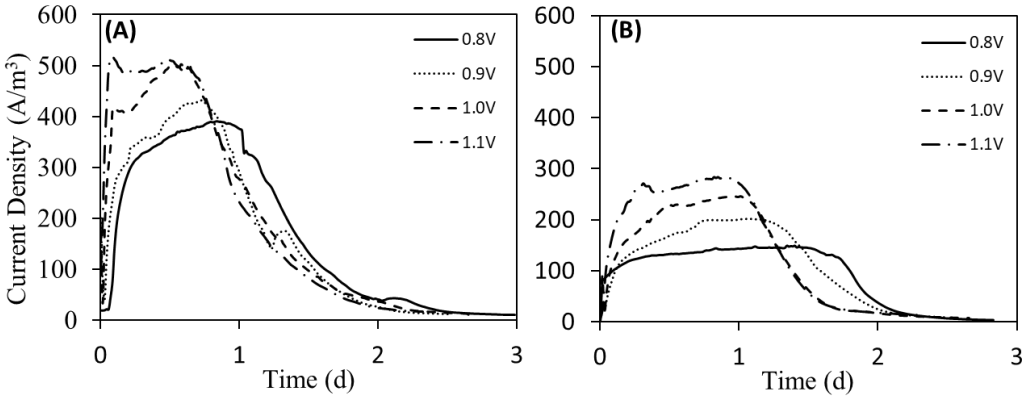

Figure 2.3. The electric current generation with different applied voltage during the recycle operation. A: MEC-10; B: MEC-5.

For the continuous recycle operation, the Coulombic efficiency (CE) in MEC-10 was higher in the range of 81-90% compared to 67-84% in MEC-5 (Figure A4). The higher electric current density in MEC-10 resulted in a shorter time for substrate utilization compared to MEC-5 (Figure 2.3), allowing more organic substrates to be utilized by exoelectrogens at the bioanode. Similarly, the increasing applied voltage from 0.8 to 1.1 V gradually increased the CE in both MEC-10 and MEC-5 (Figure A4).

2.3.4 Continuous-flow MEC operation

The electric current density varied over a relatively wide range from 260 to 500 A m^{-3} for MEC-10 and from 110 to 360 A m^{-3} for MEC-5 during continuous-flow operation of MEC-10 and MEC-5 in series (no recycle) (Figures 2.1D and 2.4). The wide variation in electric current has been commonly reported in the continuous-flow operation of bioelectrochemical systems [7,11,33]. Even with the substantial variation, the maximum

current density (506 A m^{-3} in MEC-10) was consistent with the peak current values during continuous recycle operation (512 A m^{-3} in MEC-10). Thus, the stacked electrode design can be applied for continuous flow MEC operation either with or without effluent recycle.

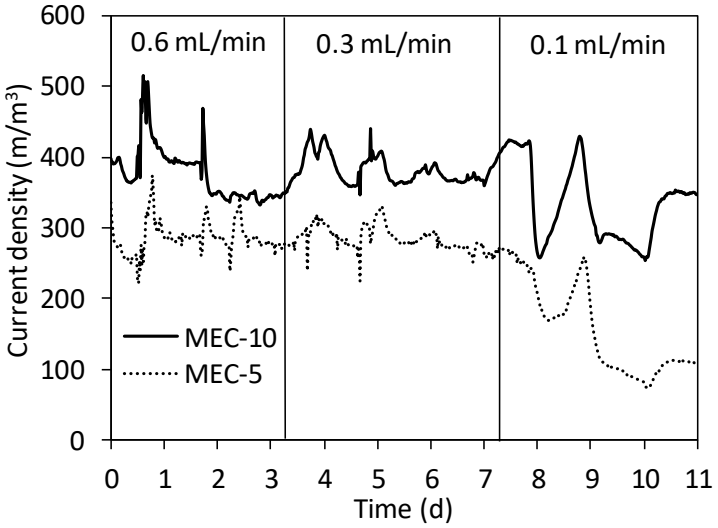

Figure 2.4. Electric current generation in the continuous-flow MEC system fed with acetate.

Effects of the flow rate on the electric current generation were not clearly observed until the flow rate was reduced to 0.1 mL min^{-1}. When the flow rate decreased from 0.6 to 0.3 mL min^{-1}, the current density of both MEC-10 and MEC-5 was stationary (Figure 2.4). This negligible change in the current density can be explained by the high COD concentration of influent (677-711 mg-COD L^{-1}) (Figure 2.5A), providing sufficient substrates in the MEC system even with the short retention time. High COD concentration also was shown in the effluent, which was 503 ± 10 mg-COD L^{-1} at 0.6 mL min^{-1} and 298 ± 59 mg-COD L^{-1} at 0.3 mL min^{-1} (Figure 2.5A). However, when the flow rate was reduced to 0.1 mL min^{-1}, the effluent COD dropped to 148.5 ± 18.5 mg-COD L^{-1} (Figure 2.5A). As

a result, the average electric current decreased with a wider variation in electric current both in MEC-10 and MEC-5.

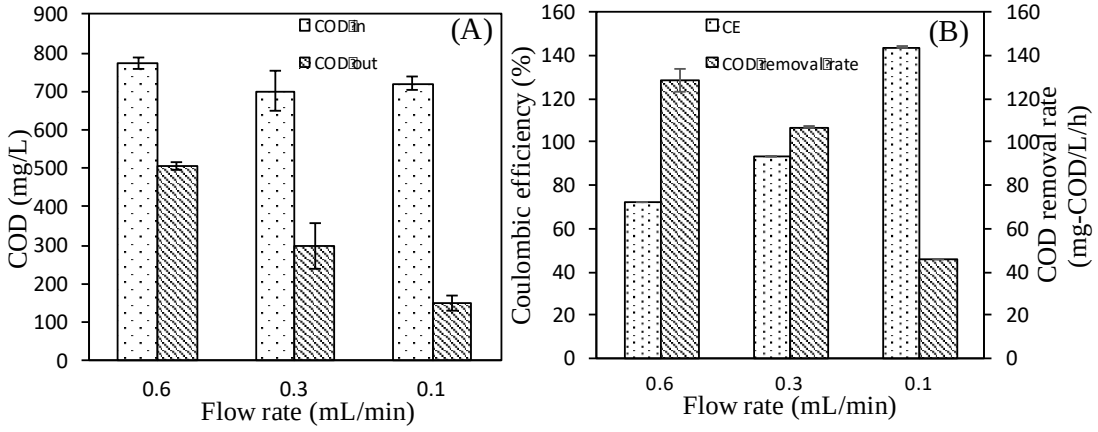

Figure 2.5. Operation results of continuous-flow MEC system. A: COD treatment, B: Columbic efficiency and COD removal rate.

The COD removal increased from 35 to 79% with the decreasing flow rate from 0.6 to 0.1 mL min^{-1} (Figure 2.5A), because the mean hydraulic retention time increased from 2.1 to 12.5 h. The COD removal rate was 106.8 - 128.8 mg-COD L^{-1} h^{-1} for 0.3 and 0.6 mL min^{-1} while it dropped to 45.7 mg-COD L^{-1} h^{-1} for 0.1 mL min^{-1} (Figure 2.5B). In previous studies on MEC applications for organic removal, the COD removal rate was 14 - 246 mg L^{-1} h^{-1} [12,14,34]. The COD removal rate was 14 – 21 mg-COD L^{-1} h^{-1} in the multi-electrode continuous flow MEC with 8 separate graphite fiber brush anodes [14]. Varying COD removal rates ranged from 7.6 to 10.8 mg-COD L^{-1} h^{-1} were achieved in a single pair electrode MEC with a working volume of 580 mL [34]. In another study, the COD removal rate was 78-110.5 mg-COD L^{-1} h^{-1} in a MEC with Pt-catalyzed cathode [12]. Compared with the reported COD removal rates, the stacked electrode design can substantially improve

the MEC performance for rapid organic removal rate without using expensive Pt catalysts or large amounts of electrode materials.

The Coulombic efficiency (CE) was 72.5 ± 0.9% for 0.6 mL min^{-1} and 93.6 ± 1.3 % for 0.3 mL min^{-1} (Figure 2.5B). These results were consistent with previous MECs that the CE in the range of 80-100% [3,12]. When the flow rate was decreased to 0.1 mL min^{-1}, the CE was 140.7 ± 14.4% (Figure 2.5B). The mean hydraulic residence time for 0.1 mL min^{-1} was 12.5 h. Hydrogen gas produced at the cathode stayed in the reactor system for a relatively long time (12.5 h) and as a result, a certain fraction of the produced H_2 gas was used as an electron donor by exoelectrogens on the anode, resulting in the high CE above 100% as previously reported [14]. However, the CE values lower than 100% and relatively high COD removal rates (>100 mg-COD L^{-1} h^{-1}) for 0.6 and 0.3 mL min^{-1} indicate that potential hydrogen oxidation at the anode was controlled with the reduced hydraulic retention time (4.2 and 2.1 h). This observation indicates that stacked electrode MECs need to be operated at a certain flow rate or higher to avoid generating extra electric current by oxidation of hydrogen gas. In addition, the short resistance time will also help control methanogenesis reactions at the MEC cathode and contribute to high energy recovery.

2.3.5 Electric current generation of individual electrodes under continuous-flow operation

Significant variation in the electric current among the individual electrodes was observed during the continuous flow operation (Table 2.1). For instance, the electric current in individual electrodes ranged from 0.9 to 2.7 mA for 0.6 mL min^{-1} and similar variation was found for the lower flow rate conditions (0.3 and 0.1 mL min^{-1}). Even with

the variation, the electrode pair with the lowest electric current always produced at least 60% of the average current of all electrode pairs. This finding indicates that every electrode pair contributed to the total electric current generation; that is, the MEC performance was not dependent on only a few healthy electrode pairs. Similar to the fed-batch operation, electrode pair #10 in MEC-10 and electrode pair #5 in MEC-5 produced the highest electric current regardless of the flow rate condition because they are located next to the large volume of solution. This finding implies that the stacked electrode design can be further improved by slightly increasing the distance between electrode pairs (currently 2.8 mm) to increase the current generation of individual electrode pairs.

Table 2.1. Electric current generation (mA) for individual electrode pairs during continuous flow operation of MEC-10 and MEC-5 in series

Reactor	Electrode pair	0.6 mL min^{-1}	0.3 mL min^{-1}	0.1 mL min^{-1}
MEC-10	#1	0.98 ± 0.34	1.11 ± 0.21	1.28 ± 0.24
	#2	0.90 ± 0.14	1.04 ± 0.15	0.98 ± 0.16
	#3	1.60 ± 0.22	1.53 ± 0.12	1.40 ± 0.21
	#4	1.20 ± 0.17	1.18 ± 0.08	1.13 ± 0.15
	#5	1.62 ± 0.25	1.58 ± 0.12	1.43 ± 0.23
	#6	1.58 ± 0.26	1.55 ± 0.15	1.40 ± 0.26
	#7	1.93 ± 0.17	2.04 ± 0.11	1.94 ± 0.22
	#8	1.58 ± 0.15	1.49 ± 0.08	1.40 ± 0.25
	#9	1.59 ± 0.17	1.54 ± 0.10	1.41 ± 0.30
	#10	2.10 ± 0.21	2.20 ± 0.10	1.89 ± 0.42
MEC-5	#1	1.58 ± 0.18	1.69 ± 0.13	1.46 ± 0.33
	#2	1.67 ± 0.23	1.57 ± 0.17	1.15 ± 0.45
	#3	1.29 ± 0.23	1.04 ± 0.21	0.79 ± 032
	#4	1.97 ± 0.16	2.04 ± 0.09	1.59 ± 0.62
	#5	2.61 ± 0.18	2.81 ± 0.09	2.04 ± 0.90

2.4 Conclusions

The electric current generation was almost linearly proportional to the number of electrode pairs and significantly high electric current densities were achieved. MECs stacked with a larger number of electrode pairs can achieve the maximum electric capacity at low applied voltages, minimizing energy requirement for wastewater treatment. The high COD removal rate up to 128.8 mg-COD L^{-1} h^{-1} indicates the strong wastewater treatability of the stacked MEC design. The higher CE than 100% (~140%) observed at the lowest flow rate (0.1 mL min^{-1}) implies that hydrogen gas was utilized at the anode as previously reported [14] and the stacked MEC should be operated at a certain flow rate or higher to avoid the loss of produced hydrogen gas. The electric current generation from individual electrode pairs was also monitored and we found that all electrodes contributed to the total electric current but the inter-electrode distance (~2 mm) can be increased for optimized electrode performance with reduced mass transport limitation. In future studies, the stacked MEC design can be further improved by optimizing individual electrode sizes.

References

[1] Liu, H., Grot, S., & Logan, B. E. (2005). Electrochemically assisted microbial production of hydrogen from acetate. *Environmental Science & Technology*, *39*(11), 4317-4320.

[2] Rozendal, R. A., Hamelers, H. V., Euverink, G. J., Metz, S. J., & Buisman, C. J. (2006). Principle and perspectives of hydrogen production through biocatalyzed electrolysis. *International Journal of Hydrogen Energy*, *31*(12), 1632-1640.

[3] Logan, B. E., Call, D., Cheng, S., Hamelers, H. V., Sleutels, T. H., Jeremiasse, A. W., & Rozendal, R. A. (2008). Microbial electrolysis cells for high yield hydrogen gas production from organic matter. *Environmental Science & Technology*, *42*(23), 8630-8640.

[4] Ghangrekar, M. M., & Shinde, V. B. (2007). Performance of membrane-less microbial fuel cell treating wastewater and effect of electrode distance and area on electricity production. *Bioresource Technology*, *98*(15), 2879-2885.

[5] Ahn, Y., Hatzell, M. C., Zhang, F., & Logan, B. E. (2014). Different electrode configurations to optimize performance of multi-electrode microbial fuel cells for generating power or treating domestic wastewater. *Journal of Power Sources*, *249*, 440-445.

[6] Zhang, F., Xia, X., Luo, Y., Sun, D., Call, D. F., & Logan, B. E. (2013). Improving startup performance with carbon mesh anodes in separator electrode assembly microbial fuel cells. *Bioresource Technology*, *133*, 74-81.

[7] Fan, Y., Han, S. K., & Liu, H. (2012). Improved performance of CEA microbial fuel cells with increased reactor size. *Energy & Environmental Science*, *5*(8), 8273-8280.

[8] Hays, S., Zhang, F., & Logan, B. E. (2011). Performance of two different types of anodes in membrane electrode assembly microbial fuel cells for power generation from domestic wastewater. *Journal of Power Sources*, *196*(20), 8293-8300.

[9] Zhang, X., Cheng, S., Wang, X., Huang, X., & Logan, B. E. (2009). Separator characteristics for increasing performance of microbial fuel cells. *Environmental Science & Technology*, *43*(21), 8456-8461.

[10] He, W., Zhang, X., Liu, J., Zhu, X., Feng, Y., & Logan, B. E. (2016). Microbial fuel cells with an integrated spacer and separate anode and cathode modules. *Environmental Science: Water Research & Technology*, *2*(1), 186-195.

[11] Lee, H. S., & Rittmann, B. E. (2009). Significance of biological hydrogen oxidation in a continuous single-chamber microbial electrolysis cell. *Environmental Science & Technology*, *44*(3), 948-954.

[12] Tartakovsky, B., Manuel, M. F., Wang, H., & Guiot, S. R. (2009). High rate membrane-less microbial electrolysis cell for continuous hydrogen production. *International Journal of Hydrogen Energy*, *34*(2), 672-677.

[13] Hu, H., Fan, Y., & Liu, H. (2008). Hydrogen production using single-chamber membrane-free microbial electrolysis cells. *Water Research*, *42*(15), 4172-4178.

[14] Rader, G. K., & Logan, B. E. (2010). Multi-electrode continuous flow microbial electrolysis cell for biogas production from acetate. *International Journal of Hydrogen Energy*, *35*(17), 8848-8854.

[15] Logan, B., Cheng, S., Watson, V., & Estadt, G. (2007). Graphite fiber brush anodes for increased power production in air-cathode microbial fuel cells. *Environmental Science & Technology*, *41*(9), 3341-3346.

[16] Clauwaert, P., & Verstraete, W. (2009). Methanogenesis in membraneless microbial electrolysis cells. *Applied Microbiology and Biotechnology*, *82*(5), 829-836.

[17] Lee, H. S., Torres, C. I., Parameswaran, P., & Rittmann, B. E. (2009). Fate of H_2 in an upflow single-chamber microbial electrolysis cell using a metal-catalyst-free cathode. *Environmental Science & Technology*, *43*(20), 7971-7976.

[18] Xiao, Y., Zheng, Y., Wu, S., Yang, Z. H., & Zhao, F. (2016). Nitrogen recovery from wastewater using microbial fuel cells. *Frontiers of Environmental Science & Engineering*, *10*(1), 185-191.

[19] Wang, A., Liu, W., Ren, N., Cheng, H., & Lee, D. J. (2010). Reduced internal resistance of microbial electrolysis cell (MEC) as factors of configuration and stuffing with granular activated carbon. *International Journal of Hydrogen Energy*, *35*(24), 13488-13492.

[20] Sleutels, T. H., Hamelers, H. V., & Buisman, C. J. (2011). Effect of mass and charge transport speed and direction in porous anodes on microbial electrolysis cell performance. *Bioresource Technology*, *102*(1), 399-403.

[21] Sleutels, T. H., Lodder, R., Hamelers, H. V., & Buisman, C. J. (2009). Improved performance of porous bio-anodes in microbial electrolysis cells by enhancing mass and charge transport. *International Journal of Hydrogen Energy*, *34*(24), 9655-9661.

[22] Jeremiasse, A. W., Hamelers, H. V., & Buisman, C. J. (2010). Microbial electrolysis cell with a microbial biocathode. *Bioelectrochemistry*, *78*(1), 39-43.

[23] Rozendal, R. A., Jeremiasse, A. W., Hamelers, H. V., & Buisman, C. J. (2007). Hydrogen production with a microbial biocathode. *Environmental Science & Technology*, *42*(2), 629-634.

[24] Yang, Y., Ren, H., Ben-Tzvi, P., Yang, X., & He, Z. (2017). Optimal interval of periodic polarity reversal under automated control for maximizing hydrogen production in microbial electrolysis cells. *International Journal of Hydrogen Energy*, *42*(31), 20260-20268.

[25] Schwartz, E., & Friedrich, B. (2006). The H_2-metabolizing prokaryotes. *The Prokaryotes: Volume 2: Ecophysiology and Biochemistry*, 496-563.

[26] Guo, K., Soeriyadi, A. H., Patil, S. A., Prévoteau, A., Freguia, S., Gooding, J. J., & Rabaey, K. (2014). Surfactant treatment of carbon felt enhances anodic microbial electrocatalysis in bioelectrochemical systems. *Electrochemistry Communications*, *39*, 1-4.

[27] Guo H, Kim Y. Stacked multi-electrode design of microbial electrolysis cells for rapid and sludge-free treatment of municipal wastewater. under review.

[28] Cheng, S., Xing, D., Call, D. F., & Logan, B. E. (2009). Direct biological conversion of electrical current into methane by electromethanogenesis. *Environmental Science & Technology*, *43*(10), 3953-3958.

[29] Selembo, P. A., Merrill, M. D., & Logan, B. E. (2009). The use of stainless steel and nickel alloys as low-cost cathodes in microbial electrolysis cells. *Journal of Power Sources*, *190*(2), 271-278.

[30] Kondaveeti, S., Lee, S. H., Park, H. D., & Min, B. (2014). Bacterial communities in a bioelectrochemical denitrification system: the effects of supplemental electron acceptors. *Water Research*, *51*, 25-36.

[31] Sun, J., Bi, Z., Hou, B., Cao, Y. Q., & Hu, Y. Y. (2011). Further treatment of decolorization liquid of azo dye coupled with increased power production using microbial fuel cell equipped with an aerobic biocathode. *Water Research*, *45*(1), 283-291.

[32] He, Z., & Angenent, L. T. (2006). Application of bacterial biocathodes in microbial fuel cells. *Electroanalysis*, *18*(19-20), 2009-2015.

[33] Ahn, Y., & Logan, B. E. (2012). A multi-electrode continuous flow microbial fuel cell with separator electrode assembly design. *Applied Microbiology and Biotechnology*, *93*(5), 2241-2248.

[34] Xafenias, N., & Mapelli, V. (2014). Performance and bacterial enrichment of bioelectrochemical systems during methane and acetate production. *International Journal of Hydrogen Energy*, *39*(36), 21864-21875.

3 Stacked Multi-electrode Design of Microbial Electrolysis Cells for Rapid and Low-sludge Treatment of Municipal Wastewater

The multi-electrode stack design was demonstrated that can increase the electric current generation in MECs. However, the wastewater treatment efficiency of the newly designed MEC was not clear. Therefore, in this study, the stacked design MECs were applied to treat municipal wastewater with different operating conditions. The organic removal rate, biosolids production rate, and energy consumption were examined and used to represent the wastewater treatment efficiency.

The following published journal article is included in this chapter.

- Guo, H., & Kim, Y. (2019). Stacked multi-electrode design of microbial electrolysis cells for rapid and low-sludge treatment of municipal wastewater. *Biotechnology for biofuels*, *12*(1), 1-10.

The co-author's contributions include:

- Funding acquisition
- Supervision and technical support
- Manuscript review and revision

Abstract

Microbial electrolysis cells (MECs) can be used for energy recovery and sludge reduction in wastewater treatment. Electric current density, which represents the rate of wastewater treatment and H_2 production, is not sufficiently high for practical applications of MECs with real wastewater. Here a sandwiched electrode stack design was proposed and examined in a continuous-flow MEC system for more than 100 days to demonstrate enhanced electric current generation with a large number of electrode pairs. For primary effluent from a municipal wastewater treatment plant, the current density was boosted up to 190 A/m^3 with 10 electrode pairs stacked in a MEC. In continuous-flow operation with two stacked MECs in series, the biochemical oxygen demand (BOD) removal was 90 ± 2%, the chemical oxygen demand (COD) removal was 75 ± 9%, and the sludge production was 0.06 g-volatile suspended solids (VSS)/g-COD removal at a hydraulic retention time of only 0.63 h. The electric energy consumption was low at 0.40 kWh/kg-COD removal (0.058 kWh/m^3-wastewater treated) without Pt catalysts due to the magnified electrode surface area. The demonstrated results indicate that MECs with the stacked electrode design can be used for the rapid and sludge-free treatment of domestic wastewater.

Keywords

Microbial electrolysis cells; high electric current; stacked electrode design; primary clarifier treatment; rapid organic removal; low-sludge wastewater treatment system.

3.1 Introduction

In conventional wastewater treatment using activated sludge, organic substrates are oxidized in bioreactors by aerobic microorganisms (1). To maintain aerobic conditions in the bioreactors, oxygen is provided using aeration systems, such as fine bubble diffusers or mechanical aerators (2, 3). Aeration systems are responsible for a large amount of energy consumption in wastewater treatment. In addition to aeration, return activated sludge pumping also consumes a large amount of electric energy (2, 3). Therefore, high energy demand is one of the main challenges in municipal wastewater treatment. Another key challenge in wastewater treatment is the management and final disposal of wastewater sludge that is collected in sedimentation processes. Stabilization of wastewater sludge requires additional processes, such as thickening, anaerobic digestion, and dewatering, and thus makes wastewater treatment expensive and inefficient. In this study, we focused on demonstrating rapid wastewater treatment with minimized biosolids production as well as reduced energy consumption.

Microbial electrolysis cells (MECs) can be used for wastewater treatment and simultaneous energy production (4-7). In a MEC, organic substrates are removed at the bioanode through an oxidation reaction driven by exoelectrogenic bacteria while hydrogen gas is produced at the cathode by applying a small electric voltage (>0.13 V) (8-11). The magnitude of the electric current induced in a MEC represents the rate of the electrode reactions. Thus, the performance of MECs in terms of removing organics in wastewater and producing hydrogen gas is directly dependent on the magnitude of electric current. The current generation in acetate-fed MECs is usually high (12-14) compared to MECs with

low acetate concentration. As a result, high electric current (e.g., 40-400 A/m^3, 12-14, 21) was feasible because acetate was used as the primary substrate for exoelectrogenic microorganisms (10). However, electric current is often low if real wastewater is fed in MECs. It ranged from 7.4 to 42 A/m^3 (6, 15-19) and increased up to 60 A/m^3 with Pt catalysts on the cathode (20). The limited electric current generation, especially with municipal wastewater, indicates that breakthrough improvements are necessary to magnify electric current generation and such improvements should be scalable for pilot-scale and continuous-flow operation for practical wastewater treatment and energy recovery using MECs.

The current generation is proportional to the number of electrode pairs (21) and governed by various other factors, such as organic loading rate, acetate concentration, electrode catalysts, and solution conductivity. In MEC operation using real wastewater, low conductivity is known to be one of limiting factors for the high current generation. The design of separator electrode assembly was proven to effectively reduce the internal resistance in MEC and thus allow high electric current (22-24). However, the separator electrode assembly is not ideal for continuous-flow systems because electrode separator materials can block the flow of wastewater in the MEC reactor. In this study, we modified the separator electrode assembly design by using coarse plastic meshes instead of fine separators, such as glass fiber membrane or filter paper. In addition, a cloth-type anode was used to reduce the thickness of the sandwiched electrodes to avoid potential electric short-circuiting. Furthermore, the multi-electrode design was employed in this study to increase the volume-based electric current. In previous studies, multiple electrodes were applied to

improve the COD removal efficiency and electric current generation; however, the total number of electrode pairs was not sufficiently high with 10 anodes and 5 cathodes in a relatively large reactor (25). In this study, we applied the sandwiched stack design to increase the number of electrode pairs to 10 in a compact MEC reactor, allowing substantially high electric current densities. Although this study examined MECs with 5 and 10 electrode pairs, additional electrode pairs can be added in the modulated MEC design.

In practical wastewater treatment, MECs are expected to produce a much smaller amount of waste sludge than conventional activated sludge because of the small yield coefficient (0.02 g-VSS/g-COD) of exoelectrogenic microorganisms (26, 27). In this study, we also focused on estimating biosolids production in the newly designed MEC reactors fed with real wastewater. Other specific objectives of this study are to: demonstrate high electric current generation in MECs continuously fed with real wastewater by using sandwiched electrode stacks; investigate the effects of various reactor designs and operation factors, such as wastewater flow rate and organic loading rate on electric current density; examine the wastewater treatability in terms of the rate of organic removal and biosolids production; and compare the MEC performance with conventional activated sludge regarding energy consumption for the treatment of primary clarifier effluent. It should be emphasized that the main novelty of this study is the lab-scale demonstration of low-sludge municipal wastewater treatment using the easily scalable electrode-stack MEC.

3.2 Methods

3.2.1 Stacked MEC construction and start-up

Three MEC reactors were built using polypropylene blocks by drilling a cylindrical hole (7 cm^2 in cross-section). The structure of these reactors is same as the structure of our previous study (21). The liquid volumes of MEC-10 (10 electrode pairs), MEC-5 (5 electrode pairs), and MEC-1 (1 electrode pair) were 40, 35, and 28 mL, respectively. The anode was activated carbon cloth (ACC100, Evertech Envisafe Ecology, Taiwan) and pretreated in a surfactant solution (28). The cathode was stainless steel mesh (304 stainless steel, 200 × 200 mesh, McMaster Carr, USA) without any precious metal catalysts. Each electrode pair consisted of one carbon cloth piece and one stainless steel mesh piece, which were sandwiched and separated using two rubber gaskets and one plastic mesh. The thickness of the two gaskets (i.e., the distance between the anode and cathode) was 2.8 mm. Each electrode pair was operated independently (i.e., no electrical connections between the electrode pairs). The feed wastewater flowed in the normal direction to the sandwiched electrodes (Figure 3.1a). To ensure proper wastewater flow and biogas collection through the stacked electrode pairs, the upper and lower parts of each electrode (both the anode and cathode) were cut off by 0.3 cm from the circular edge (Appendix B, Figure B1), resulting in 5.42 cm^2 of the total surface area per electrode. A plastic tube was placed on the top of the polypropylene block for biogas collection (Figure 3.1b). The constructed MECs were inoculated using effluent from existing MECs and operated using synthetic wastewater for approximately 3 months (1 g/L sodium acetate in 20 mM PBS buffer with vitamins and

minerals, 21, 29) before the main part of the experiment was conducted with real wastewater.

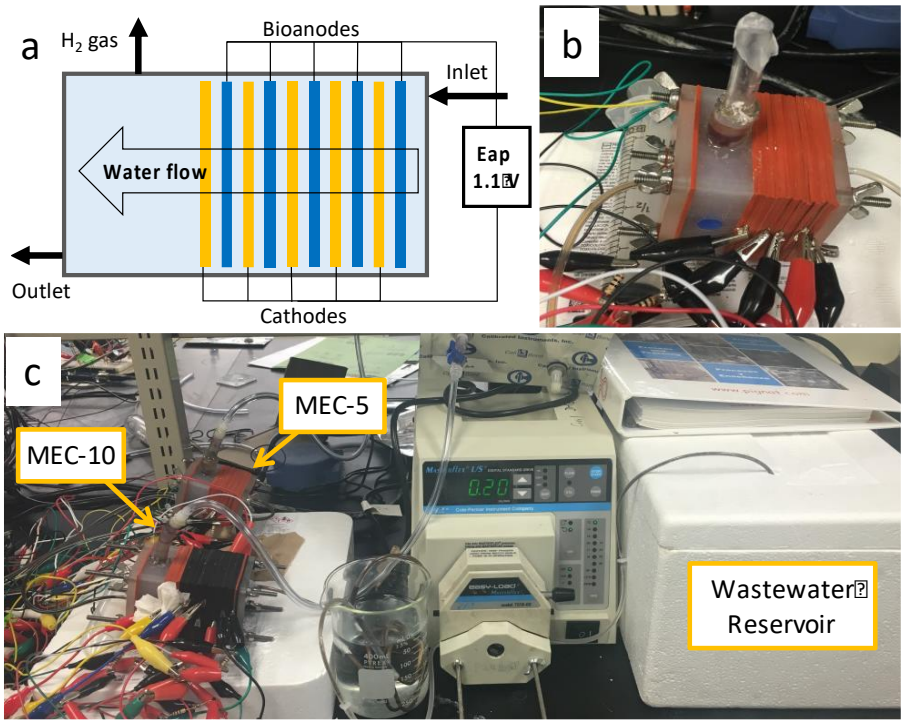

Figure 3.1. (a) Schematic of the sandwiched electrode stack; (b) MEC-5; (c) continuous-flow system with MEC-10 and MEC-5 in series.

3.2.2 MEC operation

The feed wastewater (primary clarifier effluent) was collected from a local wastewater treatment plant (Woodward Wastewater Treatment Plant, Hamilton, ON, Canada). The collected wastewater was used immediately in the experiment or stored at 4°C for no longer than 7 days. The quality parameters of the primary clarifier were measured before feeding into the systems. MEC-10 and MEC-5 were serially arranged where the wastewater flowed through MEC-10 and then MEC-5 to achieve the maximum treatability of our MEC reactors. The MEC system was operated in the continuous-flow mode with 3 different

flow rates (0.1, 0.2, and 2.0 mL/min). It was operated for 32 days at 0.1 mL/min, 36 days at 0.2 mL/min, and 32 days at 2.0 mL/min. The feed wastewater reservoir was kept in an icebox and refilled with fresh wastewater every day under the low flow rate conditions (0.1 and 0.2 mL/min) and filled twice a day at the high flow rate (2 mL/min). Between the reservoir and MEC-10, a 30-cm long copper tube was submerged in a beaker filled with water to equilibrate the influent wastewater temperature to the room temperature (22.2 ± 0.7°C) (Figure 3.1c). MEC-1 with a single electrode pair was operated in a fed-batch mode using the same primary clarifier effluent but independently from the continuous operation of MEC-10 and MEC-5.

The applied voltage (E_{ap}) to each of the electrode pairs was 1.1 V using an external power supplier (GPS-1850D; GW Instek, Taiwan). The electric current for each electrode pair was determined by measuring the electric voltage across a 10-Ω external resistor. A digital multimeter and data acquisition system was used to record the voltage every 20 min (Model 2700, Keithley Instruments, OH). The electric current for individual electrode pairs was added for all electrode pairs in the reactor and then normalized by the effective volume of the MEC reactor to obtain volume-based current density. In addition to the volume-based current density, the area-based current density was also provided using the total anode surface area of the MEC reactors (54.2 cm^2 for MEC-10 and 27.1 cm^2 for MEC-5).

3.2.3 Experimental analysis

The influent and effluent of the serial MEC system were collected every weekday and analyzed for total suspended solids (TSS), volatile suspended solids (VSS), chemical oxygen demand (COD), and biochemical oxygen demand (BOD) in accordance with the

standard method (30). The COD analysis was conducted using commercial COD test tubes (Method 8000u, Hach Company, USA).

The wastewater treatment plant applied ferric sulfate for phosphorus removal. The high concentration of ferric ions can be used as the electron acceptors and further contributes to the COD removal in MECs. Therefore, the influent and effluent samples were also analyzed to quantify ferric iron in the wastewater. The collected sample (4.5 mL) was immediately acidified with 1.5 mL 70% nitric acid (v/v) and filtered using a syringe filter (pore size 0.45 μm, polyethersulfone membrane, VWR International, USA). The filtered sample was analyzed in ICP-OES (Vista Pro, Varian Inc., Australia) to determine iron concentration.

The wastewater influent and effluent were also analyzed for pH and conductivity (SevenMulti, Mettler-Toledo International Inc., USA). In MEC-10 and MEC-5, pH of the wastewater was slightly increased from 6.7 ± 0.3 (influent) to 7.3 ± 0.2 (effluent) since the hydroxide ions were produced at the cathode with hydrogen production. The wastewater conductivity was 1.22 ± 0.15 mS/cm and did not change in the MEC experiment. No additional pre-treatment or modification was conducted to improve the wastewater treatability.

3.2.4 Coulombic efficiency and energy consumption

The Coulombic efficiency (*CE*) is the electron-based ratio between the amount of electric current generated and COD removed (31):

$$CE = \frac{8I}{QF\Delta COD} \quad \text{(Eq 3.1)}$$

I is the summation of the electric current for all electrode pairs in the MEC, *F* is the Faraday's constant (96485 C/mol), and ΔCOD is the COD change between the influent and effluent, and *Q* is the flow rate of wastewater.

The COD-based energy consumption (W_{COD}) in kWh per kg-COD removed is calculated by dividing the electric energy consumption by the rate of COD removal as:

$$W_{COD} = \frac{E_{ap} I}{Q \Delta COD} \quad \text{(Eq 3.2)}$$

The volume-based energy consumption (W_v) in kWh per m^3 of treated wastewater is calculated by dividing the total energy consumption by the flow rate during the experiment as:

$$W_v = \frac{E_{ap} I}{Q} \quad \text{(Eq 3.3)}$$

3.3 Results and Discussion

3.3.1 Rapid wastewater treatment with high current generation

The multi-electrode MEC showed substantially enhanced electric current generation as the maximum current density was 190 A/m^3 or 1.4 A/m^2 in MEC-10 (MEC of 10 electrode pairs) with continuously fed real wastewater (Figure 3.2). The maximum current density in MEC-1 (MEC of 1 electrode pair) was only ~4 A/m^3 or 0.2 A/m^2, which was much smaller than that in MEC-10. This result indicates that a large number of electrode pairs in the sandwiched design can significantly enhance the rate of wastewater treatment using MECs without any precious metal catalysts on the cathode, such as platinum. The current density in MEC-5 (MEC of 5 electrode pairs) was sensitively affected by the flow rate of wastewater and varied in a wide range up to 92 A/m^3 or 1.2 A/m^2 (Figure 3.2). Note that

the primary clarifier effluent was fed to MEC-10 and the effluent from MEC-10 was introduced to MEC-5 during the continuous MEC operation. The low current density at the low flow rates can be explained by the low organic substrate concentration in the effluent from MEC-10. For instance, the measured COD concentration in the MEC-10 effluent (i.e., influent to MEC-5) was 10.4 mg/L while it was 10.0 mg/L in the MEC-5 effluent at 0.2 mL/min. This negligible COD removal in MEC-5 indicates that the wastewater was sufficiently treated in MEC-10 and thus MEC-5 did not generate high electric current for 0.2 mL/min (and 0.1 mL/min) due to the low COD concentration. In previous MEC studies conducted with municipal wastewater, the reported electric current density ranging from 11 to 42 A/m^3 (15-17) is much lower than the current density results in this study. This comparison confirms that the stacked electrode design allowed sufficiently high current generation with primary clarifier effluent. The high current generation can be explained by the significantly high anode surface area (136 m^2/m^3 for MEC-10,77 m^2/m^3 for MEC-5), enhancing the rate of the electrode reactions in the small MEC reactors.

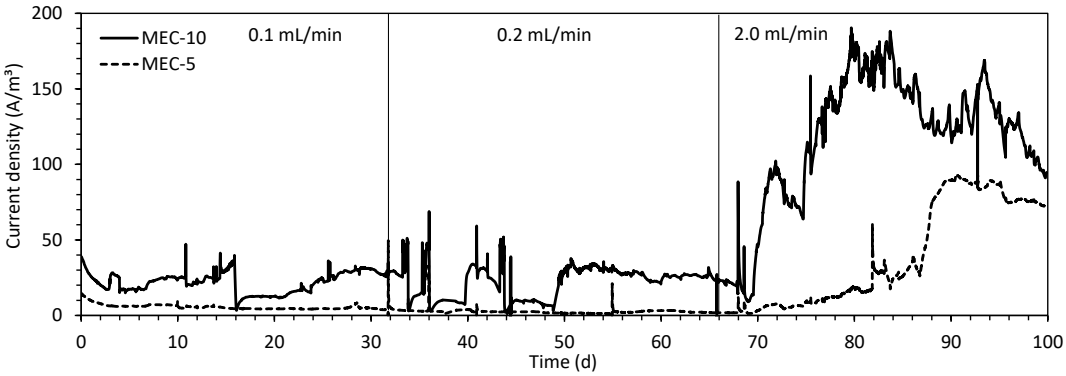

Figure 3.2. Electric current generation in the continuous-flow MEC system fed with primary clarifier effluent.

It should be emphasized that the mean hydraulic residence time (HRT) in the system was 0.63 h at 2 mL/min. Considering the typical residence time of 6-8 h in aeration tanks of conventional activated sludge systems (1, 2), the new MEC stack design can reduce the size of wastewater treatment reactors to approximately 10% of typical aeration tanks in conventional activated sludge for municipal wastewater treatment.

3.3.2 Organic loading rate and electric current

The current density was governed by the organic loading rate (OLR) rather than the COD concentration as the high OLR resulted in high electric current density (Figure 3.3a). However, the electric current density was not clearly correlated with the COD concentration (Figure 3.3b). This finding is consistent with the previous report that the magnitude of electric current is governed by the OLR rather than other operation factors, such as substrate concentration and conductivity, especially when real wastewater is used as the feed for MEC operation (32). Even with significant variations in the influent COD concentration, the OLR was governed by the flow rate because the average influent COD was below 150 mg/L (Figure 3.4). For the slow flow rates (0.1 and 0.2 mL/min), the OLR was smaller than 2 kg-COD/m^3/d (0.4 – 0.5 kg-COD/m^3/d at 0.1 mL/min and 0.7 – 1.8 kg-COD/m^3/d at 0.2 mL/min), resulting in low current densities below 40 A/m^3 (Figure 3.3a). In addition, there was no significant increase in the current densities when the flow rate increased from 0.1 to 0.2 mL/min. However, for the high flow rate of 2 mL/min, the current density increased up to 190 A/m^3 with the relatively high OLR between 8 and 16 kg-COD/m^3/d (Figure 3.3a). The OLR for the high flow rate was much greater than the typical OLR in conventional activated sludge systems (usually smaller than 2 kg-COD/m^3/d)

(2,33), indicating that the stacked MEC design can treat clarified domestic wastewater faster more efficiently than conventional activated sludge systems. The relatively short hydraulic residence time in MEC-10 (0.33 h at 2.0 mL/min) did not negatively affect the electric current generation in MEC-10. This finding indicates that exoelectrogenic bacteria can rapidly utilize organic substrates in municipal wastewater, allowing very short hydraulic retention time (i.e., 0.33 h) and thus small MEC reactors for wastewater treatment.

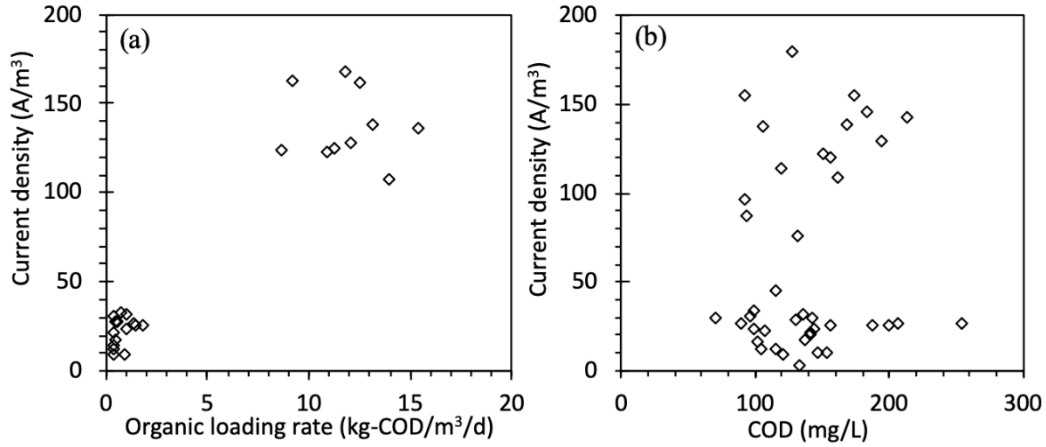

Figure 3.3. The electric current density in MEC-10 vs (a) organic loading rate; (b) COD.

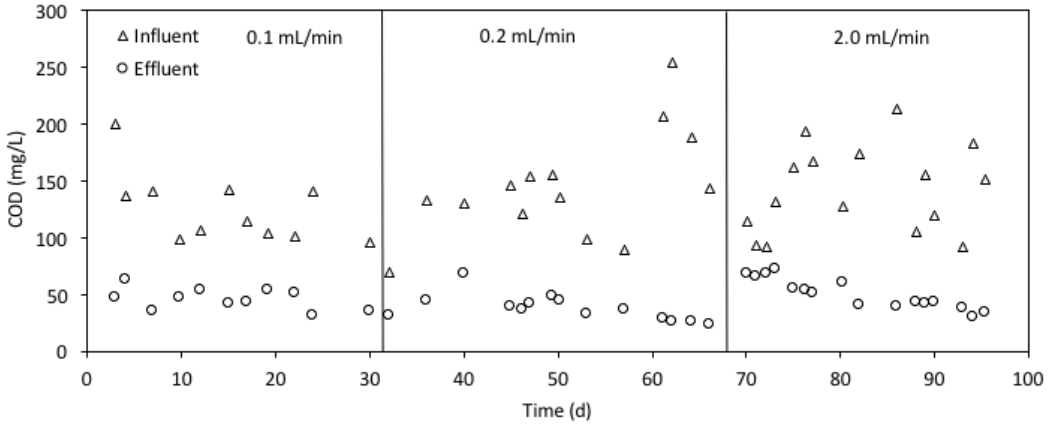

Figure 3.4. The COD concentration of the influent and effluent.

It should be noted that a gradual decrease was observed in the electric current of MEC-10 and MEC-5 between 83 and 93 days. This result can be explained by decreased OLR for the MEC operation. From 83 to 93 days, the OLR decreased from 15.4 to 6.6 kg-COD/m^3/d when the COD concentration of the influent decreased from 214 to 92 mg/L simultaneously (Figure 3.4).

3.3.3 Wastewater treatability on organic removal

The rate of organic removal was rapid since 75 ± 9% of COD was removed in MEC-10 and MEC-5 for 2 mL/min or the hydraulic residence time (HRT) of 0.63 h. The COD removal was similar or slightly lower at 64 ± 15% and 59 ± 11% for the longer HRT conditions of 12.5 h (0.1 mL/min) and 6.3 h (0.2 mL/min), respectively (Figure 3.5a). The average current density was 106.4 A/m^3 (MEC-10) and 35.0 A/m^3 (MEC-5) at 2 mL/min while it was around 23 A/m^3 (MEC-10) and 3 A/m^3 (MEC-5) at low flow rates (0.1 mL/min and 0.2 mL/min) (Figure 3.2). The electric current in MECs represents the rate of the electrode reactions, which are the organic removal at the anode and hydrogen production at the cathode. Therefore, the higher electric current density contributes to the faster organic removal. In conventional activated sludge systems, the typical HRT in the aeration tank is 6 to 8 h with approximate 80% COD removal (2). Considering the rapid COD removal of the examined MEC system (75% COD removal in 0.63 h), the stacked MEC design can be used for effective treatment of municipal wastewater. The BOD removal was high at 90 ± 2% with the effluent BOD of 19.4 ± 4.1 mg/L at 2 mL/min. Note that, for real wastewater without its chemical composition, the BOD-based removal efficiency provides more reliable organic removal treatability for biological wastewater treatment (1).

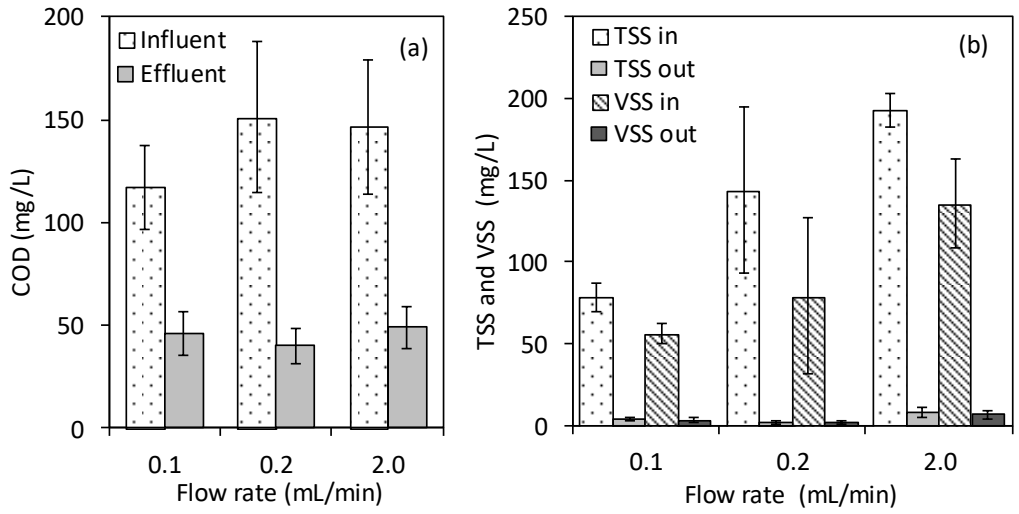

Figure 3.5. Wastewater treatability of the MEC system: (a) COD removal; (b) TSS and VSS removal.

3.3.4 Wastewater treatability on biosolids reduction

TSS (total suspended solids) and VSS (volatile suspended solids) were reduced substantially in the continuous-flow MEC system. Nearly complete reduction of biosolids (>94%) for both VSS and TSS was observed regardless of the flow rate conditions (Figure 3.5b). This observed biosolids removal was much higher than 60% of TSS removal reported in single-chamber MEC reactors (250 mL) that were fed with domestic wastewater and the MECs were built with only 1 electrode pair (27). This comparison indicates that the stacked electrode design is beneficial to minimizing sludge generation. The apparent yield coefficient measured in this study ranged from 0.01 to 0.06 g-VSS/g-COD, which is an order of magnitude smaller than the yield coefficient of the other anaerobic microorganisms (typical 0.1 to 0.6 g-VSS/g-COD) (1, 34, 35). In this study, the concentration of biosolids in the effluent was 3.67 ± 1.25 mg-TSS/L or 2.02 ± 1.21 mg-

VSS/L at 0.1 mL/min, 2.02 ± 1.21 mg-TSS/L or 1.60 ± 0.90 mg-VSS/L at 0.2 mL/min, and 10.36 ± 8.06 mg-TSS/L or 6.4 ± 2.76 mg-VSS/L at 2 mL/min (Figure 3.5b). These consistently low VSS and TSS concentrations imply that the MEC effluent can be discharged even without secondary clarification. In addition, the enhanced reduction of biosolids clearly indicates that MECs can dramatically reduce the sludge production in wastewater treatment as well as the cost for sludge treatment and disposal.

3.3.5 Coulombic efficiency and energy consumption

Coulombic efficiency (CE) varied in a wide range (Figure 3.6). The wide variation of CE can be explained by the use of real wastewater where its composition, especially the readily biodegradable portion of COD, changes continuously. A certain degree of variations in CE has been commonly found in previous studies where the primary clarifier effluent from wastewater treatment plants was fed in bioelectrochemical systems (15, 16, 36). The CE was 66 ± 27% at 0.1 mL/min while it dropped to 22 ± 14% at 0.2 mL/min and 20 ± 11% at 2 mL/min (Figure 3.6).

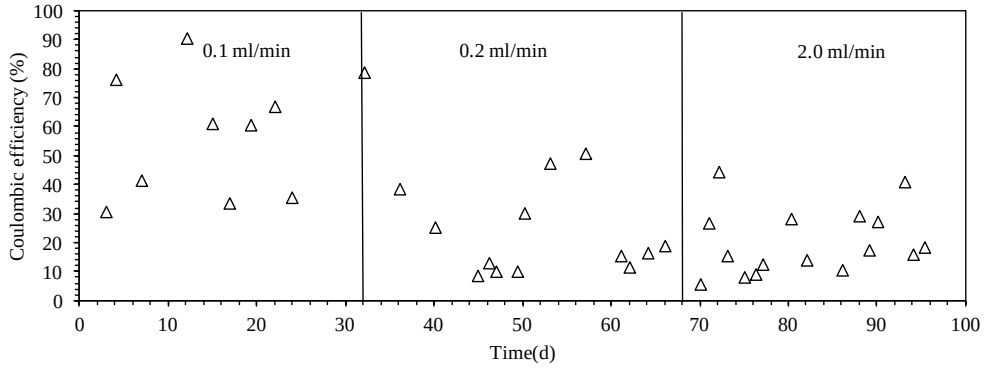

Figure 3.6. Coulombic efficiency during the continuous-flow MEC system operation.

A significant decrease was shown in CE when the flow rate increased from 0.1 mL/min to 0.2 mL/min. The significant decrease was due to the increase in ΔCOD (Figure 3.5a)

and the similar electric current generation at 0.2 mL/min. The CE value was much lower than the CE of our previous study (>72%) where the reactor was fed with synthetic wastewater (21). The low CE results indicate other biological reactions in the MEC reactors can affect CE. When the MEC reactors were disassembled, thick biofilms were found both on the anode and cathode (Appendix B, Figure B1), indicating that there was a substantial amount of microorganisms in the system. The observed biomass on the electrodes did not affect the sludge production during the MEC operation because the sludge production was consistently low over the course of 3-month operation. The presence of other terminal electron acceptors such as ferric iron and sulfate can contribute to the COD removal without electric current generation in MECs (16). In the ICP-OES (inductive coupled plasma-optical emission spectrometry) analysis, the dissolved iron was detected in the feed wastewater because the local wastewater treatment plant applied ferric sulfate in the preliminary treatment for phosphorus removal. Note that many of the known exoelectrogenic bacteria (*Geobacter* and *Shewanella* spp.) can utilize iron as the terminal electron acceptor (37, 38). In addition, other iron-reducing bacteria are commonly found in domestic sewer systems (38). However, the concentration of iron in the influent and effluent decreased from 1.45 mg/L to 0.19 mg/L, which only results in the 0.54 mg/L COD removal. Thus, the effects of iron ions were negligible. Sulfate can also contribute to additional COD removal without electric current generation by sulfate reducing bacteria (39). Sulfate concentration in the wastewater was consistently high at 82-122 mg/L (40), which can potentially oxidize up to 81 mg/L of COD assuming H_2S production. In addition, the methane production in MEC can also result in the low CE.

The electric energy consumption was as low as 0.40 kWh per kg-COD removed or 0.058 kWh per m^3 wastewater treated (Appendix B, Figure B2). The low energy consumption for the MEC operation can be explained by the stacked electrode design with the reduced inter-electrode distance (2.8 mm) and significantly magnified electrode surface area with a total of 15 electrode pairs sandwiched in the small reactors. The short inter-electrode distance contributed to the low inter resistance (229.5 Ω cm^2 based on 1.22 mS/cm and 2.8 mm) and thus resulted in the low voltage drop between the electrodes (3 to 18 mV). Compared to the energy consumption of conventional activated sludge systems which typically ranged from 0.7 to 2 kWh per kg-COD removed (2), the energy consumption for MEC operation was much lower. In conclusion, the stacked multi-electrode MECs can replace the activated sludge system because of the great treatability of primary clarifier effluent and low energy consumption.

Note that the energy recovered as H_2 gas production was not included in the energy requirement calculation because biogas production, including H_2 gas, was very small. The small biogas production can be explained by the short hydraulic residence time in the MEC reactor (37.5 min at 2 mL/min). For the short residence time, tiny H_2 gas bubbles from the cathode were flowing with the wastewater rather than separated by gravity in the MEC reactors. Also, H_2 gas is rapidly converted into CH_4 in MECs without proper inhibition of hydrogenotrophic methanogens. According to the Henry's law constant (769 atm/M) (41), the examined highest flow rate can carry more methane (606 mg CH_4/d) than the maximum amount of methane that can be produced in the MEC (155 mg CH_4/d; 100% conversion of H_2 into CH_4; 100% H_2 production from electric current).

3.3.6 Individual electrode performance

During the continuous flow operation, the wastewater flowed through 10 independent electrode pairs serially in MEC-10 and then 5 electrode pairs in MEC-5. The electric current generation was similar among the multiple electrode pairs (Table 3.1), and this result was not consistent with our recent study with synthetic wastewater that is considered to have resulted in a significant variation in the electric current generation among the electrode pairs (21). The different performances of the reactor with real wastewater and synthetic wastewater were due to the low readily biodegradable organics concentration of real wastewater. The slow conversion of biodegradable organics to readily biodegradable organics in the reactor contributes to the stable electric current results.

Table 3.1. Average electric current (mA) for each electrode pair in MEC-10

Electrode pair	0.1 mL/min	0.2 mL/min	2.0 mL/min
#1	0.11 ± 0.09	0.08 ± 0.03	0.15 ± 0.08
#2	0.14 ± 0.05	0.09 ± 0.05	0.53 ± 0.19
#3	0.12 ± 0.05	0.10 ± 0.06	0.50 ± 0.15
#4	0.08 ± 0.03	0.10 ± 0.04	0.54 ± 0.17
#5	0.08 ± 0.03	0.09 ± 0.04	0.54 ± 0.18
#6	0.08 ± 0.03	0.09 ± 0.05	0.55 ± 0.20
#7	0.08 ± 0.03	0.11 ± 0.04	0.56 ± 0.20
#8	0.08 ± 0.03	0.09 ± 0.04	0.47 ± 0.17
#9	0.07 ± 0.02	0.09 ± 0.04	0.49 ± 0.18
#10	0.07 ± 0.03	0.08 ± 0.04	0.53 ± 0.22

In addition, the consistent electric current results indicate the operation of the MEC stack was reliable even though a single reactor was operated. The location of individual electrode pairs did not affect the current generation except for the first pair from the inlet (electrode

pair #1). For instance, there was no significant variation in the electric current for electrode pairs #2 through #10 in MEC-10 (Table 3.1). However, electrode pair #1 generated noticeably lower electric current compared to the other electrode pairs only at the high flow rate of 2 mL/min (Table 3.1).

3.4 Conclusions and outlook

The stacked-electrode design demonstrates excellent wastewater treatability with minimal biosolids production and consistently low COD in the MEC effluent. Even though the demonstration was achieved in lab-scale experiments, the MEC design is readily applicable in practical applications as the experiment was conducted with primary clarifier effluent from a local wastewater treatment plant. The demonstrated MEC design does not need further scale-up for practical applications. Many MEC reactors with 10-20 electrode pairs can be used to receive the primary clarifier effluent in parallel just like a modulated membrane filtration system where individual membrane modules receive feed water in parallel and operate independently one another. Without further scale-up of the MEC design, the stacked electrode MECs can be used to treat municipal wastewater with stable effluent quality and minimal biosolids generation.

References

1. Grady CPL, Daigger GT, Love NG, Filipe CDM. Biological Wastewater Treatment, third ed. Boca Raton: CRC press; 2011.

2. Burton F, Tchobanoglous G, Tsuchihashi R, Stensel HD, Metcalf & Eddy Inc. Wastewater engineering treatment and resource recovery. 5th ed. New York: McGraw-Hill Education; 2013.

3. Rittmann, BE, McCarty PL. Environmental biotechnology: principles and applications. New York: McGraw-Hill Education; 2013.

4. Call D; Logan BE. Hydrogen production in a single chamber microbial electrolysis cell lacking a membrane. Environ Sci Technol. 2008; 42(9): 3401-3406.

5. Wagner RC, Regan JM, Oh SE, Zuo Y, Logan BE. Hydrogen and methane production from swine wastewater using microbial electrolysis cells. Water Res. 2009; 43(5): 1480-1488.

6. Cusick RD, Bryan B, Parker DS, Merrill MD, Mehanna M, Kiely PD, Liu G, Logan BE. Performance of a pilot-scale continuous flow microbial electrolysis cell fed winery wastewater. App Microbiol Biotechnol. 2011; 89(6): 2053-2063.

7. Heidrich ES, Dolfing J, Scott K, Edwards SR, Jones C, Curtis TP. Production of hydrogen from domestic wastewater in a pilot-scale microbial electrolysis cell. APP Microbiol Biotechnol. 2013; 97(15): 6979-6989.

8. Liu H, Grot S, Logan BE. Electrochemically assisted microbial production of hydrogen from acetate. Environ Sci Technol. 2005; 39(11): 4317-4320.

9. Rozendal RA, Hamelers HV, Euverink GJ, Metz SJ, Buisman CJ. Principle and perspectives of hydrogen production through biocatalyzed electrolysis. Int J Hydrog Energy. 2006; 31(12): 1632-1640.

10.Cheng S, Logan BE, Sustainable and efficient biohydrogen production via electrohydrogenesis. Proc Natl Acad Sci. 2007; 104(47):18871-18873.

11. Schröder U. From Wastewater to Hydrogen: Biorefineries Based on Microbial Fuel-Cell Technology. *ChemSusChem.* 2008; (4): 281-282.

12. Rozendal RA, Hamelers HV, Molenkamp RJ, Buisman CJ. Performance of single chamber biocatalyzed electrolysis with different types of ion exchange membranes. Water Res. 2007; 41(9): 1984-1994.

13. Hu H, Fan Y, Liu H. Hydrogen production using single-chamber membrane-free microbial electrolysis cells. Water res. 2008; 42(15): 4172-4178.

14. Hussain A, Manuel M, Tartakovsky B. A comparison of simultaneous organic carbon and nitrogen removal in microbial fuel cells and microbial electrolysis cells. J environ manag. 2016; 173:23-33.

15. Cusick RD, Kiely PD, Logan BE. A monetary comparison of energy recovered from microbial fuel cells and microbial electrolysis cells fed winery or domestic wastewaters. Int J Hydrog Energy. 2010; 35(17): 8855-8861.

16. Escapa A, Gil-Carrera L, García V, Morán A. Performance of a continuous flow microbial electrolysis cell (MEC) fed with domestic wastewater. Bioresour technol. 2012; 117: 55-62.

17. Escapa A, San-Martín MI, Mateos R, Morán A. Scaling-up of membraneless microbial electrolysis cells (MECs) for domestic wastewater treatment: Bottlenecks and limitations. Bioresour technol. 2015; 180: 72-78.

18. Hussain A, Lebrun FM, Tartakovsky B. Removal of organic carbon and nitrogen in a membraneless flow-through microbial electrolysis cell. Enzym Microb Technol. 2017; 102: 41-48.

19. Zhang F, He Z. Scaling up microbial desalination cell system with a post-aerobic process for simultaneous wastewater treatment and seawater desalination. Desalination. 2015; 360: 28-34.

20. Tenca A, Cusick RD, Schievano A, Oberti R, Logan BE. Evaluation of low cost cathode materials for treatment of industrial and food processing wastewater using microbial electrolysis cells. Int J Hydrog Energy. 2013; 38(4): 1859-1865.

21. Guo H, Kim Y. Scalable multi-electrode microbial electrolysis cells for high electric current and rapid organic removal. J Power Sources. 2018; 391: 67-72.

22. Jwa E, Yun YM, Kim H, Jeong N, Park SC, Nam JY. Domestic wastewater treatment in a tubular microbial electrolysis cell with a membrane electrode assembly. Int J Hydrog Energy. 2019; 44(2): 652-660.

23. Cotterill S E, Dolfing J, Jones C, Curtis T P, Heidrich ES. Low Temperature Domestic Wastewater Treatment in a Microbial Electrolysis Cell with 1 m^2 Anodes: Towards System Scale-Up. Fuel cells. 2017; 17(5): 584-592.

24. Hu H, Fan Y, Liu H. Hydrogen production in single-chamber tubular microbial electrolysis cells using non-precious-metal catalysts. Int J Hydrog Energy. 2009; 34(20): 8535-8542.

25. Ahn Y, Logan BE. A multi-electrode continuous flow microbial fuel cell with separator electrode assembly design. Appl microbiol biotechnol. 2012; 93(5): 2241-2248.

26.Wilson EL, Kim Y. The yield and decay coefficients of exoelectrogenic bacteria in bioelectrochemical systems. Water res. 2016; 94: 233-239.

27. Brown RK, Harnisch F, Dockhorn T, Schröder U. Examining sludge production in bioelectrochemical systems treating domestic wastewater. Bioresour technol. 2015; 198: 913-917.

28. Guo K, Soeriyadi A.H, Patil S.A, Prévoteau A, Freguia S, Gooding JJ, Rabaey K. Surfactant treatment of carbon felt enhances anodic microbial electrocatalysis in bioelectrochemical systems. Electrochem Commun. 2014; 39: 1-4.

29. Cheng S, Xing D, Call DF, Logan BE. Direct biological conversion of electrical current into methane by electromethanogenesis. Environ Sci Technol. 2009; 43(10): 3953-3958.

30. APHA (American Public Health Association). Standard methods for the examination of water and wastewater. Washington, DC, USA, 2005.

31. Logan BE, Call D, Cheng S, Hamelers HV, Sleutels TH. Jeremiasse, A.W.; Rozendal, R.A. Microbial electrolysis cells for high yield hydrogen gas production from organic matter. Environ Sci Technol. 2008; 42(23): 8630-8640.

32. Asztalos JR, Kim Y. Enhanced digestion of waste activated sludge using microbial electrolysis cells at ambient temperature. Water res. 2015; 87: 503-512.

33. Beun JJ, Hendriks A, Van Loosdrecht, M CM, Morgenroth E, Wilderer PA, Heijnen JJ. Aerobic granulation in a sequencing batch reactor. Water res. 1999; 33(10): 2283-2290.

34. Henze M, Gujer W, Mino T, Van Loosdrecht MCM. Activated sludge models ASM1, ASM2, ASM2d and ASM3. London: IWA publishing. 2000.

35. Batstone DJ, Keller J, Angelidaki I, Kalyuzhnyi SV, Pavlostathis SG, Rozzi A, Sanders, WTM, Siegrist H, Vavilin VA. The IWA anaerobic digestion model no 1 (ADM1). Water Sci and Technol. 2002; 45(10): 65-73.

36. Heilmann J, Logan BE. Production of electricity from proteins using a microbial fuel cell. Water Environt Res. 2006; 78(5): 531-537.

37. Johnson DB, McGinness S. Ferric iron reduction by acidophilic heterotrophic bacteria. App environ microbiol. 1991; 57(1): 207-211.

38. Nielsen JL, Juretschko S, Wagner M, Nielsen PH. Abundance and phylogenetic affiliation of iron reducers in activated sludge as assessed by fluorescence in situ hybridization and microautoradiography. App environ microbiol. 2002; 68(9): 4629-4636.

39. Ditzig J, Liu H, Logan BE. Production of hydrogen from domestic wastewater using a bioelectrochemically assisted microbial reactor (BEAMR). Int J Hydrog Energy. 2007; 32(13): 2296-2304.

40. Routledge I. City of Hamilton wastewater treatment facilities-2011 annual report, City of Hamilton, Hamilton, 2011.

41. Benjamin MM, Lawler DF. Water quality engineering: Physical/chemical treatment processes. New York: John Wiley & Sons, 2013.

4 Mechanisms of Heavy Metal Separation in Bioelectrochemical Systems and Relative Significance of Precipitation

Bioelectrochemical systems (BES) have emerged as a novel technology for wastewater treatment and energy production. Recently, BES has attracted more attention in heavy metal separation from industrial wastewater since heavy metal ions can be reduced to metallic metals on the cathode in BES. Many papers were published in the last 10 years. Therefore, a comprehensive review including the fundamentals and mechanisms of heavy metal separation in BES is meaningful for BES development. Although some researchers summarized the heavy metal separation efficiency in their review papers, the mechanisms of heavy metal separation especially the precipitation of heavy metal in BES were not completely investigated. Thus, we review the mechanism of heavy metal separation with an emphasis on the precipitation of heavy metals in BES.

The following published book chapter is included in this chapter.

- Guo, H., & Kim, Y. (2020). Mechanisms of Heavy Metal Separation in Bioelectrochemical Systems and Relative Significance of Precipitation. *Microbial Electrochemical Technologies*, 128.

The co-author's contributions include:

- Funding acquisition
- Supervision and technical support
- Manuscript review and revision

Abstract

Heavy metal pollution is a severe environmental issue. Most heavy metals are toxic and can threaten human health. Conventional methods such as precipitation and adsorption have been used to separate heavy metals from aqueous solutions. Due to high energy and chemical costs of conventional methods, there is a need for new cost-effective and sustainable technologies to separate heavy metals. Bioelectrochemical systems (BES) have been reported as an efficient method. To provide a clear understanding of heavy metal separation in BES, this review summarized previous research work on BES applications for separating heavy metals and discussed various removal mechanisms including electrochemical reduction, precipitation, and adsorption. The separation of various heavy metals, such as cobalt, cadmium, copper, mercury, gold, silver, vanadium, chromium, nickel, zinc, and selenium, was also discussed. Comparing with previous reviews which focused on the mechanism of the electrochemical reduction of heavy metal separation in BES, we emphasize important roles of precipitation in metal separation.

Keywords

Reduction potential; removal efficiency; solubility products; microbial electrolysis cells; microbial fuel cells.

4.1 Introduction

Heavy metals are the elements having high atomic weights or high densities (Fergusson and Erric 1990). Some heavy metals such as copper, iron, mercury, and zinc are important trace elements in natural waters (Manahan 2017). These heavy metals are essential nutrients for plants and animals at low levels but toxic at high concentrations. The toxicity of heavy metals to microorganisms and plants was reported by Giller et al. (1998) and Nagajyoti et al. (2010). Some heavy metals are of particular concern because of their toxicities to humans. For instance, cadmium can affect several enzymes and cause kidney damage and bone disease (Manahan 2017). Exposure to uranium can increase the risk of cancer (Achparaki et al. 2012). Lead adversely affects the central and peripheral nervous systems (Hu 20002; Tchounwou et al. 2012). The industrial wastewater from metal plating facilities, mining operations, and pesticide producing are the main sources of heavy metal pollution (Srivastava and Majumder 2008; Fu and Wang 2011). Because heavy metals are non-biodegradable (Kurniawan et al. 2006) and can be accumulated in soils and living organisms, effective treatments of the waste sources should be conducted. Many methods, which include chemical precipitation, coagulation-flocculation, flotation, membrane filtration, ion exchange, electrodialysis, and adsorption, have been developed to separate heavy metal ions from aqueous solutions (Fu and Wang 2011; Kurniawan et al. 2006; He and Chen 2014). However, the conventional methods require high energy consumption and chemical costs. Therefore, an innovative method that can separate heavy metals effectively and sustainably is in need.

Bioelectrochemical systems (BES) have emerged as a novel technology for wastewater treatment and energy production (Rabaey et al. 2010; Wang et al. 2015; ElMekawy et al. 2015). In the literature, BES is used to present both Microbial fuel cells (MFCs) and microbial electrolysis cells (MECs) (Nancharaiah et al. 2015). MFCs can oxidize the substrates with current generation (Liu et al. 2005; He et al. 2005; Logan et al. 2006) while MECs can produce hydrogen gas with a small applied voltage (Call and Logan 2008; Logan et al. 2008). During the process, the electrons produced from the substrates are transferred to the anode and flow to the cathode. The oxidized heavy metal ions can gain the electrons from the cathode and be reduced to metallic metals. This reduction process makes the separation of heavy metals achievable in BES. Many studies reported the utility of BES for separating heavy metals. Therefore, in this review, we gave a summary of previous studies that focus on the heavy metal separation in BES.

Nancharaiah et al. (2015), Wang and Ren (2014), and Dominguez-Benetton et al. (2018) reviewed the removal and recovery of metals in BES. In the study of Wang and Ren (2014), the BES were classified into four categories based on the cathode type (abiotic cathode or biocathode) and reactor type (MEC or MFC). The category of the reactor with bipolar membranes was added in the study conducted by Nancharaiah et al. (2015). Dominguez-Benetton et al. (2018) reported a division of BES into four categories based on the mechanisms for metal transformation and recovery. In these three reviews, the performance of previous reactors was summarized and the reduction of heavy metal ions was discussed. However, the precipitation of heavy metal ions, which is possible in BES, was not included in their study. Some precipitates such as cadmium hydroxide, cadmium carbonate, and

cobalt hydroxide were detected in previous studies (Colantonio and Kim 2016, Huang et al. 2015). Thus, in this study, we reviewed the mechanism of heavy metal separation with an emphasis on the precipitation of metals in BES. In summary, the objectives of this review are to: summarize the previous studies related to the heavy metal separation in BES; report the fundamentals for separating heavy metals in BES; discuss the mechanisms that include reduction, precipitation, and adsorption of heavy metal separation in BES.

4.2 Fundamentals of heavy metal separation using microbial electrochemistry

4.2.1 Reduction potential

In most of microbial electrochemistry systems, organic substrates are oxidized at the anode to provide the electrons. The electrons flowed from the anode to the cathode where most of the reduction of heavy metals occurs. The reduction potential represents the possibility of a chemical species gaining electrons. The typical cathode potential in MFCs is from 0.1 to 0. 3V vs. SHE (Logan et al. 2006). For the metal ions whose reduction potential is higher than the typical cathode potential, they can be reduced in MFCs and the reduction is spontaneous. For instance, the reduction of Co^{3+} to Co^{2+} (1.82 V vs. SHE), Au^{3+} to Au^{0} (1.00 V vs. SHE), and Cr^{6+} to Cr^{3+} (1.33 V vs. SHE) have been reported in MFCs (Huang et al. 2013; Choi and Hu 2013; Gangadharan and Nambi 2015). The cathode potential in MECs depends on the applied voltage and varies from -0.25 to -1.5 V (Logan et al. 2016; Huang et al. 2014; Colantonio and Kim 2016). The broad range of the cathode potentials makes the heavy metals such as Cd^{2+}, Co^{2+}, and Ni^{2+} whose reduction potential

is lower than -0.4 V (Table 4.1) reduced in MECs (Wang et al. 2016; Jiang et al. 2014; Qin et al. 2012;).

Table 4.1. Standard reduction potential of redox couples and theoretical reduction potential of redox couples when [M_{ox}] =1 mM or 10 μM[a]

Redox couples	Standard (V vs. SHE)	1 mM (V vs. SHE)	10 μM (V vs. SHE)
Co^{3+}/Co^{2+}	1.82	1.88[b]	1.88[b]
Cr^{6+}/Cr^{3+}	1.33	0.39[b]	0.41[b]
Au^{3+}/Au^{0}	1.00	0.94	0.90
V^{6+}/V^{4+}	0.991	0.55[b]	0.55[b]
Hg^{2+}/Hg^{0}	0.855	0.77	0.71
Ag^{+}/Ag^{0}	0.799	0.62	0.51
Fe^{3+}/Fe^{2+}	0.77	0.74[b]	0.74[b]
Se^{4+}/Se^{0}	0.74	0.29	0.26
Cu^{2+}/Cu^{0}	0.34	0.25	0.19
U^{6+}/U^{4+}	0.327	-0.53[b]	-0.53[b]
Ni^{2+}/Ni^{0}	-0.257	-0.34	-0.40
Co^{2+}/Co^{0}	-0.28	-0.37	-0.43
Cd^{2+}/Cd^{0}	-0.4	-0.49	-0.55
Zn^{2+}/Zn^{0}	-0.76	-0.85	-0.91

a: [M_{ox}]: the concentration of oxidized heavy metals; pH=7; at 20°C
b: $M_{ox} = 0.1M_{red}$ (the concentration of reduced heavy metals)

The redox potential, which is affected by different conditions such as pH and temperature, can be calculated using the Nernst equation (Eq 4.1, Sawyer et al. 1994).

$$E = E^{0} - \frac{RT}{nF} \ln Q \qquad \text{Eq 4.1}$$

In equation 4.1, E is the half-cell redox potential at the operating conditions; E^{0} is the standard half-cell redox potential; R is the gas constant (8.314 J/K/mol); T is the temperature (K); n is the number of electrons transferred in the half-cell reaction; F is the

Faraday constant (9.6485 $\times$ 10^4 C/mol); Q is the reaction quotient. Table 4.1 shows the theoretical reduction potential of heavy metals with different concentrations at pH 7.

4.2.2 Precipitation

The oxygen reduction in MFCs (Eq 4.2) and the hydrogen production (Eq 4.3) in MECs can result in the high pH near the cathode (Van Phuong et al. 2011, Van Phuong et al. 2012; Cusick and Logan 2012). Some heavy metal ions can easily form the precipitation with hydroxide (OH^-) at high pH. The equilibrium concentration of the heavy metal ions ($[M_{eq}]$) can be calculated based on the solubility product (K_{sp}). Table 4.2 shows the summary of the pK_{sp} value of hydroxide precipitation and $[M_{eq}]$ at pH 7 and 12.

Table 4.2. Equilibrium concentration (M) of heavy metal ions $[M_{eq}]$ at pH 7 and pH 12 with hydroxide

Reactions	pK_{sp}[a]	$[M_{eq}]$ at pH = 7	$[M_{eq}]$ at pH = 12
$Co^{2+} + 2OH^- \rightarrow Co(OH)_2\,(s)$	15.7	$10^{-1.7}$	$10^{-11.7}$
$Ni^{2+} + 2OH^- \rightarrow Ni(OH)_2\,(s)$	17.2	$10^{-3.2}$	$10^{-13.2}$
$Cu^{2+} + 2OH^- \rightarrow Cu(OH)_2\,(s)$	20.4	$10^{-6.4}$	$10^{-16.4}$
$Zn^{2+} + 2OH^- \rightarrow Zn(OH)_2\,(s)$	16.8	$10^{-2.8}$	$10^{-12.8}$
$Hg^{2+} + 2OH^- \rightarrow Hg(OH)_2\,(s)$	25.4	$10^{-11.4}$	$10^{-21.4}$
$Cd^{2+} + 2OH^- \rightarrow Cd(OH)_2\,(s)$	14.3	$10^{-0.3}$	$10^{-10.3}$
$Ag^{+} + OH^- \rightarrow AgOH\,(s)$	7.7	$10^{-0.7}$	$10^{-5.7}$
$Cr^{3+} + 3OH^- \rightarrow Cr(OH)_3\,(s)$	30.0	10^{-9}	$10^{-24.0}$

a: Werener and Morgan (2012)

From Table 4.2, it can be seen that the formation of some heavy metal hydroxide precipitation requires a high pH condition. For example, $10^{-0.3}$ M (or 56 mg/L) Cd^{2+}can dissolve in the solution at pH 7 while only $10^{-11.7}$ M (or 1.12×10^{-10} mg/L) can dissolve at

pH 12. For some other heavy metals such as Cu^{2+}, Hg^{2+}, and Cr^{3+}, the dissolved concentration is low even at natural pH.

$$O_2 + 4H^+ + 2e^- \rightarrow 2H_2O \qquad \text{Eq 4.2}$$

$$2H^+ + 2e^- \rightarrow H_2 \qquad \text{Eq 4.3}$$

Carbonate precipitation is also possible in BES. The oxidation of organics at the anode can produce bicarbonate (HCO_3^-) (Eq 4.4). The HCO_3^- can convert to CO_3^{2-} with OH^- in the cathode chamber (Eq 4.5). The concentration of HCO_3^- and CO_3^{2-} depend on the pH. When the concentration of total carbonate ($C_{T, CO32-}$) equal to 10 mM, the concentration of CO_3^{2-} is $10^{-5.4}$ M (pH 7) and 10^{-2} M (pH 12). With these CO_3^{2-}, some heavy metals are easy to form carbonate precipitation. Table 4.3 shows the summary of pK_{sp} of carbonate precipitation and $[M_{eq}]$ at different pH.

Table 4.3. Equilibrium concentration (M) of heavy metal ions at pH 7 and pH 12 with $C_{T, CO_3^{2-}} = 10$ mM

Reactions	pK_{sp}[a]	pH = 7 ($[CO_3^{2-}] = 10^{-5.4}$ M)	pH = 12 ($[CO_3^{2-}] = 10^{-2}$ M)
$Co^{2+} + CO_3^{2-} \rightarrow CoCO_3\,(s)$	10.0	$10^{-4.6}$	10^{-8}
$Ni^{2+} + CO_3^{2-} \rightarrow NiCO_3\,(s)$	6.9	$10^{-1.5}$	$10^{-4.9}$
$Cu^{2+} + CO_3^{2-} \rightarrow CuCO_3\,(s)$	9.6	$10^{-4.2}$	$10^{-7.6}$
$Zn^{2+} + CO_3^{2-} \rightarrow ZnCO_3\,(s)$	10	$10^{-4.6}$	$10^{-8.0}$
$Hg^{2+} + CO_3^{2-} \rightarrow HgCO_3\,(s)$	16.1	$10^{-10.7}$	$10^{-14.1}$
$Cd^{2+} + CO_3^{2-} \rightarrow CdCO_3\,(s)$	13.7	$10^{-8.3}$	$10^{-11.7}$
$2Ag^{+} + CO_3^{2-} \rightarrow Ag_2CO_3\,(s)$	11.1	$10^{-2.85}$	$10^{-4.55}$

a: Werener and Morgan (2012)

From the Table 4.3, it can be seen that some heavy metal ions such as Ni^{2+} and Ag^+ require a higher pH or higher $C_{T, CO32-}$ to form the carbonate precipitation. Some heavy metal ions

such as Cd^{2+} and Hg^{2+} can easily form the precipitation even with the low concentration at neutral pH.

$$\text{Organics} \rightarrow HCO_3^- + e^- \quad \text{Eq 4.4}$$

$$HCO_3^- + OH^- \rightarrow CO_3^{2-} + H_2O \quad \text{Eq 4.5}$$

4.3 Mechanisms of heavy metal separation in BES

4.3.1 Overview

Reduction, precipitation, and adsorption have been reported as the three mechanisms for heavy metal separation in BES (Table 4.4). The heavy metal ions can be reduced at the cathode (Figure 4.1A). They can also be reduced at the anode by the microorganisms (Figure 4.1B). Figure 4.1C shows the formation of hydroxide precipitation of heavy metals. In addition, the heavy metal ions can also combine with the carbonate to form the carbonate precipitation (Figure 4.1D). The adsorption by the electrode or biosorption by the microorganisms contributes to the heavy metal separation in BES as well.

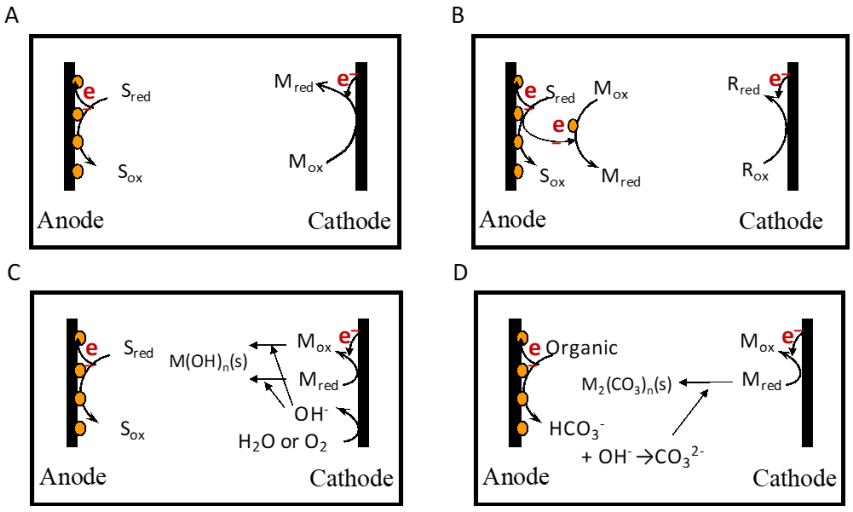

Figure 4.1. Mechanisms of heavy metal separation in BES. A. reduction at the cathode; B. reduction at the anode; C. precipitation with OH^-; D. precipitation with CO_3^{2-}.

Table 4.4. The summary of heavy metal separation in BES

Heavy metals	Concentration (mM)	Reactor mode	Removal efficiency	Mechanisms	Reference
Cadmium Cd^{2+}	0.1	MEC	71-91% in 48 h	Cathodic reduction, Precipitation,	Colantonio and Kim (2016)
	0.45-1.8	MFC	89-93% in 60 h	Cathodic reduction	Choi et al. (2014)
	0.45	MEC	39-47% in 4 h	Cathodic reduction, Adsorption	Wang et al. (2016)
	10^{-4}-10^{-1} μM 0.02 mM	MEC	69% in 168 h	Cathodic reduction, biosorption	Colantonio et al. (2016)
Cobalt (Co^{2+} or Co^{3+})	Co^{2+} 0.847	MEC	92% in 6 h	Cathodic reduction, Adsorption	Jiang et al. (2014)
	$LiCoO_2$ (s) and Co^{2+} 0.34	MFC-MEC	88% in 6 h	Cathodic reduction, Adsorption	Huang et al. (2014)
	$LiCoO_2$ (s)	MFC	62-70% in 48 h	Cathodic reduction	Huang et al. (2013)
	Co^{2+} 0.36	MFC	93% in 6 h	Cathodic reduction, Precipitation	Huang et al. (2015)
Copper (Cu^{2+})	15.6	MFC	~100% in 168 h	Cathodic reduction, Precipitation	Heijne et al. (2010)
	0.79-100	MFC	>99% in 144h	Cathodic reduction	Tao et al. (2011a)
	31.25	MFC	90% in 24 h	Cathodic reduction	Rodenas et al. (2015)
	0-100	MFC	70% in 144 h	Cathodic reduction, Precipitation	Tao et al. (2011b)

Copper (Cu^{2+})	9.4, 31.3	MFC	92% in 480 h	Cathodic reduction	Tao et al. (2011c)
	$Cu(NH_3)_4^{2+}$	MFC	84% in 8 h	Cathodic reduction	Zhang et al. (2012)
	5-15	MFC	98% in 24 h	Cathodic reduction	Wu et al. (2018)
Nickle (Ni^{2+})	0.85-17	MEC	33-99% in 19.8 h	Cathodic reduction, Adsorption	Qin et al. 2012
Mercury (Hg^{2+})	0.125-0.5	MFC	>94% in 5 h	Cathodic reduction, Precipitation	Wang et al. (2011)
Gold (Au^{4+})	0-10.1	MFC	~100% in 12 h	Cathodic reduction, Precipitation	Choi and Hu (2013)
Silver (Ag^{+})	0.46-1.84	MFC	>98% in 8 h	Cathodic reduction	Choi and Cui (2012)
	$AgNO_3$ or AgS_2O_3	MFC	95% in 35 h	Cathodic reduction	Tao et al. (2012)
	9.26	MFC	~100% in 21 h	Cathodic reduction	Wang et.al (2013)
Vanadium (V^{5+})	9.8	MFC	25.3% in 72 h	Cathodic reduction	Zhang et al. (2009)
	4-8	MFC	~100% in 168 h	Cathodic reduction	Qiu et al. (2017)
	4.9, 9.8	MFC	67.9% in 240 h	Cathodic reduction	Zhang et al. (2010)
	4.9-19.6	MFC	26.1% in 72 h	Cathodic reduction	Zhang et al. (2010)
Zinc (Zn^{2+})	0.23-0.63	MEC	17%-99% in 48 h	Precipitation	Tang et.al (2016)

Zinc (Zn^{2+})	1.54 -12.3	MEC	60%-99% in 23 h	Cathodic reduction, Precipitation	Modin et al. (2017)
	0.2-0.5	MFC	94-99% in 48 h	Precipitation. Biosorption	Abourached et al. (2014)
Selenium (Se^{4+})	0-5.1	MFC	~99%	Bio-reduction	Catal et al. (2009)
Chromium (Cr^{6+})	0.96-9.6	MFC	99.5% in 25 h	Cathodic reduction	Li et al. (2008)
	0.48-3.84	MFC	~100% in 150 h	Cathodic reduction	Wang et al. (2008)
	1.44-5.77	MFC	~100% in 48 h	Cathodic reduction	Gangadharan and Nambi (2015)
	0.5	MFC	97% in 26 h	Cathodic reduction	Li et al. (2009)
	1.8-19.2	MFC	19.2~100% in 14 d	Cathodic reduction, Precipitation	Kim et al. (2017)
	0.76	MFC	>80%% in 4 h	Cathodic reduction, precipitation	Huang et al. (2011)
	0.38-0.77	MFC	~100% in 7 h	Cathodic reduction	Huang et al. (2010)
	0.42-1.2	MFC	~100% in 120 h	Cathodic reduction, precipitation	Tandukar et al. (2009)
	0.19-0.57	MFC	97.5 % in 4.5 h	Cathodic reduction	Shi et al. (2017)
	0.19	MFC	~100% or 42.5% in 3.5 h	Chemical reduction, Cathodic reduction	Liu et al. (2011)
	0-2.88	MFC	65.6% in 3 h	Chemical reduction, Cathodic reduction	Wang et al. (2017)

4.3.2 Cobalt

Cobalt can be found in some minerals and most cobalt is produced as a by-product of nickel refining. Cobalt has many industrial and medical applications. It is widely used in lithium-ion batteries where the cathode is made by lithium cobalt oxide ($LiCoO_2$). Various technologies such as ion exchange, chemical precipitation, and solvent extraction have been used to recover cobalt (Marafi and Stanislaus 2008). BES was also proposed to separate the cobalt from aqueous solutions.

Cobalt can be reduced at the cathode in BES. The reduction of Co^{3+} to Co^{2+} at the cathode is spontaneous since the redox potential of Co^{3+}/ Co^{2+} couple is high (1.81 V vs. SHE). In the work conducted by Huang et al. (2013), the Co^{3+} from insoluble $LiCoO_2$ (s) was reduced to the soluble Co^{2+} in two chambers MFCs (Eq 4.6). The recovery efficiencies from 62.5% to 70.5% were achieved under different conditions such as initial pH and external resistor with 48 hours of operation (Table 4.4). To further recover the cobalt, the soluble Co^{2+} needs to be reduced to insoluble Co^0 (Eq 4.7). This reduction demands an external power supply due to the low redox potential of Co^{2+}/ Co^0 (-0.232 V SHE). The reduction of Co^{2+} to Co^0 was enhanced by using biocathode in the study of Huang et al. (2014) and Jiang et al. (2014). In addition, the applied voltage can affect the reduction of Co^{2+} and a higher applied voltage condition results in a higher reduction rate. However, when the applied voltage was larger than 0.5 V, more electrons were provided for hydrogen evolution instead of cobalt reduction. Therefore, the optimal applied voltage of Co^{2+} reduction was 0.3 to 0.5 V (Jiang et al. 2014). A self-drive system that the $LiCoO_2$/ Co^{2+} MFC was used to provide the energy for the Co^{2+}/Co^0 MEC was proposed by Huang et al.

(2014). In their study, 46 ± 2 mg/L • h of cobalt leaching rate was achieved in the MFC when 7 ± 0 mg/L • h cobalt reduction rate was shown in the MEC. The overall cobalt yield was 0.15 ± 0.01 g Co/ g Co.

$$LiCoO_2(s) + 4H^+ + e^- \rightarrow Li^+ + Co^{2+} + 2H_2O \qquad \text{Eq 4.6}$$

$$Co^{2+} + 2e^- \rightarrow Co \qquad \text{Eq 4.7}$$

Co^{2+} can be separated by precipitation in BES as well. Co^{2+} ions can easily combine with OH^- and CO_3^{2-} to form the precipitation of $Co(OH)_2$ and $Co(CO)_3$ because of the low K_{sp} (Table 4.2 and Table 4.3). Huang et al. (2015) reported that 93.3% of cobalt was removed by $Co(OH)_2$ precipitation in MFCs with 6 h operation. The cobalt precipitation was formed on bacterial surfaces, which demonstrated the contribution of the oxygen-reducing biocathode. There was no $Co(CO)_3$ formed in these MECs because the cation exchange membrane limited the transfer of HCO_3^- between the anode chamber and cathode chamber. However, the precipitation of $Co(CO)_3$ in BES without the membrane is possible. It can be seen from Table 4.3 that only $10^{-4.6}$ M Co^{2+} (1.5 mg-Co/L) can dissolve in the water with $C_{T,\ CO32-}$ of 10 mM at pH 7. The concentration decreases to 10^{-8} M (0.59 μg-Co/L) at pH 12.

The mechanism of adsorption has been reported by Huang et al. (2014) and Jiang et al. (2014). 46.1% and 27% of cobalt were removed under open circuit conditions in their studies.

4.3.3 Cadmium

Cadmium is toxic and has been listed as a group-B1 carcinogen element by the US Environment Protection Agency (EPA, Purkayastha et al. 2014). The sources of cadmium

in the environment include coal combustion, iron and steel production, usage of NiCd batteries, and electroplating. A number of technologies such as precipitation, coagulation, and membrane filtration have been applied to remove cadmium (Purkayastha et al. 2014). BES was also used to separate cadmium from aqueous solutions.

Cadmium removal in BES can be achieved by the cathodic reduction (Eq 4.8). The reduction of Cd^{2+} to Cd^0 requires an external power supply because of the low redox potential of Cd^{2+}/Cd^0 (-0.403V vs. SHE). Choi et al. (2014) used Cr^{6+} a cathodic reactant to remove Cd^{2+} in an MFC. 94.5 % of Cd^{2+} was removed with 60 hours of operation in the study. An enhanced reduction rate was reported in the study of Wang et al. (2016) by using the deposited Cu cathodes. Cd^{2+} removal rates in the MECs with deposited Cu (4.96-5.86 mg/L • h with different cathode materials) were 1.8-4.2 times higher than that in the MECs without deposited Cu (1.18-3.26 mg/L • h).

$$Cd^{2+} + 2e^- \rightarrow Cd \qquad \text{Eq 4.8}$$

Precipitation of cadmium hydroxide ($Cd(OH)_2$) and cadmium carbonate ($CdCO_3$) were reported by Colantonio and Kim (2016). They found that the precipitation was responsible for more than 60% of cadmium removal under the applied voltage of 0.4 V in a single chamber MEC. To avoid the dissociation of $Cd(OH)_2$ and $CdCO_3$, sufficient amounts of substrates were suggested to feed to the reactor in their study. From Table 4.2 and 4.3, $10^{-8.3}$ M Cd^{2+} (0.56 μg-Cd/L) can result in the formation of $CdCO_3$ while $Cd(OH)_2$ can be formed with $10^{-0.3}$ M Cd^{2+} (56 mg-Cd/L) at pH 7. At pH 12, the equilibrium concentration of Cd^{2+} decrease to $10^{-10.3}$ M (5.6×10^{-3} μg/L).

In addition, the separation of cadmium by biosorption at the anode was demonstrated in an MFC by Abourached et al. (2014). The precipitation process of Cd^{2+} on the cathode is difficult when oxygen exists in the MFC because the standard redox potential of Cd^{2+} is much lower than O_2. However, more than 89% of cadmium was removed in the study of Abourached et al. (2014) by using the air-cathode-MFCs. This result can be explained by the biosorption of Cd^{2+} at the anode. The performance of the MFC was affected by the initial cadmium concentration. The maximum tolerable concentration of cadmium was 200 μM in MFCs. Cadmium removal by anode biosorption was also reported in MECs with low cadmium concentration in the study conducted by Colantonio et al. (2016). In their study, 59.3%, 6.3%, and 4.4% of cadmium were removed by anode biosorption with different initial Cd^{2+} concentrations.

4.3.4 Copper

Copper is an essential element to living organisms because it is a key constituent of the respiratory enzyme complex. However, a high dose of copper is toxic to all life forms. Copper commonly exists in the effluent from electronics plating, wire drawing, copper polishing, and paint. (Zamani et al. 2007). Numerous treatment technologies, which include adsorption, biosorption, and co-precipitation with calcium carbonate, are available for copper removal and recovery (Aston et al. 2010; Khosravi and Alamdari 2009).

Copper can be separated by reduction at the cathode in BES. The reduction of Cu^{2+} to Cu^0 at the cathode occurs spontaneously because of the positive standard redox potential of Cu^{2+}/Cu^0 couple (0.337 V vs. SHE). There are two major ways for the reduction of Cu^{2+}: Cu^{2+} is directly reduced to Cu^0 at the cathode (Eq 4.9); Cu^{2+} is first reduced to Cu_2O and

then Cu_2O is reduced to Cu^0 (Eq 4.10 and 4.11). Although the standard reduction potential of Cu^{2+}/Cu^0 (0.337 V vs. SHE) is higher than that of Cu^{2+}/Cu_2O (0.207 V vs. SHE), the reduction of Cu^{2+} to Cu_2O is more favorable when pH > 4.7 based on the Nernst equations (Tao et al. 2011a). Both metallic copper Cu^0 and cuprous oxide (Cu_2O) appeared on the cathode in studies conducted by Tao et al. (2011a) and Wu et al. (2018). The formation of Cu_2O can be governed by pH. It was shown that only metallic Cu was formed on the cathode by controlling the pH < 3 in the study of Heijne et al. (2010) and Rodenas et al. (2015). In addition to the pH, the formation of Cu_2O can be controlled by providing enough electrons (substrates) since the formation of Cu requires 1 more electron than the formation of Cu_2O (Tao et al. 2011c).

$$Cu^{2+} + 2e^- = Cu(s) \quad \text{Eq 4.9}$$

$$2Cu^{2+} + 2H_2O + 2e^- = Cu_2O + 2H^+ \quad \text{Eq 4.10}$$

$$Cu_2O + 2H^+ + 2e^- = 2Cu + H_2O \quad \text{Eq 4.11}$$

Apart from Cu^{2+}, some copper complexes can also be reduced at the cathode. For instance, ammonia-copper complexes ($Cu(NH_3)_4^{2+}$) were fed to a dual-chamber MFC in the study of Zhang et al. (2012). The reduction of $Cu(NH_3)_4^{2+}$ can be achieved in two ways: Cu^{2+} that released from $Cu(NH_3)_4^{2+}$ was reduced to Cu or Cu_2O directly; $Cu(NH_3)_4^{2+}$ accepted an electron to form $Cu(NH_3)_4^+$ and then $Cu(NH_3)_4^+$ deposited as Cu or Cu_2O on the cathode. These two ways were affected by the pH. $Cu(NH_3)_4^{2+}$ was dissociated to Cu^{2+} at pH < 5.34 while it was reduced to $Cu(NH_3)_4^+$ at pH > 8.83. In the study conducted by Zhang et al. (2012), 84% of copper was removed with the initial concentration of 350 mg-Cu/L at pH 3.0 after 8 h.

Copper can also be separated by precipitation in BES because of the low K_{sp} of $Cu(OH)_2$ and $CuCO_3$ (Table 4.2 and 4.3). For instance, $10^{-6.4}$ M Cu^{2+} (25.5 µg-Cu/L) can result in the formation of $Cu(OH)_2$ at pH 7. In addition, the formation of insoluble copper complex brochantite ($CuSO_4 \cdot 3Cu(OH)_2$, Eq 4.12) also contributed to the separation of Cu^{2+}. This complex was detected on the cathode in the studies of Tao et al. (2011a, 2011b). Brochantite can be formed at the high initial Cu^{2+} concentration (~6400 mg/L). With the high concentration of Cu^{2+}, low removal efficiencies of 18.6% and 28.1 % were shown in a dual-chamber MFC and a membrane-free MFC respectively (Tao et al. 2011a, Tao et al. 2011b). The precipitation of copper sulfide was also observed in the study of Miran et al. (2017).

$$4Cu^{2+} + 6H_2O + SO_4^{2-} = CuSO_4 \cdot 3Cu(OH)_2 + 6H^+ \quad \text{Eq 4.12}$$

The mechanism of anode biosorption was reported by Tao et al. (2011a). In the study, the Cu^{2+} concentration in the anode chamber decreased from 5.3 mg/L to 0.17 mg/L.

4.3.5 Mercury

Mercury is harmful and toxic to human beings. The major sources of mercury contamination include dental practice wastes, fertilizers, pulp paper wastes, and coal combustors used in electricity generation (Baeyens et al. 2016; Bender 2008; Morimoto et al. 2005). Many technologies such as activated carbon adsorption, ion exchange, and precipitation have been used to remove mercury (Monteagudo and Ortiz 2000; Hutchison et al. 2008).

Similar to cobalt and cadmium, the separation of Hg^{2+} was also achieved in BES. The reduction of Hg^{2+} to Hg^0 in BES is spontaneous since the Hg^{2+}/Hg^0 couple has a high redox

potential (0.851 V vs. SHE). The reduction at the cathode has two ways: Hg^{2+} was reduced to Hg^0 directly (Eq 4.13); Hg^{2+} was reduced to Hg_2^{2+} first, then Hg_2^{2+} was reduced to Hg^0 (Eq 4.14 and 4.15). In the study of Wang et al. (2011), the removal efficiency larger than 94% was achieved under different conditions (e.g., initial pH, initial Hg concentration).

$$Hg^{2+} + 2e^- \rightarrow Hg\ (l) \qquad (0.851\ V\ vs.\ SHE) \quad Eq\ 4.13$$

$$2Hg^{2+} + 2e^- \rightarrow Hg_2^{2+}\ (l) \qquad (0.911\ V\ vs.\ SHE)\ Eq\ 4.14$$

$$Hg_2^{2+} + 2e^- \rightarrow 2Hg\ (l) \qquad (0.796\ V\ vs.\ SHE) \quad Eq\ 4.15$$

Precipitation also contributed to the separation of Hg^{2+} since Hg_2Cl_2 was detected on the cathode in the study of Wang et al. (2011). There were no $Hg(OH)_2$ and $HgCO_3$ formed in the system because of the low initial pH. However, the precipitation of these two precipitates is possible in BES because of the low K_{sp} of $Hg(OH)_2$ and $HgCO_3$ (Table 4.2 and 4.3). For instance, less than $10^{-10.7}$ M Cu^{2+} (4×10^{-3} μg-Hg/L) can dissolve in the solution at pH 7. The mechanism of precipitation of $Hg(OH)_2$ and $HgCO_3$ can be investigated in future studies.

4.3.6 Gold

Gold is widely used in the electronics industry because of its great electrical conductivity and outstanding corrosion resistance. Gold is commonly present in leach solutions and electroplating wastes (Flores and Okeefe 1995). Many methods such as ion-exchange and biosorption can be used to separate gold from wastewater (Gomes et al. 2001; Das 2010).

Gold ions (Au^{3+}) can deposit on the cathode by reducing Au^{3+} in BES (Eq 4.16). The transfer of electrons from the cathode to Au^{3+} is spontaneous because of the high standard

redox potential of Au^{3+}/Au^0 (1.002 V vs. SHE). Choi and Hu (2013) reported that 99.89% of gold was recovered in a cubical dual-chamber MFC with 12 hours. pH and initial Au^{3+} concentration can affect the removal efficiency.

$$AuCl_4^- + 3e^- = Au(s) + 4Cl^- \quad \text{Eq 4.16}$$

Au^{3+} is likely to form precipitates of $Au(OH)_3$ at the high pH conditions allowing the separation of gold. In the study of Choi and Hu (2013), the power density of MFC decreased from 1.37 to 0.78 W/m^2 with the pH increasing from 2 to 5. The low current density was due to the low conductivity of the catholyte with the $Au(OH)_3$ formation.

4.3.7 Silver

Silver is widely used in jewelry, electronics, and photographic industries. It is a precious metal and only exists in nature with limited amounts. High concentrations of some silver compounds are toxic to aquatic life (Naddy et al. 2007). Several methods such as ion exchange, chemical reduction, and electrolysis are available to recover or remove silver from aqueous solutions (Blondeau and Veron 2010).

Separation of Ag^+ can be achieved by reducing Ag^+ to Ag^0 at the cathode in BES. The reduction of Ag^+ to Ag is spontaneous because of the high redox potential of Ag^+/Ag^0 (0.799V vs. SHE, Eq 4.17). In the study of Choi and Cui (2012), more than 98% of silver was recovered in the MFC with different initial concentrations of $AgNO_3$ (50 to 200 mg/L) in 8 h. High removal efficiencies (>89%) were shown in using MFCs that started with 1 mM $AgNO_3$ (170 mg/L) with pH ranging from 2 to 6.6 (Tao et al. 2012). In addition to $AgNO_3$, some silver complex compounds such as silver thiosulfate($[AgS_2O_3]^-$) and diamine silver ($[Ag(NH_3)_2^+]$) were used as cathodic solutions in the studies of Tao et al.

(2012) and Wang et al. (2013). The slower removal rates (95% in 35 h and 99.9% in 21 h, Table 4.4) were shown for complexes reduction since the redox potentials of $[AgS_2O_3]^-/Ag$ (0) (0.25 V vs. SHE) and $[Ag(NH_3)_2^+]/ Ag^0$ (0.373 V vs. SHE) were lower (Eq 4.18, 4.19, and 4.20) than that of Ag^+/Ag^0. Through the SEM-EDS analysis, Ag^0 crystals were shown on the cathode. A small fraction of Ag_2S was also detected at pH 4.0 and 6.5 with $[AgS_2O_3]^-$ reduction (Eq 4.19).

$$Ag^+ + e^- = Ag(s) \quad \text{Eq 4.17}$$

$$[AgS_2O_3]^- + e^- = Ag(s) + S_2O_3^- \quad \text{Eq 4.18}$$

$$[AgS_2O_3]^- + 8e^- + 6\ H^+ = 2Ag_2S(s) + 3H_2O + 3S_2O_3^- \quad \text{Eq 4.19}$$

$$[Ag(NH_3)_2]^+ + e^- = Ag(s) + 2NH_3 \quad \text{Eq 4.20}$$

The precipitation of Ag_2CO_3 and AgOH requires high pH conditions. At pH 7, the solubility of Ag^+ is $10^{-2.85}$ M (152 mg-Ag/L) and $10^{-0.7}$ M (21.5 g-Ag/L) with CO_3^{2-} and OH^-, respectively. Therefore, the formation of Ag_2CO_3 and AgOH is difficult at pH 7. The solubility of Ag^+ is smaller than $10^{-5.7}$ M (0.2 mg-Ag/L) at pH 12. The low solubility makes the formation of Ag_2CO_3 and AgOH possible. There were no previous BES related to the results of AgOH or Ag_2CO_3 precipitation. The precipitation can be investigated in the future as a potential method to separate silver in BES.

4.3.8 Vanadium

Vanadium is the main pollutant found in wastewater from vanadium mining and vanadium pentoxide (V_2O_5) production (Bauer et al. 2000). Most of the vanadium is used as a steel additive and vanadium-steel alloys for tools, piston rods, and armor plates. Vanadium is a trace element in living organisms. However, some vanadium compounds

are harmful to people and sometimes can be fatal. V^{5+} is more toxic than V^{4+} which is insoluble at high pH (neutral or alkaline pH). Therefore, the reduction of V^{5+} to V^{4+} is an applicable method to remove or recover vanadium from aqueous solutions.

The reduction of V^{5+} to V^{4+} is spontaneous because the V^{5+}/V^{4+} couple has a high positive redox potential (0.991 V vs. SHE, Eq 4.21). The removal efficiency ranged from 25 to 100% was achieved in previous studies (Table 4.4, Zhang et al. 2009; Zhang et al. 2012; Zhang et al. 2010, Qiu et al. 2017). The color of cathodic electrolyte changed from yellow brow to sky-blue during the reduction process of V^{5+} to V^{4+}. To separate V^{4+} from cathodic solution, the pH of the cathodic electrolyte was adjusted to 6 by using $NH_3 \cdot H_2O$. During the pH increasing process, the color changed from sky-blue to dark grey due to the re-oxidization of some V^{4+}. Both Cr^{6+} and V^{5+} were reduced in the study of Zhang et al. (2012), which contributed to a better MFC performance. The recovery of Cr^{6+} and V^{5+} can be separated since chromium was mainly deposited on the cathode surface while vanadium stayed in the catholyte. The vanadium can be removed later by increasing the pH.

$$VO_2^{2+} + e^- + 2\ H^+ = VO^{2+} + H_2O \quad \text{Eq 4.21}$$

4.3.9 Chromium

The main sources of hexavalent chromium in the environment are from electroplating, leather tanning, and wood product processes (Jadhav et al. 2012). Methods such as chemical precipitation, ion exchange, membrane filtration, and biosorption have been developed to treat chromium in aqueous solutions (Kurniawan et al. 2006; Quintelas et al.2006). Cr(III) is the form of chromium with less toxicity and less solubility comparing

with Cr(VI). Thus, the reduction of Cr(VI) to Cr(III) is regarded as a safe and efficient process for Cr(VI) removal.

The reduction of Cr(VI) is achievable at the cathode of MFCs since the redox potential of Cr(VI)/Cr(III) couple is high (1.33 V vs. SHE, Eq 4.22). There are three different ways for Cr(VI) reduction at the cathode: Cr(VI) is reduced at the abiotic cathode directly; Cr(VI) is reduced by microorganisms at the biocathode; the cathode products such as H_2O_2 can also reduce Cr(VI). 99.5% of Cr(VI) was removed in a dual-chamber MFC with abiotic cathode after 25 h treatment in the study of Li et al. (2008). The removal efficiency was affected by the pH and initial concentration of Cr(VI). The similar removal efficiency was shown in previous studies of Wang et al. (2008) and Gangadharan and Nambi (2015). The cathode materials also affect the reduction rates at the cathode. Li et al. (2009) improved the reduction rates and power generation by using the rutile-coated cathode. In addition, various removal efficiencies (19.2-100%) were shown in MFCs feed with chromium wastewater (Kim et al. 2017).

$$Cr_2O_7^{2-} + 4e^- + 8H^+ = Cr_2O_3 + 4H_2O \quad \text{Eq 4.22}$$

The reduction of Cr(VI) was also investigated in several MFCs with biocathode. In these MFCs, the cathode chambers were inoculated with various mediums, which include healthy MFC effluent (Huang et al. 2011a), primary clarifier effluent (Huang et al. 2011b), Cr(VI) reducing bacteria cultures from Cr(VI) contaminated soil (Huang et al. 2010), and a mixture of denitrifying and anaerobic mixed cultures (Tandukar et al. 2009). The removal efficiencies of Cr(VI) ranged from 60-100% (i.e., 0.46 to 20.4 mg/VSS • h) in these MFCs. In addition to the inoculated mediums, many other factors can also affect the removal

efficiency of Cr(VI) in MFCs. For instance, Huang et al. (2010) evaluated the effects of different biocathode materials, i.e., graphite fibers, graphite felt, and graphite granules. The highest removal efficiency of 90.2% was achieved in the MFC with graphite fibers. The removal efficiency of 97.5% within 4.5 h was achieved in the study of Shi et al. (2017) by using the natural pyrrhotite-coated cathode. The effects of pH and initial concentration of Cr(VI) were studied by Huang et al. (2011b) and Huang et al. (2010). In addition, Liu et al. (2011) evaluated the effects of different inoculums for the anode on Cr(VI) removal efficiency. Among the MFCs that inoculated with *Shewanella decolorationis* S12, *Klebsiella pneumonia* L17, and anaerobic activated sludge, the MFC inoculated with anaerobic activated sludge had the best performance with 97% Cr(VI) removal efficiency after 3 h operation.

Cr(VI) can also be reduced by hydrogen peroxide which was produced at the cathode with oxygen reduction (Eq 4.23). The mechanism was demonstrated in the study of Liu et al. (2011) with an air-bubbling-cathode MFC and a nitrogen-bubbling-cathode MFC. Complete reduction of Cr(VI) was achieved in the air-bubbling-cathode MFC after 4 h of operation while only 42.5% of Cr(VI) was reduced in the MFC without air. The faster removal rate of Cr(VI) with the air-bubbling-cathode MFC can be explained by the production of H_2O_2 which was electrochemically generated via the reaction of O_2 reduction (Eq 4.24). After adding H_2O_2, the increased Cr(VI) removal rates of the nitrogen-bubbling-cathode MFC indicated the contribution of H_2O_2. Similar to H_2O_2, Fe^{3+} was used as an electron shuttle mediator to enhance the reduction of Cr(VI) in the study of Wang et al. (2017).

$$O_2 + 2H^+ + 2e^- \rightarrow H_2O_2 \quad \text{Eq 4.23}$$

$$2HCrO_4^- + 3H_2O_2 + 8H^+ = 2Cr^{3+} + 8H_2O + 3O_2 \quad \text{Eq 4.24}$$

After reduction, Cr(III) ions can easily combine with OH^- to form the precipitates in BES (Table 4.2). $Cr(OH)_3$ was detected in many previous studies (Tandukar et al. 2009, Kim et al. 2017, Huang et al. 2011a). The formation of $Cr(OH)_3$ was highly pH-dependent and it was usually generated at pH from 6.5 to 10.

4.3.10 Nickel

Nickel is the 5th most common element on the earth. The dominant use of nickel is the production of ferronickel for stainless steel (Reck et al. 2008). It is also widely used for producing batteries, alloy steels, and non-ferrous alloys. A high dose of nickel can cause various pathological effects such as kidney diseases, lung fibrosis, and even cancer in humans (Denkhaus and Salnikow 2002). Various technologies, including chemical precipitation, ion exchange, membrane filtration, and adsorption, were investigated for nickel recovery and removal (Papadopoulos et al. 2004; Chen et al. 2009; Landaburu-Aguirre et al. 2012).

BES can also be used to separate nickel from aqueous solutions by reducing Ni^{2+} to Ni^0. Direct reduction of soluble Ni^{2+} to metal Ni^0 at the cathode requires an external power supply because of the negative standard redox potential (-0.25 V vs. SHE) (Eq 4.25). Ni^{2+} recovery from a nickel sulfate solution was studied in a MEC with different applied voltages from 0.5 V to 1.1 V (Qin et al. 2012). The maximum removal efficiency of 67 ± 5.3% was achieved under the applied voltage of 1.1 V. The pH and initial Ni^{2+} concentration can affect the performance of MEC. 87% of Ni^{2+} was removed in the single

test with the initial concentration of 530 mg-Ni^{2+}/L when the MEC was fed with artificial acid mine drainage in the study of Luo et al. (2014). For the mixed metal (nickel, copper, and iron) test, copper was deposited on the cathode first, followed by nickel and ferric.

$$Ni^{2+} + 2e^- \rightarrow Ni \quad \text{Eq 4.25}$$

Precipitation is the potential mechanism of nickel separation in BES although it has not been reported in previous studies. The precipitation of $Ni(OH)_2$ and $NiCO_3$ requires high pH conditions. At pH 7, $10^{-3.2}$ M Ni^{2+} (37 mg/L) can dissolve in the water based on the K_{sp} of $Ni(OH)_2$ (Table 4.2). The high solubility of $10^{-1.5}$ M Ni^{2+} (1.86 g/L) was shown for $NiCO_3$ because of the high Ksp. At pH 12, the negligible amount of Ni^{2+} ($10^{-13.2}$ M Ni^{2+} or $10^{-5.4}$ μg/L) can dissolve in the water because of the formation of $Ni(OH)_2$.

Adsorption at the cathode also contributes to the nickel removal, which was proved by Qin et al. (2012). The nickel removal efficiency of 9 ± 0.1 % was achieved in a MEC under open-circuit conditions.

4.3.11 Zinc

Zinc is an essential trace element for living things, but it can be carcinogenic in excess. Various technologies, which include ion exchange, precipitation, and adsorption are used to remove or recover zinc from aqueous solutions (Alyüz et al. 2009; Chen et al. 2011).

Direct reduction of zinc at the cathode in a BES system requires an external power supply because of the low standard redox potential (-0.764 vs. SHE) (Eq 4.26). The reduction of zinc at the cathode was investigated in a MEC using sodium acetate as the substrate (Modin et al. 2017). 60-99% of zinc was removed with different operating conditions such as initial zinc concentration and catholyte type. The removal efficiency can

be affected by the hydrogen generation since Zn^{2+} was reduced at the cathode potential of -1.0 V which was close to the potential when hydrogen generation occurred.

$$Zn^{2+} + 2e^- \rightarrow Zn \quad \text{Eq 4.26}$$

The separation of zinc by precipitation of $Zn(OH)_2$ and ZnS has been reported in previous studies (Modin et al.2017; Teng et al. 2016; Abourached et al. 2014). The formation of $Zn(OH)_2$ contributed to the majority removal of zinc in the study of Teng et al. (2016) since the reduction of Zn^{2+} was difficult at the cathode when sulfide existed in the system. Up to 99% of Zn^{2+} was removed with the initial concentration ranged from 10 to 40 mg-Zn/L. This result is consistent with the study of Abourached et al. (2014) that up to 99% of Zn^{2+} was removed by the precipitation of ZnS with the initial concentration ranged from 13 to 32.5 mg-Zn/L. In addition, the formation of $ZnCO_3$ is possible in BES because of the low K_{sp}. At pH 7, $10^{-4.6}$ M Zn^{2+} (1.4 mg/L) can result in the precipitation of $ZnCO_3$ while 10^{-8} M Zn^{2+} (0.56 μg/L) can result in the precipitation at pH 12.

Zinc also can be separated from aqueous solution by biosorption at the anode. In the study of Abourached et al. (2014), the removal of zinc was studied in an air cathode MFC. When the oxygen existed in the system, Zn^{2+} was difficult to reduce because of the low standard redox potential (-0.764 V vs. SHE). However, more than 94% of zinc was removed in this MFC and this high removal efficiency was due to the biosorption at the anode. In addition, the lower removal efficiency was shown in the autoclave MFC with non-living microbial cells, which indicated that the microorganisms played an important role in zinc removal in MFCs.

4.3.12 Selenium

Selenium is an essential trace element for some species, but large amounts of selenium are toxic. Selenium is used in various industrial products and processes, such as pigments, electronics, photoelectric cells, and glass manufacturing. Current methods for removing selenium include precipitation, adsorption, ion exchange, and reduction (Twidwell et al. 1999).

The separation of selenium was studied in the single-chamber MFCs by reducing Se^{4+} to Se^0. Se^{4+} can be reduced spontaneously since the redox potential of Se^{4+}/Se^0 is +0.41 V vs. SHE. However, there was no current generated when the MFC was converted from aerobic condition to anaerobic condition in the study of Catal et al. (2009). This result indicated that oxygen was reduced on the cathode while the reduction of Se^{4+} to Se^0 was caused by the respiring microorganisms at the anode. 99% of 50 mg/L selenite was removed in 48 h with acetate as the substrate. Also, 99% of 200 mg/L selenite was removed in 72 h with glucose as the substrate. In addition, Lee et al. (2007) and Banuelos et al. (2013) illustrated that *Shewanella* species, well known for their capability to generate current in MFCs, can use selenite as the electron acceptor.

4.4 Conclusions

BES shows great efficiency for separating heavy metals from aqueous solutions. Many factors govern the removal efficiency, such as the operation time, pH, initial concentration, and cathode potential (MFC) or applied voltage (MEC). The mechanism of cathodic reduction has been demonstrated for metal separations in many previous studies. In addition, the mechanism of precipitation can also contribute to the metal separation in BES

since some heavy metals are easy to form precipitates with OH^- or CO_3^{2-}. For instance, Hg^{2+}, Cu^{2+}, Au^{3+}, Cd^{2+}, and Cr^{3+} can form the precipitants even at neutral pH with low metal ion concentration. Some heavy metals such as Co^{2+}, Ni^{2+}, Zn^{2+}, and Ag^+ require a high pH condition. Thus, it is still possible for the metals to form precipitants near the BES cathode since the oxygen reduction in MFC and hydrogen production in MEC can result in high pH conditions near the BES cathode. The mechanism of precipitation has been investigated in some previous studies, but more future studies are needed to understand this mechanism.

4.5 Future perspectives

There were many previous studies focused heavily on the reduction mechanism of the heavy metal separation in BES. However, a few studies discussed the mechanism of the precipitation. The electrode reactions such as hydroxide production at the cathode and carbonate production at the anode enhance the separation of heavy metal by precipitation. Therefore, we suggested that future studies should investigate the mechanism of precipitation for heavy metal separation in BES.

References

Abourached C, Catal T, Liu H (2014) Efficacy of single-chamber microbial fuel cells for removal of cadmium and zinc with simultaneous electricity production. Water Research 51:228-33.

Achparaki M, Thessalonikeos E, Tsoukali H, Mastrogianni O, Zaggelidou E, Chatzinikolaou F, Vasilliades N, Raikos N (2012) Heavy metals toxicity. Aristotle University Medical Journal 39(1):29-34.

Alyüz B, Veli S (2009) Kinetics and equilibrium studies for the removal of nickel and zinc from aqueous solutions by ion exchange resins. Journal of Hazardous Materials 167(1-3):482-8.

Aston JE, Apel WA, Lee BD, Peyton BM (2010) Effects of cell condition, pH, and temperature on lead, zinc, and copper sorption to Acidithiobacillus caldus strain BC13. Journal of Hazardous Materials 184(1-3):34-41.

Baeyens W, Ebinghaus R, Vasiliev O, editors (2016) Global and regional mercury cycles: sources, fluxes and mass balances. Springer Science & Business Media.

Bauer G, Güther V, Hess H, Otto A, Roidl O, Roller H, Sattelberger S, Köther-Becker S, Beyer T (2000) Vanadium and vanadium compounds. Ullmann's Encyclopedia of Industrial Chemistry.

Banuelos GS, Lin ZQ, Yin X (2013) Selenium in the environment and human health. CRC Press.

Bender M (2008) Facing Up to the Hazards of Mercury Tooth Fillings. Mercury.

Blondeau JP, Veron O (2010) Precipitation of silver nanoparticles in glass by multiple wavelength nanosecond laser irradiation. Journal of Optoelectronics and Advanced Materials 445-50.

Call D, Logan BE (2008) Hydrogen production in a single chamber microbial electrolysis cell lacking a membrane. Environmental Science & Technology 42(9):3401-6.

Catal T, Bermek H, Liu H (2009) Removal of selenite from wastewater using microbial fuel cells. Biotechnology Letters 31(8):1211-6.

Chen C, Hu J, Shao D, Li J, Wang X (2009) Adsorption behavior of multiwall carbon nanotube/iron oxide magnetic composites for Ni (II) and Sr (II). Journal of Hazardous Materials 164(2-3):923-8.

Chen X, Chen G, Chen L, Chen Y, Lehmann J, McBride MB, Hay AG (2011) Adsorption of copper and zinc by biochars produced from pyrolysis of hardwood and corn straw in aqueous solution. Bioresource Technology 102(19):8877-84.

Choi C, Cui Y (2012) Recovery of silver from wastewater coupled with power generation using a microbial fuel cell. Bioresource Technology 107:522-5.

Choi C, Hu N (2013) The modeling of gold recovery from tetrachloroaurate wastewater using a microbial fuel cell. Bioresource Technology 133:589-98.

Choi C, Hu N, Lim B (2014) Cadmium recovery by coupling double microbial fuel cells. Bioresource Technology 170:361-9.

Colantonio N, Guo H, Kim Y (2016) Effect of Low Cadmium Concentration on the Removal Efficiency and Mechanisms in Microbial Electrolysis Cells. ChemistrySelect 1(21):6920-4.

Colantonio N, Kim Y (2016) Cadmium (II) removal mechanisms in microbial electrolysis cells. Journal of Hazardous Materials 311:134-41.

Cusick RD, Logan BE (2012) Phosphate recovery as struvite within a single chamber microbial electrolysis cell. Bioresource Technology 107:110-5.

Das N (2010) Recovery of precious metals through biosorption—a review. Hydrometallurgy 103(1-4):180-9.

Denkhaus E, Salnikow K. Nickel essentiality, toxicity, and carcinogenicity (2002) Critical reviews in oncology/hematology 42(1):35-56.

Dominguez-Benetton X, Varia JC, Pozo G, Modin O, ter-Heijne A, Fransaer J, Rabaey K (2018) Metal recovery by microbial electro-metallurgy. Progress in Materials Science.

ElMekawy A, Srikanth S, Bajracharya S, Hegab HM, Nigam PS, Singh A, Mohan SV, Pant D (2015). Food and agricultural wastes as substrates for bioelectrochemical system (BES): the synchronized recovery of sustainable energy and waste treatment. Food Research International 73:213-25.

Fergusson JE (1990). Heavy elements: chemistry, environmental impact and health effects. Pergamon.

Flores C, OKeefe TJ (1995) Gold recovery from organic solvents using galvanic stripping. Minerals, Metals and Materials Society, Warrendale, PA (United States).

Fu F, Wang Q (2011) Removal of heavy metal ions from wastewaters: a review. Journal of Environmental Management 92(3):407-18.

Gangadharan P, Nambi IM (2015) Hexavalent chromium reduction and energy recovery by using dual-chambered microbial fuel cell. Water Science and Technology 71(3):353-8.

Giannopoulou I, Panias D (2008) Differential precipitation of copper and nickel from acidic polymetallic aqueous solutions. Hydrometallurgy 90(2-4):137-46.

Giller KE, Witter E, Mcgrath SP (1998) Toxicity of heavy metals to microorganisms and microbial processes in agricultural soils: a review. Soil Biology and Biochemistry 30(10-11):1389-414.

Gomes CP, Almeida MF, Loureiro JM (2001) Gold recovery with ion exchange used resins. Separation and Purification Technology 24(1-2):35-57.

Heijne AT, Liu F, Weijden RV, Weijma J, Buisman CJ, Hamelers HV (2010) Copper recovery combined with electricity production in a microbial fuel cell. Environmental Science & Technology 44(11):4376-81.

He J, Chen JP (2014) A comprehensive review on biosorption of heavy metals by algal biomass: materials, performances, chemistry, and modeling simulation tools. Bioresource Technology 160:67-78.

He Z, Minteer SD, Angenent LT (2005) Electricity generation from artificial wastewater using an upflow microbial fuel cell. Environmental Science & Technology 39(14):5262-7.

Huang L, Chai X, Chen G, Logan BE (2011a) Effect of set potential on hexavalent chromium reduction and electricity generation from biocathode microbial fuel cells. Environmental Science & Technology 45(11):5025-31.

Huang L, Chai X, Cheng S, Chen G (2011b) Evaluation of carbon-based materials in tubular biocathode microbial fuel cells in terms of hexavalent chromium reduction and electricity generation. Chemical Engineering Journal 166(2):652-61.

Huang L, Chen J, Quan X, Yang F (2010) Enhancement of hexavalent chromium reduction and electricity production from a biocathode microbial fuel cell. Bioprocess and Biosystems Engineering 33(8):937-45.

Huang L, Jiang L, Wang Q, Quan X, Yang J, Chen L (2014) Cobalt recovery with simultaneous methane and acetate production in biocathode microbial electrolysis cells. Chemical Engineering Journal 253:281-90.

Huang L, Li T, Liu C, Quan X, Chen L, Wang A, Chen G (2013) Synergetic interactions improve cobalt leaching from lithium cobalt oxide in microbial fuel cells. Bioresource Technology 128:539-46.

Huang L, Liu Y, Yu L, Quan X, Chen G (2015) A new clean approach for production of cobalt dihydroxide from aqueous Co (II) using oxygen-reducing biocathode microbial fuel cells. Journal of Cleaner Production 86:441-6.

Huang L, Yao B, Wu D, Quan X (2014) Complete cobalt recovery from lithium cobalt oxide in self-driven microbial fuel cell–microbial electrolysis cell systems. Journal of Power Sources 259:54-64.

Hu H (2002) Human health and heavy metals. Life Support: The Environment and Human Health; MIT Press: Cambridge, MA, USA.

Hutchison A, Atwood D, Santilliann-Jiminez QE (2008) The removal of mercury from water by open chain ligands containing multiple sulfurs. Journal of Hazardous Materials 156(1-3):458-65.

Jadhav UU, Hocheng H (2012) A review of recovery of metals from industrial waste. Journal of Achievements in Materials and Manufacturing Engineering 54(2):159-67.

Jiang L, Huang L, Sun Y (2014) Recovery of flakey cobalt from aqueous Co (II) with simultaneous hydrogen production in microbial electrolysis cells. International Journal of Hydrogen Energy 39(2):654-63.

Khosravi J, Alamdari A (2009) Copper removal from oil-field brine by coprecipitation. Journal of Hazardous Materials 166(2-3):695-700.

Kim C, Lee CR, Song YE, Heo J, Choi SM, Lim DH, Cho J, Park C, Jang M, Kim JR (2017) Hexavalent chromium as a cathodic electron acceptor in a bipolar membrane microbial fuel cell with the simultaneous treatment of electroplating wastewater. Chemical Engineering Journal 15;328:703-7.

Kurniawan TA, Chan GY, Lo WH, Babel S (2006) Physico–chemical treatment techniques for wastewater laden with heavy metals. Chemical Engineering Journal 118(1-2):83-98.

Landaburu-Aguirre J, Pongrácz E, Sarpola A, Keiski RL (2012) Simultaneous removal of heavy metals from phosphorous rich real wastewaters by micellar-enhanced ultrafiltration. Separation and Purification Technology 88:130-7.

Lee JH, Han J, Choi H, Hur HG (2007) Effects of temperature and dissolved oxygen on Se (IV) removal and Se (0) precipitation by Shewanella sp. HN-41. Chemosphere 68(10):1898-905.

Liu H, Cheng S, Logan BE (2005) Production of electricity from acetate or butyrate using a single-chamber microbial fuel cell. Environmental Science & Technology 39(2):658-62.

Liu L, Yuan Y, Li FB, Feng CH (2011) In-situ Cr (VI) reduction with electrogenerated hydrogen peroxide driven by iron-reducing bacteria. Bioresource Technology 102(3):2468-73.

Li Z, Zhang X, Lei L (2008) Electricity production during the treatment of real electroplating wastewater containing Cr6+ using microbial fuel cell. Process Biochemistry 43(12):1352-8.

Logan BE, Call D, Cheng S, Hamelers HV, Sleutels TH, Jeremiasse AW, Rozendal RA (2008) Microbial electrolysis cells for high yield hydrogen gas production from organic matter. Environmental Science & Technology 42(23):8630-40.

Logan BE, Hamelers B, Rozendal R, Schröder U, Keller J, Freguia S, Aelterman P, Verstraete W, Rabaey K (2006) Microbial fuel cells: methodology and technology. Environmental Science & Technology 40(17):5181-92.

Luo H, Liu G, Zhang R, Bai Y, Fu S, Hou Y (2014) Heavy metal recovery combined with H2 production from artificial acid mine drainage using the microbial electrolysis cell. Journal of Hazardous Materials 270:153-9.

Manahan S (2017) Environmental chemistry. CRC press.

Marafi M, Stanislaus A (2008) Spent hydroprocessing catalyst management: A review: Part II. Advances in metal recovery and safe disposal methods. Resources, Conservation and Recycling 53(1-2):1-26.

Miran W, Jang J, Nawaz M, Shahzad A, Jeong SE, Jeon CO, Lee DS (2017). Mixed sulfate-reducing bacteria-enriched microbial fuel cells for the treatment of wastewater containing copper. Chemosphere. 189:134-42.

Modin O, Fuad N, Rauch S (2017) Microbial electrochemical recovery of zinc. Electrochimica Acta 248:58-63.

Monteagudo JM, Ortiz MJ (2000) Removal of inorganic mercury from mine waste water by ion exchange. Journal of Chemical Technology and Biotechnology 75(9):767-72.

Morimoto T, Wu S, Uddin MA, Sasaoka E (2005) Characteristics of the mercury vapor removal from coal combustion flue gas by activated carbon using H2S. Fuel 84(14-15):1968-74.

Naddy RB, Gorsuch JW, Rehner AB, McNerney GR, Bell RA, Kramer JR (2007) Chronic toxicity of silver nitrate to Ceriodaphnia dubia and Daphnia magna, and potential mitigating factors. Aquatic Toxicology 84(1):1-0.

Nagajyoti PC, Lee KD, Sreekanth TV (2010) Heavy metals, occurrence and toxicity for plants: a review. Environmental Chemistry Letters 8(3):199-216.

Nancharaiah YV, Mohan SV, Lens PN (2015) Metals removal and recovery in bioelectrochemical systems: a review. Bioresource Technology 195:102-14.

Purkayastha D, Mishra U, Biswas S (2014) A comprehensive review on Cd (II) removal from aqueous solution. Journal of Water Process Engineering 2:105-28.

Qin B, Luo H, Liu G, Zhang R, Chen S, Hou Y, Luo Y (2012) Nickel ion removal from wastewater using the microbial electrolysis cell. Bioresource Technology 121:458-61.

Qiu R, Zhang B, Li J, Lv Q, Wang S, Gu Q (2017) Enhanced vanadium (V) reduction and bioelectricity generation in microbial fuel cells with biocathode. Journal of Power Sources. 359: 379-83.

Quintelas C, Sousa E, Silva F, Neto S, Tavares T (2006) Competitive biosorption of ortho-cresol, phenol, chlorophenol and chromium (VI) from aqueous solution by a bacterial biofilm supported on granular activated carbon. Process Biochemistry 41(9):2087-91.

Rabaey K, Bützer S, Brown S, Keller J, Rozendal RA (2010) High current generation coupled to caustic production using a lamellar bioelectrochemical system. Environmental Science & Technology 44(11):4315-21.

Rabaey K (2006) Microbial fuel cells: methodology and technology. Environmental Science & Technology 40(17):5181-92.

Reck BK, Müller DB, Rostkowski K, Graedel TE (2008) Anthropogenic nickel cycle: Insights into use, trade, and recycling. Environmental Science & Technology 42(9):3394-400.

Rodenas Motos P, Ter Heijne A, van der Weijden R, Saakes M, Buisman CJ, Sleutels TH (2015) High rate copper and energy recovery in microbial fuel cells. Frontiers in microbiology 6:527.

Sawyer CN, McCarty PL, Parkin GF (1994) Chemistry for environmental engineers. New York. Mc Graw-Hill Book Company.

Shi J, Zhao W, Liu C, Jiang T, Ding H (2017) Enhanced Performance for Treatment of Cr (VI)-Containing Wastewater by Microbial Fuel Cells with Natural Pyrrhotite-Coated Cathode. Water. 9(12):979.

Srivastava NK, Majumder CB (2008) Novel biofiltration methods for the treatment of heavy metals from industrial wastewater. Journal of Hazardous Materials 151(1):1-8.

Stumm W, Morgan JJ (2012) Aquatic chemistry: chemical equilibria and rates in natural waters. John Wiley & Sons.

Tandukar M, Huber SJ, Onodera T, Pavlostathis SG (2009) Biological chromium (VI) reduction in the cathode of a microbial fuel cell. Environmental Science & Technology 43(21):8159-65.

Tao HC, Gao ZY, Ding H, Xu N, Wu WM (2012) Recovery of silver from silver (I)-containing solutions in bioelectrochemical reactors. Bioresource Technology 111:92-7.

Tao HC, Liang M, Li W, Zhang LJ, Ni JR, Wu WM (2011a) Removal of copper from aqueous solution by electrodeposition in cathode chamber of microbial fuel cell. Journal of Hazardous Materials 189(1-2):186-92.

Tao HC, Li W, Liang M, Xu N, Ni JR, Wu WM (2011b) A membrane-free baffled microbial fuel cell for cathodic reduction of Cu (II) with electricity generation. Bioresource Technology 102(7):4774-8.

Tao HC, Zhang LJ, Gao ZY, Wu WM (2011c) Copper reduction in a pilot-scale membrane-free bioelectrochemical reactor. Bioresource Technology 102(22):10334-9.

Tchounwou PB, Yedjou CG, Patlolla AK, Sutton DJ (2012) Heavy metal toxicity and the environment. InMolecular, clinical and environmental toxicology. Springer, Basel.

Teng W, Liu G, Luo H, Zhang R, Xiang Y (2016) Simultaneous sulfate and zinc removal from acid wastewater using an acidophilic and autotrophic biocathode. Journal of hazardous materials 304:159-165.

Twidwell LG, McCloskey J, Miranda P, Gale M (1999) Technologies and potential technologies for removing selenium from process and mine wastewater. InProceedings of the TMS Fall Extraction and Processing Conference Vol. 2, pp. 1645-1656.

Van Phuong N, Kwon SC, Lee JY, Lee JH, Lee KH (2012). The effects of pH and polyethylene glycol on the Cr (III) solution chemistry and electrodeposition of chromium. Surface and Coatings Technology 206(21):4349-55.

Van Phuong N, Kwon SC, Lee JY, Shin J, Lee YI (2011) Mechanistic study on the effect of PEG molecules in a trivalent chromium electrodeposition process. Microchemical Journal 99(1):7-14.

Wang G, Huang L, Zhang Y (2008) Cathodic reduction of hexavalent chromium [Cr (VI)] coupled with electricity generation in microbial fuel cells. Biotechnology Letters 30(11):1959.

Wang H, Luo H, Fallgren PH, Jin S, Ren ZJ (2015) Bioelectrochemical system platform for sustainable environmental remediation and energy generation. Biotechnology Advances 33(3):317-34.

Wang H, Ren ZJ (2014) Bioelectrochemical metal recovery from wastewater: a review. Water Research 66:219-32.

Wang Q, Huang L, Pan Y, Quan X, Puma GL (2017) Impact of Fe (III) as an effective electron-shuttle mediator for enhanced Cr (VI) reduction in microbial fuel cells: Reduction of diffusional resistances and cathode overpotentials. Journal of Hazardous Materials 321:896-906.

Wang Q, Huang L, Pan Y, Zhou P, Quan X, Logan BE, Chen H (2016) Cooperative cathode electrode and in situ deposited copper for subsequent enhanced Cd (II) removal and hydrogen evolution in bioelectrochemical systems. Bioresource Technology 200:565-71.

Wang YH, Wang BS, Pan B, Chen QY, Yan W (2013) Electricity production from a bio-electrochemical cell for silver recovery in alkaline media. Applied Energy 112:1337-41.

Wang Z, Lim B, Choi C (2011) Removal of Hg2+ as an electron acceptor coupled with power generation using a microbial fuel cell. Bioresource Technology 102(10):6304-7.

Wu Y, Zhao X, Jin M, Li Y, Li S, Kong F, Nan J, Wang A (2018) Copper removal and microbial community analysis in single-chamber microbial fuel cell. Bioresource Technology.

Zamani HA, Rajabzadeh G, Firouz A, Ganjali MR (2007) Determination of copper (II) in wastewater by electroplating samples using a PVC-membrane copper (II)-selective electrode. Journal of Analytical Chemistry 62(11):1080-7.

Zhang B, Feng C, Ni J, Zhang J, Huang W (2012) Simultaneous reduction of vanadium (V) and chromium (VI) with enhanced energy recovery based on microbial fuel cell technology. Journal of Power Sources 204:34-9.

Zhang BG, Zhou SG, Zhao HZ, Shi CH, Kong LC, Sun JJ, Yang Y, Ni JR (2010) Factors affecting the performance of microbial fuel cells for sulfide and vanadium (V) treatment. Bioprocess and Biosystems Engineering 33(2):187-94.

Zhang B, Zhao H, Shi C, Zhou S, Ni J (2009) Simultaneous removal of sulfide and organics with vanadium (V) reduction in microbial fuel cells. Journal of Chemical Technology and Biotechnology 84(12):1780-6.

Zhang LJ, Tao HC, Wei XY, Lei T, Li JB, Wang AJ, Wu WM (2012) Bioelectrochemical recovery of ammonia–copper (II) complexes from wastewater using a dual chamber microbial fuel cell. Chemosphere 89(10):1177-82.

5 Ammonium Sulfate Production from Wastewater and Low-grade Sulfuric Acid Using Bipolar- and Cation-exchange Membranes

The ammonia concentration in the dewatering centrate is significantly high. On the one hand, ammonia needs to be removed since high ammonia concentration in water can cause algal blooms. On the other hand, ammonia products (e.g., ammonium sulfate) are widely used as fertilizers for food products. Therefore, we proposed a novel technology to recover ammonia from municipal wastewater and produce high-purity ammonium sulfate as final products. An electrodialysis reactor with bipolar membranes (BMPs) and cation exchange membranes (CEMs) but without anion exchange membranes (AEMs) was built in this study. Various operating conditions, such as applied voltage and linear velocity, were examined to maximize the ammonia recovery rate. Energy consumption was evaluated and compared with other ammonia production methods.

The following published journal article is included in this chapter.

- Guo, H., Yuan, P., Pavlovic, V., Barber, J., & Kim, Y. (2021). Ammonium sulfate production from wastewater and low-grade sulfuric acid using bipolar- and cation-exchange membranes. *Journal of Cleaner Production*, *285*, 124888.

The co-author’s contributions: Funding acquisition; membrane supply; Supervision; technical support; manuscript review and revision.

Abstract

Conventional electrodialysis can be used to recover ammonia from dewatering centrate (i.e., down-stream wastewater from digested sludge dewatering). However, ionic impurities of the recovered ammonia solution are still a limiting factor for broad applications of ion-exchange membranes (IEMs) in wastewater treatment and resource recovery. In this study, an electrodialysis stack with bipolar membranes (BPMs) and cation exchange membranes (CEMs) but without anion exchange membranes (AEMs) was examined under various operation conditions to demonstrate high-purity ammonium sulfate production using low-grade sulfuric acid and dewatering centrate. Two significant benefits of removing AEMs from the bipolar membrane electrodialysis (BMED) are no more membrane fouling problems on AEMs and complete exclusion of impurity anions (e.g., chloride ions) in the recovered ammonium sulfate solution. A higher applied voltage condition (30 V over 7 pairs of CEM and BPM) resulted in a substantially high ammonia recovery (88.4%) and concentration (4.34 g-N/L) in 90 min. The ammonia recovery and concentration were also improved by increasing the flow rate through the BMED stack. The lowest electric energy consumption in the membrane stack was 9.6 kWh/kg-N, indicating energy efficient production of high-purity ammonium sulfate from wastewater. The amount of divalent cation scales accumulated in the BMED stack was linearly proportional to the average electric current, implying that the scaling problem can be controlled by reducing the applied voltage. Even with the scale accumulation, the electric current generation (i.e., separation performance) was hardly affected during the experiment.

These findings demonstrated the strong potential of AEM-lacking BMED for practical ammonia separation from wastewater with reduced impurities.

Keywords

Bipolar membrane, Electrodialysis, Ammonia recovery, Clean-in-place (CIP), Membrane fouling, Divalent cation scaling

5.1 Introduction

The ammonia concentration in dewatering centrate (down-stream wastewater from dewatering process of digested sludge) is significantly high (often 1000 mg-N/L or higher) (Holloway et al., 2007; Galvagno et al., 2016) because of the breakdown of proteins during anaerobic digestion. In conventional wastewater treatment plants, dewatering centrate is usually sent back to the mainstream wastewater treatment processes and mixed with raw wastewater. As a result, dewatering centrate contributes to 15 – 20% of influent nitrogen load (Flux et al., 2002). The high nitrogen load leads to high operating costs (e.g., intensive aeration and high return sludge pumping) and poor water quality of the final effluent. In most developed countries, including Canada, treated wastewater effluents are strictly regulated for nearly complete removal of ammonia and organic nitrogen (CCME 2001). Several new methods, such as SHARON, anammox, and struvite precipitation (Mulder et al., 2001; Flux et al., 2002; Strous et al., 1997; Huang et al., 2016), are under development for the removal or recovery of ammonia from dewatering centrate. However, these methods have various challenges, such as long sludge retention time, low recovery efficiency, and a large amount of chemical consumption.

Electrodialysis (ED) has been investigated and examined for ammonia recovery from wastewater (Mondor et al., 2008; Ippersiel et al., 2012; Ward et al., 2018). A conventional ED stack, consisting of cation-exchange membranes (CEMs) and anion-exchange membranes (AEMs), can achieve ionic separation from the dilute to concentrate cells. In previous studies, significantly high ammonia concentration (> 14 g-N/L) was demonstrated using swine manure (Mondor et al., 2008; Ippersiel et al., 2012). A pilot ED system achieved 7.1 g-N/L of ammonia recovery from centrate (Ward et al., 2018). These results indicated that ED can be used to recover ammonia efficiently from wastewater. However, fouling of IEMs especially AEMs is one of the common problems in ED application (Lee et al., 2002a; Lee et al., 2002b; Ruiz et al., 2007; and Lee et al., 2008; Choi et al., 2016). In addition, anions, such as Cl^- and HCO_3^-, are also concentrated through AEMs in conventional ED systems. Such impurity anions reduce the commercial value of the concentrated ammonia solution and thus require further treatment to make it a readily applicable ammonia product. In this study, bipolar membranes (BPMs) were proposed to replace AEMs in an ED system so that serious membrane fouling problems and unwanted anions can be excluded. Thus, a high purity ammonia solution can be produced from wastewater (e.g., dewatering centrate).

A BPM is manufactured by chemically attaching a CEM and an AEM (Simon, 1993; Bauer et al., 1988). At the interface between the CEM and AEM, water is dissociated into protons (H^+) and hydroxyl ions (OH^-) under a sufficiently strong electrical field. Thus, bipolar membrane electrodialysis (BMED) has been regarded as an efficient tool for acid and base production (Pourcelly, 2002; Audinos, 1997; Cherif et al., 1997; Paleologou et

al., 1997; Huang and Xu, 2006; Zhang et al., 2011; Ye et al., 2015; Tran et al., 2015; Sun et al., 2017; Lei et al., 2020; Marta et al., 2020; Melnikov et al., 2020; Yao et al., 2019; Heinonen et al., 2020; Herrero-Gonzalez et al., 2020a; Herrero-Gonzalez et al., 2020b; Kumar et al., 2019). BMED also has been applied in wastewater treatment (Tian et al., 2019; Lin et al., 2019; Gao et al., 2020). Applications of BMED in ammonia recovery from simulated wastewater were reported (Li et al., 2016; Shi et al., 2018; van Linden et al., 2020). However, BMED operation requires relatively high electric energy consumption for water dissociation compared to conventional ED (Strathmann, 2004). The energy consumption in a two-cell BMED (BPMs with AEMs or CEMs) is lower than that in a three-cell BMED (BPMs, CEMs, and AEMs) (Xu and Yang, 2002; Li et al., 2016). In addition, organic anions in dewatering centrate (e.g., conjugate base anions of organic acids) are relatively low in concentration after proper digestion; thus, it is difficult to concentrate them to a sufficiently high concentration for commercial uses. Inorganic anions in dewatering centrate are mostly chloride and bicarbonate ions while phosphate is usually low (Yuan and Kim, 2017). Since acid recovery from dewatering centrate is not meaningful, we removed the acid cells by removing AEMs from a BMED stack. An additional benefit of removing the acid cells is very low pH conditions in the feed cells where dewatering centrate flows through in the BMED stack. As a result, inorganic scaling and organic fouling can be effectively controlled in the feed cells.

Among various ammonia products, ammonium sulfate has broad industrial demand and high market values. For instance, approximately 2 million tons of ammonium sulfate are demanded in the United States per year (Chou et al., 2005). Ammonium sulfate is also

known to have a high commercial value as one ton of granular ammonium sulfate ranges from $75 to $130 (Chou et al., 2005). Ammonium sulfate is usually produced by mixing ammonia and sulfuric acid or produced as a coke oven by-product (Weston et al., 2000). These methods are expensive because of high energy consumption and a large amount of chemical demand. Thus, in this study, we focused on recovering ammonia from dewatering centrate in the form of ammonium sulfate using low-grade sulfuric acid solutions (< 0.1 M H_2SO_4).

The applied voltage is an important operation factor that governs the performance of ED separation, including BMED stacks. High applied voltages enhance the rate of separation of ions and accelerate the rate of water dissociation. In addition, the high flow rate can reduce the mass transfer limitation (Walker et al., 2014; Kim et al., 2011) and thus contribute to the rapid transfer of ions. Therefore, we investigated various applied voltage and flow rate conditions to optimize and accelerate ammonium sulfate production using an AEM-lacking BMED system (ED with BPMs and CEMs). Scaling is a challenge in the application of IEM systems for water and wastewater treatment (Gryta, 2009; Warsinger et al., 2015). Common divalent cations in dewatering centrate, such as Ca^{2+} and Mg^{2+}, can form precipitates with CO_3^{2-}, SO_4^{2-}, or OH^-. These precipitates cause serious scaling problems on IEMs and reduce the energy and separation efficiencies of the ED systems. The effects of scaling on the performance of an ED system with long-term operations were reported in a previous study (De Paepe et al., 2018). Thus, clean-in-place (CIP) is essential for ED operation to restore IEM performance. NaOH and NaCl solutions are common cleaning solutions for removing organic foulants (Mikhaylin and Bazinet, 2016; Mondor

et al., 2009; Pronk et al., 2007) while acid reagents (such as HCl and citric acid) can be used to remove both inorganic scalants and organic foulants (Mikhaylin and Bazinet, 2016; Guo et al., 2015; Talebi et al., 2019; Wang et al., 2011; Mondor et al., 2019; Pronk et al., 2007). Therefore, a two-step CIP was employed using NaCl and HCl in this study, and we analyzed the cleaning solutions after CIP for Ca^{2+} and Mg^{2+} to investigate the effects of the applied voltage and flow rate on scaling control.

5.2 Material and methods

5.2.1 BMED construction

Two polypropylene blocks were used to build the BMED reactor. The BMED stack consisting of 7 pairs of CEM (CR67, SUEZ Water Technologies & Solutions, Canada) and BPM (made of AR103 and CR61, SUEZ Water Technologies & Solutions, Canada) was sandwiched between the anode and cathode (Figure 5.1A). The anode and cathode were platinum plates coated with titanium. The main characteristics of ion-exchange membranes (IEMs) were shown in Table 5.1. A silicone spacer with non-tortuous plastic mesh (36.7 cm^2 of open area, 0.08 cm of thickness) was placed between membranes (Appendix, Figure C1). The thin inter-membrane distance, which reduced the resistance for ionic separation, was maintained since the thickness of the spacer was around 1 mm. An AEM (AR 204, SUEZ Water Technologies & Solutions, Canada) was placed next to the cathode while an extra CEM (CR67, SUEZ Water Technologies & Solutions, Canada) was placed to the anode. These two membranes prevent the transfer of ions from the feed cells to the electrode rinse cells (Figure 5.1A).

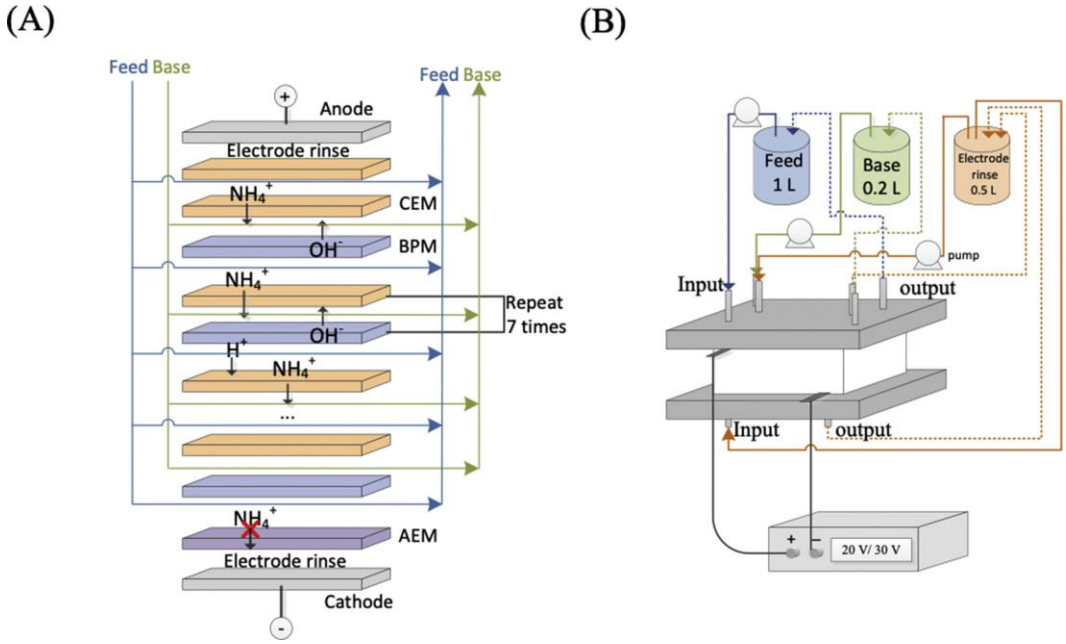

Figure 5.1. Schematic of (A) the BMED stack and (B) the operating system.

Table 5.1. IEM characteristics

	CR67	AR204	BPM
Thickness (mm)	0.6	0.5	1.1
Burst strength (kPa)	1034.2	1034.2	> 2206.3
Ion-exchange capacity (meq/dry gram membrane)	≥ 2.1	≥ 2.4	-
Resistivity[a] (Ω-cm^2)	10.0	7.0	-
Transport number[b]	95%	82%	-
pH operation range	1-14	< 10	1-14
Maximum current density (mA/cm^2)	100	100	100

[a.] Resistivity in 10 mM NaCl

[b.] Transport number at 0.5 N NaCl: 1 N NaCl

5.2.2 BMED operation

Dewatering centrate was collected from the local wastewater treatment plant and stored at 4°C for no longer than 2 weeks. The main characteristics of the dewatering centrate were shown in Table 5.2. During the operation, dewatering centrate (1.0 L) was used as the feed solution. Sodium sulfate (100 mM Na_2SO_4, VWR International, Canada) was used as the electrode rinse reagent (0.5 L). The base solution was initially prepared with 0.2 L (20% of the feed volume) of low-grade sulfuric acid (0.09 M, pH of 1.65 ± 0.05, Thermo Fisher Scientific, USA). The BMED system was operated for 2 hours in the continuous-recycle mode where dewatering centrate feed, electrode rinse, and the base solution were recirculated between the BMED reactor and the reservoirs using peristaltic pumps (Figure 5.1B). The feed solution (dewatering centrate) and base solution (low-grade sulfuric acid) were operated at three different flow rates (60, 120, and 180 mL/min or linear velocities of 0.47, 0.93, and 1.40 cm/s, respectively) while the electrode rinse was operated at 90 mL/min (4.90 cm/s). Two different applied voltages of 20 and 30 V were applied to the BMED system by using an external power supplier (Model 9201, BK Precision, USA). The electric current of the BMED stack was monitored and recorded every 10 seconds using a digital multimeter and data acquisition system (34970A, Agilent Technologies, USA) and then normalized by the effective area of the membrane (36.7 cm^2) to obtain the area-based current density. It should be noted that the constructed BMED was operated using dewatering centrate and deionized water at various flow rates and applied voltages before the operation with dewatering centrate and sulfuric acid.

Table 5.2. Dewatering centrate characteristics (n = 4)

Component	Average ± standard deviation
NH_3-N	1.19 ± 0.03 g/L
Ca^{2+}	120.66 ± 3.46 mg/L
Mg^{2+}	81.66 ± 2.42 mg/L
K^+	101.58 ± 4.24 mg/L
Na^+	275.21 ± 7.66 mg/L
Conductivity	10.38 ± 0.05 mS/cm
pH	7.63 ± 0.08

Divalent cations, such as Ca^{2+} and Mg^{2+}, can form precipitates in the base cells. A two-step CIP was conducted with two cleaning reagents: 5% (w/w) sodium chloride (0.2 L NaCl, VWR International, Canada); and 5% (w/w) hydrochloric acid (0.2 L HCl, VWR International, Canada) by following the guidance of the manufacturer after each experiment. The feed, base, and electrode rinse solutions were operated independently with 0.2 L NaCl for 1.5 hours first and then operated with 0.2 L HCl for the other 1.5 hours. The feed and base pumps were operated at 180 mL/min while the electrode rinse flowed at 90 mL/min during CIP. Also, the flow direction was changed every 45 min during CIP.

5.2.3 Single CEM and AEM unit

The voltage loss at each cell pair (E_{cp}) was evaluated from the overall applied voltage of the BMED system ($E_{overall}$) and the voltage loss at the electrodes and electrode membranes ($E_{electrode}$) (Eq 5.1). To determine $E_{electrode}$, a single CEM and AEM unit was designed by removing the CEM and BPM stack from BMED system (Appendix, Figure C2A). The experiment was operated with 1 L of dewatering centrate and 0.5 L of 100 mM

Na_2SO_4. These solutions were circulated at the same linear velocity as the feed flow and electrode rinse flow during the BMED operation. The applied voltage of the single unit ranged from 2 to 7 V. The electric current was linearly proportional to $E_{electrode}$ (Appendix, Figure C2B).

$$E_{cp}\ (V/\text{cell pair}) = \frac{E_{overall}\ (V) - E_{electrode}(V)}{7\ \text{cell pair}} \quad (Eq\ 5.1)$$

5.2.4 Experimental measurement

Samples from the base (1 mL), feed (5 mL), and electrode rinse (5 mL) were collected from the reservoirs at 0, 15, 30, 60, and 120 min. These samples were analyzed for ammonia concentration by using commercial ammonia test vials (Method 10205, Hach Company, USA). Apart from the NH_4^+, the collected samples were analyzed by inductive coupled plasma-optical emission spectrometry (ICP-OES, Vista Pro, Varian Inc., Australia) to quantify the concentration of cations (Ca^{2+}, Mg^{2+}, Na^+, and K^+). Before the analysis, the collected samples were acidified with 70% nitric acid (w/w) and filtered using syringe filters (pore size 0.45 μm, polyethersulfone membrane, VWR International, USA). The cleaning solutions after each CIP were collected and analyzed in ICP-OES for Ca^{2+} and Mg^{2+} to quantify the scaling problem in the BMED stack and the cleaning efficiency of CIP. In addition, the pH and conductivity of the feed and base solutions were analyzed and recorded (Orion Versa Star Pro, Thermo Fisher Scientific, USA).

5.2.5 Ammonia recovery, current efficiency, and energy consumption

The ammonia recovery is the ratio between the ammonia mass in the base solution and the initial ammonia mass in the feed solution (Eq 5.2):

$$\text{Ammonia recovery} = \frac{(C_B(t)V_B(t) - C_{B,0}V_{B,0})}{C_{F,0}V_{F,0}} \quad \text{(Eq 5.2)}$$

$C_{B,0}$ (g/L) and $C_B(t)$ (g/L) are the concentration of the ammonia in the base solution at time 0 and t (s), $V_{B,0}$ (L) and $V_B(t)$ (L) are the volumes of the base solution at time 0 and t (s), $C_{F,0}$ (g/L) is the concentration of the ammonia in the feed solution at time 0, and $V_{F,0}$ (L) is the initial volume of the feed solution.

The current efficiency based on ammonia removal (CE_{NH4^+}) is the ratio between the amount of ammonium that was separated from the feed to the base and the number of electrons that were generated from electric current (Eq 5.3):

$$CE_{NH4^+} = \frac{F(C_F(t)V_F(t) - C_{F,0}V_{F,0})}{n\sum I_t \Delta t} \quad \text{(Eq 5.3)}$$

$C_F(t)$ (M) is the concentration of the ammonia in the feed solution at time t (s), $V_F(t)$ (L) is the volume of the feed solution at time t (s), F is the Faraday's constant (96485 C/mol), n is the number of cell units (repeated units of CEM and BPM, n = 7), I_t (A) is the electric current at t (s), and Δt is the time interval for recording the electric current (Δt = 10 s).

The energy consumption (kWh/kg-N) of the membrane stack was calculated based on Eq 5.4:

$$\text{Energy consumption} = \frac{\Sigma(E_{overall} - E_{electrode})I_t \Delta t}{3600 \times (C_B(t)V_B(t) - C_{B,0}V_{B,0})} \quad \text{(Eq 5.4)}$$

Note that the pumping energy was not included because ED is not a pressurized membrane system and thus the energy cost for pumping is relatively low compared to the energy requirement for voltage applications (Strathmann, 2004).

The solubility index (SI) was given by the log of the ratio between the ion activity product (IAP) and the solubility constant (K_{sp}) (Davis and Masten, 2013):

$$SI = \log \frac{IAP}{K_{sp}} \quad \text{(Eq 5.5)}$$

If SI is positive, then the solution is supersaturated (i.e., precipitates are likely formed).

5.3 Results and discussion

5.3.1 Effects of applied voltage on ammonia recovery

The ammonia recovery and maximum ammonia concentration in the base solution increased with the increasing applied voltage (Figures 5.2A and 5.2B). The maximum ammonia recovery was 88.4% at 30 V while it was 69.8% at 20 V (Figure 5.2A). This result is consistent with the previous study where high electric current densities (Figure 5.2C) enhanced the transport of ions and thus increased the concentration of the base solution (Li et al., 2016). Ammonia was concentrated by a factor of 3.1 at 20 V (from 1.176 ± 0.012 to 3.623 ± 0.025 g-N/L) while the concentration factor was even higher at 3.7 for the 30 V application (from 1.170 ± 0.003 to 4.345 ± 0.002 g-N/L) (Figure 5.2B). The concentration factors were lower than the volume ratio (5) of the feed and base reservoirs due to the ammonia loss and increased ammonia concentration gradient (Figure 5.2B). Because of the small volume of the base reservoir (i.e., 1/5 of the feed reservoir), the ammonia concentration gradient was substantial, resulting in the decreased ammonia recovery rate (i.e., decreased slope) (Figure 5.2A).

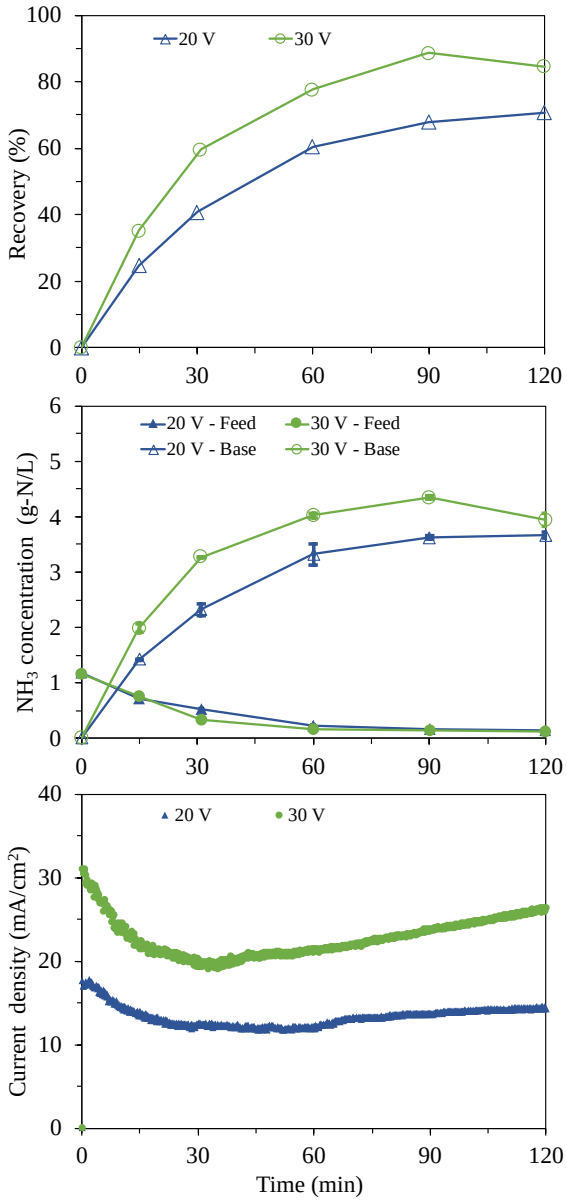

Figure 5.2. Effects of the applied voltage on (A) ammonia recovery, (B) ammonia concentration in the feed and base reservoirs, and (C) electric current density.

The electric current decreased gradually in the early stage of the BMED operation and then increased steadily (Figure 5.2C). The change of the electric current can be explained by the variable conductivity of the feed and base solution (Appendix, Figure C3). The

conductivity in the feed reservoirs decreased gradually in the early stage of the experiment because of the separation of NH_4^+. Meanwhile, the conductivity of the base reservoir dropped sharply because hydroxide ions from BPMs consumed protons from sulfuric acid. In the late stage of the experiment, the conductivity of the feed reservoir increased steadily (Appendix, Figure C3) since the production of H^+ was more dominant than NH_4^+ removal. The conductivity in the base reservoir was stationary due to the slow ammonia recovery. Therefore, the electric current density increased gradually in the late stage of BMED operation (Figure 5.2C). $E_{electrode}$ of the system was 4.85 V ($E_{overall}$ = 20 V) and 6.42 V ($E_{overall}$ = 20 V) since the average current was 0.49 A (20 V) and 0.83 A (30 V) (Appendix, Figure C2B). Thus, E_{cp} at 20 V and 30 V was 2.16 and 3.37 V/cell pair (Eq 5.1), respectively. It should be noted that the electric current density in the BMED (12-32 mA/cm^2, Figure 5.2C) was much smaller than the maximum allowable electric current density for the BPMs (100 mA/cm^2, Table 5.1). Therefore, the bipolar membrane did not limit the overall performance of the BMED operation (Krol et al., 2001; Aritomi et al., 1996).

The higher applied voltage resulted in the lower $CE_{NH_4^+}$ (Appendix, Figure C4A). This result can be explained by the accelerated separation of other cations such as H^+ and K^+ at the high applied voltage (30 V). At 30 V, more H^+ was produced (lower pH in the feed chamber as shown in Appendix, Figure C4B) because of the accelerated water splitting. The high concentration of H^+ enhanced the transfer of H^+, resulting in the lower $CE_{NH_4^+}$. Also, the increased ammonia concentration gradient across the CEMs (Figure 5.2B) resulted in the decreased $CE_{NH_4^+}$ (Appendix, Figure C4A). The $CE_{NH_4^+}$ decreased from 86%

(15 min) to 28% (120 min) at 20 V. The demonstrated $CE_{NH_4^+}$ (Appendix, Figure C4A) was lower than the CEs in previous BMED systems feed with salt solution or pretreated wastewater (> 80%) (Tran et al., 2015, Li et al., 2015). The low $CE_{NH_4^+}$ in this study can be explained by the separation of other cations, such as H^+ and K^+.

$CE_{NH_4^+}$ was 64% (30 min) at 30 V for 60% ammonia recovery (Figure 5.2B and Appendix, Figure C4A). Assuming an example full-scale BMED stack with 500 cell pairs under typical operation conditions (an effective membrane area of 0.96 m^2; electric current density of 100 A/m^2) (Strathmann, 2010; Porter, 1989; Baker, 2012; Pawlowski, 2014; Tsiakis and Papageorgiou, 2005), the ammonia separation rate is expected to be 16 kg-N/h. Assuming that the same dewatering centrate (Table 5.1) is treated in the full-scale BMED system, the ammonia loading rate will be 108 kg-N/hr (for an assumed flow rate of 90 m^3/hr in full-scale ED systems, Tsiakis and Papageorgiou, 2005). Therefore, the dewatering centrate needs to be treated in 4 BMED stacks in series to achieve 60% ammonia recovery in a full-scale BMED system. This sample calculation indicates high feasibility of BMED applications in high-purity ammonia production from dewatering centrate or high-nutrient wastewater streams.

5.3.2 Ammonia loss by volatilization

It should be emphasized that the maximum ammonia concentration in the base reservoir was observed at 90 min and the ammonia concentration decreased from 4.345 ± 0.002 to 3.938 ± 0.114 g-N/L after 90 min for 30 V (Figure 5.2B). This decreased ammonia concentration can be explained by the ammonia loss by volatilization from the base reservoir. During the operation, the substantially high pH (up to 10) of the base solution

(Appendix, Figure C4B) resulted in more than 50% of un-ionized ammonia existed in aqueous solutions. In addition, the high ammonia concentration (Figure 5.2B) in the base solution likely contributed to the volatilization of ammonia from the base reservoir. During the operation, the strong smell of ammonia gas also indicated the volatilization of ammonia. Note that ammonia loss from the base to electrode rinse was not feasible because of the AEM located next to the cathode in the BMED stack design (Figure 5.1A). Furthermore, the ammonia concentration in the electrode rinse was always smaller than 0.01 g/L at the end of the operation, indicating that the negligible amount of ammonia was transferred to the electrode rinse solution. Thus, the majority of the ammonia loss can be explained by volatilization from the base reservoir. For instance, at the end of the experiments, 5.2% of ammonia was lost for the operation at 30 V and 180 mL/min.

5.3.3 Effects of flow rate or linear velocity on ammonia recovery

The higher flow rate (i.e., water flow velocity in the BMED stack) resulted in the higher ammonia recovery (Figure 5.3A). The highest ammonia recovery of 88.4% was observed at the flow rate of 180 mL/min (water flow velocity of 1.40 cm/s) while the ammonia recovery was 76.1% at 120 mL/min (0.93 cm/s) and 68.7% at 60 mL/min (0.47 cm/s) (Figure 5.3A). The maximum ammonia concentration in the base reservoir was 4.345 ± 0.002 g-N/L (180 mL/min), which was higher than 3.813 ± 0.064 g-N/L at 120 mL/min and 3.703 ± 0.004 g-N/L at 60 mL/min (Figure 5.3B). The high electric current density at the high flow rate (Figure 5.3C) was consistent with the high ammonia

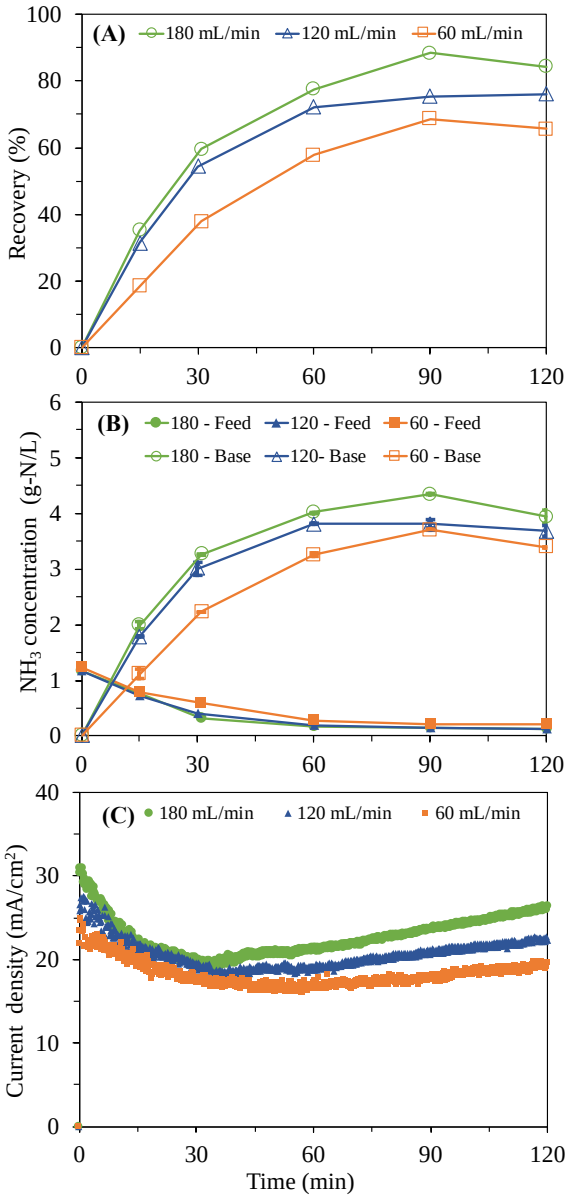

Figure 5.3. The effects of flow rate (i.e., linear velocity in the BMED stack) on (A) ammonia recovery, (B) ammonia concentration in the feed and base chamber, and (C) electric current density.

recovery results (Figure 5.3A). The increased electric current density can be explained by the decreased mass-transfer limitation near the membrane surfaces. This result was

consistent with previous studies where a high flow rate increased the degree of mixing conditions and further increased the electric current (Walker et al., 2014; Kim et al., 2011).

It should be noted that the increase in the ammonia recovery was significant when the flow rate increased from 60 to 120 mL/min for the first 60 min (Figure5.3A). However, there was a subtle increase in the ammonia recovery when the flow rate increased from 120 to 180 mL/min. Therefore, a further increase in the flow rate above 180 mL/min (1.40 cm/s) was not expected to improve ammonia recovery using the BMED system. The ammonia volatilization also resulted in the decrease in ammonia concentration (Figure 5.3B). 18.7 % of ammonia was lost at 60 mL/min while 13.3% and 5.2% of ammonia were lost at 120 and 180 mL/min, respectively.

It was found that the examined flow rate conditions did not have significant effects on CE_{NH4^+} (Appendix, Figure C5) while the applied voltage directly affected CE_{NH4^+} (Appendix, Figure C4A). This result indicated that the increased electric current by increasing the flow rate is directly contributed by the increased ammonia separation. However, the high voltage conditions not only enhanced the ammonia separation but also accelerated the production of H^+ and OH^- at the bipolar membranes.

5.3.4 Competing cations in ammonia removal

The high applied voltage application (30 V) in the BMED system resulted in enhanced removal of cations (Figures 5.4A and 5.4B).

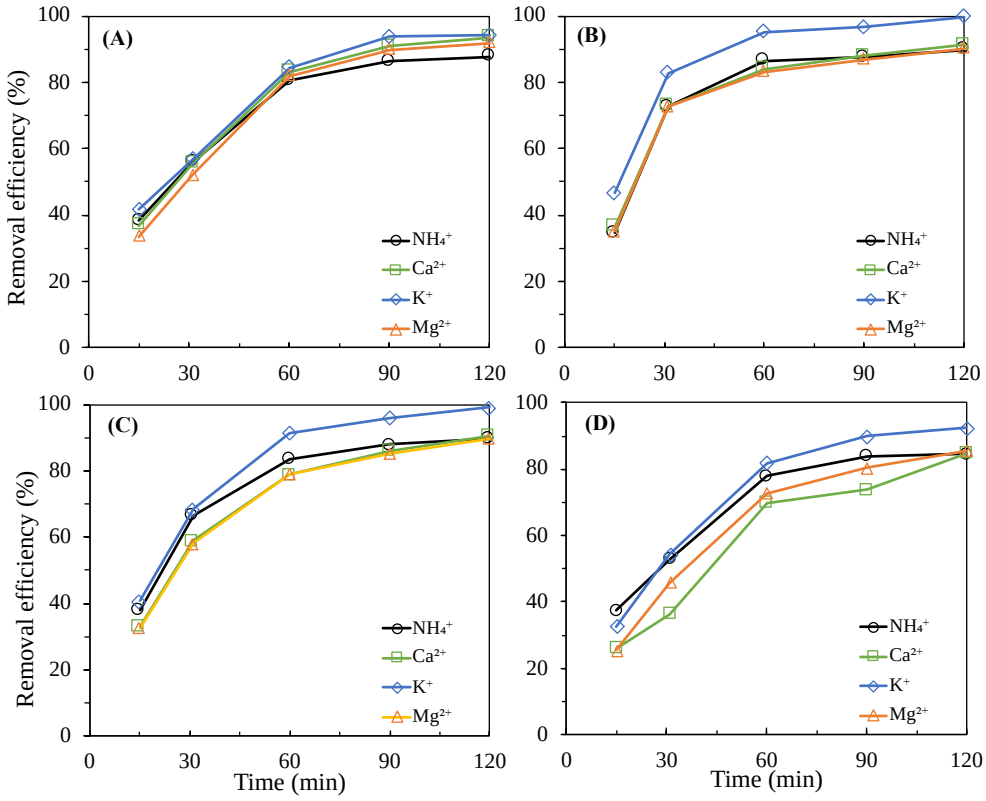

Figure 5.4. The removal efficiency of cations based on the feed reservoir concentration for (A) 20 V and 180 mL/min; (B) 30 V and 180 mL/min; (C) 30 V and 120 mL/min; (D) 30 V and 60 mL/min.

The highest removal efficiency was observed for K^+ at 30V (Figures 5.4A and 5.4B). For 30 V application, 99.7% of K^+ was separated from the feed and transferred into the base at the end of the operation (Figure 5.4B and Table 5.3). The rapid removal (i.e. large slope) of K^+ can be explained by the high equivalent ionic conductivity (Table 5.3). The removal of NH_4^+ was slower than the removal of K^+ (Figures 5.4A, 5.4B, and Table 5.3) although the equivalent ionic conductivities of NH_4^+ and K^+ were close (Table 5.3). This result indicated that the high ammonia concentration gradient between the base and feed cells

slowed down the ammonia separation in the BMED stack. The high ammonia concentration gradient also resulted in the lowest removal efficiency of NH_4^+ at 20 V. Comparing removal efficiency of all cations at 20 V, the removal efficiency of NH_4^+ was lower than 88% while the other cations were higher than 92% (Figure 5.4A). The removal efficiency of Ca^{2+} and Mg^{2+} was similar (Figures 5.4A and 5.4B) because of the close equivalent ionic conductivity (Table 5.3). In addition, the removal efficiency of cations was significantly improved by increasing the applied voltage, especially in the early stage of BMED operation. The removal efficiency of NH_4^+ was 55.8% at 20 V (Figure 5.4A) while that was 72.6% at 30 V in the first 30 min (Figure 5.4B). The results for K^+, Mg^{2+}, and Ca^{2+} removal were consistent with the results of NH_4^+ removal that more than 70% of cations were removed at 30 V while less than 60% of cations were removed at 20 V. The removal efficiency of Na^+ did not include in the discussion since the feed cells received the Na^+ from the electrode rinse cells.

Table 5.3. Equivalent ionic conductivity of major cations in dewatering centrate (adapted from Weast et al., 1988) and the removal efficiency of cations at 30 V and 180 mL/min

ions	Λ (10^{-4} m^2 S mol^{-1})	Removal efficiency (%)				
		15 min	30 min	60 min	90 min	120 min
NH_4^+	73.50	34.5	72.6	86.5	87.4	89.8
K^+	73.48	46.5	82.8	95.1	96.7	99.8
Ca^{2+}	59.47	36.5	72.9	84.0	88.0	91.3
Mg^{2+}	53.00	35.0	72.6	63.2	86.8	90.3

The high flow rate resulted in the high removal efficiency for all ions (Figures 5.4B, 5.4C, and 5.4D). The highest removal efficiency was observed for K^+ and more than 90%

of K^+ was removed at the end of the operation regardless of the flow rate (Figures 5.4B, 5.4C, and 5.4D). The NH_4^+ removal efficiency increased from 84.6% to 89.7% when the flow rate increased from 60 mL/min to 120 mL/min (Figures 5.4C and 5.4D). However, there was a subtle increase (0.1%) in NH_4^+ removal when the flow rate increased from 120 to 180 mL/min (Figures 5.4B and 5.4C). Similar trends were observed for the removal of Ca^{2+} and Mg^{2+} (Figures 5.4B, 5.4C, and 5.4D). The removal efficiency increased by 5.9% (84.7% at 60 mL/min, 90.6% at 120 mL/min) and 0.7% (91.3% at 180 mL/min) for Ca^{2+} while that increased by 4.2% (85.5% at 60 mL/min, 89.7% at 120 mL/min) and 0.6% (90.3% at 180 mL/min) for Mg^{2+} (Figures 5.4B, 5.4C, and 5.4D).

The BMED stack design without AEMs played an important role in increasing the purity of the ammonia product. Anions, such as Cl^- and HCO_3^-, were excluded in the ammonium sulfate solution. The non-ideal transfer of anions through CEMs was negligible since the transport number for the CEMs was 95% at 0.5 N NaCl to 1 N NaCl (Table 5.1). In addition, the concentration of anions in the dewatering centrate was lower than 0.5 N.

5.3.5 Scaling control in BMED operation

The amount of divalent cation scales accumulated in the BMED system was linearly proportional to the average electric current (Figure 5.5). The high electric current contributed to a sharp concentration gradient by concentration polarization in the boundary layer on the base side of the CEM (Strathmann, 2004). As a result, the higher ionic concentration at the CEM surface with a higher electric current induced a greater amount of precipitates on the CEM. In addition, the high electric current produced more hydroxide in the base cell (Appendix, Figure C4B), resulting in substantially intensified scale

formation. In the ICP-OES analysis results, 82.6 - 91.8% of Ca^{2+} and 62.6 - 76.0% of Mg^{2+} (compared with the mass of Ca^{2+} and Mg^{2+} in the feed dewatering centrate) were precipitated during the BMED operation (Appendix, Table C1 and C2). Among these precipitates, 48.0 - 59.4% of Ca^{2+} and 36.3 - 43.9% of Mg^{2+} were observed in the cleaning solution after the post-operation CIP (Appendix, Table C1 and C2). These results indicated that half of Ca^{2+} and Mg^{2+} precipitates were accumulated in the membrane stack when half of the precipitates were deposited in the base reservoir. It should be emphasized that the scales hardly affected the separation performance since the electric current density was stable (Figures 5.2C and 5.3C).

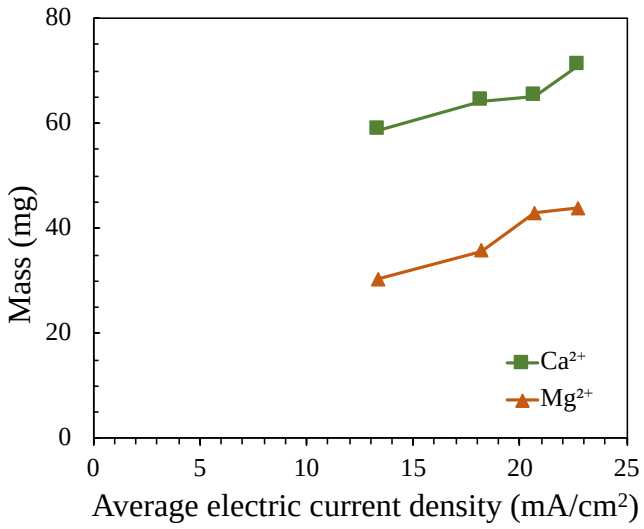

Figure 5.5. The mass of Ca^{2+} and Mg^{2+} in the cleaning solution with different current density. (13.3 mA/cm^2 under 20 V and 180 mL/min; 18.2 mA/cm^2 under 30 V and 60 mL/min; 20.7 mA/cm^2 under 30 V and 120 mL/min; and 22.7 mA/cm^2 under 30 V and 180 mL/min).

The formation of precipitates resulted in the low concentration of Ca^{2+} and Mg^{2+} in the base aqueous solution (Figures 5.6A and 5.6B).

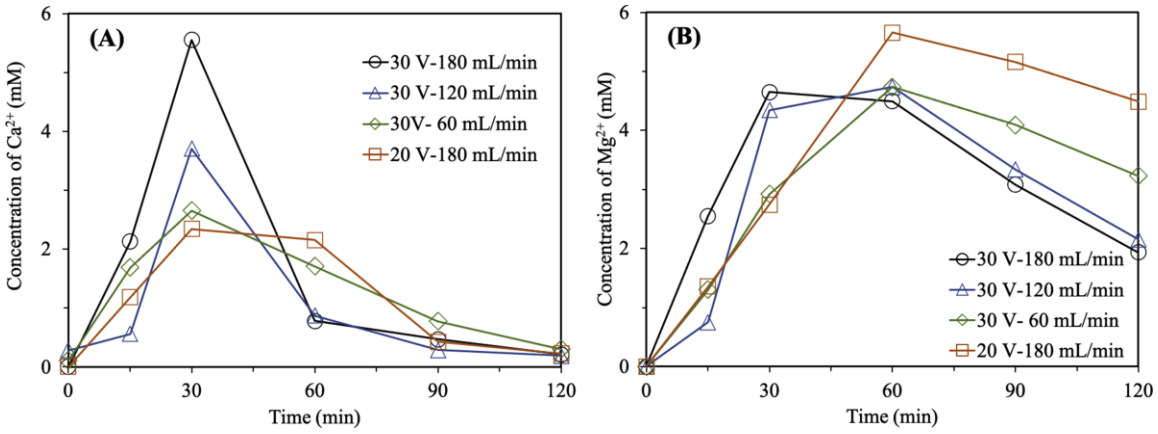

Figure 5.6. The concentration of aqueous phase cations in the base reservoir: (A) Ca^{2+} and (B) Mg^{2+}.

The base solution in the reservoir became cloudy during the BMED operation, indicating the formation of the precipitates. The dominant precipitates in the base solution were $CaSO_{4,(s)}$ and $Mg(OH)_{2,(s)}$ according to SI for potential precipitates (Table 5.4). This theoretical prediction was also consistent with the ICP-OES analysis results of the CIP solution (Figure 5.6). The base chamber was initially prepared with 90 mM H_2SO_4. The low pH (< 4) (Appendix, Figure C4B) and low divalent cations concentration prevented the formation of precipitates in the early stage of the BMED operation (0 - 30 min). Along with the pH increase after 30 min, the formation of precipitates ($CaSO_{4,(s)}$) resulted in a significant decrease in the concentration of Ca^{2+} (Figure 5.6). The decrease in Mg^{2+} concentration was slower than the decrease in Ca^{2+} concentration. The slower decrease in Mg^{2+} concentration indicated that $Mg(OH)_{2,(s)}$ precipitation occurred in the later stage (i.e., 60 min or later) while $CaSO_{4,(s)}$ precipitation was dominant in the early stage of the BMED

operation (i.e., 30 - 60 min) (Figure 5.6). It should be noted that even with tens of the repeated experiments for various experimental conditions that resulted in serious scaling problems, noticeable membrane damages or failures (e.g., punctured membranes) were not observed.

Table 5.4. The solubility indices for the main compounds in the base solution[a].

Compounds	$Log(K_{sp})$[b]	Log(IAP)[c]	SI
$Mg(OH)_{2,(s)}$	−11.0	−10.3	0.7
$Ca(OH)_{2,(s)}$	−5.3	−10.3	−5.0
$CaSO_{4,(s)}$	−4.6	−3.3	1.3

[a.] The main cations in the base were only OH^- and SO_4^{2-} without AEMs in the BMED stack.

[b.] Davis and Masten, 2013.

[c.] pH = 10, $[SO_4^{2-}]$ = 90 mM, $[Mg^{2+}]$ and $[Ca^{2+}]$ were the maximum concentration in the base solution (from Figure 5.6).

5.3.6 Electric energy consumption

The electric energy consumption of the membrane stack for ammonia recovery was calculated using Eq 5.4 and it was ranged from 9.6 to 24.2 kWh/kg-N for the examined experimental conditions (Figure 5.7). The electric energy consumption of the membrane stack decreased with the increasing flow rate (Figure 5.7), indicating that high flow rate conditions are more beneficial for energy-efficient ammonia production using BMED. Although the high applied voltage generally resulted in the high electric energy consumption, the electric energy consumption of the membrane stack relatively insensitive to the applied voltage for the relatively high ammonia recovery of 70% (Figure 5.7). For the low ammonia recovery (50% and 60%), the energy consumption was much smaller for

20 V compared to 30 V (Figure 5.7). However, the BMED operation time at 20 V was 2.5 times that of 30 V (Figure 5.2A). In addition, the stack energy consumption for the high ammonia recovery (70%) was much higher than the energy consumption for the low ammonia recovery (50% and 60% recoveries). This result can be explained by the low ammonia recovery rate because of the low ammonia concentration in feed solution in the late stage of the experiment (Figures 5.2 and 5.3). Therefore, considering the energy consumption, ammonia recovery, and ammonia separation rate, 30 V, 180 mL/min, and 60 min operating time is the optimal operating conditions for the examined BMED system.

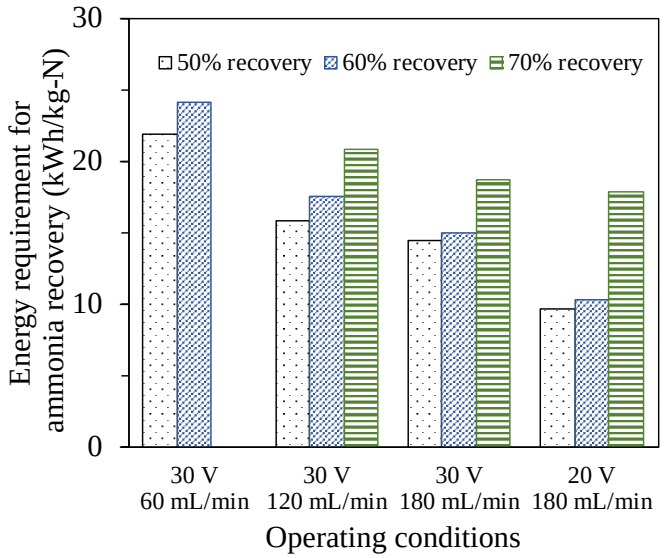

Figure 5.7. The electric energy requirement for ammonia recovery under different operating conditions for ammonium sulfate production. For the 30 V applications, E_{cp} was 3.4 V/cell pair while E_{cp} was 2.2 V/cell pair for the 20 V application. For the 120 min experiment, 70% ammonia recovery was not achieved for 30 V - 60 mL/min.

The electric energy consumption of the membrane stack for the recommended conditions (60% ammonia recovery, 30 V, and 180 mL/min) was 15.0 kWh/kg-N (Figure

5.7). This electric energy consumption is smaller than the electric energy consumption in previous studies (Table 5.5). Although a lower energy consumption of 4.9 kWh/kg-N was reported in a pilot-scale ED system (Table 5.5) (Ward et al., 2018), impurities of the ammonia product (inorganic anions, such as Cl^-) were not considered in the study. Also, the use of conventional ED with CEMs and AEMs allowed lower energy consumption compared to BMED; however, AEM fouling problems and unwanted anions (e.g., Cl^- and organic anions) are still remained as challenges in conventional ED applications.

Table 5.5. Reported energy requirements for ammonia production and recovery

Methods	Energy consumption (kWh/kg-N)	References
BMED with CEM and AEM	5 - 30	Li et al., 2016 van Linden et al., 2020 Shi et al., 2018
Ammonia stripping	25 - 44	Maurer et al., 2003 Morales et al., 2013 Antonini et al., 2011
Struvite precipitation	28 - 120	Maurer et al., 2003 Cao et al., 2019
Electrochemical cell	13 - 26	Desloover et al., 2012 Kuntke et al., 2017
Steam reforming	8 - 22	Appl, 1999; Rafiqul et al., 2005
ED	2 – 25	Ward et al., 2018 Van et al., 2019 Pan et al., 2020
Haber-Bosch	> 11	Razon 2013; Rouwenhorst et al, 2019
BMED with CEM	15	This study

Considering the high purity of the produced ammonium sulfate, BMED can also be compared with the Haber-Bosch process that has a high energy consumption (usually > 11 kWh/kg-N) (Razon 2013; Rouwenhorst et al, 2019). The Haber-Bosch ammonia synthesis

process is wildly used in industry to produce ammonia by fixing 130 million tons of nitrogen per year (Patil et al., 2015). However, with serious challenges, such as high energy consumption for hydrogen production and greenhouse gas emission (Baltrusaitis, 2017), the Haber-Bosch process is not considered as a sustainable method for ammonia production. It should be emphasized that there was no additional chemical consumption for pH adjustment or no toxic byproduct chemical creation during the BMED process. Also, the used dewatering centrate as the feed to BMED system did not need an extra pretreatment (e.g., filtration) because AEMs, that are vulnerable to organic fouling, were excluded in the examined BMED stack design (except for the electrode rinse cell). In addition, if the ammonia concentration in the feed is higher with other wastewater streams (e.g., source-separated human urine, liquid portion of food waste digestate), the energy requirement per nitrogen production using BMED can significantly be reduced, implying the strong potential of BMED for broad applications for high purity ammonia production.

The pumping energy is negligible because BMED is not a pressurized membrane system and thus the electric energy consumption will be dominant for BMED applications (Strathmann, 2004). It should be noted that the flow velocity in the BMED was much lower than the flow velocity for full-scale ED systems (Tsiakis and Papageorgiou, 2005). Therefore, the energy consumption will be lower for full-scale BMED. In addition, the cost for using BPMs is comparable to the cost for using IEMs since BPMs are manufactured by chemically attaching a CEM and an AEM (Simon, 1993; Bauer et al., 1988). Considering the market price for ammonium sulfate ranged from $75 to $130 (Chou et al., 2005), the BMED is an economical technology for resource recovery in wastewater treatment.

5.4 Conclusions

BMED with BPMs and CEMs (but without AEMs) was examined for efficient and rapid production of high-purity ammonia sulfate from dewatering centrate wastewater. The removal of AEMs in the BMED system simplified the IEM stack design, reduced the energy consumption, enhanced the ammonia recovery, increased the purity of ammonium sulfate by excluding anions, minimize the fouling on IEMs, and shortened the operation time. The ammonia recovery was enhanced by increasing the applied voltage and the flow rate. However, the increased applied voltage and flow rate also resulted in the raised electric energy consumption. CE_{NH4}^{+} decreased with the increasing applied voltage while CE_{NH4}^{+} was not significantly affected by the flow rate. It was found that the separation of NH_4^+ was slower than the separation of K+ because of the high concentration gradient of NH_4^+ across the CEMs. However, ammonium sulfate was the main compound in the base chamber due to the high initial ammonia concentration (compared with other cations). The decreased concentration of Ca^{2+} and Mg^{2+} in the base reservoir indicated the formation of precipitants, such as $CaSO_{4,(s)}$ and $Mg(OH)_{2,(s)}$, implying that a regular BMED stack cleaning is necessary. Pretreatment of dewatering centrate such as remove divalent cations using ion-exchange resins can be considered and examined in future studies to control the scaling problem. Compared to the energy consumption in the conventional ED system, the energy consumption in the BMED system was relatively high. However, high energy consumption is inevitable in BMED for water dissociation to generate H^+ and OH^- while production of ammonium sulfate from wastewater is a highly feasible method for practical IEM applications in nutrient separation from wastewater. Therefore, ammonium sulfate

production using wastewater and low-grade sulfuric acid will reduce the nutrient discharge into natural water systems with sustainable ammonia supplies to various industries, helping to establish a new green circular economy for resource recovery in wastewater treatment.

References

Appl, M., 1999. Ammonia: principles and industrial practice. Future, 245, 12.

Antonini, S., Paris, S., Eichert, T., and Clemens, J., 2011. Nitrogen and phosphorus recovery from human urine by struvite precipitation and air stripping in Vietnam. CLEAN–Soil, Air, Water, 39(12), 1099-1104.

Aritomi, T., Van den Boomgaard, T., and Strathmann, H., 1996. Current-voltage curve of a bipolar membrane at high current density. Desalination, 104(1-2), 13-18.

Audinos, R., 1997. Ion-Exchange membrane processes for clean industrial chemistry. Chemical Engineering & Technology: Industrial Chemistry-Plant Equipment-Process Engineering-Biotechnology, 20(4), pp.247-258.

Baker, R. W., 2012. Membrane technology and applications. John Wiley & Sons.

Baltrusaitis, J., 2017. Sustainable ammonia production.

Bauer, B., Gerner, F.J., and Strathmann, H., 1988. Development of bipolar membranes. Desalination, 68(2-3), pp.279-292.

Canadian Council of Ministers of the Environment, 2001. Canadian Water Quality Guidelines for the Protection of Aquatic Life.

Cao, L., Wang, J., Xiang, S., Huang, Z., Ruan, R., and Liu, Y., 2019. Nutrient removal from digested swine wastewater by combining ammonia stripping with struvite precipitation. Environmental Science and Pollution Research, 26(7), 6725-6734.

Cherif, A.T., Molenat, J., and Elmidaoui, A., 1997. Nitric acid and sodium hydroxide generation by electrodialysis using bipolar membranes. Journal of applied electrochemistry, 27(9), pp.1069-1074.

Choi, S. Y., Yu, J. W., and Kweon, J. H., 2013. Electrodialysis for desalination of brackish groundwater in coastal areas of Korea. Desalination and Water Treatment, 51(31-33), 6230-6237.

Chou, M.I.M., Bruinius, J.A., Benig, V., Chou, S.F.J., and Carty, R.H., 2005. Producing ammonium sulfate from flue gas desulfurization by-products. Energy sources, 27(11), pp.1061-1071.

Davis, M. L., and Masten, S. J., 2013. Principles of Environmental Engineering. McGraw-Hill Education.

De Paepe, J., Lindeboom, R. E., Vanoppen, M., De Paepe, K., Demey, D., Coessens, W., ... & Vlaeminck, S. E., 2018. Refinery and concentration of nutrients from urine with electrodialysis enabled by upstream precipitation and nitrification. Water research, 144, 76-86.

Desloover, J., Abate Woldeyohannis, A., Verstraete, W., Boon, N., and Rabaey, K., 2012. Electrochemical resource recovery from digestate to prevent ammonia toxicity during anaerobic digestion. Environmental science & technology, 46(21), pp.12209-12216.

Fux, C., Boehler, M., Huber, P., Brunner, I., and Siegrist, H., 2002. Biological treatment of ammonium-rich wastewater by partial nitritation and subsequent anaerobic ammonium oxidation (anammox) in a pilot plant. Journal of biotechnology, 99(3), pp.295-306.

Gao, F., Wang, L., Wang, J., Zhang, H., and Lin, S., 2020. Nutrient recovery from treated wastewater by a hybrid electrochemical sequence integrating bipolar membrane electrodialysis and membrane capacitive deionization. Environmental Science: Water Research & Technology, 6(2), 383-391.

Galvagno, G., Eskicioglu, C., and Abel-Denee, M. (2016). Biodegradation and chemical precipitation of dissolved nutrients in anaerobically digested sludge dewatering centrate. Water research, 96, 84-93.

Gryta, M., 2009. Calcium sulphate scaling in membrane distillation process. Chemical Papers, 63(2), pp.146-151.

Guo, H., You, F., Yu, S., Li, L., and Zhao, D., 2015. Mechanisms of chemical cleaning of ion exchange membranes: A case study of plant-scale electrodialysis for oily wastewater treatment. Journal of Membrane Science, 496, 310-317.

Heinonen, J., Zhao, Y., and Van der Bruggen, B., 2020. A process combination of ion exchange and electrodialysis for the recovery and purification of hydroxy acids from secondary sources. Separation and Purification Technology, 240, 116642.

Herrero-Gonzalez, M., Admon, N., Dominguez-Ramos, A., Ibañez, R., Wolfson, A., and Irabien, A., 2020. Environmental sustainability assessment of seawater reverse osmosis brine valorization by means of electrodialysis with bipolar membranes. Environmental Science and Pollution Research, 27(2), 1256-1266.

Herrero-Gonzalez, M., Diaz-Guridi, P., Dominguez-Ramos, A., Irabien, A., and Ibañez, R., 2020a. Highly concentrated HCl and NaOH from brines using electrodialysis with bipolar membranes. Separation and Purification Technology, 116785.

Holloway, R.W., Childress, A.E., Dennett, K.E., and Cath, T.Y., 2007. Forward osmosis for concentration of anaerobic digester centrate. Water research, 41(17), pp.4005-4014.

Huang, C. and Xu, T., 2006. Electrodialysis with bipolar membranes for sustainable development. Environmental science & technology, 40(17), pp.5233-5243.

Huang, H., Zhang, P., Zhang, Z., Liu, J., Xiao, J., and Gao, F., 2016. Simultaneous removal of ammonia nitrogen and recovery of phosphate from swine wastewater by struvite electrochemical precipitation and recycling technology. Journal of Cleaner production, 127, 302-310.

Ippersiel, D., Mondor, M., Lamarche, F., Tremblay, F., Dubreuil, J., and Masse, L., 2012. Nitrogen potential recovery and concentration of ammonia from swine manure using electrodialysis coupled with air stripping. Journal of environmental management, 95, S165-S169.

Kim, Y., Walker, W.S., and Lawler, D.F., 2011. Electrodialysis with spacers: Effects of variation and correlation of boundary layer thickness. Desalination, 274(1-3), pp.54-63.

Krol, J. J., Jansink, M., Wessling, M., and Strathmann, H., 1998. Behaviour of bipolar membranes at high current density: water diffusion limitation. Separation and purification technology, 14(1-3), 41-52.

Kumar, A., Phillips, K. R., Cai, J., Schröder, U., and Lienhard, J. H., 2019. Integrated valorization of desalination brine through NaOH recovery: opportunities and challenges. Angewandte Chemie International Edition, 58(20), 6502-6511.

Kuntke, P., Rodríguez Arredondo, M., Widyakristi, L., ter Heijne, A., Sleutels, T. H., Hamelers, H. V., and Buisman, C. J., 2017. Hydrogen gas recycling for energy efficient ammonia recovery in electrochemical systems. Environmental Science & Technology, 51(5), 3110-3116.

Lee, H. J., Choi, J. H., Cho, J., and Moon, S. H., 2002a. Characterization of anion exchange membranes fouled with humate during electrodialysis. Journal of membrane science, 203(1-2), 115-126.

Lee, H. J., Moon, S. H., and Tsai, S. P., 2002b. Effects of pulsed electric fields on membrane fouling in electrodialysis of NaCl solution containing humate. Separation and Purification Technology, 27(2), 89-95.

Lee, H. J., Hong, M. K., Han, S. D., Cho, S. H., & Moon, S. H., 2009. Fouling of an anion exchange membrane in the electrodialysis desalination process in the presence of organic foulants. Desalination, 238(1-3), 60-69.

Lei, C., Li, Z., Gao, Q., Fu, R., Wang, W., Li, Q., & Liu, Z., 2020. Comparative study on the production of gluconic acid by electrodialysis and bipolar membrane electrodialysis: Effects of cell configurations. Journal of Membrane Science, 118192.

Li, C., Wang, G., Feng, H., He, T., Wang, Y., and Xu, T., 2015. Cleaner production of Niacin using bipolar membranes electrodialysis (BMED). Separation and Purification Technology, 156, pp.391-395.

Li, Y., Shi, S., Cao, H., Wu, X., Zhao, Z., and Wang, L., 2016. Bipolar membrane electrodialysis for generation of hydrochloric acid and ammonia from simulated ammonium chloride wastewater. Water research, 89, pp.201-209.

Lin, J., Lin, F., Chen, X., Ye, W., Li, X., Zeng, H., and Van der Bruggen, B., 2019. Sustainable management of textile wastewater: a hybrid tight ultrafiltration/bipolar-membrane electrodialysis process for resource recovery and zero liquid discharge. Industrial & Engineering Chemistry Research, 58(25), 11003-11012.

Maurer, M., Schwegler, P., and Larsen, T.A., 2003. Nutrients in urine: energetic aspects of removal and recovery. Water Science and technology, 48(1), pp.37-46.

Melnikov, S. S., Mugtamov, O. A., and Zabolotsky, V. I., 2020. Study of electrodialysis concentration process of inorganic acids and salts for the two-stage conversion of salts into acids utilizing bipolar electrodialysis. Separation and Purification Technology, 235, 116198.

Mikhaylin, S., & Bazinet, L., 2016. Fouling on ion-exchange membranes: Classification, characterization and strategies of prevention and control. Advances in colloid and interface science, 229, 34-56.

Mondor, M., Masse, L., Ippersiel, D., Lamarche, F., and Masse, D. I., 2008. Use of electrodialysis and reverse osmosis for the recovery and concentration of ammonia from swine manure. Bioresource technology, 99(15), 7363-7368.

Mondor, M., Ippersiel, D., Lamarche, F., & Masse, L., 2009. Fouling characterization of electrodialysis membranes used for the recovery and concentration of ammonia from swine manure. Bioresource technology, 100(2), 566-571.

Morales, N., Boehler, M. A., Buettner, S., Liebi, C., and Siegrist, H., 2013. Recovery of N and P from urine by struvite precipitation followed by combined stripping with digester sludge liquid at full scale. Water, 5(3), 1262-1278.

Mulder, J.W., Van Loosdrecht, M.C.M., Hellinga, C., and Van Kempen, R., 2001. Full-scale application of the SHARON process for treatment of rejection water of digested sludge dewatering. Water science and technology, 43(11), pp.127-134.

Paleologou, M., Thibault, A., Wong, P.Y., Thompson, R., and Berry, R.M., 1997. Enhancement of the current efficiency for sodium hydroxide production from sodium sulphate in a two-compartment bipolar membrane electrodialysis system. Separation and purification technology, 11(3), pp.159-171.

Patil, B. S., Wang, Q., Hessel, V., and Lang, J., 2015. Plasma N2-fixation: 1900–2014. Catalysis today, 256, 49-66.

Pawlowski, S., Crespo, J. G., and Velizarov, S., 2014. Pressure drop in reverse electrodialysis: Experimental and modeling studies for stacks with variable number of cell pairs. Journal of membrane science, 462, 96-111.

Pan, Y., Zhu, T., and He, Z., 2020. Minimizing effects of chloride and calcium towards enhanced nutrient recovery from sidestream centrate in a decoupled electrodialysis driven by solar energy. Journal of Cleaner Production, 121419.

Porter, M. C., 1989. Handbook of industrial membrane technology.

Pourcelly, G., 2002. Electrodialysis with bipolar membranes: principles, optimization, and applications. Russian journal of electrochemistry, 38(8), pp.919-926.

Pronk, W., Zuleeg, S., Lienert, J., Escher, B., Koller, M., Berner, A., and Boller, M. (2007). Pilot experiments with electrodialysis and ozonation for the production of a fertiliser from urine. Water science and technology, 56(5), 219-227

Rafiqul, I., Weber, C., Lehmann, B., and Voss, A., 2005. Energy efficiency improvements in ammonia production—perspectives and uncertainties. Energy, 30(13), pp.2487-2504.

Razon, L. F., 2014. Life cycle analysis of an alternative to the haber-bosch process: Non-renewable energy usage and global warming potential of liquid ammonia from cyanobacteria. Environmental Progress & Sustainable Energy, 33(2), 618-624.

Rouwenhorst, K. H., Van der Ham, A. G., Mul, G., and Kersten, S. R., 2019. Islanded ammonia power systems: Technology review & conceptual process design. Renewable and Sustainable Energy Reviews, 114, 109339.

Ruiz, B., Sistat, P., Huguet, P., Pourcelly, G., Araya-Farias, M., and Bazinet, L., 2007. Application of relaxation periods during electrodialysis of a casein solution: impact on anion-exchange membrane fouling. Journal of membrane science, 287(1), 41-50.

Shi, L., Hu, Y., Xie, S., Wu, G., Hu, Z., and Zhan, X., 2018. Recovery of nutrients and volatile fatty acids from pig manure hydrolysate using two-stage bipolar membrane electrodialysis. Chemical Engineering Journal, 334, pp.134-142.

Simons, R., 1993. Preparation of a high performance bipolar membrane. Journal of membrane science, 78(1-2), pp.13-23.

Strathmann, H., 2004. Ion-exchange membrane separation processes (Vol. 9). Elsevier.

Strathmann, H., 2010. Electrodialysis, a mature technology with a multitude of new applications. Desalination, 264(3), 268-288.

Strous, M., Van Gerven, E., Zheng, P., Kuenen, J.G., and Jetten, M.S., 1997. Ammonium removal from concentrated waste streams with the anaerobic ammonium

oxidation (anammox) process in different reactor configurations. Water Research, 31(8), pp.1955-1962.

Sun, X., Lu, H., & Wang, J., 2017. Recovery of citric acid from fermented liquid by bipolar membrane electrodialysis. Journal of Cleaner Production, 143, 250-256.

Talebi, S., Chen, G. Q., Freeman, B., Suarez, F., Freckleton, A., Bathurst, K., and Kentish, S. E., 2019. Fouling and in-situ cleaning of ion-exchange membranes during the electrodialysis of fresh acid and sweet whey. Journal of Food Engineering, 246, 192-199.

Tian, W., Wang, X., Fan, C., and Cui, Z., 2019. Optimal treatment of hypersaline industrial wastewater via bipolar membrane electrodialysis. ACS Sustainable Chemistry & Engineering, 7(14), 12358-12368.

Tongwen, X. and Weihua, Y., 2002. Effect of cell configurations on the performance of citric acid production by a bipolar membrane electrodialysis. Journal of membrane Science, 203(1-2), pp.145-153.

Tran, A.T., Mondal, P., Lin, J., Meesschaert, B., Pinoy, L., and Van der Bruggen, B., 2015. Simultaneous regeneration of inorganic acid and base from a metal washing step wastewater by bipolar membrane electrodialysis after pretreatment by crystallization in a fluidized pellet reactor. Journal of membrane science, 473, pp.118-127.

Tsiakis, P., and Papageorgiou, L. G., 2005. Optimal design of an electrodialysis brackish water desalination plant. Desalination, 173(2), 173-186.

van Linden, N., Bandinu, G. L., Vermaas, D. A., Spanjers, H., & van Lier, J. B.. 2020. Bipolar membrane electrodialysis for energetically competitive ammonium removal and dissolved ammonia production. Journal of Cleaner Production, 120788.

van Linden, N., Spanjers, H., and van Lier, J. B., 2019. Application of dynamic current density for increased concentration factors and reduced energy consumption for concentrating ammonium by electrodialysis. Water research, 163, 114856.

Walker, W.S., Kim, Y., and Lawler, D.F., 2014. Treatment of model inland brackish groundwater reverse osmosis concentrate with electrodialysis—Part I: sensitivity to superficial velocity. Desalination, 344, pp.152-162.

Wang, Q., Yang, P., and Cong, W., 2011. Cation-exchange membrane fouling and cleaning in bipolar membrane electrodialysis of industrial glutamate production wastewater. Separation and purification technology, 79(1), 103-113.

Ward, A. J., Arola, K., Brewster, E. T., Mehta, C. M., and Batstone, D. J., 2018. Nutrient recovery from wastewater through pilot scale electrodialysis. Water research, 135, 57-65

Warsinger, D.M., Swaminathan, J., Guillen-Burrieza, E., and Arafat, H.A., 2015. Scaling and fouling in membrane distillation for desalination applications: a review. Desalination, 356, pp.294-313.

Weast, R. C., Astle, M. J., & Beyer, W. H. (1988). CRC handbook of chemistry and physics (Vol. 69). Boca Raton, FL: CRC press.

Weston, C. W., Papcun, J. R., and Dery, M. (2000). Ammonium compounds. Kirk-Othmer Encyclopedia of Chemical Technology.

Ye, W., Huang, J., Lin, J., Zhang, X., Shen, J., Luis, P., and Van der Bruggen, B., 2015. Environmental evaluation of bipolar membrane electrodialysis for NaOH production from

wastewater: conditioning NaOH as a CO2 absorbent. Separation and Purification Technology, 144, pp.206-214.

Yuan, P. and Kim, Y., 2017. Increasing phosphorus recovery from dewatering centrate in microbial electrolysis cells. Biotechnology for biofuels, 10(1), p.70.

Zhang, X., Li, C., Wang, Y., Luo, J., and Xu, T., 2011. Recovery of acetic acid from simulated acetaldehyde wastewaters: Bipolar membrane electrodialysis processes and membrane selection. Journal of membrane science, 379(1-2), pp.184-190.

6 Membrane Scaling in Electrodialysis for Nutrients Separation from High-strength Wastewater

Electrodialysis (ED) has been regarded as an emerging technology to recover nutrients from wastewater. High-strength wastewater such as food processing wastewater is an ideal source for nutrients recovery since it contains a high concentration of ammonia. However, divalent cations such as calcium and magnesium ions in high-strength wastewater can form various precipitates during ED operation. The formation of inorganic scalants (i.e., membrane scaling) can limit the broad applications of ED because inorganic scalants can cause high energy consumption and reduce the life span of membranes. Therefore, in this study, we investigated the calcium and magnesium scale formation in a lab-scale ED reactor fed with high-strength wastewater. Different operating conditions, such as applied voltage and the type of membranes, were examined in the study.

- Guo, H., & Kim, Y. (under review). Membrane Scaling in Electrodialysis for Nutrients Separation from High-strength Wastewater. *Environmental Engineering Science.*

The co-author's contributions include:

- Funding acquisition
- Supervision and technical support
- Manuscript revision

Abstract

Membrane scaling problems can limit broad applications of electrodialysis (ED) for nutrients recovery from wastewater. In this study, we investigated the calcium and magnesium scale precipitation on ion-exchange membranes (IEMs) using a lab-scale ED reactor. Two high-strength wastewater streams, including municipal waste (MW) liquid digestate and food waste (FW) liquid digestate, were fed into the ED reactor. For the operation with MW liquid digestate, the cumulative Ca^{2+} loss increased with the increasing electric current while the electric current conditions did not affect the cumulative Mg^{2+} loss. After 8-h operation, 60.1% of Ca^{2+} and 39.0% of Mg^{2+} in the MW liquid digestate were lost in the form of precipitates. Observed scalants on cation-exchange membranes (CEMs) were vaterite, amorphous calcium carbonate (ACC), and struvite while ACC was not found on anion-exchange membranes (AEMs). Observed scalants of calcium carbonate with MW liquid digestate (vaterite and ACC) were different from scalants (calcite) found with synthetic solutions. Among these scalants, struvite was formed as sharp (needle-shaped) crystals that can potentially damage the IEM. The gradual loss of Mg^{2+} was observed with FW liquid digestate because of high PO_4^{3-} concentration, indicating the formation of struvite. The membrane with high selectivity for divalent ions resulted in the rapid decrease in electric current, implying serious membrane scaling on IEMs. These findings demonstrated that the membrane scaling problems by calcium and magnesium precipitation are ubiquitous in ED for nutrients recovery from wastewater.

Keywords

Calcium and magnesium scaling; electrodialysis for nutrients recovery; liquid digestate;

shapes of scalants; struvite; membrane selectivity

6.1 Introduction

Electrodialysis (ED) is a membrane separation process where ions are transferred through the ion exchange membranes (IEMs) by an electric field between two electrodes (Strathmann, 2004; Moran, 2018). ED has been widely applied in brackish water desalination (AI-Amshawee et al., 2020; Mei et al., 2020; Xu et al., 2018; Patel et al., 2020; Nguyen et al., 2019), wastewater treatment (Lafi et al., 2018; Chao and Liang, 2008; Benvenuti et al., 2014), and food processing (Mondor et al., 2012, Wang et al., 2019). Recently, ED has been regarded as an emerging technology to recover nutrients from wastewater (Ward et al., 2018; Wang et al., 2017; Liu et al., 2017; Ye et al., 2019; Shi et al., 2018; Ippersiel et al., 2012). For instance, 7.1 g/L NH_4-N was recovered from the municipal centrate wastewater using a pilot-scale ED system (Ward et al., 2018). Substantially high levels of ammonia separation (up to 21.4 g-N/L) were achieved using bipolar membrane ED reactors that were fed with pig manures (Shi et al., 2018; Ippersiel et al., 2012). These studies demonstrated the high feasibility of ED in nutrients recovery from wastewater.

Membrane scaling problems (i.e., inorganic salt precipitates deposited on IEM surfaces) can limit broad applications of the ED technology since the inorganic scalants cause substantially high energy consumption in ED operation as well as permanent IEM damages (Phuntsho et al., 2014; Brewster et al., 2017; Li et al., 2015). Membrane scaling is triggered in ED systems when the feed wastewater contains divalent cations such as Mg^{2+}, and Ca^{2+} (Andreeva et al., 2018). In previous studies, various IEM scaling precipitates, including

gypsum ($CaSO_4 \cdot 2H_2O$), calcium carbonate ($CaCO_3$), and magnesium hydroxide ($Mg(OH)_2$), were observed in ED reactors that were fed with synthetic solutions (Asraf-Snir et al., 2016, Andreeva et al., 2018, Bazinet and Araya-Farias, 2005, Casademont et al., 2007). The relatively high concentration of Mg^{2+} and Ca^{2+} coupled with abundant carbonate species in liquid digestate after anaerobic digestion can lead to serious scale formation for nutrients recovery using ED systems (Ward et al., 2018; Brewster et al., 2017). As a result, a mechanistic model was developed to predict scale formation in electrodialytic nutrients recovery from liquid digestate (Brewster et al., 2017). However, the effects of operation conditions on scalants formation were not systematically investigated for high-strength wastewater treatment using ED. Therefore, in this study, we focused on various aspects of IEM scaling problems in ED fed with two high-strength wastewater streams: municipal waste (MW) liquid digestate (dewatering centrate after anaerobic digestion); and food waste (FW) liquid digestate (the liquid portion after dewatering of anaerobically digested food waste).

Calcium carbonate, gypsum, and struvite are common scalants in wastewater treatment using ED systems (Ward et al., 2018; Brewster et al., 2017; Asraf-Snir et al., 2016). The formation of scalants on IEMs surfaces increases the electrical resistance and decreases the permselectivity of IEMs (Mikhaylin and Bazinet, 2016). The scalants also can cause physical damages to the membrane because of the sharp edge (e.g., needle-shaped aragonite, struvite, and gypsum) (Asraf-Snir et al., 2016; Andritsos et al., 1997; Le Corre et al., 2005; Cusick and Logan, 2012). Therefore, in this study, we investigated the shape of scalants especially for magnesium and calcium precipitates in ED for nutrients recovery.

In an ED reactor, the separation rate of ions is governed by the electric current density (İpekçi et al., 2020; Bunani et al., 2017). A high separation rate of ions contributes to a rapid increase in the ions concentration in the concentrate cell and likely to result in more serious scaling problems. Therefore, we investigated the effects of electric current density on membrane scaling in the ED system. Other specific objectives of this study are to: examine the calcium and magnesium precipitation with the MW and FW liquid digestates; investigate the effects of membrane selectivity on precipitation of calcium and magnesium; study the morphology of scalants on IEMs.

6.2 Materials and methods

6.2.1 Reactor construction

The ED reactor was constructed using polypropylene blocks with a cylindrical chamber (7 cm^2 in cross-section). Two pieces of stainless steel mesh (2 cm × 2 cm; 304 stainless steel, 200× 200 mesh, McMaster Carr, USA) were used as the anode and cathode. The anode and cathode were separated by 2 CEMs and 2 AEMs, creating an anode cell (15 mL), a feed cell next to the anode (Feed Cell-A, 25 mL), a concentrate cell (3 mL), a feed cell next to the cathode (Feed Cell-C, 25 mL), and a cathode cell (15 mL) (Figure 6.1). Two types of IEMs were used in the ED reactor: CR 67 and AR 908 (SUEZ Water Technologies & Solutions, Canada); Selemion CMV and Selemion AMV (Asahi Glass, Japan) (Table 6.1).

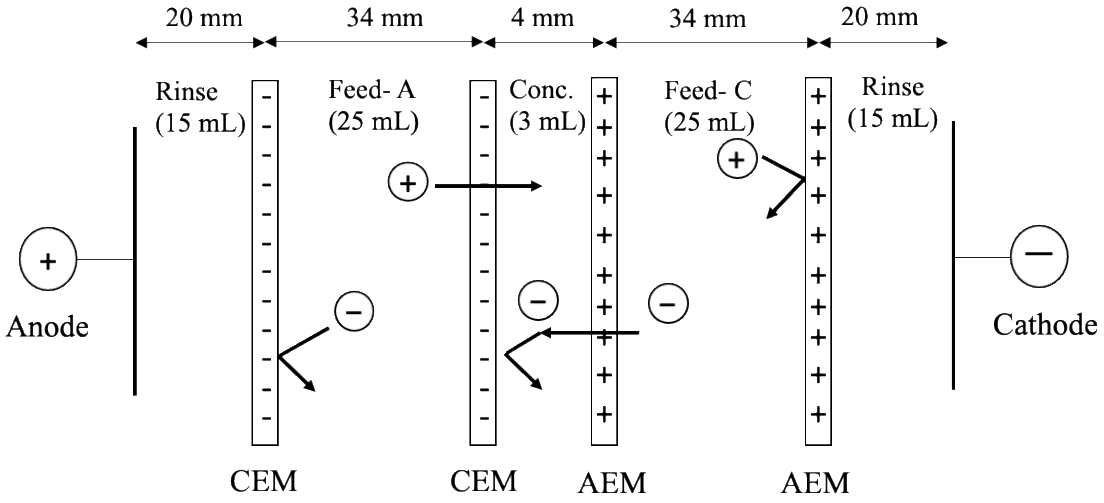

Figure 6.1. Schematic arrangement of CEMs and AEMs for enhanced scale formation in ED.

Table 6.1. IEM characteristics

	CR67	AR908	Selemion CMV	Selemion AMV
Thickness (mm)	0.6	0.6	0.1	0.1
Burst strength (kPa)	827.3	827.3	200	250
Ion-exchange capacity (meq/dry gram resin)	≥ 2.3	≥ 2.0	≥ 2.2[a]	≥ 1.9[b]
Resistivity (Ω-cm^2)	5.5[c]	7.0[c]	2.0[d]	2.0[d]
Transport number [e]	0.94	0.94	0.97	0.95

[a.] Miyoshi et al., 1992; Verbanck et al., 2006.

[b.] Le et al., 2009.

[c.] In 10 mM NaCl.

[d.] In 500 mM NaCl.

[e.] t-Na+. t-Cl-.

6.2.2 Feed wastewater and reactor operation

The Feed cell -A and -C were fed with the MW liquid digestate or the FW liquid digestate (Table 6.2). The MW liquid digestate was collected from the local wastewater treatment plant (Hamilton, Canada) and stored at 4°C for no longer than 2 weeks. The FW liquid digestate was collected from StormFisher Environmental Ltd (London, Canada) and centrifuged at 8000 rpm for 5 minutes. High ammonia concentration was observed in the MW and FW liquid digestate (Table 6.2). The concentration of Ca^{2+} in the MW and FW liquid digestates was similar while Mg^{2+} concentration in the FW liquid digestate was lower than that in the MW liquid digestate (Table 6.2). The anolyte was prepared with 100 mM Na_2SO_4 and 100 mM NaOH while the catholyte was started with 100 mM NaCl and 100 mM HCl. The alkaline and acid solutions were used to avoid significant changes in pH. The concentrate cell was filled with 10 mM NaCl.

Table 6.2. The main characteristics of the MW liquid digestate and FW liquid digestate (average ± standard deviation, n =3)

component	MW liquid digestate	FW liquid digestate
NH_3-N	64.4 ± 8.6 mM	157.7 ± 0.8 mM
Ca^{2+}	3.5 ± 0.1 mM	2.6 ± 0.03 mM
Mg^{2+}	3.3 ± 0.3 mM	0.4 ± 0.03 mM
PO_4^{3-}	0.1 ± 0.01 mM	4.8 ± 1.5 mM
Soluble COD	457 ± 29 mg/L	3215 ± 714 mg/L
pH	8.2 ± 0.1	8.2 ± 0.03
Conductivity	7.7 ± 0.8 mS/cm	22.8 ± 1.5 mS/cm

The reactor was operated under batch mode to investigate the effects of electric current density, feed sources, and types of membranes on the formation of precipitates (Table 6.3). The solutions in the Feed Cell-A and -C were replaced every 2 hours when the applied voltage was 8 and 12 V. A frequent change (every 1 hour) of feed solutions was applied for the high applied voltage (16 V) to ensure sufficient ions separation from the feed cell into the concentrate cell. The electrode rinse solutions were replaced every 1 hour for all tests while the concentrate cell solutions were maintained throughout the experiment. Three different applied voltages were provided by an external power supplier (Model 9201, BK Precision, USA). The electric current of the ED reactor was measured and recorded every 1 minute by using a digital multimeter and data acquisition system (34970A, Agilent Technologies, USA). Then the electric current was normalized by the effective area of membranes (7 cm^2). The average current density ranged from 5.1 to 16.9 mA/cm^2 depends on the feed sources and IEMs (Table 6.3). All the tests were operated at room temperature (22.4 ± 0.3℃).

6.2.3 Experiment measurement

Samples from the concentrate cell were collected every 2 hours (test 1 and 2, Table 6.3) or every 1 hour (test 3-6; Table 6.3). These samples were analyzed by inductive coupled plasma-optical emission spectrometry (ICP-OES, Vista Pro, Varian Inc., Australia) to measure the concentration of Ca^{2+} and Mg^{2+}. Before the ICP-OES analysis, the collected samples were acidified using 70% nitric acid (w/w) and filtered with syringe filters (pore size 0.45 μm, polyethersulfone membrane, VWR International, USA). The ammonia concentration in the collected samples was analyzed by using commercial ammonia test

vials (Method 10205, Hach Company, USA). Apart from the concentrate samples, the feed solutions (initial and final solutions of each batch) of test-1 and -2 (Table 6.3) were also collected and analyzed by ICP-OES to observe the separation rate of Ca^{2+} and Mg^{2+} in the feed cell. The pH and conductivity of all the solutions (electrode rinse, feed, and concentrate) were analyzed and recorded (Orion Versa Star Pro, Thermo Fisher Scientific, USA). In addition, the precipitated crystals on the membrane from test 3 (Table 6.3) were analyzed in scanning electron microscopy and energy-dispersive X-ray spectroscopy (SEM-EDS, JEOL JSM-6610LV, Japan) to study the morphology and elements of the crystals.

Table 6.3. Operation conditions in the ED system

	Applied voltage (V)	Average current density (mA/cm^2)	Feed source	Operation time (h)	IEM
Test 1	8	5.1 ± 0.5	MW liquid digestate	8	CR 67/AR 908
Test 2	12	7.6 ± 1.0	MW liquid digestate	8	
Test 3	16	10.6 ± 0.6	MW liquid digestate	6	
Test 4	16	16.9 ± 1.6	FW liquid digestate	6	
Test 5	16	9.6 ± 0.9	MW liquid digestate	6	Selemion CMV/AMV
Test 6	16	6.7 ± 2.3	FW liquid digestate	6	

6.3 Results and discussions

6.3.1 Precipitates formation in the concentrate cell with different applied voltage

A high electric current density resulted in a rapid increase in Ca^{2+} concentration in the concentrate cell during the early stage of the experiment (Figure 6.2a). The rapid increase in Ca^{2+} concentration can be explained by the enhanced Ca^{2+} separation through the CEM from Feed Cell-A (Figure 6.2a). However, the concentration of concentrate Ca^{2+} decreased gradually after 4 h for 5.1 mA/cm^2 and 2 h for 7.6 mA/cm^2 (Figure 6.2a). Considering the

continued Ca^{2+} separation from Feed Cell-A (Figure 6.2a), the decrease in the concentrate Ca^{2+} concentration can only be explained by the formation of calcium precipitates in the concentrate cell (e.g., $CaCO_3$) as carbonate and bicarbonate anions were transported from Feed Cell-C. When the reactors were disassembled after the 8 h experiment, white powders were observed on IEM surfaces (Appendix, Figure D1), indicating the active formation of inorganic precipitates (including $CaCO_3$) during the reactor operation.

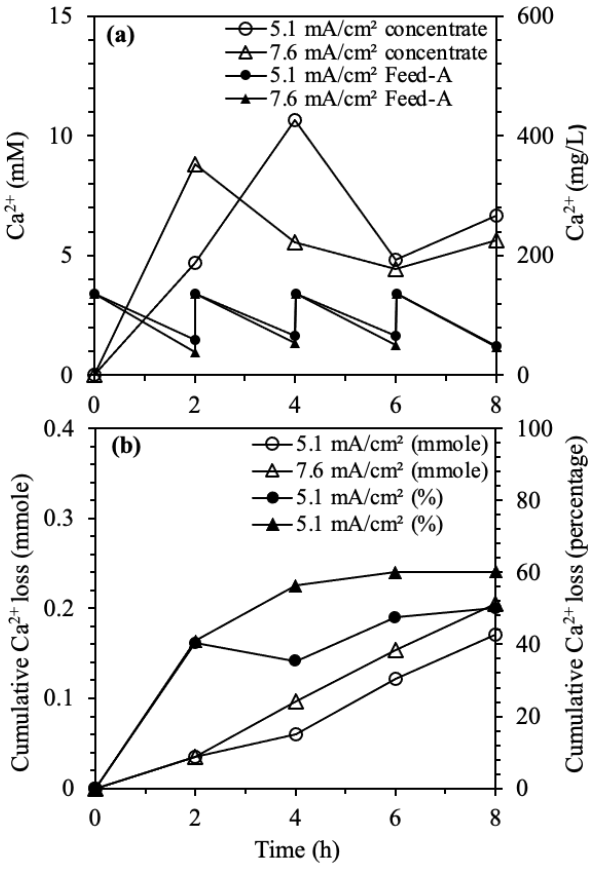

Figure 6.2. (a) Concentration of calcium in the concentrate cell and the Feed Cell-A; (b) cumulative calcium loss (no fill label: the amount of calcium loss; solid fill label: the percentage of calcium loss).

In addition, the calcium loss (i.e., the cumulative mass of Ca^{2+} removed from Feed Cell-A minus the mass of Ca^{2+} remaining in the concentrate cell) increased linearly with the ED operating time (Figure 6.2b). Note that the Feed Cell-A and -C were replaced every 2 h by fresh wastewater while the concentrate cell was maintained throughout the experiment. At the end of the 8 h experiment, 50.0% (5.1 mA/cm^2) and 60.1 % (7.6 mA/cm^2) of the total Ca^{2+} provided in the feed digestate was lost in the form of calcium precipitates (Figure 6.2b), indicating serious precipitation and scaling challenges in ED applications for nutrients separation from wastewater.

The Mg^{2+} concentration in the concentrate cell increased gradually with the maximum concentration of ~20 mM (Figure 6.3a). High electric current density contributed to the high concentrate Mg^{2+} concentration (Figure 6.3a). However, the high concentrate Mg^{2+} concentration limited the separation rate of Mg^{2+} from Feed Cell-A, resulting in a similar remaining Mg^{2+} concentration in Feed Cell-A for 5.1 and 7.6 mA/cm^2 (Figure 6.3a). For 7.6 mA/cm^2, a slight decrease in the concentrate Mg^{2+} concentration was observed (Figure 6.3a), indicating the potential formation of magnesium precipitates in the concentrate cell. Two expected magnesium precipitates in the concentrate cell were struvite and magnesium hydroxide (Table 6.4). Considering the neutral to slightly basic pH in the concentrate cell (pH 7.6 - 8.5), the hydroxide concentration was not sufficient to induce the formation of magnesium hydroxide. The solubility index for the magnesium hydroxide in the concentrate cell was -1.7 for pH 8.5, indicating the magnesium hydroxide was not precipitated in the concentrate cell. Therefore, the Mg^{2+} loss can be explained by struvite precipitation in the concentrate cell.

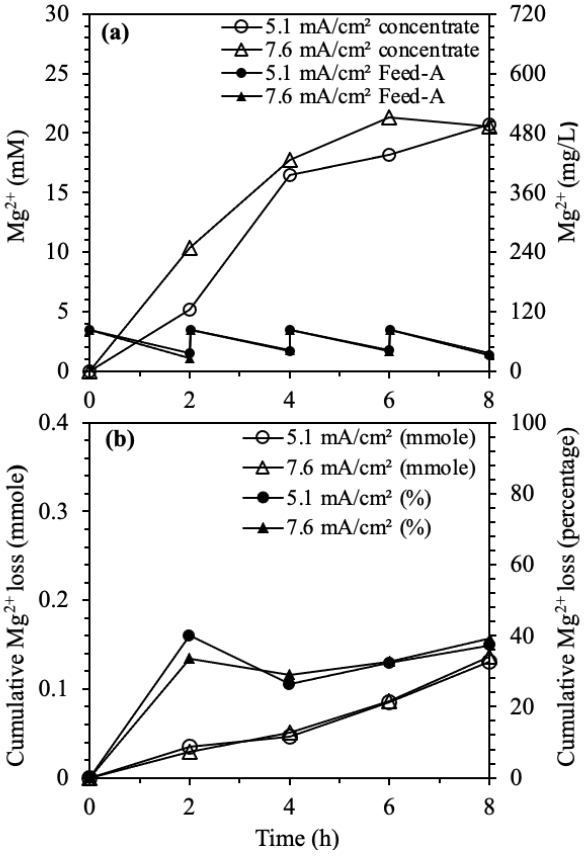

Figure 6.3. (a) Concentration of magnesium in the concentrate cell and the Feed Cell-A; (b) cumulative magnesium loss (no fill label: the amount of magnesium loss; solid fill label: the percentage of magnesium loss).

Table 6.4. The solubility constant (pK_{sp}) for the main potential precipitates in the concentrate cell

Mineral	Chemical formula	pK_{sp}
Calcite	$CaCO_3$	8.5[a]
Aragonite	$CaCO_3$	8.3 [a]
Vaterite	$CaCO_3$	7.9 [a]
Struvite	$MgNH_4PO_4 \cdot 6H_2O$	13.3[b]
Brucite	$Mg(OH)_2$	11.0[c]

[a.] Walker et.al., 2014
[b.] Ohlinger et.al., 1998
[c.] Davis, 2004

Another interesting finding is the negligible differences in the cumulative Mg^{2+} loss between 5.1 and 7.6 mA/cm^2 (~40% of the total Mg^{2+} provided in the feed digestate as shown in Figure 6.3b). The almost identical results in the cumulative Mg^{2+} loss can be explained by the limited amount of struvite precipitation. In the MW liquid digestate, the relatively low phosphate concentration (0.1 mM PO_4^{3-} vs. 3.3 mM Mg^{2+} and 64.4 mM NH_4^+ as shown in Table 6.2) and the competitive separation (e.g., Cl^- or HCO_3^-) are considered to limit the rate of struvite precipitation in the reactor.

6.3.2 Precipitation with the FW liquid digestate

The average electric current density for the FW liquid digestate (16.9 ± 1.6 mA/cm^2, Table 6.3) was much higher than that with the MW liquid digestate (10.6 ± 0.6 mA/cm^2, Table 6.3) because of the high conductivity of the FW liquid digestate (Table 6.2). Even with the high average electric current density, the separation of divalent cations (Ca^{2+} and Mg^{2+}) was slower with the FW liquid digestate (Figures 6.4a and 6.4b) mainly due to the lower initial Ca^{2+} and Mg^{2+} concentration in the FW liquid digestate compared to the MW liquid digestate (Table 6.2). Even with the lower concentration of Ca^{2+} and Mg^{2+} in the concentrate, gradual decreases in the concentrate Ca^{2+} and Mg^{2+} concentration were also observed in the later stage of the experiment for the FW liquid digestate (Figures 6.4a and 6.4b). This finding implied the formation of calcium and magnesium occurring in the concentrate cell.

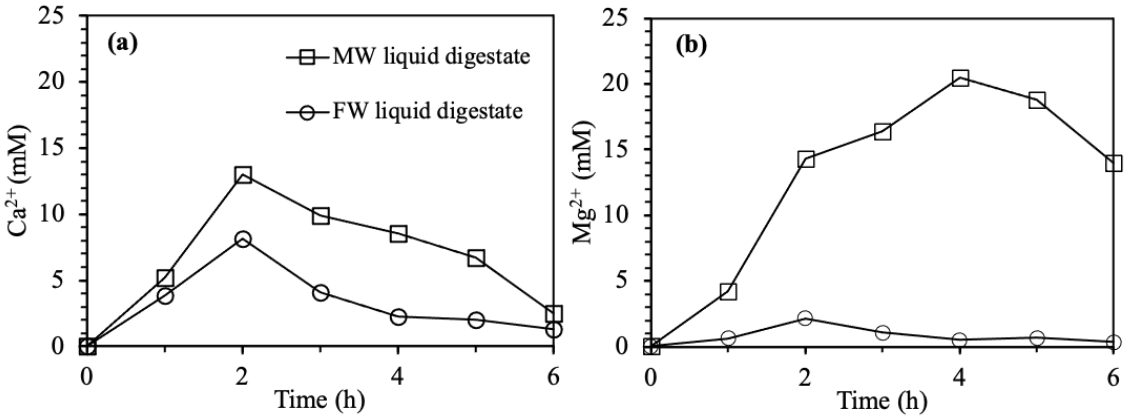

Figure 6.4. Concentration of (a) calcium and (b) magnesium in the concentrate cell with different feed sources.

The concentrate Mg^{2+} concentration started decreasing only at 2.6 mM for the FW liquid digestate (Figure 6.4b) while it increased above 20 mM with the MW liquid digestate (Figure 6.4b). The low Mg^{2+} concentration for the FW liquid digestate can be explained by the high phosphate concentration in the FW liquid digestate (Table 6.2). The molar concentration ratio between Mg^{2+} and PO_4^{3-} for the FW liquid digestate was 1:12 while the ratio for the MW liquid digestate was 33:1 (Table 6.2). Thus, the struvite precipitation was limited by Mg^{2+} for the FW liquid digestate while it was limited by PO_4^{3-}concentration for the MW liquid digestate. These observations clearly indicated that IEM scaling problems by calcium and magnesium precipitation can be ubiquitous for ED nutrient separation from wastewater.

6.3.3 Precipitation with different IEMs

The application of CMV contributed to better separation of the divalent cations (Ca^{2+} and Mg^{2+}) compared to CR 67 (Figures 6.5a and 6.5b) while similar electric current

densities were observed with the MW liquid digestate between CMV and CR 67 (Figure 6.5c). This result is consistent with previous studies where CMV highly favors divalent cations over monovalent cations (Van der Bruggen et al., 2004; Kim and Lawler, 2011; Dong et al., 2020). As CR 67 is less selective for divalent cations, consistently higher ammonia concentration was observed in the concentrate with CR 67 compared to CMV (Appendix, Figure D2, and Figures 6.5a, 6.5b). Thus, we recommend that CR 67 for ammonia separation from wastewater while CMV is recommended in separation process for water softening or groundwater desalination.

While the electric current density was similar between CMV/AMV and CR 67/AR 908 for the MW liquid digestate, CR 67/AR 908 resulted in a much higher electric current density for FW liquid digestate (Figure 6.5c). For the FW liquid digestate, one important difference from the MW liquid digestate is the soluble COD (3215 ± 714 mg/L for FW liquid digestate vs. 457 ± 29 mg/L for MW liquid digestate as shown in Table 6.2). This substantially high COD of the FW liquid digestate triggered serious organic fouling on the CMV/AMV membranes, resulting in the rapid decrease in the electric current density from 13.8 to 4.6 mA/cm^2 (Figure 6.5c). On the other hand, the electric current density for CR 67/AR 908 was maintained high between 14.4 to 21.7 mA/cm^2 over the 6-h operation. Based on these experimental results, CR 67 and AR 908 can be applied for efficient ammonia separation from high-strength wastewater with reduced organic fouling problems.

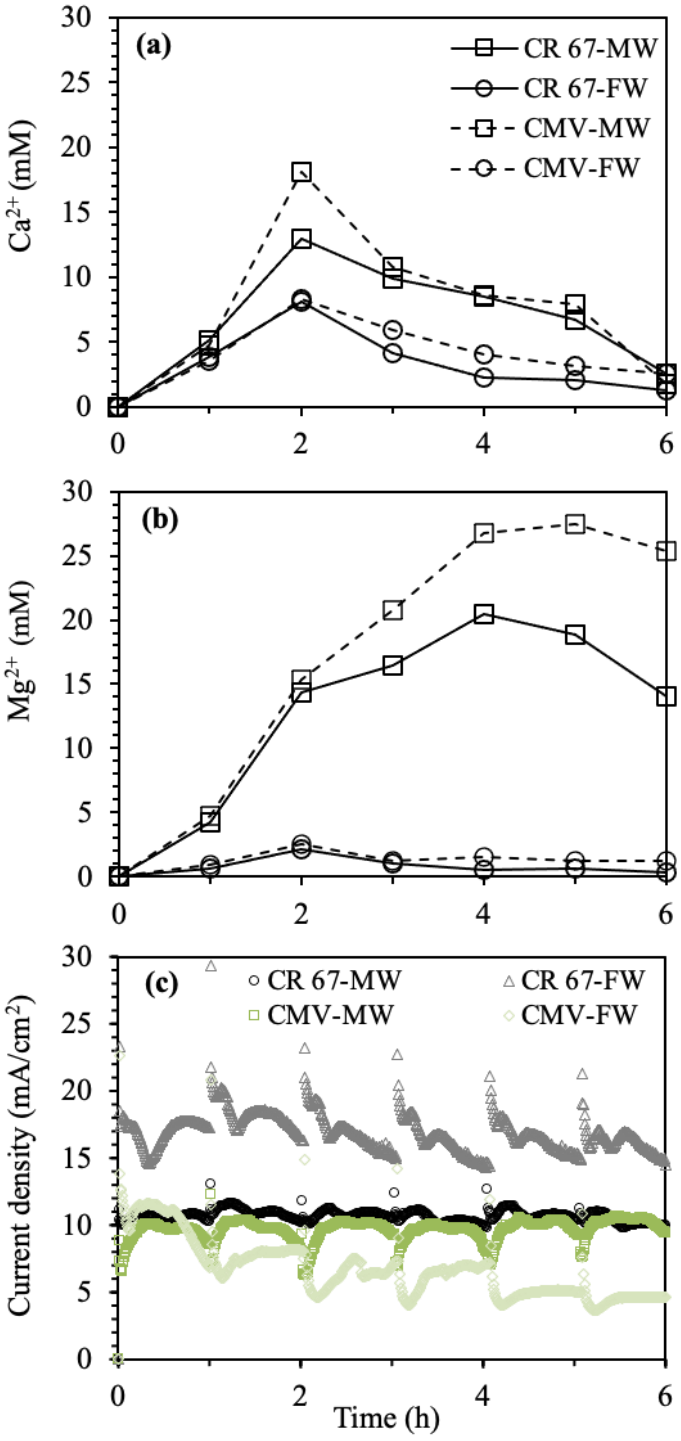

Figure 6.5. Concentration of (a) calcium and (b) magnesium in the concentrate cell with different membranes and feed sources; (c) the electric current density of the ED system.

6.3.4 SEM-EDS analysis

The majority of IEM scalants were found to be calcium carbonate in the SEM-EDS analysis (Figure 6.6). Two types of calcium carbonate crystals (amorphous powders and spherical solid) were found on the CEM surfaces (Figure 6.6a) while only spherical calcium carbonate precipitates were formed on the AEM surfaces (Figures 6.6b). Amorphous calcium carbonate (ACC) is a metastable precursor for crystalline calcium carbonate polymorphs (Ogino et al., 1987; Rodriguez-Blanco et al., 2012; Bots et al., 2012). Thus, ACC is rapidly transformed into more stable anhydrous polymorphs for calcium carbonate (i.e., calcite, vaterite, and aragonite) (Ogino et al., 1987). However, this transformation is inhibited and thus slowed with a presence of magnesium ions that increase the stability of ACC (Rodriguez-Blanco et al., 2012; Loste et al., 2003). The large amount of ACC on the CEM surface (i.e., amorphous small and cloudy particles in Figure 6.6a) can be explained by the high magnesium concentration near the CEM surface (Figure 6.4b) because Mg^{2+} was continuously supplied from Feed Cell-A through the CEM. On the other hand, ACC was not found on the AEM surface (Figure 6.6b), supporting the role of Mg^{2+} in increasing ACC stability (Rodriguez-Blanco et al., 2012; Loste et al., 2003). It should be noted that Mg^{2+} concentration is negligible on the surface of an AEM because high positive fixed charges effectively repel multi-valent cations from the surface (Strathmann, 2004).

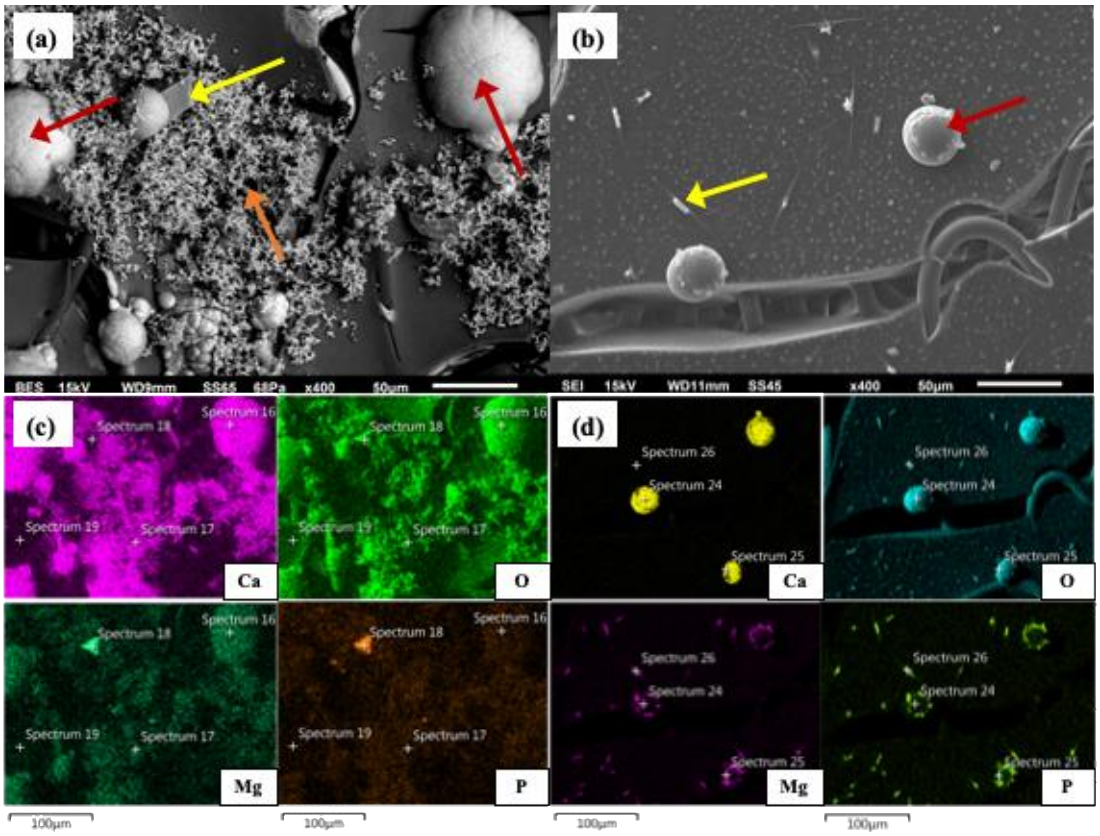

Figure 6.6. SEM-EDS images of SUEZ membranes after 6 h operation with the MW liquid digestate at 10.6 mA/cm^2. (a) CEM, 50 μm; (b) AEM, 50 μm; (c) CEM mapping; (d) AEM mapping. (Orange arrow: ACC; yellow arrow: struvite; Red arrow: vaterite).

There are three major anhydrous polymorphs for calcium carbonate: calcite; vaterite; and aragonite. Among these, calcite is thermodynamically most stable with rhombohedral structure (Andritsos et al., 1997; Ševčík et al., 2018; Tzotzi et al., 2007). Vaterite commonly has 3 different crystalline structures: rough-surfaced spheroids; cauliflower-surfaced spheroids; and disk-shaped particles (Andritsos et al., 1997). Aragonite crystals are known to form needle-shaped and sharp agglomerates (Andritsos et al., 1997). According to the SEM images, the relatively large spherical calcium carbonate precipitates

(10 – 50 μm in diameter) were identified as vaterite crystals (Figures 6.6a and 6.6b). Thus, vaterite and ACC were found on the IEM surface when the MW liquid digestate was used for nutrient separation. However, when the MW liquid digestate was replaced by a synthetic salt solution (10 mM $CaCl_2$ in Feed Cell-A and 10 mM Na_2CO_3 in Feed Cell-C), only calcite (rhombohedral calcium carbonate) was observed on IEM surfaces (Appendix, Figure D3). This inconsistency in the observed $CaCO_3$ scalants on IEMs clearly indicates that experimental results with synthetic solutions cannot present scaling problems in real ED applications for nutrient separation from wastewater.

In the SEM-EDS analysis, struvite was found to be the only magnesium precipitate both on the CEM and AEM surfaces (Figure 6.6). Compared to the calcium precipitates, the visible amount of struvite crystals was relatively minor (Figures 6.6a and 6.6b) even though the molar concentration of Mg^{2+} was similar to that of Ca^{2+} (Table 6.2). In the SEM images, needle-shaped struvite was observed on the IEM surfaces (Figures 6.6a and 6.6b). This typical needle-shaped struvite was also observed in previous studies (Le Corre et al., 2005; Cusick and Logan, 2012). In addition, the struvite crystals on the CEM surface were larger than those on the AEM surface (Figures 6.6a and 6.6b) since the high calcium concentration near the CEM surface contributed to the rapid agglomeration of struvite particles (Le Corre et al., 2005). Considering the sharp struvite can puncture membranes and cause irreversible damages to the membranes, the formation of struvite needs to be controlled in membrane systems.

6.4 Conclusions

Inorganic scale precipitation with Ca^{2+} and Mg^{2+} was investigated using a lab-scale ED reactor fed with the MW and FW liquid digestates. Serious $CaCO_3$ precipitation was observed for both the MW and FW liquid digestates. The magnesium precipitation was limited by the phosphate concentration for the MW liquid digestate while the magnesium scale precipitation was limited by Mg^{2+} concentration for the FW liquid digestate. However, even with the low concentration of Mg^{2+} or phosphate, the significant precipitation of magnesium was observed on IEMs, indicating the IEM scaling problems are ubiquitous in ED applications for nutrients recovery. In the SEM-EDS analysis, vaterite and struvite crystals were found on the CEM and AEM surfaces while ACC crystals were only observed on the CEM surface. Although the amount of struvite was relatively minor compared to the amount of vaterite and ACC, the struvite formation needs to be controlled in the ED since the needle-shaped struvite can puncture the IEMs. For the ED fed with synthetic solutions, calcite was observed on IEMs, indicating the experimental results with synthetic solutions can not present scaling problems in practical ED applications for nutrients separation from wastewater. In addition, the CEM with high selectivity to divalent cations works well with the MW liquid digestate (low soluble COD). However, a significant decrease in the electric current was observed when the ED reactor was operated with the FW liquid digestate (high soluble COD). Therefore, the CEM with high selectivity to divalent cations is not recommended to apply in high-strength wastewater such as FW liquid digestate.

References

Al-Amshawee, S., Yunus, M. Y. B. M., Azoddein, A. A. M., Hassell, D. G., Dakhil, I. H., and Hasan, H. A., 2020. Electrodialysis desalination for water and wastewater: A review. Chemical Engineering Journal, 380, 122231.

Andreeva, M. A., Gil, V. V., Pismenskaya, N. D., Dammak, L., Kononenko, N. A., Larchet, C., Grande, D., and Nikonenko, V. V., 2018. Mitigation of membrane scaling in electrodialysis by electroconvection enhancement, pH adjustment and pulsed electric field application. Journal of Membrane Science, 549, 129-140.

Andritsos, N., Karabelas, A. J., and Koutsoukos, P. G., 1997. Morphology and structure of CaCO3 scale layers formed under isothermal flow conditions. Langmuir, 13(10), 2873-2879.

Asraf-Snir, M., Gilron, J., and Oren, Y., 2016. Gypsum scaling of anion exchange membranes in electrodialysis. Journal of Membrane Science, 520, 176-186.

Bazinet, L., and Araya-Farias, M., 2005. Effect of calcium and carbonate concentrations on cationic membrane fouling during electrodialysis. Journal of colloid and interface science, 281(1), 188-196.

Benvenuti, T., Krapf, R. S., Rodrigues, M. A. S., Bernardes, A. M., and Zoppas-Ferreira, J., 2014. Recovery of nickel and water from nickel electroplating wastewater by electrodialysis. Separation and Purification Technology, 129, 106-112.

Bots, P., Benning, L. G., Rodriguez-Blanco, J. D., Roncal-Herrero, T., and Shaw, S., 2012. Mechanistic insights into the crystallization of amorphous calcium carbonate (ACC). Crystal Growth and Design, 12(7), 3806-3814.

Brewster, E. T., Ward, A. J., Mehta, C. M., Radjenovic, J., and Batstone, D. J., 2017. Predicting scale formation during electrodialytic nutrient recovery. Water research, 110, 202-210.

Bunani, S., Yoshizuka, K., Nishihama, S., Arda, M., and Kabay, N., 2017. Application of bipolar membrane electrodialysis (BMED) for simultaneous separation and recovery of boron and lithium from aqueous solutions. Desalination, 424, 37-44.

Casademont, C., Pourcelly, G., and Bazinet, L., 2007. Effect of magnesium/calcium ratio in solutions subjected to electrodialysis: Characterization of cation-exchange membrane fouling. Journal of colloid and interface science, 315(2), 544-554.

Chao, Y. M., and Liang, T. M., 2008. A feasibility study of industrial wastewater recovery using electrodialysis reversal. Desalination, 221(1-3), 433-439.

Cusick, R. D., and Logan, B. E., 2012. Phosphate recovery as struvite within a single chamber microbial electrolysis cell. Bioresource technology, 107, 110-115.

Davis, M. L., and Masten, S. J., 2013. Principles of Environmental Engineering. McGraw-Hill Education.

Dong, T., Yao, J., Wang, Y., Luo, T., and Han, L., 2020. On the permselectivity of di- and mono-valent cations: Influence of applied current density and ionic species concentration. Desalination, 488, 114521.

İpekçi, D., Kabay, N., Bunani, S., Altıok, E., Arda, M., Yoshizuka, K., and Nishihama, S., 2020. Application of heterogeneous ion exchange membranes for simultaneous separation and recovery of lithium and boron from aqueous solution with bipolar membrane electrodialysis (EDBM). Desalination, 479, 114313.

Ippersiel, D., Mondor, M., Lamarche, F., Tremblay, F., Dubreuil, J., and Masse, L., 2012. Nitrogen potential recovery and concentration of ammonia from swine manure using electrodialysis coupled with air stripping. Journal of environmental management, 95, S165-S169.

Kim, Y., and Lawler, D. F., 2011. Selectivity coefficients of cation-exchange membranes: Maximizing consistency and minimizing error amplification. Separation and purification technology, 81(3), 357-362.

Lafi, R., Gzara, L., Lajimi, R. H., and Hafiane, A., 2018. Treatment of textile wastewater by a hybrid ultrafiltration/electrodialysis process. Chemical Engineering and Processing-Process Intensification, 132, 105-113.

Le Corre, K. S., Valsami-Jones, E., Hobbs, P., and Parsons, S. A., 2005. Impact of calcium on struvite crystal size, shape and purity. Journal of crystal growth, 283(3-4), 514-522.

Le, X. T., Bui, T. H., Viel, P., Berthelot, T., and Palacin, S., 2009. On the structure–properties relationship of the AMV anion exchange membrane. Journal of Membrane Science, 340(1-2), 133-140.

Li, Z., Linares, R. V., Bucs, S., Aubry, C., Ghaffour, N., Vrouwenvelder, J. S., and Amy, G., 2015. Calcium carbonate scaling in seawater desalination by ammonia–carbon dioxide forward osmosis: Mechanism and implications. Journal of Membrane Science, 481, 36-43.

Liu, R., Wang, Y., Wu, G., Luo, J., and Wang, S., 2017. Development of a selective electrodialysis for nutrient recovery and desalination during secondary effluent treatment. Chemical Engineering Journal, 322, 224-233.

Loste, E., Wilson, R. M., Seshadri, R., and Meldrum, F. C., 2003. The role of magnesium in stabilising amorphous calcium carbonate and controlling calcite morphologies. Journal of Crystal Growth, 254(1-2), 206-218.

Mei, Y., Li, X., Yao, Z., Qing, W., Fane, A. G., and Tang, C. Y., 2020. Simulation of an energy self-sufficient electrodialysis desalination stack for salt removal efficiency and fresh water recovery. Journal of Membrane Science, 598, 117771.

Mikhaylin, S., and Bazinet, L., 2016. Fouling on ion-exchange membranes: Classification, characterization and strategies of prevention and control. Advances in colloid and interface science, 229, 34-56.

Miyoshi, H., Chubachi, M., Yamagami, M., and Kataoka, T., 1992. Characteristic coefficients for equilibrium between solution and Neosepta or Selemion cation exchange membranes. Journal of Chemical and Engineering Data, 37(1), 120-124.

Mondor, M., Ippersiel, D., and Lamarche, F., 2012. Electrodialysis in food processing. In Green technologies in food production and processing (pp. 295-326). Springer, Boston, MA.

Moran, S., 2018. An Applied Guide to Water and Effluent Treatment Plant Design. Butterworth-Heinemann.

Nguyen, L. D., Gassara, S., Bui, M. Q., Zaviska, F., Sistat, P., and Deratani, A., 2019. Desalination and removal of pesticides from surface water in Mekong Delta by coupling

electrodialysis and nanofiltration. Environmental Science and Pollution Research, 26(32), 32687-32697.

Ogino, T., Suzuki, T., and Sawada, K., 1987. The formation and transformation mechanism of calcium carbonate in water. Geochimica et Cosmochimica Acta, 51(10), 2757-2767.

Ohlinger, K. N., Young, T. M., and Schroeder, E. D., 1998. Predicting struvite formation in digestion. Water Research, 32(12), 3607-3614.

Patel, S. K., Qin, M., Walker, W. S., and Elimelech, M., 2020. Energy Efficiency of Electro-Driven Brackish Water Desalination: Electrodialysis Significantly Outperforms Membrane Capacitive Deionization. Environmental Science and Technology, 54(6), 3663-3677.

Phuntsho, S., Lotfi, F., Hong, S., Shaffer, D. L., Elimelech, M., and Shon, H. K., 2014. Membrane scaling and flux decline during fertiliser-drawn forward osmosis desalination of brackish groundwater. Water research, 57, 172-182.

Rodriguez-Blanco, J. D., Shaw, S., Bots, P., Roncal-Herrero, T., and Benning, L. G., 2012. The role of pH and Mg on the stability and crystallization of amorphous calcium carbonate. Journal of Alloys and Compounds, 536, S477-S479.

Ševčík, R., Šašek, P., and Viani, A., 2018. Physical and nanomechanical properties of the synthetic anhydrous crystalline CaCO 3 polymorphs: vaterite, aragonite and calcite. Journal of materials science, 53(6), 4022-4033.

Shi, L., Hu, Y., Xie, S., Wu, G., Hu, Z., and Zhan, X., 2018. Recovery of nutrients and volatile fatty acids from pig manure hydrolysate using two-stage bipolar membrane electrodialysis. Chemical Engineering Journal, 334, 134-142.

Strathmann, H., 2004. Ion-exchange membrane separation processes. Elsevier.

Tzotzi, C., Pahiadaki, T., Yiantsios, S. G., Karabelas, A. J., and Andritsos, N., 2007. A study of CaCO3 scale formation and inhibition in RO and NF membrane processes. Journal of membrane science, 296(1-2), 171-184.

Van der Bruggen, B., Koninckx, A., and Vandecasteele, C., 2004. Separation of monovalent and divalent ions from aqueous solution by electrodialysis and nanofiltration. Water research, 38(5), 1347-1353.

Verbanck, M., Buess-Herman, C., and Hurwitz, H. D., 2006. Properties of CMV cation exchange membranes in sulfuric acid media. Journal of membrane science, 284(1-2), 67-78.

Walker, W. S., Kim, Y., and Lawler, D. F., 2014. Treatment of model inland brackish groundwater reverse osmosis concentrate with electrodialysis—Part I: sensitivity to superficial velocity. Desalination, 344, 152-162.

Wang, Y., Jiang, C., Bazinet, L., and Xu, T., 2019. Electrodialysis-Based Separation Technologies in the Food Industry. In Separation of Functional Molecules in Food by Membrane Technology (pp. 349-381). Academic Press.

Wang, Y. K., Geng, Y. K., Pan, X. R., and Sheng, G. P., 2017. In situ utilization of generated electricity for nutrient recovery in urine treatment using a selective electrodialysis membrane bioreactor. Chemical Engineering Science, 171, 451-458.

Ward, A. J., Arola, K., Brewster, E. T., Mehta, C. M., and Batstone, D. J., 2018. Nutrient recovery from wastewater through pilot scale electrodialysis. Water research, 135, 57-65.

Xu, X., He, Q., Ma, G., Wang, H., Nirmalakhandan, N., and Xu, P., 2018. Selective separation of mono-and di-valent cations in electrodialysis during brackish water desalination: Bench and pilot-scale studies. Desalination, 428, 146-160.

Ye, Z. L., Ghyselbrecht, K., Monballiu, A., Pinoy, L., and Meesschaert, B., 2019. Fractionating various nutrient ions for resource recovery from swine wastewater using simultaneous anionic and cationic selective-electrodialysis. Water research, 160, 424-434.

7 Modeling Ammonia and Acetic Acid Inhibition on Mesophilic Anaerobic Digestion Fed with Thickened Waste Activated Sludge

Anaerobic digestion (AD) in wastewater treatment is essential for sludge stabilization and biosolids reduction. Many factors, such as ammonia, volatile fatty acids (VFA), and pH, are regarded as inhibitors in AD processes. Although many studies reported the toxicity of ammonia on methanogens, there is still limited understanding on the inhibition of ammonia on hydrogenotrophic methanogenesis. In addition, the inhibition of acetic acid on methanogenesis was not investigated in previous studies. Therefore, we investigated the effects of high concentrations of ammonia and acetic acid on AD performance through biogas methane production tests. A modified AD model with various inhibition functions was built to translate lab-scale experimental results on methane production.

This paper is prepared for future journal publication.

- Guo, H., Fernandes, S., and Kim, Y. Modeling Ammonia and Acetic Acid inhibition on Mesophilic Anaerobic Digestion Fed with thickened Waste Activated Sludge

The co-author's contributions include:

Sarah Fernades: experiments operation, data collection.

Younggy Kim: supervision, technical support, funding acquisition, manuscript revision.

Abstract

Anaerobic digestion (AD) has been regarded as an environmental-friendly technology to treat wastewater and produce renewable energy. Inhibition of ammonia, volatile fatty acids (VFAs), and pH have been investigated and modelled in AD. However, limited studies presented ammonia inhibition on hydrogenotrophic methanogenesis. In addition, the inhibition of acetic acid (the most common VFA product during AD processes) on methane production was not considered in many AD studies. Therefore, in this study, we investigated the inhibition of high ammonia concentrations and acetate concentrations on AD through biochemical methane potential (BMP) tests. The results indicated that the AD fed with thickened waste activated sludge (TWAS) could be tolerated up to 6.8 g-N/L of total ammonia (TAN). The high initial pH (~8.8) increased the concentration of free ammonia (FAN) and significantly decreased methane production. The methane production in the BMP tests with 0 and 20 g-COD/L of additional acetate was similar. However, more than 50% of methane was reduced when the additional acetate concentration increased to 40 g-COD/L. A modified anaerobic digestion model (ADM) with various inhibition functions was proposed to simulate the inhibition of ammonia and acetic acid on methanogenesis. The acetate uptake rate in ADM was introduced by a Haldane function. In addition, sensitivity analysis was conducted to quantify the degree of inhibitions of free ammonia, acetate, and acetic acid on individual microbial activities in the ADM.

Keywords

Anaerobic digestion model; Non-competitive inhibition; Haldane inhibition; Threshold inhibition; Relative sensitivity

7.1 Introduction

Anaerobic digestion (AD) is an essential wastewater treatment method for energy recovery and sludge management [1]. AD that involves multi-step biological processes (i.e., hydrolysis, acidogenesis, and methanogenesis) can degrade organic matters and convert them into renewable energy sources (biogas of methane and carbon dioxide) [1][2][3]. Acetoclastic and hydrogenotrophic methanogenesis play important roles in methane production and thus have been regarded as essential indicators of AD stability [2][4][5]. Many inhibitors, such as ammonia [5][6][7][8], sulfide [9][10], volatile fatty acids (VFAs) [11][12], heavy metals [13], and nanomaterials [14], can affect methanogens activities and cause AD failures. Among these inhibitors, ammonia, whose concentration is usually high in municipal and food waste sludge [15], has attracted more attention due to significant inhibition [5].

Ammonia is an essential nutrient for bacteria growth. However, a high concentration of ammonia is toxic to methanogens since ammonia can change intracellular pH or inhibit the methane synthesizing enzyme directly [16][17][18]. Diffusion of ammonia into bacterial cells causes proton imbalance or potassium deficiency [16][17][18]. Free ammonia (FAN) and ammonium (NH_4^+) are two forms of ammonia in aqueous solutions. FAN is more toxic than NH_4^+ for methanogens because of the high permeability of FAN to bacterial cell membranes [19]. The concentration of total ammonia (TAN) that ranged from 1.4 to 15 g-N/L (concentration of FAN was in the range of 0.03 to 1.4 g-N/L) resulted in 50% to 100% inhibition on methane production under different operating conditions [6][8][20][21][22][23]. Through the analysis of methanogenic populations, acetoclastic

methanogens seem to be more sensitive to FAN than hydrogenotrophic methanogens [24][25][26]. However, hydrogenotrophic methanogenesis was the main pathway for methane production in high FAN levels [25][27].

VFAs (i.e., propionic, butyric, valeric, and acetic acid) are intermediate products during AD processes. The accumulation of VFAs especially acetic acid indicates the instability of AD. The reasonable VFA concentration in a stable AD system should be in the range of 50 to 250 mg/L [12]. However, the concentration of VFA in the AD fed with kitchen wastes could be increased to 18 g/L [28]. The widely accepted mechanisms for VFA inhibition are the activity loss of enzymes and the inhibition of bacterial cell activity due to significant pH changes [29][30][31]. Among the four VFAs in AD, acetic acid is the main VFA product during hydrolysis and acidogenesis processes [32]. Although many studies reported the inhibition of total VFAs (TVFA) on AD [28][33], limited studies investigated the inhibition of acetic acid on methane production especially the AD fed with thickened waste activated sludge (TWAS). Therefore, we focused on investigating the inhibition of acetic acid on AD in this study.

Inhibition models that represent the response of methane production for inhibitors have been developed based on many inhibition experiments [34]. Un-competitive and non-competitive inhibition functions have been used to model ammonia inhibition on AD [35]. Ammonia affects the overall uptake rate and affinity of the substrate in un-competitive inhibition functions [35][36] while ammonia linearly affects the biomass growth rate (or substrate uptake rate) in the non-competitive inhibition functions [37][38][39]. Non-competitive inhibition of FAN was involved in Anaerobic Digestion Model No.1 (ADM1)

[39]. However, the ADM1 only considered the inhibition of FAN on acetoclastic methanogenesis. In fact, hydrogenotrophic methanogenesis is the leading pathway for methane production when FAN concentrations are high [25][27]. The hydrogenotrophic methanogens (especially *Methanobacterium congolense* and *Methanoculleus thermautotophicus*) are sensitive to the ammonia concentration under mesophilic conditions [40][41]. Therefore, this study aims to modify the ammonia inhibition functions in ADM1 by introducing the FAN inhibition functions for hydrogenotrophic methanogenesis. Methane production in AD with a high concentration of TAN was evaluated.

High concentrations of VFAs especially the accumulation of acetic acid showed serious inhibition on the activity of methanogens [28][31][42][43][44]. However, the acetic acid inhibition on AD was not considered in the original ADM1 [39]. In previous studies, a non-competitive function was added into ADM1 to simulate the inhibition of TVFAs on methanogenesis [45][46]. The effects of acetic acid on the degradation of propionic and butyric acid were also introduced using non-competitive functions in a modified ADM1 [41]. Many studies demonstrated that a threshold inhibition is more suitable to simulate methane production with different concentrations of inhibitors [41][47][48]. Therefore, the acetic acid inhibitions on acetoclastic and hydrogenotrophic methanogenesis were introduced by threshold inhibition functions in the modified ADM1. Since acetate is an important substrate for acetoclastic methanogenesis, the uptake rate of acetate was modeled by Haldane inhibition which is frequently used to represent methanogenesis reactions[49][50].

The main objectives of this study are to: investigate the effects of high concentrations of ammonia and acetate on methane production; modify the ADM1 by introducing various inhibition functions; calibrate model parameters for inhibition functions; examine the sensitivity of individual model parameters.

7.2 Methods and Materials

7.2.1 Experimental methods

The biochemical methane potential (BMP) tests were performed with batch AD reactors. The lab-scale AD reactors were built using 160 mL glass bottles and operated at a mesophilic temperature of 37.5 ℃ in a shaking incubator (700L Stackable Incubated 126 Shaker, Eppendorf, USA) for 28 d. TWAS collected from the local wastewater treatment plant (Woodward Avenue Wastewater treatment plant, Hamilton, Ontario, Canada) was used as the substrate for the AD reactors. The solids concentration (42.7 ± 7.4 g/L of total suspended solids, TSS) was observed in TWAS (Table 7.1).

Table 7.1. The main characteristics of the TWAS (average ± standard deviation, n =4)

Component	TWAS	Seed sludge
NH_3-N	0.30 ± 0.03 g/L	2.45 ± 0.39 g/L
Total Suspended Solids (TSS)	42.7 ± 7.4 g/L	32.3 ± 5.5 g/L
Volatile Suspended Solids (VSS)	31.8 ± 5.0 g/L	19.0 ± 2.8 g/L
Total Chemical Oxygen Demand (TCOD)	50.5 ± 7.4 g/L	27.0 ± 0.9 g/L
Soluble Chemical Oxygen Demand (Soluble COD)	5.1 ± 0.7 g/L	1.4 ± 0.2 g/L
Conductivity	3.7 ± 0.2 mS/cm	15.7 ± 1.1 mS/cm
pH	6.6 ± 0.3	7.7 ± 0.1

The total sludge volume in AD reactors was 90 mL which consists of 70 mL TWAS and 20 mL seed sludge (Table 7.1). The seed sludge was collected from a lab-scale inoculum reactor that was fed with TWAS for 10 months (sludge retention time of 21 d) at 37.5 ℃. The seed sludge and TWAS were both purged with nitrogen gas before feeding into the AD reactors.

The BMP tests were performed with various concentrations of TAN and acetate (Table 7.2). Ammonium chloride (NH_4Cl, VWR international, Canada) and ammonium hydroxide (NH_4OH, VWR international, Canada) were used as TAN sources while sodium acetate ($CH_3COONa \cdot 3H_2O$, VWR international, Canada) was used as acetate source. The effects of TAN concentrations on AD performance were estimated by comparing the experimental results of the BMP tests under two different additional TAN concentrations (0 and 4 g-N/L). The initial pH of the BMP tests was controlled by changing the concentration ratio of NH_4Cl and NH_4OH. NH_4Cl was the only TAN source for the BMP tests with neutral pH (ranged from 7.24 to 7.34 as shown in Appendix, Table E1) while the 4 g-N/L of TAN in the BMP tests with high initial pH (ranged from 8.78 to 8.89 as shown in Appendix, Table E1) was supplied by NH_4Cl (90%) and NH_4OH (10%). To investigate the inhibition of acetate on AD, sodium acetate was added to AD reactors, resulting in the additional acetate concentration of 0, 20, 40 g-COD/L in the BMP tests. In summary, 9 BMP tests (Table 7.2) were completed with three different ammonia conditions (0 g-N/L with neutral pH; 4 g-N/L with neutral pH; 4 g-N/L with high pH) and three different acetate concentrations (0, 20, 40 g-COD/L).

Table 7.2. Experimental conditions of BMP tests

Additional acetate→ Additional TAN ↓	0 g-COD/L (0COD)	20 g-COD/L (20COD)	40 g-COD/L (40COD)
0 g-N/L	0COD | 0N	20COD | 0N	40COD | 0N
4 g-N/L as NH_4Cl	0COD | 4N-NPH	20COD | 4N-NPH	40COD | 4N-NPH
4 g-N/L as NH_4Cl and NH_4OH	0COD | 4N-HPH	20COD | 4N-HPH	40COD | 4N-HPH

7.2.2 Experimental measurement

The headspace biogas from AD reactors was collected and analyzed every two days. The biogas volume was measured using gas-tight syringes (50 mL, Dyna Medical Corporation, Canada). The fraction of carbon dioxide and methane was analyzed with nitrogen gas using a thermal conductivity detector – gas chromatograph (TCD-GC) (SRI 8610C, SRI Instruments, USA). The TCD-GC used a molecular sieve column (ShinCarbon ST 19808, Restek, USA) with helium as the carrier gas. Initial biogas analysis with the TCD-GC confirmed that nitrogen was the only gas present in the first few minutes of the BMP tests since the feed sludge was purged by nitrogen for 1-3 minutes.

The initial and final pH of the sludge was measured (Orion Versa Star Pro, Thermo Fisher Scientific, USA) and recorded (Appendix, Table E1). The pH in the BMP tests of 0N and 4N-NpH increased from 7.3 to 7.7 while the pH in the BMP tests of 4N-HpH decreased from 8.8 to 7.7 after 28 d (Appendix, Table E1). The TAN concentrations in the initial and final sludge were analyzed by using commercial ammonia test vials (Method 10,205, Hach Company, USA). More than 1.5 g-N/L of TAN was produced during the BMP tests (Appendix, Table E1). The total solids (TS, 51.2 ± 1.7 g/L) and volatile solids

(VS, 26.2 ± 6.7 g/L) were measured in accordance with the standard method [51]. The methane yield in the BMP tests was normalized by the volatile solids (VS) concentration (26.2 g/L).

7.3 Model development

7.3.1 FAN inhibition on methanogenesis

In the original ADM1, the ammonia inhibition on acetoclastic methanogenesis was introduced by a non-competitive inhibition function (Eq 7.1) [39]. However, the effects of ammonia on hydrogenotrophic methanogenesis were not considered. Previous studies indicated that hydrogenotrophic methanogenesis dominates methane production when FAN concentrations were high [25][27]. Therefore, a non-competitive inhibition function was added in the modified ADM to show the effects of FAN concentration on hydrogenotrophic methanogens (Eq 7.2).

$$I_{NH_3,Xac} = \frac{1}{1+{S_{NH_3}}/{K_{INH_3,Xac}}} \qquad \text{Eq 7.1}$$

$$I_{NH_3,Xh_2} = \frac{1}{1+{S_{NH_3}}/{K_{INH_3,Xh_2}}} \qquad \text{Eq 7.2}$$

$I_{NH_3,Xac}$ and I_{NH_3,Xh_2} denote the inhibition degree of FAN on acetoclastic and hydrogenotrophic methanogenesis, respectively. The value of 1 stands for no inhibition while the value around 0 represents complete inhibition. S_{NH_3} is the concentration of FAN. $K_{INH_3,Xac}$ and $K_{INH_3,Xh2}$ are the FAN concentrations that cause 0.5 inhibition. The values of $K_{INH_3,Xac}$ and $K_{INH_3,Xhe}$ need to be calibrated in this study.

7.3.2 Haldane kinetics for acetate inhibition on acetoclastic methanogenesis

The uptake rate of acetate was introduced by Haldane kinetics (Eq 7.3) which is frequently used to represent the acetate inhibition on acetoclastic methanogenesis [49][50].

$$Rate\ of\ uptake\ of\ aetate = k_{ac}\frac{S_{AC}}{K_{sac}+S_{AC}+{S_{AC}^2}/{K_{IAC,Xac}}}X_{AC}I_1 \qquad \text{Eq 7.3}$$

S_{AC} is the concentration of acetate. k_{ac} is the maximum specific acetoclastic methanogenesis rate. K_{sac} is the half-saturation value for acetoclastic methanogenesis (Appendix, Table E2). $K_{IAC,Xac}$ is the inhibition constant causes half inhibition and the value of $K_{IAC,Xac}$ needs to be determined in this study.

7.3.3 Acetic acid inhibition on methanogenesis

Threshold functions have been used to simulate methane production with different concentrations of inhibitors [41][47][48]. In this study, threshold inhibition functions were introduced in an ADM to represent the effects of the concentration of acetic acid on acetoclastic methanogenesis and hydrogenotrophic methanogenesis (Eq 7.4 and 7.5).

$$I_{Hac\_xac} = \begin{cases} 1 & HAC \le HAC_{min} \\ \dfrac{p+e^{a\left(\frac{HAC-HAC_{min}}{HAC_{max}-HAC_{min}}\right)^2}}{p+1} & HAC > HAC_{max} \end{cases} \qquad \text{Eq 7.4}$$

$$I_{Hac\_xh2} = \begin{cases} 1 & HAC \le HAC_{min,} \\ \dfrac{q+e^{b\left(\frac{HAC-HAC_{min,}}{HAC_{max,}-HAC_{min,}}\right)^2}}{q+1} & HAC > HAC_{max,} \end{cases} \qquad \text{Eq 7.5}$$

I_{Hac_xac} and I_{Hac_xh2} indicate the inhibition degree of acetic acid on acetoclastic methanogenesis. HAC_{min} and $HAC_{min,}$ are the acetic acid concentrations where inhibition starts. The maximum inhibition is reached when the acetic acid concentration is equal to

HAC_{max} and $HAC_{max\prime}$. The values of p and q determine the maximum inhibition. The maximum inhibition is $\frac{p}{p+1}$ for acetoclastic methanogenesis and $\frac{q}{q+1}$ for hydrogenotrophic methanogenesis. The exponent a or b provides a progressive increase in inhibition when the concentration of acetic acid is higher than the lower limit.

7.3.4 ADM validation

A non-steady-state ADM with inhibition functions of FAN, acetic acid, and acetate was built based on ADM1 [39]. Kinetic rate expressions including 19 reactions and 21 biological components of the ADM were listed in Appendix, Table E2. Kinetic coefficients were slightly changed from the original ADM1 model [39] with minor adjustments to the mesophilic temperature of 37.5 ºC (Appendix, Table E3). Some fractions including the acetate from sugars, hydrogen from sugars, acetate from amino acids, and hydrogen from amino acids were modified to represent the contribution of hydrogenotrophic methanogenesis to methane production (Appendix, Table E3).

The numerical model ADM was implemented using the visual basic application (VBA) and solved implicitly using fixed-point iterations. The initial concentrations of the 21 biological components in TWAS (Appendix, Table E4) were obtained from the characterization of TWAS (Table 7.1) and the previous studies that used similar substrates [52][53][54]. The initial values of TWAS were used in a steady-state ADM 1 (21 d of sludge retention time) to simulate the concentration of biological components in the seed sludge (Appendix, Table E4). The initial concentration used in the ADM was obtained from 28.6% of concentrations in the seed sludge (20 ml/70 mL) and 71.4% of concentrations in TWAS (50 mL/70 mL). Linear changes of pH and ammonia were

assumed in the model based on the experimental measurements (as shown in Appendix, Table E1).

7.3.5 Sensitivity analysis

To compare the sensitivity of parameters during the experimental period, the average relative sensitivity of individual parameters is calculated based on Eq 7.6 and 7.7 [55][56].

$$average\ relative\ sensitivity = \frac{\sum_{k0}^{kn}(\frac{\partial y(k)}{\partial \theta} \times \frac{\theta}{y(k)})}{n} \quad \text{Eq 7.6}$$

$$\frac{\partial y(k)}{\partial \theta} = \frac{y(k,\theta+\Delta\theta)-y(k,\theta-\Delta\theta)}{2\Delta\theta} \quad \text{Eq 7.7}$$

y is the simulation result of methane production at k which represents the time when the biogas was measured during experiments. n is the total number of measurements in experiments. θ is the parameter in inhibition functions. $\Delta\theta$ is used to study the sensitivity of y to θ. $\Delta\theta$ is equal to 0.01θ in this study.

7.4 Results and discussions

7.4.1 Model calibration with experimental results

The ADM reliably simulated the effects of FAN, acetate, and acetic acid on methane yield (Figures 7.1a, 7.1b, 7.1c). In the ADM, the small values of $K_{INH_3,Xac}$ (1.8 mM) and K_{INH_3,Xh_2} (0.65 mM) (Table 7.3) indicated the significant inhibition of FAN on acetoclastic and hydrogenotrophic methanogenesis.

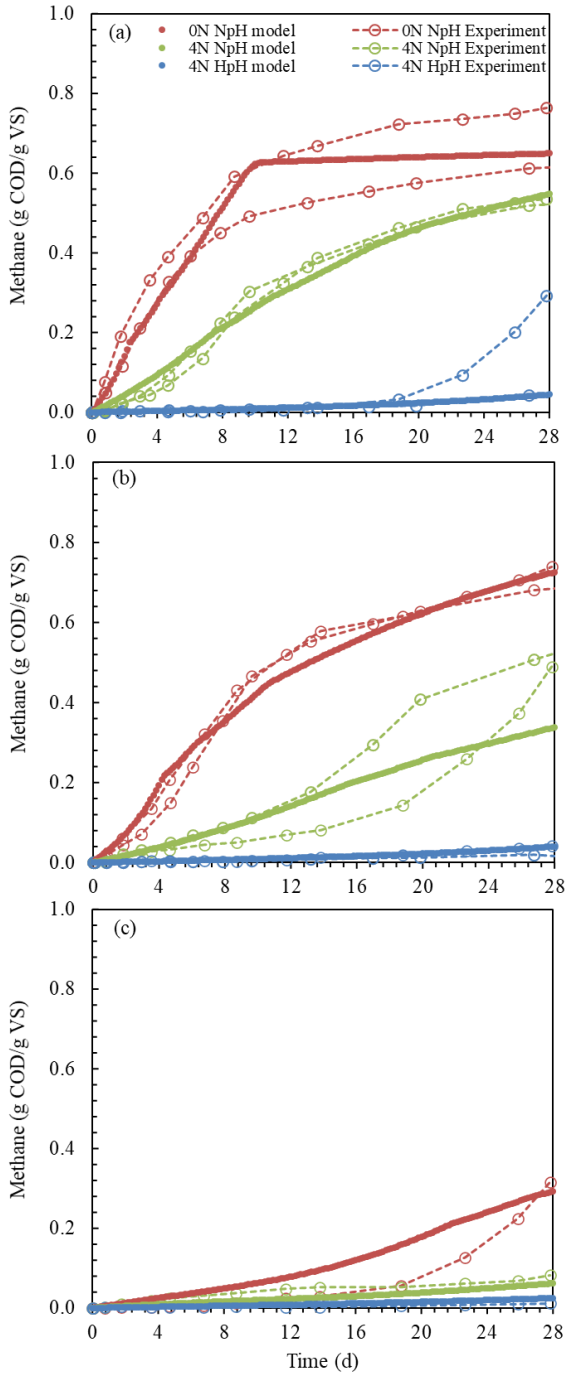

Figure 7.1. Methane yield from BMP tests and model simulation: (a) without additional acetate; (b) with 20 g-COD/L of acetate; (c) with 40 g-COD/L of acetate.

Table 7.3. Parameter values in inhibition functions

Type	Inhibition Functions
FAN inhibition on X_{AC}	$K_{INH_3,Xac} = 1.8\ mM$
FAN inhibition on X_{H2}	$K_{INH_3,Xh_2} = 0.065\ mM$
Acetate inhibition on X_{AC}	$K_{IAC,Xac} = 85\ g\ COD/L$
Acetic acid inhibition on X_{AC}	$a = -0.45$ $p = 0.4$ $HAC_{min} = 38\ mg/L$ $HAC_{max} = 100\ mg/L$
Acetic acid inhibition on X_{H2}	$b = -0.45$ $q = 0.15$ $HAC_{min'} = 40\ mg/L$ $HAC_{max'} = 90\ mg/L$

The large value of $K_{IAC,Xac}$ (85 g COD/L as shown in Table 7.3) was applied in Haldane inhibition functions to represent the substrate (i.e., acetate) inhibition. The acetic acid inhibition on acetoclastic methanogenesis starts from 38 mg/L of acetic acid while it starts from 40 mg/L of acetic acid for hydrogenotrophic methanogenesis (Table 7.3). Maximum inhibition is observed on the methanogenesis when the acetic acid concentration is higher than 100 mg/L for acetoclastic methanogenesis and 90 mg/L for hydrogenotrophic methanogenesis, respectively. Constant *p* (0.4 for acetoclastic methanogenesis as shown in Table 7.3) and *q* (0.15 for hydrogenotrophic methanogenesis as shown in Table 7.3) determine the maximum inhibition (0.29 for acetoclastic methanogenesis while 0.13 for hydrogenotrophic methanogenesis). The exponent -4.5 (Table 7.3) provides acceleration in inhibition.

The experimental and simulation results were consistent in showing that the methane yield was reduced more than 10% when the TAN concentration increased from 1 (TAN in the initial sludge as shown in Appendix, Table E1) to 5 g-N/L (initial 1 g-N/L and

additional 4 g-N/L) without additional acetate (Figure 7.1a). The slight decrease in methane yield indicated that 5 g-N/L TAN could be tolerated for TWAS with a pH around 7.55 (Appendix, Table E1). Similar results were observed in a previous study that a TAN concentration of 5980 mg/L resulted in 27% biogas reduction with a pH of 7.43 [57]. The reduction of methane yield raised to 90% when the initial pH increased from 7.27 to 8.85 (Appendix, Table E1 and Figure 7.1a). The significant methane reduction can be explained by the sharp increase in the FAN concentration (less than 0.1 g-N/L for neutral pH while more than 2 g-N/L for high pH as shown in Appendix, Figure E1) with high pH. In the early stage of the anaerobic digestion process (0 to 10 d), more than 50% of methane reduction was observed in both experimental and model simulation results (Figure 7.1a). The significant decrease in the methane reduction was due to the high inhibition of hydrogenotrophic methanogenesis which was presented by the low value of K_{INH3_xh2} (0.065 mM) in the ADM. The methane reduction decreased with increasing sludge retention time (Figure 7.1a), indicating that methanogens need time to adapt to the severe conditions. This result was consistent with a previous study that high sludge retention time helps an AD system to tolerate relatively high TAN concentration [5].

A slight increase in the methane yield was observed when the concentration of additional acetate increased from 0 g-COD/L to 20 g-COD/L with 1 g-N/L of TAN (initial TAN in the sludge as shown in Appendix, Table E1) (Figures 7.1a and 7.1b). The slight increase can be explained by the substantial substrate of acetate in 20 g-COD/L. The substrate (i.e., acetate) inhibition in 20 g-COD/L was maintained at ~0.8 (1 means no inhibition) while the fully consumed acetate contributed to the complete acetate inhibition

(around 0) in 0 g-COD/L after 11 d (Appendix, Figures E2a and E2b). There was no acetic acid inhibition in 0 g-COD/L since the concentration of acetic acid was lower than 10 mg/L during 28 d (Appendix, Figures E3a, E4a, E5a). The concentration of acetic acid in 20 g-COD/L was in the range of 10 to 58 mg/L, resulting in ~30% acetic acid inhibition on acetoclastic methanogenesis and ~40% inhibition on hydrogenotrophic methanogenesis during the early stage of the AD process (Figure 7.1b, Appendix, Figures E3b, E4b, E5b). It should be noted that the maximum methane yield rate in 20 g-COD/L (0.049 g-COD/g-VS/d) was around half of that in 0 g-COD/L (0.09 g-COD/ g-VS/d). This result was consistent with a previous study that 20 g-COD/L of acetate resulted in 50% inhibition in maximum methane yield rate [58].

Compared to the methane yield in 0 and 20 g-COD/L with 1 g-N/L, the methane yield in 40 g-COD/L with 1 g-N/L was much lower (around 40% as shown in Figure 7.1c). The lower methane concentration can be explained by the severe inhibition of methanogenesis due to the high concentration of acetic acid and acetate (Appendix, Figures E2c, E3c, E4c, and E5c). It should be noted that a slight increase was observed in methane yield in 40 g-COD/L with 1 g-N/L during the late stage of the BMP tests (Figure 7.1c). This result indicates that a longer retention time can help the AD system to tolerate severely high acetate concentration (40 g-COD/L).

FAN was the dominant inhibitor when the acetate concentration was lower than 20 g-COD/L since the similar methane yield was detected in both 0 g-COD/L with 5 g-N/L and 20 g-COD/L with 5 g-N/L under neutral pH (Figures 7.1a and 7.1b). For the high pH conditions, acetic acid inhibition was negligible while the FAN inhibition was complete

(Appendix, Figures E1, and E2). High acetate concentration (40 g-COD/L) reduced the utilization rate of acetate (Figure 7.1c and Appendix, Figure E2c) while acetic acid inhibits the activity of methanogens during the early stage of the AD process (Appendix, Figures E4c, and E5c).

7.4.2 Effects of pH on model simulation

FAN inhibition was sensitive to the pH and TAN concentration (Figure 7.2).

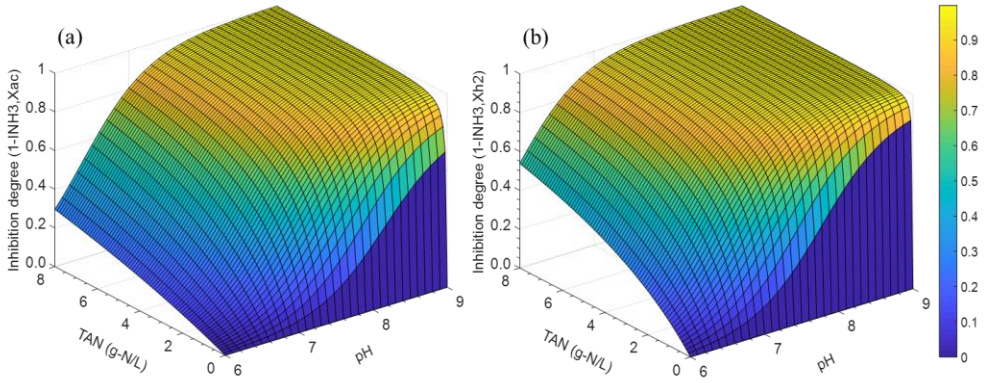

Figure 7.2. Inhibition degree with pH and different concentration of TAN (1 means complete inhibition): (a) I_{NH3_xac}; (b) I_{NH3_xh2}.

More than 50% inhibition was observed in both acetoclastic and hydrogenotrophic methanogenesis when the pH was higher than 8 with the TAN concentration of 0.1 g-N/L. This result indicated that neutral pH in the AD is necessary to maintain the activity of methanogens. FAN inhibition was mainly determined by the TAN concentration when the pH was lower than 7.5 (Figure 7.2) since less than 5% of TAN existed as un-ionized ammonia (i.e., FAN) at neutral pH. For the BMP tests in this study, the pH was in the range of 7.1 to 8.9 while the TAN concentration ranged from 1.0 to 8.5 g-N/L (Appendix, Table E1). Therefore, the inhibition degree for acetoclastic methanogenesis was higher than 0.50

(or less than 0.50 for $I_{NH_3,Xac}$) while the inhibition degree for hydrogenotrophic methanogenesis was higher than 0.73 (or less than 0.27 forI_{NH_3,Xh_2}) (Figure 7.2). The high FAN inhibition on hydrogenotrophic methanogenesis resulted in the slow methane yield rate in the early stage of the AD process (Figure 7.1).

Acetic acid inhibition was extremely sensitive to pH and acetate concentrations. There was no acetic acid inhibition on methanogenesis when the pH was higher than 7.8 and the acetate concentration varied from 0 to 60 g-COD/L (Figure 7.3). However, the maximum inhibition was reached in both acetoclastic and hydrogenotrophic methanogenesis with only 5 g-COD/L of acetate when the pH is lower than 6.6 (Figure 7.3). For the pH in the range of 7 to 7.5, the AC concentration of 19-58 g-COD/L and 15-36 g-COD/L resulted in the maximum acetic acid inhibition on acetoclastic methanogenesis and hydrogenotrophic methanogenesis, respectively.

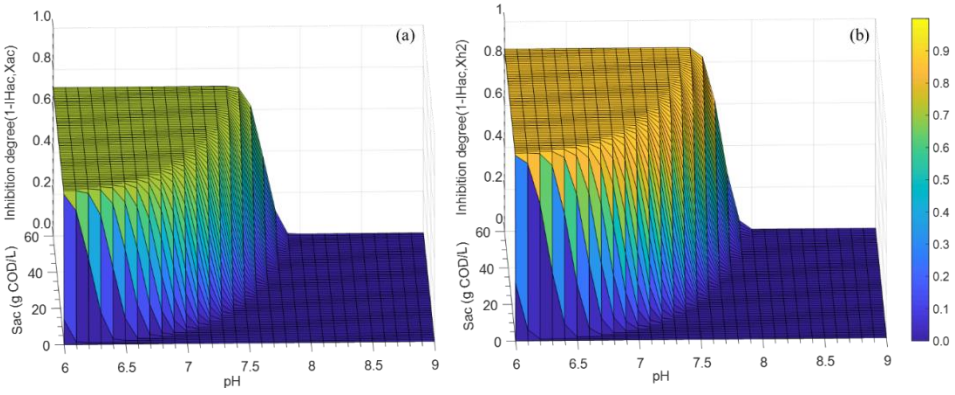

Figure 7.3. Inhibition degree with pH and different concentrations of AC (1 means complete inhibition): (a) 1- I_{Hac_xac}; (b) 1- I_{Hac_xh2}.

The methane yield was sensitive to the pH conditions (Figures 7.4).

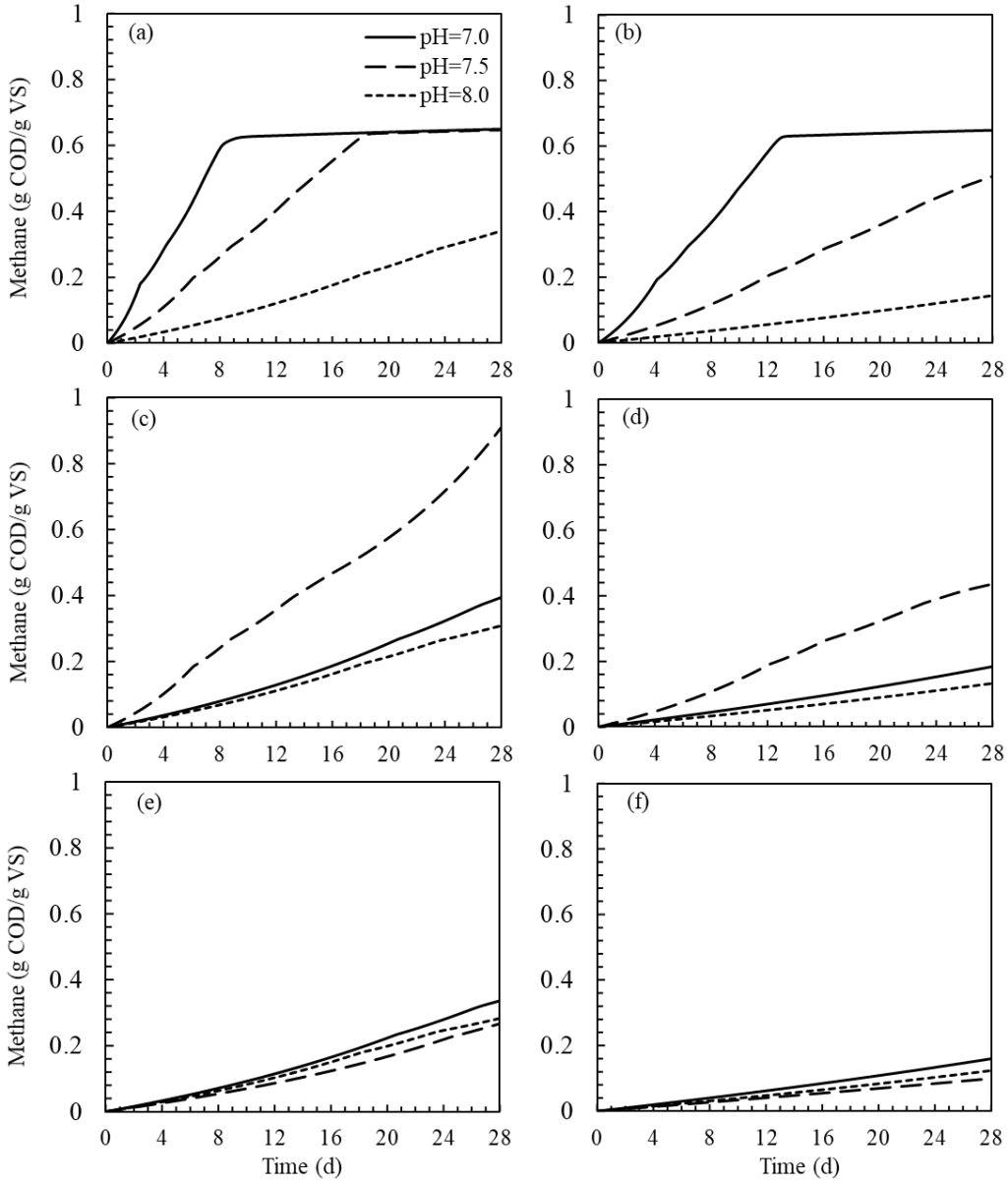

Figure 7.4. Model simulation results under different conditions. (a) 0 g AC-COD/L and 2 g TAN-N/L; (b) 0g AC-COD/L and 4 g TAN-N/L; (c) 20g AC-COD/L and 2 g TAN-N/L; (d) 20g AC-COD/L and 4 g TAN-N/L; (e) 40g AC-COD/L and 2 g TAN-N/L; (f) 40g AC-COD/L and 4 g TAN-N/L.

High pH resulted in low methane yield when the TAN concentration was 2 and 4 g-N/L without additional acetate (Figures 7.4a and 7.4b). The low methane yield can be explained by the severe FAN inhibition at high pH (Figure 7.2). For 20 g-COD/L of additional acetate, the methane yield at pH 7 decreased significantly because of the high acetic acid inhibition (Figures 7.3, 7.4c, and 7.4d). In addition, the maximum methane yield was achieved at pH 7.5 due to the relatively low inhibition of acetic acid (compared to the inhibition at pH 7) and FAN (compared to the inhibition at pH 8). Conversely, the minimum methane yield was observed at pH 7.5 when the concentration of additional acetate increased to 40 g-COD/L (Figures 7.4e and 7.4f). The sharp decrease in the methane yield at pH 7.5 was due to the significant increase in the acetic acid inhibition ($I_{NH3,Xac}$ decreased from ~0.99 to ~0.50 while $I_{NH3,Xh2}$ decreased from ~0.98 to ~0.30). It should be noted that acetate is also an inhibitor for methane yield since acetate is the substrate of acetoclastic methanogens. Therefore, high methane yield was observed at pH 7.5 with 20 g-COD/L of acetate and 2 g TAN-N/L because of the substantial substrate.

7.4.3 Sensitivity analysis

The relative sensitivity of $K_{INH_3,Xac}$ and K_{INH_3,Xh_2} were increased with increasing pH when the pH was lower than 9 (Figure 7.5a). The increased sensitivity can be explained by the enhanced FAN inhibition at high pH. For the low pH (6 and 7), higher sensitivity was shown in $K_{INH_3,Xac}$ compared to the sensitivity of K_{INH_3,Xh_2}. This result is consistent with previous studies where acetoclastic methanogens were found to be more sensitive to FAN than hydrogenotrophic methanogens [24][25][26]. A higher sensitivity of K_{INH_3,Xh_2} was observed at pH 8, indicating the hydrogenotrophic dominants methane yield with high FAN

levels [25][27]. Similar sensitivity was observed at $K_{INH_3,Xac}$ and K_{INH_3,Xh_2} with a pH of 9 due to the almost complete inhibition of acetoclastic and hydrogenotrophic methanogenesis.

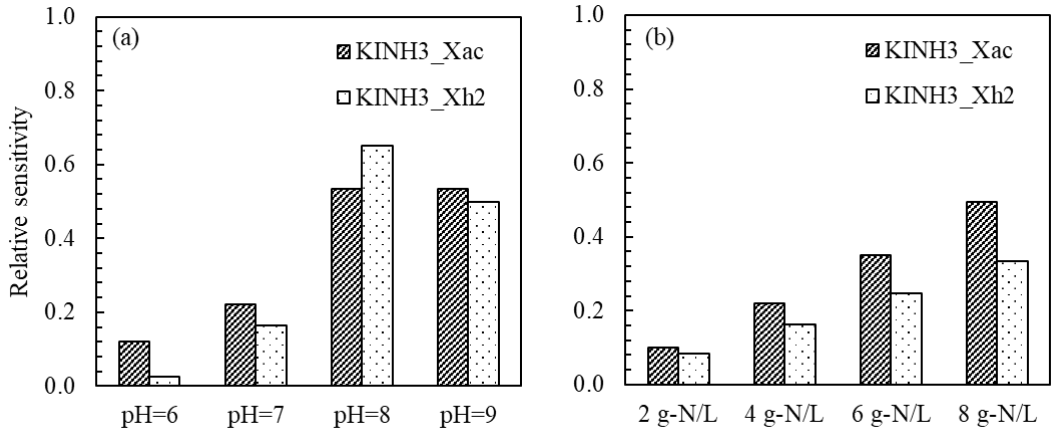

Figure 7.5. The relative sensitivity of $K_{INH_3,Xac}$ and K_{INH_3,Xh_2} at (a) various pH with TAN of 4 g-N/L and (b) different TAN concentrations with pH of 7.

The relative sensitivity of $K_{INH_3,Xac}$ and K_{INH_3,Xh_2} were linearly proportional to the concentration of TAN (Figure 7.5b). Higher TAN concentration resulted in higher relative sensitivity, implying that methane yield was more sensitive to FAN inhibition at high FAN levels. It should be noted that a significant increase was observed in the relative sensitivity of $K_{INH_3,Xac}$ and K_{INH_3,Xh_2} when pH increased from 7 to 8. A gradual rise was shown in the relative sensitivity of $K_{INH_3,Xac}$ and K_{INH_3,Xh_2} when the concentration of TAN increased from 4 to 8 g-N/L. Therefore, pH control is a more efficient method to maintain AD performance compared to TAN removal.

HAC$_{max}$ is the most sensitive parameter in the acetic acid inhibition functions (Figure 7.6a). For an AD with a high concentration of acetate (40 g-COD/L for Figure 7.6a), the acetic acid concentration usually maintained between the concentration of 50% inhibition

and HAC_{max}. Therefore, HAC_{max} (i.e., the acetic acid concentration at which the inhibition is nearly complete) dominated the acetic acid inhibition. The change in HAC_{max} contributed to a substantial sensitive simulation result. It should be noted that acetic acid inhibition is extremely sensitive to pH. For a low pH (around 6), acetic acid inhibition is almost complete regardless of the acetate concentration (Figure 7.3). Therefore, the model simulation results were only sensitive to *p* and *q* (i.e., parameters determine the maximum inhibition of acetic acid) at low pH conditions.

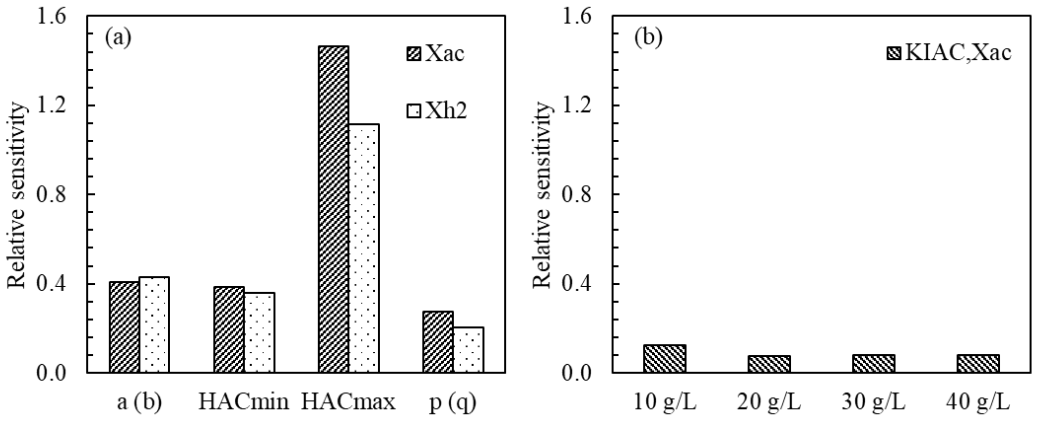

Figure 7.6. The relative sensitivity of (a) parameters in acetic acid inhibition functions (pH=7.5, the average pH of experimental sludge) and (b) $K_{IAC,Xac}$ at different acetate concentrations (pH=7.5).

The model simulation results were not sensitive to the Haldane inhibition since the relative sensitivity of $K_{IAC,Xac}$ was lower than 0.2 (Figure 7.6b). The relative sensitivity of $K_{IAC,Xac}$was decreased with increasing acetate concentrations (Figure 7.6b). Considering the large value of $K_{IAC,Xac}$ (85 g-COD/L), the acetate concentration was regarded as a substrate instead of an inhibitor because of the relatively low acetate concentration (10-40 g/L). Therefore, the increased acetate concentration provided substantial substrates for

methane yield, reducing the effects of $K_{IAC,Xac}$ changes on simulation results (Appendix, Figure E6). The insensitive Haldane inhibition indicated that methanogens can tolerate a high concentration of acetate.

7.5 Conclusions

This study presented the inhibition of ammonia and acetate on AD performance for methane production. Ammonia was found to have a minor negative impact on methane production at neutral pH with a relatively high concentration. There was no significant decrease in methane production until the additional acetate concentration increased to a substantially high level. The ADM with ammonia and acetic acid inhibition functions reliably simulated the experimental results. Inhibition functions including non-competitive inhibition of ammonia on methanogenesis, threshold inhibition of acetic acid on methanogenesis, and Haldane inhibition of acetate on the substrate uptake rate were implemented in the ADM. Methane production was sensitive to the pH based on the model simulation results. FAN was the main inhibitor at high pH while acetic acid was the dominant inhibitor at low pH. Low concentrations of acetate limited methane production by decreasing the acetate uptake rate. The relative sensitivity of $K_{INH_3,Xac}$ and K_{INH_3,Xh_2} were increased with increasing pH and TAN concentrations, indicating methanogens are sensitive to the change in pH and TAN concentration. Haldane inhibition was not sensitive to the acetate concentration, implying methanogens can tolerate a high concentration of acetate. Acetic acid inhibition was very sensitive to pH and HAC_{max} is the most sensitive parameter in acetic acid inhibition function at the pH of 7.5. Since the methane production was sensitive to the pH and TAN concentration, more frequent measurements for pH and

TAN are suggested in future AD studies.

References

[1] Grady Jr, C. L., Daigger, G. T., Love, N. G., & Filipe, C. D. (2011). Biological wastewater treatment. CRC press.

[2] Kumar, A., & Samadder, S. R. (2020). Performance evaluation of anaerobic digestion technology for energy recovery from organic fraction of municipal solid waste: A review. Energy, 197, 117253.

[3] Wu, D., Li, L., Zhao, X., Peng, Y., Yang, P., & Peng, X. (2019). Anaerobic digestion: a review on process monitoring. Renewable and Sustainable Energy Reviews, 103, 1-12.

[4] Chen, Y., Cheng, J. J., & Creamer, K. S. (2008). Inhibition of anaerobic digestion process: a review. Bioresource technology, 99(10), 4044-4064.

[5] Yenigün, O., & Demirel, B. (2013). Ammonia inhibition in anaerobic digestion: a review. Process Biochemistry, 48(5-6), 901-911.

[6] Rajagopal, R., Massé, D. I., & Singh, G. (2013). A critical review on inhibition of anaerobic digestion process by excess ammonia. Bioresource technology, 143, 632-641.

[7] Sung, S., & Liu, T. (2003). Ammonia inhibition on thermophilic anaerobic digestion. Chemosphere, *53*(1), 43-52.

[8] Chen, J. L., Ortiz, R., Steele, T. W., & Stuckey, D. C. (2014). Toxicants inhibiting anaerobic digestion: a review. Biotechnology advances, 32(8), 1523-1534.

[9] Harada, H., Uemura, S., & Momonoi, K. (1994). Interaction between sulfate-reducing bacteria and methane-producing bacteria in UASB reactors fed with low strength wastes containing different levels of sulfate. Water Research, 28(2), 355-367.

[10] Cai, J., Zheng, P., & Mahmood, Q. (2008). Effect of sulfide to nitrate ratios on the simultaneous anaerobic sulfide and nitrate removal. Bioresource Technology, 99(13), 5520-5527.

[11] Jain, S., Jain, S., Wolf, I. T., Lee, J., & Tong, Y. W. (2015). A comprehensive review on operating parameters and different pretreatment methodologies for anaerobic digestion of municipal solid waste. Renewable and Sustainable Energy Reviews, *52*, 142-154.

[12] Ren, Y., Yu, M., Wu, C., Wang, Q., Gao, M., Huang, Q., & Liu, Y. (2018). A comprehensive review on food waste anaerobic digestion: Research updates and tendencies. Bioresource technology, 247, 1069-1076.

[13] Altaş, L. (2009). Inhibitory effect of heavy metals on methane-producing anaerobic granular sludge. Journal of hazardous materials, 162(2-3), 1551-1556.

[14] Stasinakis, A. S. (2012). Review on the fate of emerging contaminants during sludge anaerobic digestion. Bioresource technology, *121*, 432-440.

[15] Guo, H., Yuan, P., Pavlovic, V., Barber, J., & Kim, Y. (2021). Ammonium sulfate production from wastewater and low-grade sulfuric acid using bipolar-and cation-exchange membranes. Journal of Cleaner Production, 285, 124888.

[16] Gallert, C., Bauer, S., & Winter, J. J. A. M. (1998). Effect of ammonia on the anaerobic degradation of protein by a mesophilic and thermophilic biowaste population. Applied microbiology and biotechnology, 50(4), 495-501.

[17] Gerardi, M. H. (2006). Wastewater bacteria (Vol. 5). John Wiley & Sons.

[18] Kayhanian, M. (1999). Ammonia inhibition in high-solids biogasification: an overview and practical solutions. Environmental technology, 20(4), 355-365.

[19] Müller, T., Walter, B., Wirtz, A., & Burkovski, A. (2006). Ammonium toxicity in bacteria. Current microbiology, 52(5), 400-406.

[20] De Baere, L. A., Devocht, M., Van Assche, P., & Verstraete, W. (1984). Influence of high NaCl and NH4Cl salt levels on methanogenic associations. Water research, 18(5), 543-548.

[21] Garcia, M. L., & Angenent, L. T. (2009). Interaction between temperature and ammonia in mesophilic digesters for animal waste treatment. Water research, 43(9), 2373-2382.

[22] Bayr, S., Rantanen, M., Kaparaju, P., & Rintala, J. (2012). Mesophilic and thermophilic anaerobic co-digestion of rendering plant and slaughterhouse wastes. Bioresource technology, 104, 28-36.

[23] Browne, J. D., Allen, E., & Murphy, J. D. (2014). Assessing the variability in biomethane production from the organic fraction of municipal solid waste in batch and continuous operation. Applied energy, *128*, 307-314.

[24] Calli, B., Mertoglu, B., Inanc, B., & Yenigun, O. (2005). Effects of high free ammonia concentrations on the performances of anaerobic bioreactors. Process Biochemistry, 40(3-4), 1285-1292.

[25] Karakashev, D., Batstone, D. J., & Angelidaki, I. (2005). Influence of environmental conditions on methanogenic compositions in anaerobic biogas reactors. Applied and environmental microbiology, 71(1), 331-338.

[26] Fotidis, I. A., Karakashev, D., & Angelidaki, I. (2014). The dominant acetate degradation pathway/methanogenic composition in full-scale anaerobic digesters operating under different ammonia levels. International Journal of Environmental Science and Technology, 11(7), 2087-2094.

[27] Song, M., Shin, S. G., & Hwang, S. (2010). Methanogenic population dynamics assessed by real-time quantitative PCR in sludge granule in upflow anaerobic sludge blanket treating swine wastewater. Bioresource Technology, 101(1), S23-S28.

[28] Xu, Z., Zhao, M., Miao, H., Huang, Z., Gao, S., & Ruan, W. (2014). In situ volatile fatty acids influence biogas generation from kitchen wastes by anaerobic digestion. Bioresource technology, 163, 186-192.

[29] Bouallagui, H., Touhami, Y., Cheikh, R. B., & Hamdi, M. (2005). Bioreactor performance in anaerobic digestion of fruit and vegetable wastes. Process biochemistry, 40(3-4), 989-995.

[30] Misi, S. N., & Forster, C. F. (2001). Batch co-digestion of multi-component agro-wastes. Bioresource technology, 80(1), 19-28.

[31] Xiao, K. K., Guo, C. H., Zhou, Y., Maspolim, Y., Wang, J. Y., & Ng, W. J. (2013). Acetic acid inhibition on methanogens in a two-phase anaerobic process. Biochemical engineering journal, 75, 1-7.

[32] Jiang, Y., Heaven, S., & Banks, C. J. (2012). Strategies for stable anaerobic digestion of vegetable waste. *Renewable energy*, *44*, 206-214.

[33] Siegert, I., & Banks, C. (2005). The effect of volatile fatty acid additions on the anaerobic digestion of cellulose and glucose in batch reactors. Process Biochemistry, 40(11), 3412-3418.

[34] Rozzi, A., & Remigi, E. (2004). Methods of assessing microbial activity and inhibition under anaerobic conditions: a literature review. Re/Views in Environmental Science & Bio/Technology, 3(2), 93-115.

[35] Hill, D. T., & Barth, C. L. (1977). A dynamic model for simulation of animal waste digestion. *Journal (Water Pollution Control Federation)*, 2129-2143.

[36] Pavlostathis, S. G., & Giraldo-Gomez, E. (1991). Kinetics of anaerobic treatment: a critical review. *Critical Reviews in Environmental Science and Technology*, *21*(5-6), 411-490.

[37] Keshtkar, A., Ghaforian, H., Abolhamd, G., & Meyssami, B. (2001). Dynamic simulation of cyclic batch anaerobic digestion of cattle manure. *Bioresource Technology*, *80*(1), 9-17.

[38] Mussati, M., Aguirre, P., & Scenna, N. J. (1998). Modeling of real biological reactors for the treatment of complex substrates. Dynamic simulation. Computers & chemical engineering, 22, S723-S726.

[39] D. J. Batstone, J. Keller, I. Angelidaki, S. V. Kalyuzhnyi, S. G. Pavlostathis, A. Rozzi, W. T. Sanders, H. Siegrist and V. A. Vavilin, "The IWA Anaerobic Digestion Model No 1 (ADM1)," Water Science and Technology, 2002.

[40] Wang, H., Fotidis, I. A., & Angelidaki, I. (2015). Ammonia effect on hydrogenotrophic methanogens and syntrophic acetate-oxidizing bacteria. FEMS microbiology ecology, 91(11).

[41] Li, X., Yang, Z., Liu, G., Ma, Z., & Wang, W. (2019). Modified anaerobic digestion model No. 1 (ADM 1) for modeling anaerobic digestion process at different ammonium concentrations. Water Environment Research, 91(8), 700-714.

[42] Wilson, C. A., Novak, J., Takacs, I., Wett, B., & Murthy, S. (2012). The kinetics of process dependent ammonia inhibition of methanogenesis from acetic acid. Water research, 46(19), 6247-6256.

[43] Fezzani, B., & Cheikh, R. B. (2010). Two-phase anaerobic co-digestion of olive mill wastes in semi-continuous digesters at mesophilic temperature. Bioresource technology, 101(6), 1628-1634.

[44] Yin, Q., Gu, M., & Wu, G. (2020). Inhibition mitigation of methanogenesis processes by conductive materials: A critical review. Bioresource Technology, 317, 123977.

[45] Fezzani, B., & Cheikh, R. B. (2008). Implementation of IWA anaerobic digestion model No. 1 (ADM1) for simulating the thermophilic anaerobic co-digestion of olive mill wastewater with olive mill solid waste in a semi-continuous tubular digester. Chemical Engineering Journal, 141(1-3), 75-88.

[46] Boubaker, F., & Ridha, B. C. (2008). Modelling of the mesophilic anaerobic co-digestion of olive mill wastewater with olive mill solid waste using anaerobic digestion model No. 1 (ADM1). Bioresource technology, 99(14), 6565-6577.

[47] Astals, S., Batstone, D. J., Tait, S., & Jensen, P. D. (2015). Development and validation of a rapid test for anaerobic inhibition and toxicity. Water Research, 81, 208-215.

[48] Astals, S., Peces, M., Batstone, D. J., Jensen, P. D., & Tait, S. (2018). Characterising and modelling free ammonia and ammonium inhibition in anaerobic systems. Water research, 143, 127-135.

[49] Bernard, O., Hadj-Sadok, Z., Dochain, D., Genovesi, A., & Steyer, J. P. (2001). Dynamical model development and parameter identification for an anaerobic wastewater treatment process. Biotechnology and bioengineering, 75(4), 424-438.

[50] Lokshina, L. Y., Vavilin, V. A., Kettunen, R. H., Rintala, J. A., Holliger, C., & Nozhevnikova, A. N. (2001). Evaluation of kinetic coefficients using integrated Monod and Haldane models for low-temperature acetoclastic methanogenesis. Water Research, 35(12), 2913-2922.

[51] American Public Health Association, American Water Works Association, Water Pollution Control Federation, & Water Environment Federation. (1912). Standard methods for the examination of water and wastewater (Vol. 2). American Public Health Association.

[52] Hirmiz, Y., Hong, Y., & Kim, Y. (2019). A new model with serial hydrolysis reactions for the anaerobic digestion of waste activated sludge under thermophilic conditions. Environmental Science: Water Research & Technology, 5(12), 2182-2192.

[53] Tong, J., & Chen, Y. (2009). Recovery of nitrogen and phosphorus from alkaline fermentation liquid of waste activated sludge and application of the fermentation liquid to promote biological municipal wastewater treatment. Water research, 43(12), 2969-2976.

[54] Chen, Y., Jiang, S., Yuan, H., Zhou, Q., & Gu, G. (2007). Hydrolysis and acidification of waste activated sludge at different pHs. Water research, 41(3), 683-689.

[55] Mozumder, M. S. I., Goormachtigh, L., Garcia-Gonzalez, L., De Wever, H., & Volcke, E. I. (2014). Modeling pure culture heterotrophic production of polyhydroxybutyrate (PHB). Bioresource technology, 155, 272-280.

[56] Smith, E. D., Szidarovszky, F., Karnavas, W. J., & Bahill, A. T. (2008). Sensitivity analysis, a powerful system validation technique. The Open Cybernetics & Systemics Journal, 2(1).

[57] Webb, A. R., & Hawkes, F. R. (1985). The anaerobic digestion of poultry manure: variation of gas yield with influent concentration and ammonium-nitrogen levels. *Agricultural Wastes*, *14*(2), 135-156.

[58] Dogan, T., Ince, O., Oz, N. A., & Ince, B. K. (2005). Inhibition of volatile fatty acid production in granular sludge from a UASB reactor. *Journal of Environmental Science and Health*, *40*(3), 633-644.

8 Conclusions and future work

This thesis presented novel methods to treat wastewater with low energy consumption. Nutrients recovery and biosolids reduction are the two main goals in this study. Bioelectrochemical systems (BES), electrodialysis (ED), and anaerobic digestion (AD) were applied to treat wastewater with different aspects.

8.1 Chapter 2: multi-electrode design in microbial electrolysis cells

The multi-electrode stack design successfully enhanced the electric current generation in microbial electrolysis cells (MECs). The electric current generation was linearly proportional to the number of electrode pairs. However, a longer start-up time was required for multi-electrode MECs. Compared to the electric current in MECs with activated carbon cloth cathodes, the electric current in MECs with stainless steel mesh cathodes was higher. High applied voltage and flow rate contributed to high electric current. A substantially high COD removal rate was achieved in stacked MECs, implying the strong wastewater treatability of the stacked MEC.

It was founded that all electrodes contributed to the total electric current generation in MECs. The short inter-electrode distance in stacked MECs reduced the resistance of systems but limited mass transport. Therefore, the effects of inter-electrode distance on electric current generation in stacked MECs should be investigated in future studies. In addition, the stacked MEC design can be further improved by optimizing individual electrode sizes.

8.2 Chapter 3: MECs for municipal wastewater treatment

The multi-electrode MECs demonstrated excellent wastewater treatability with rapid organic removal and minimized biosolids production. The electric current in the MEC with 10 pairs of electrodes was ~50 times higher than the electric current in the MEC with single pair of electrodes. Besides the number of electrodes, the electric current was also governed by the organic loading rate (OLR) and the high OLR resulted in the high electric current. Compared to the energy consumption in conventional activated sludge systems, the energy consumption in MECs was much lower. Considering the minimal biosolids production and consistently low COD in the MEC effluent, the stacked electrode MEC can be applied to replace the activated sludge systems and treat municipal wastewater efficiently.

The hydrogen gas production was very small in the stacked MECs because of the short residence time and conversion of hydrogen gas into methane gas. Therefore, the inter-electrode distance in MECs or the volume of the gas chamber can be increased to improve biogas production in future studies. In addition, the number of electrode pairs of stacked MECs was limited to 10 in this study. Stacked MECs with a large number of electrode pairs (50 to 100) can be built in future studies to improve wastewater treatment efficiency.

8.3 Chapter 4: BES for heavy metals removal/recovery

BES shows great efficiency for heavy metal removal/recovery. May factors, such as pH, operation time, cathode potential, and initial concentration of heavy metal, affect the performance of BES for heavy metal removal/recovery. Cathodic reduction, precipitation, and adsorption have been reported as three main mechanisms. In BES, heavy metal ions can be reduced and recovered at the cathode. The spontaneity of reduction is determined

by the reduction potential of the heavy metal ions and the cathode potential. The precipitation of heavy metal is also possible since the oxygen reduction in microbial fuel cells (MFCs) and the hydrogen production in MECs contribute to a high pH near the cathode. In addition, heavy metal also can be removed by electrode adsorption or microorganisms biosorption.

Although many studies presented the removal/recovery efficiency of heavy metal in BES, most of the studies focused on the mechanisms of reduction. Therefore, we suggested that future studies should investigate the mechanism of precipitation of heavy metal removal/recovery in BES.

8.4 Chapter 5: ammonia recovery from dewatering centrate

Bipolar membrane electrodialysis (BMED) (only with bipolar membranes-BPMs and cation exchange membranes-CEMs) efficiently produced high-purity ammonium sulfate from dewatering centrate. The production rate of ammonium sulfate (i.e., ammonia recovery rate) increased with increasing applied voltage and flow rate (or linear velocity). Although the high applied voltage and flow rate resulted in high electric energy consumption, the electric energy consumption in the BMED was lower than the electric energy consumption in traditional methods (e.g., ammonia stripping, struvite precipitation, and steam reforming) for ammonia recovery. It was found that the separation of ammonium was slower than the separation of potassium. However, ammonium sulfate was still the main compound in the base stream because of the high initial concentration of ammonia in the dewatering centrate. The calcium and magnesium in the base stream can result in the formation of precipitants, such as calcium sulfate and magnesium hydroxide. These

precipitates on membranes can increase energy consumption and affect the permeability of membranes. Therefore, a regular BMED stack cleaning with acids is necessary to maintain BMED performance. Considering the low energy consumption and rapid ammonia recovery in BMED, BMED is a green and sustainable technology for wastewater treatment.

BMED system was only operated for a short time (several hours) in this study, and frequent BMED stack cleaning was performed after every single test. To investigate the stability of BMED performance, long-time operations without stack cleaning should be performed in future studies. In addition, the effects of electro-osmosis or osmosis on ammonia recovery should also be investigated. BMED can also be scaled up with more membranes to improve ammonia recovery efficiency.

8.5 Chapter 6: Ion exchange membrane scaling problems

Ion exchange membrane (IEM) scaling problems are ubiquitous in ED applications for nutrients recovery. Serious calcium precipitation was observed in a lab-scale ED reactor fed with the food waste (FW) and municipal waste (MW) liquid digestate because of the high concentration of carbonate in the FW and MW liquid digestate. Struvite is one of the common magnesium precipitates during wastewater treatment processes. In the ED fed with the FW and MW liquid digestate, the magnesium precipitation was limited by the phosphate concentration for the MW liquid digestate while it was limited by magnesium concentration for the FW liquid digestate. Through the scanning electron microscope (SEM) analysis, different polymorphs of calcium carbonate were observed on AEM and CEM. Vaterite and ACC crystals were observed on the CEM while vaterite was found on the AEM. Compared to the amount of calcium carbonate, the amount of struvite on IEMs was

relatively minor. However, the struvite formation needs to be controlled in ED applications since the needle-shaped struvite can cause irreversible damage to IEMs. It was founded that calcite was the only precipitate on IEMs when the ED fed with synthetic solutions, implying the experimental results with synthetic solutions can not present scaling problems in practical ED applications. In addition, the application of CR 67 contributed to the high ammonia recovery while the application of CMV contributed to the high recovery of divalent cations. Therefore, we recommend that CR 67 for ammonia separation from wastewater while CMV is recommended in separation processes for water softening.

All the tests were examined under batch operation in this study. A continuous-flow ED system should be built in the future to simulate the industrial ED application for wastewater treatment. Although the shape of scalants on IEM were analyzed by SEM, the effects of IEM scaling on membrane performance should be evaluated by measuring membrane permeability and resistance.

8.6 Chapter 7: ammonia and acetic acid inhibition in AD

Ammonia and acetic acid inhibitions in AD with high solids sludge were investigated in this study. A relatively high total ammonia (TAN) concentration was found to have a minor negative impact on methane production at neutral pH. A high concentration of acetic acid resulted in serious methane production inhibition since the accumulation of acetic acid can change intracellular pH significantly. A modified anaerobic digestion model (ADM) with inhibition functions of free ammonia (FAN) (simple inhibition), acetate (Haldane inhibition), and acetic acid (threshold inhibition) reliably simulated the experimental results. The simulated results were extremely sensitive to pH. For the low pH,

acetic acid was the main inhibitor while FAN was the dominant inhibitor at high pH. The sensitivity analysis was conducted to quantify the degree of inhibitions by free ammonia, acetate, and acetic acid on individual microbial activities in the modified ADM. Between pH of 6 and 8, the relative sensitivity of ammonia inhibition increased with increasing pH while the relative sensitivity of acetic acid inhibition changed a lot.

Linear changes were assumed for pH and TAN concentration in the ADM. However, reactions, such as proteins and lipids degradation, affect pH and TAN concentration significantly during the AD processes. Therefore, the pH and TAN concentration should be measured more frequently in future AD experiments. For the sensitivity analysis, the selected time points may significantly affect the average relative sensitivity results (non-steady state model). Thus, the weighted average sensitivity or sensitivity on methane production rate can be used in future study to compare the sensitivity of each parameter. In addition, the effects of inhibitors on acetoclastic and hydrogenotrophic methanogenesis should be evaluated by analyzing coenzyme activities and microbial community.

Appendix A: Supplementary information for Chapter 2

Scalable multi-electrode microbial electrolysis cells for high electric current and rapid organic removal

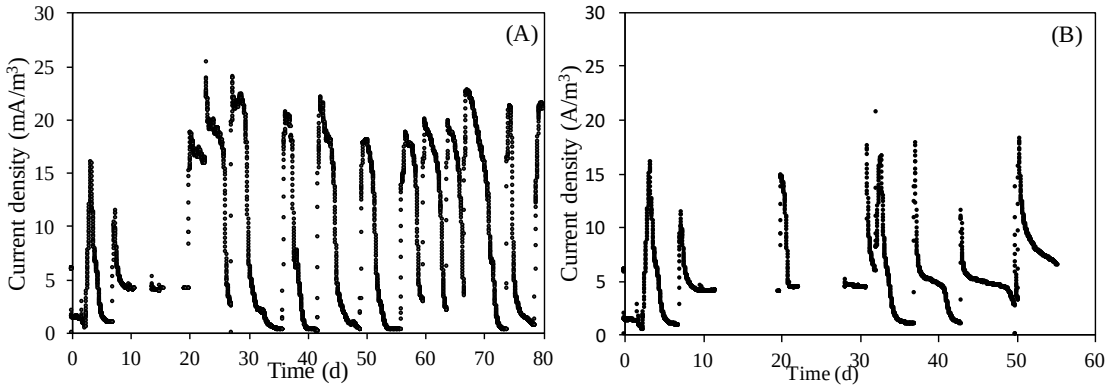

Figure A1. Electric current generation during fed-batch operation at Eap of 0.6 V for MECs with single electrode pair: (A) Stainless steel mesh cathode; and (B) Activated carbon cloth cathode.

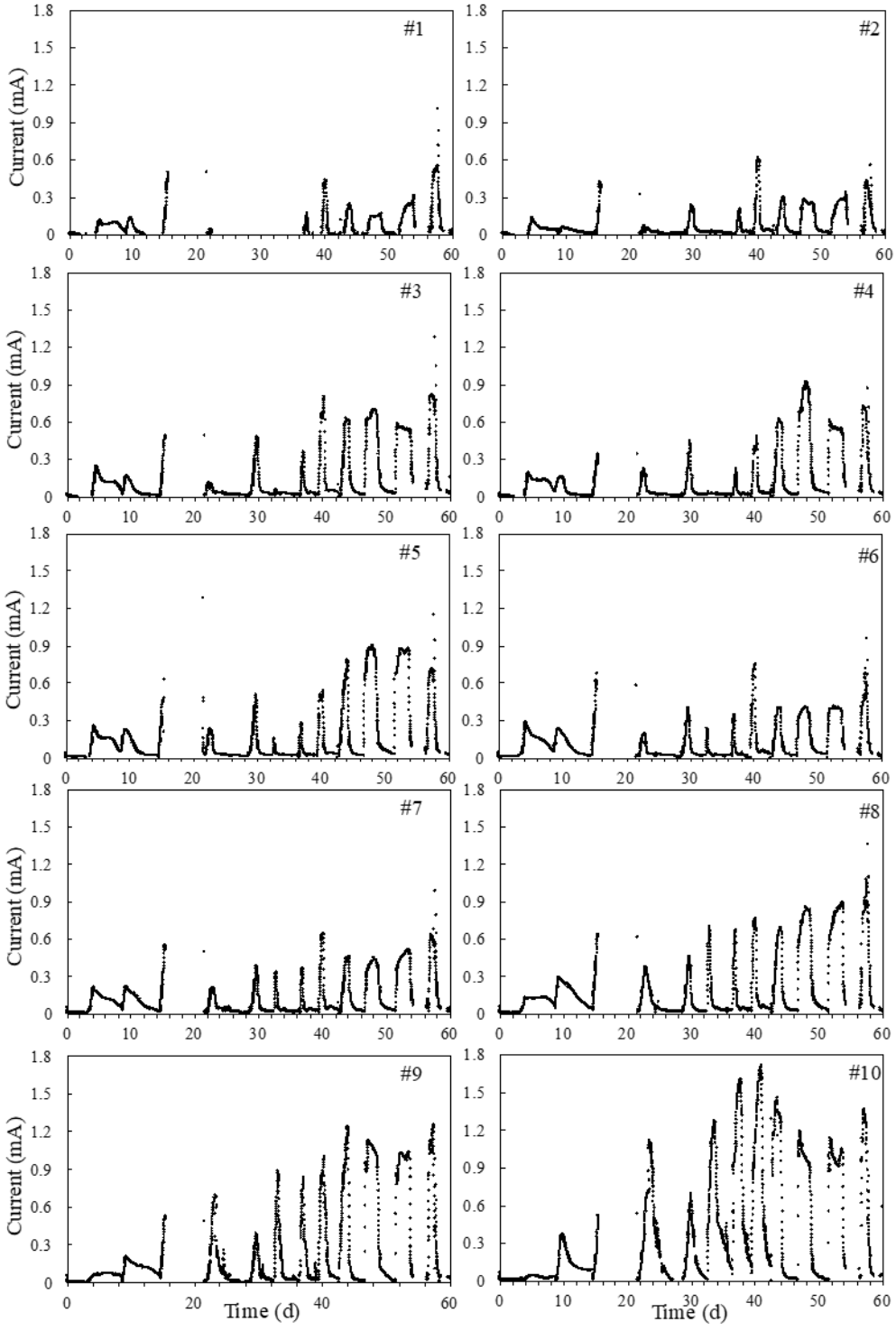

Figure A2. Electric current generation from individual electrode pairs in MEC-10.

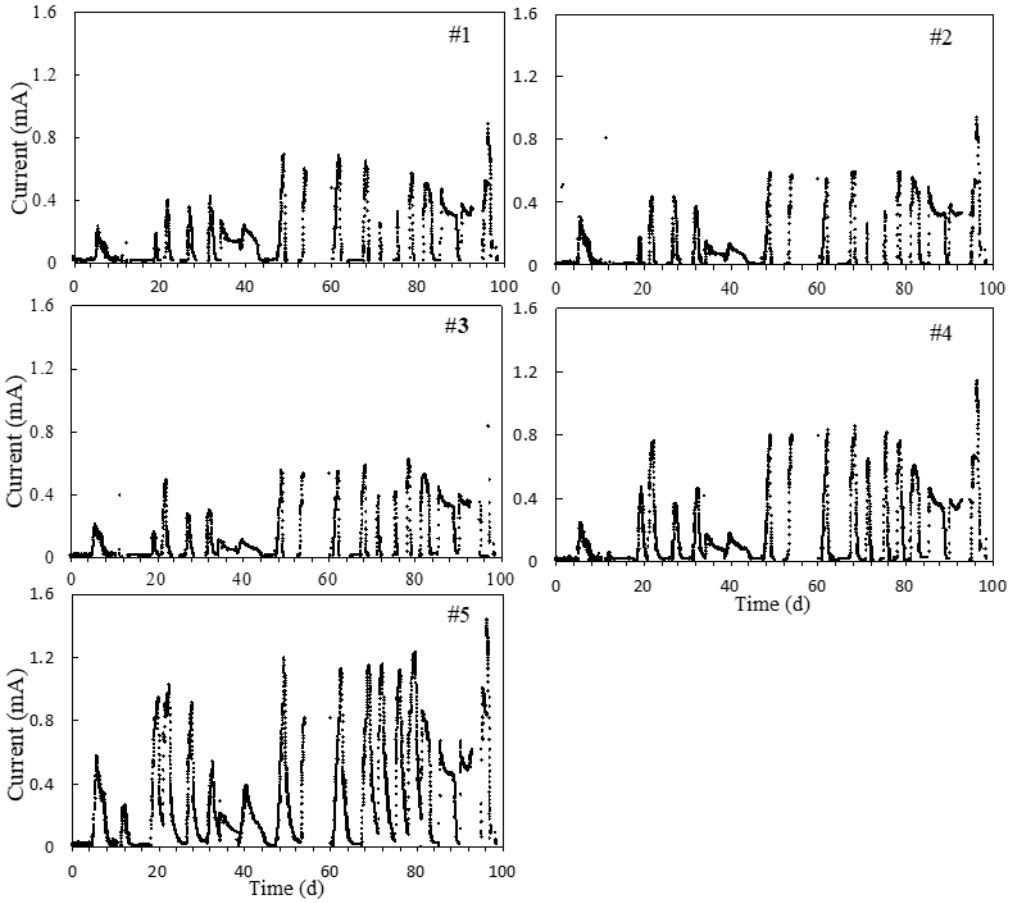

Figure A3. Electric current generation from individual electrode pairs in MEC-5.

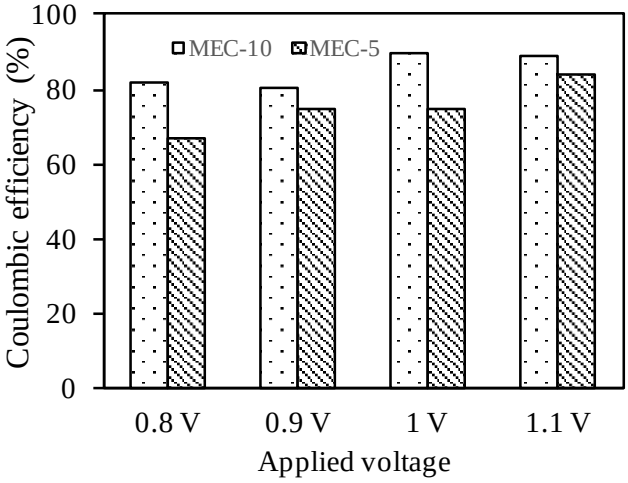

Figure A4. Coulomb efficiency during MEC operation under continuous recycle mode.

Appendix B: Supplementary information for Chapter 3

Stacked multi-electrode design of microbial electrolysis cells for rapid and low-sludge treatment of municipal wastewater

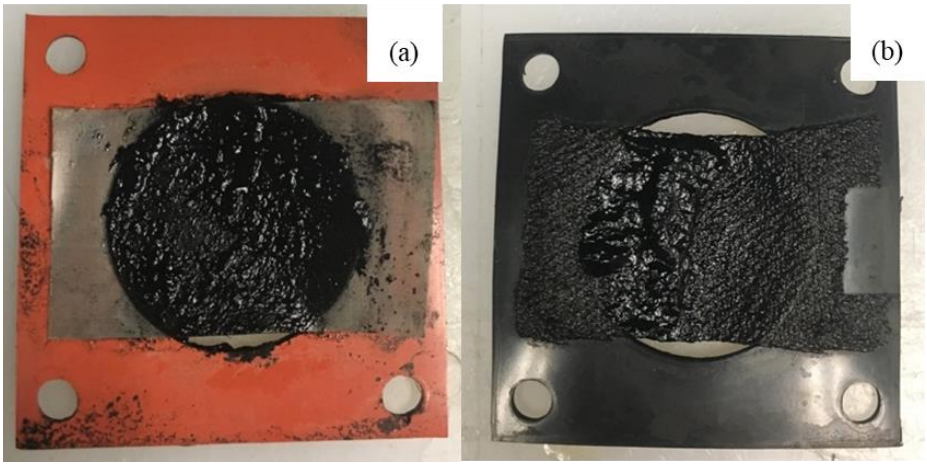

Figure B1. (a) Cathode and (b) bioanode after ~3 months of MEC operation with primary clarifier effluent.

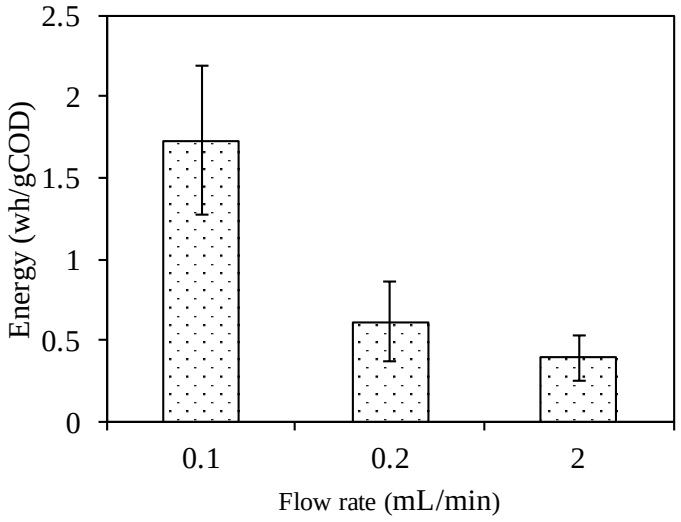

Figure B2. Electric energy consumption for continuous-flow MEC system operation.

Appendix C: Supplementary information for Chapter 5

Ammonium sulfate production from wastewater and low-grade sulfuric acid using bipolar- and cation-exchange membranes

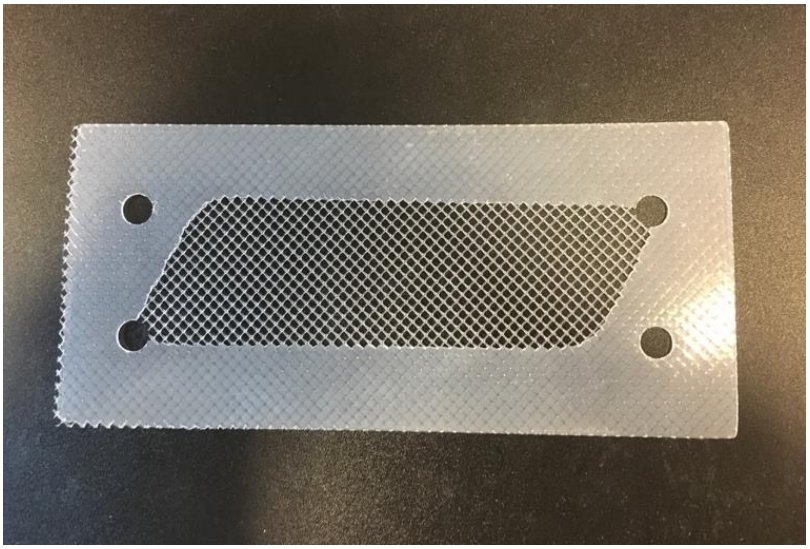

Figure C1. The photo of a plastic spacer with non-tortuous mesh.

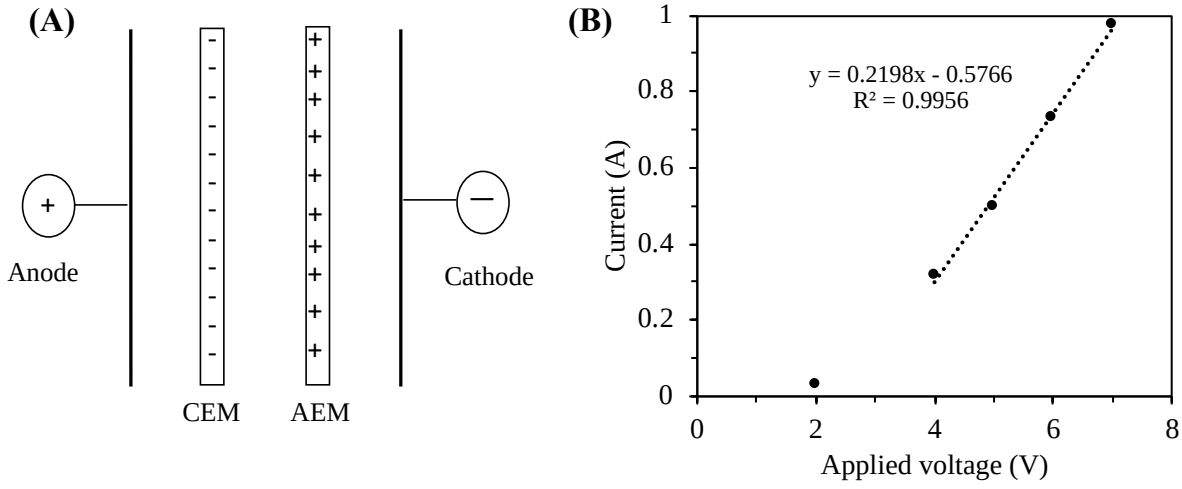

Figure C2. (A) Schematic of the single CEM and AEM unit; (B) the average electric current of the single CEM and AEM unit at various applied voltages.

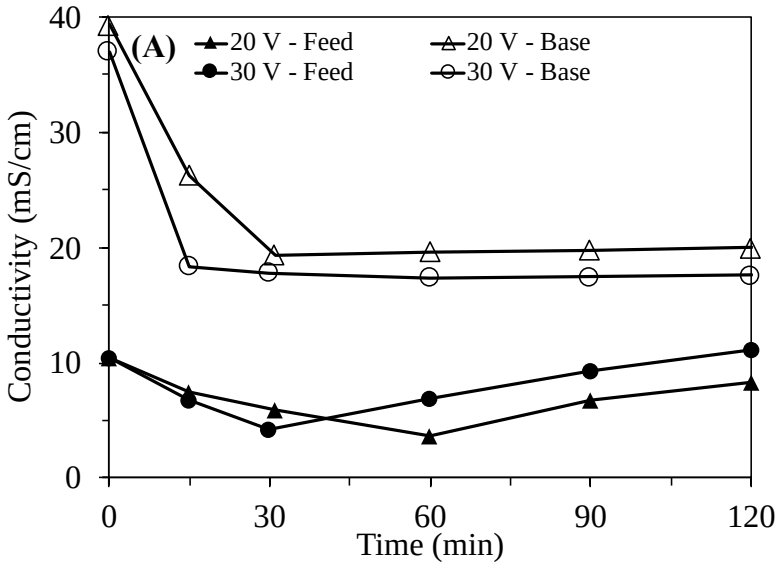

Figure C3. The conductivity of the feed and base reservoir at different applied voltage.

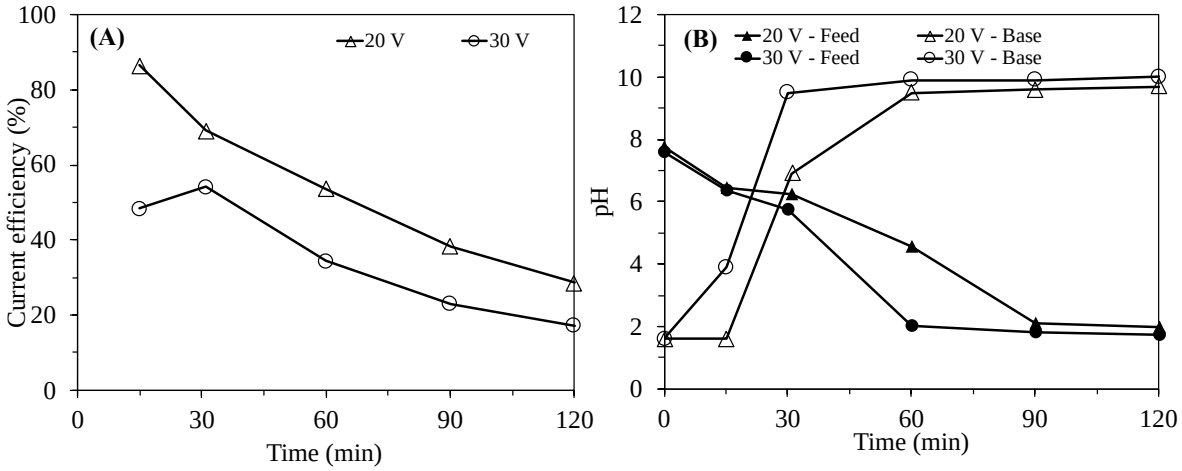

Figure C4. (A) The current efficiencies and (B) pH at different applied voltage.

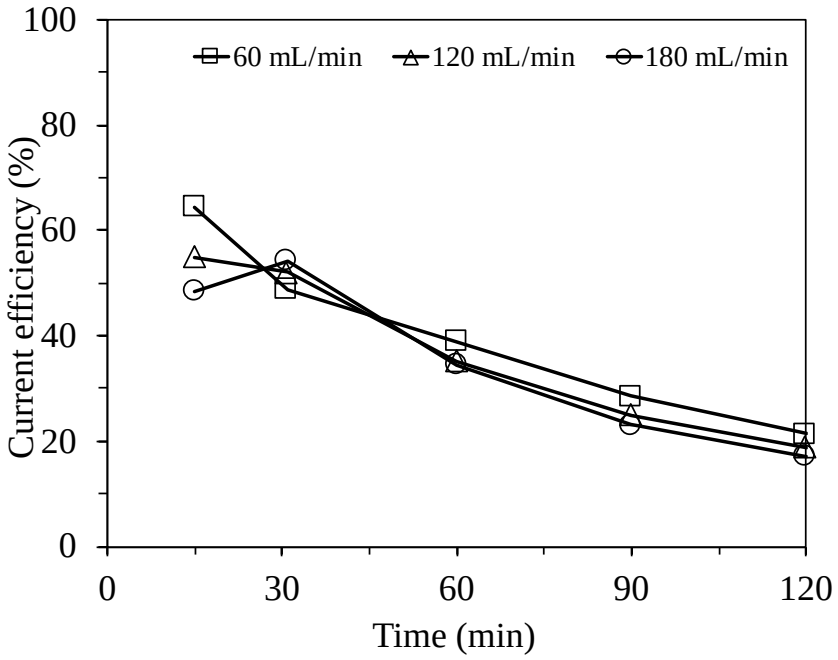

Figure C5. The current efficiency at different flow rates.

Table C1. The mass of Ca^{2+} (mg) in the feed, base, and CIP solution

	Feed-initial	Feed-end	Base-end	CIP solution
30 V -180 mL/min	119.40	10.26	2.10	71.03
30 V -120 mL/min	116.50	10.79	1.82	65.25
30 V -60 mL/min	124.46	18.74	2.88	64.30
20 V -180 mL/min	122.27	7.92	2.05	58.70

Table C2. The mass of Mg^{2+} (mg) in the feed, base, and CIP solution

	Feed-initial	Feed-end	Base-end	CIP solution
30 V -180 mL/min	80.29	7.70	11.59	43.86
30 V -120 mL/min	79.01	8.04	12.42	42.98
30 V -60 mL/min	84.23	12.08	18.45	35.70
20 V -180 mL/min	83.09	6.72	24.35	30.20

Appendix D: Supplementary information for Chapter 6

Membrane Scaling in Electrodialysis for Nutrients Separation from High-strength Wastewater

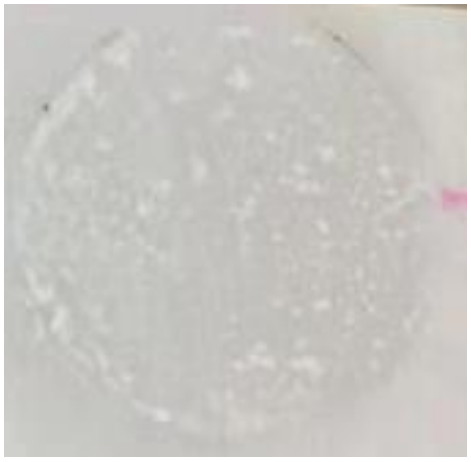

Figure D1. Cation-exchange membrane after 8 hours of ED operation 7.6 mA/cm^2 with domestic wastewater dewatering centrate.

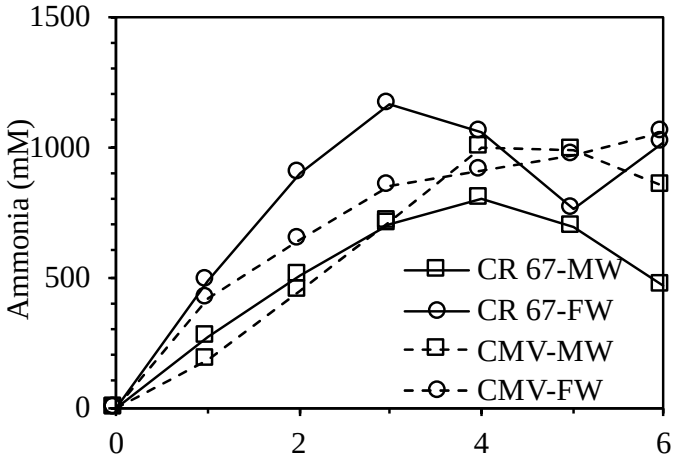

Figure D2. Ammonia concentration in the concentrate cell with different feed sources and membranes.

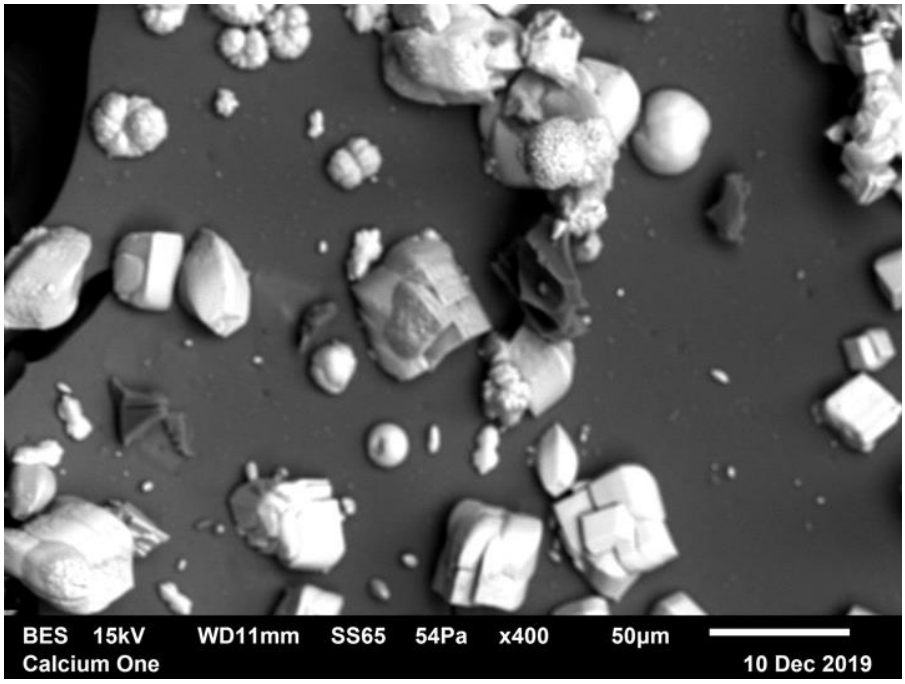

Figure D3. Membrane scalants from synthetic solution (not real wastewater) after ED operation.

Appendix E: Supplementary information for Chapter 7

Modeling Ammonia and Acetic Acid Inhibition on Mesophilic Anaerobic Digestion Fed with Thickened Waste Activated Sludge

Table E1. Initial and final experimental conditions (n=2 for 0 and 20 g-COD/L, n=1 for 40 g-COD/L)

Additional Inhibitors (g/L)	$pH_{initial}$	pH_{final}	NH_3-$N_{initial}$ (mg/L)	NH_3-N_{final} (mg/L)
0 COD 0N NpH	7.27 ± 0.31	7.57 ± 0.07	1002 ± 280	2900 ± 141
0 COD 4N NpH	7.11 ± 0.24	7.55 ± 0.05	5002 ± 280	6755 ± 1562
0 COD 4N HpH	8.85 ± 0.01	7.60 ± 0.10	5002 ± 280	8585 ± 318
20 COD 0N NpH	7.32 ± 0.24	7.98 ± 0.10	1002 ± 280	3175 ± 417
20 COD 4N NpH	7.35 ± 0.22	7.56 ± 0.08	5002 ± 280	6440 ± 318
20 COD 4N HpH	8.78 ± 0.05	7.69 ± 0.05	5002 ± 280	8000 ± 14
40 COD 4N NpH	7.34	7.75	1200	3310
40 COD 4N NpH	7.24	7.70	5200	7590
40 COD 4N HpH	8.89	7.90	5200	8370

Table E2. Kinetic rate expressions used in the mathematical model. A rate expression can be obtained: $R_{i=}\sum_{i,j=1}^{j=19} r_{i,j} * Rate_{i,j}$

	Component (i) →	1	2	3	4	5	6	7	8	9	
j	**Process**	S_{SU}	S_{AA}	S_{FA}	S_{VA}	S_{BU}	S_{PRO}	S_{AC}	S_{H2}	S_{CH4}	**Rate (mg-COD L^{-1} d^{-1})**
1	Disintegration										$k_{dis} X_C$
2	Hydrolysis of carbohydrates	1									$k_{hydc\,h} X_{CH}$
3	Hydrolysis of proteins		1								$k_{hydpr}\, X_{PR}$
4	Hydrolysis of lipids	1- $f_{fa,li}$		$f_{fa,li}$							$k_{hydli}\, X_{LI}$
5	Uptake of sugars	-1				$(1\text{-}Y_{su})f_{bu,su}$	$(1\text{-}Y_{su})f_{pro,su}$	$(1\text{-}Y_{su})f_{ac,su}$	$(1\text{-}Y_{su})f_{h2,su}$		$k_{su}\frac{S_{SU}}{K_{ssu}+S_{SU}} X_{SU} I_1$
6	Uptake of amino acids		-1		$(1\text{-}Y_{aa})f_{va,aa}$	$(1\text{-}Y_{aa})f_{bu,aa}$	$(1\text{-}Y_{aa})f_{pro,aa}$	$(1\text{-}Y_{aa})f_{ac,aa}$	$(1\text{-}Y_{aa})f_{h2,aa}$		$k_{aa}\frac{S_{AA}}{K_{saa}+S_{AA}} X_{AA} I_1$
7	Uptake of LCFA			-1				$(1\text{-}Y_{fa})0.7$	$(1\text{-}Y_{fa})0.3$		$k_{fa}\frac{S_{FA}}{K_{sfa}+S_{FA}} X_{FA} I_2$
8	Uptake of valerate				-1		$(1\text{-}Y_{c4})0.54$	$(1\text{-}Y_{c4})0.31$	$(1\text{-}Y_{c4})0.15$		$k_{c4}\frac{S_{VA}}{K_{sc4}+S_{VA}} X_{C4}\frac{1}{1+S_{BU}/S_{VA}} I_2$
9	Uptake of butyrate					-1		$(1\text{-}Y_{c4})0.8$	$(1\text{-}Y_{c4})0.2$		$k_{c4}\frac{S_{BU}}{K_{sc4}+S_{BU}} X_{C4}\frac{1}{1+S_{VA}/S_{BU}} I_2$
10	Uptake of propionate						-1	$(1\text{-}Y_{pro})0.57$	$(1\text{-}Y_{pro})0.43$		$k_{pro}\frac{S_{PRO(1)}}{K_{spro}+S_{PRO(1)}} X_{PRO} I_2$
11’	Uptake of acetate							-1		$(1\text{-}Y_{ac})$	$k_{ac}\frac{S_{AC}}{K_{sac}+S_{AC}+S_{AC}^2/K_{IAC,Xac}} X_{AC} I_3$
12’	Uptake of hydrogen								-1	$(1\text{-}Y_{h2})$	$k_{h2}\frac{S_{H2}}{K_{sh2}+S_{H2}} X_{H2} I_4$
13	Decay of X_{su}										$k_{decxsu}\, X_{SU}$
14	Decay of X_{aa}										$k_{decxaa}\, X_{AA}$
15	Decay of X_{fa}										$k_{decxfa}\, X_{FA}$
16	Decay of X_{c4}										$k_{decxc\,4} X_{C4}$
17	Decay of X_{pro}										$k_{decxpro}\, X_{PRO}$
18	Decay of X_{ac}										$k_{decxac}\, X_{AC}$
19	Decay of X_{h2}										$k_{decx\,h2} X_{H2}$

Table E2. Continued

j	Component (i) → / Process	11 X_C	12 X_{CH}	13 X_{PR}	14 X_{LI}	15 X_{SU}	16 X_{AA}	17 X_{C4}	18 X_{PRO}	19 X_{AC}	20 X_{H2}	21 X_I	Rate (mg-COD L^{-1} d^{-1})
1	Disintegration	-1											$k_{dis} X_C$
2	Hydrolysis of carbohydrates		-1										$k_{hydch} X_{CH}$
3	Hydrolysis of proteins			-1									$k_{hydpr} X_{PR}$
4	Hydrolysis of lipids				-1								$k_{hydli} X_{LI}$
5	Uptake of sugars					Y_{su}							$k_{su} \frac{S_{SU}}{K_{ssu} + S_{SU}} X_{SU} I_1$
6	Uptake of amino acids						Y_{aa}						$k_{aa} \frac{S_{AA}}{K_{saa} + S_{AA}} X_{AA} I_1$
7	Uptake of LCFA							Y_{fa}					$k_{fa} \frac{S_{FA}}{K_{sfa} + S_{FA}} X_{FA} I_2$
8	Uptake of valerate								Y_{c4}				$k_{c4} \frac{S_{VA}}{K_{sc4} + S_{VA}} X_{C4} \frac{1}{1 + S_{BU}/S_{VA}} I_2$
9	Uptake of butyrate								Y_{c4}				$k_{c4} \frac{S_{BU}}{K_{sc4} + S_{BU}} X_{C4} \frac{1}{1 + S_{VA}/S_{BU}} I_2$
10	Uptake of propionate									Y_{pro}			$k_{pro} \frac{S_{PRO(1)}}{K_{spro} + S_{PRO(1)}} X_{PRO} I_2$
11’	Uptake of acetate										Y_{ac}		$\boldsymbol{k_{ac} \frac{S_{AC}}{K_{sac} + S_{AC} + S_{AC}^2 / K_{IAC,Xac}} X_{AC} I}$
12’	Uptake of hydrogen											Y_{h2}	$k_{h2} \frac{S_{H2}}{K_{sh2} + S_{H2}} X_{H2} I_4$
13	Decay of X_{su}	1				-1							$k_{decxsu} X_{SU}$
14	Decay of X_{aa}	1					-1						$k_{decxaa} X_{AA}$
15	Decay of X_{fa}	1						-1					$k_{decxfa} X_{FA}$
16	Decay of X_{c4}	1							-1				$k_{decxc4} X_{C4}$
17	Decay of X_{pro}	1								-1			$k_{decxpro} X_{PRO}$
18	Decay of X_{ac}	1									-1		$k_{decxac} X_{AC}$
19	Decay of X_{h2}	1										-1	$k_{decxh2} X_{H2}$
$I_1 = I_{ph} I_{IN,lim}$ $I_2 = I_{ph} I_{IN,lim} I_{h2,x}$ $I_3 = I_{ph} I_{IN,lim} I_{NH3,Xac} I_{HAC,Xac}$ $I_4 = I_{ph} I_{IN,lim} I_{NH3,Xh2} I_{HAC,Xh2}$		$I_{IN,lim} = \frac{1}{1 + K_{SIN}/S_{IN}}$		$I_{PHn\ (1,2,3)} = \begin{pmatrix} e^{\left[-3*\left(\frac{pH - pH_{ul,n}}{pH_{ul,n} - pH_{ll,n}}\right)^2\right]}, & if\ pH \le pH_{ul,n} \\ 1, & if\ pH > pH_{Hl,n} \end{pmatrix}$					$I_{H_2,x} = \frac{1}{1 + S_{h_2}/K_{Ih_2,x}}$		$I_{NH3,Xac}$; $I_{HAC,Xac}$ $I_{NH3,Xh2}$; $I_{HAC,Xh2}$ see section 3

Table E3. Kinetic parameters, rates and stoichiometric coefficients used in mathematical model for a temperature of 37.5 ºC.

Model parameter	Symbol	Value	Unit
First order decay rate of degraders, beta-oxidizers, methanogens	k_{dec}	0.022	d^{-1}
First order composite disintegration rate	k_{dis}	0.545	d^{-1}
First order hydrolysis rate	k_{hyd}	10.00	d^{-1}
Monod Max. specific sugar utilization rate	k_{su}	31.29	d^{-1}
Monod Max. specific amino acid utilization rate	k_{aa}	52.15	d^{-1}
Monod Max. specific long-chain fatty acid utilization rate	k_{fa}	6.40	d^{-1}
Monod Max. specific valerate and butyrate utilization rate	k_{c4}	21.02	d^{-1}
Monod Max. specific propionate utilization rate	k_{pro}	13.73	d^{-1}
Monod Max. specific acetoclastic methanogenesis rate	k_{ac}	9.10	d^{-1}
Monod Max. specific hydrogenotrophic methanogenesis rate	k_{h2}	35.00	d^{-1}
Half-saturation value for sugar utilization	$K_{S,su}$	544.90	mg-COD L^{-1}
Half-saturation value for amino acid utilization	$K_{S,aa}$	300.00	mg-COD L^{-1}
Half-saturation value for fatty acid utilization	$K_{S,fa}$	400.00	mg-COD L^{-1}
Half-saturation value for valerate and butyrate utilization	$K_{S,c4}$	217.96	mg-COD L^{-1}
Half-saturation value for propionate utilization	$K_{S,pro}$	114.59	mg-COD L^{-1}
Half-saturation value for acetoclastic methanogenesis utilization	$K_{S,ac}$	163.47	mg-COD L^{-1}
Half-saturation value for hydrogenotrophic methanogenesis utilization	$K_{S,h2}$	0.0089	mg-COD L^{-1}
Yield of fermenters on sugar	Y_{su}	0.10	g-COD g-COD^{-1}
Yield of fermenters on amino acids	Y_{aa}	0.08	g-COD g-COD^{-1}
Yield of beta-oxidizers on long-chain fatty acids	Y_{fa}	0.06	g-COD g-COD^{-1}
Yield of beta-oxidizers on valerate and butyrate	Y_{c4}	0.06	g-COD g-COD^{-1}
Yield of beta-oxidizers on propionate	Y_{pro}	0.04	g-COD g-COD^{-1}
Yield of acetoclastic methanogens on acetic acid	Y_{ac}	0.05	g-COD g-COD^{-1}
Yield of hydrogenotrophic methanogens on hydrogen	Y_{h2}	0.06	g-COD g-COD^{-1}
Fraction of particulate inert from composites	$f_{xi,xc}$	0.30	-
Fraction of carbohydrates from composites	$f_{ch,xc}$	0.20	-
Fraction of proteins from composites	$f_{pr,xc}$	0.20	-
Fraction of lipids from composites	$f_{li,xc}$	0.30	-
Fraction of fatty acids from lipids	$f_{fa,li}$	0.95	-
Fraction of hydrogen from sugars	$f_{h2,su}$	0.30	-
Fraction of butyrate from sugars	$f_{bu,su}$	0.13	-
Fraction of propionate from sugars	$f_{pro,su}$	0.27	-
Fraction of acetate from sugars	$f_{ac,su}$	0.30	-
Fraction of hydrogen from amino acids	$f_{h2,aa}$	0.22	-
Fraction of valerate from amino acids	$f_{va,aa}$	0.23	-
Fraction of butyrate from amino acids	$f_{bu,aa}$	0.26	-
Fraction of propionate from amino acids	$f_{pro,aa}$	0.05	-
Fraction of acetate from amino acids	$f_{ac,aa}$	0.24	-

Table E4. Initial composition of TWAS, seed sludge, and ADM simulation

Model parameter	Symbol	TWAS (g-COD/L)	Seed (g-COD/L)	ADM
Composites	X_C	1400	210	1060
Particulate Inerts	X_I	12780	13381	12952
Carbohydrates	X_{CH}	4000	21	2863
Proteins	X_{PR}	14000	69	10020
Lipids	X_{LI}	4000	22	2863
Sugar fermenters	X_{SU}	10	410	124
Amino acid fermenters	X_{AA}	10	863	254
Long-chain fatty acid beta-oxidizers	X_{FA}	10	183	59
Valerate and butyrate beta-oxidizers	X_{C4}	10	344	106
Propionate beta-oxidizers	X_{PRO}	10	121	42
Acetoclastic methanogens	X_{AC}	10	466	140
Hydrogenotrophic methanogens	X_{H2}	10	261	82
Sugars	S_{SU}	1200	12	861
Amino acids	S_{AA}	1200	5	859
Long-chain fatty acids	S_{FA}	10	90	33
Valerate	S_{VA}	250	12	182
Butyrate	S_{BU}	250	14	182
Propionate	S_{PRO}	250	14	182
Acetate	S_{AC}	250	450	307
Hydrogen gas	S_{H2}	0	0	0
Methane gas	S_{CH4}	0	0	0

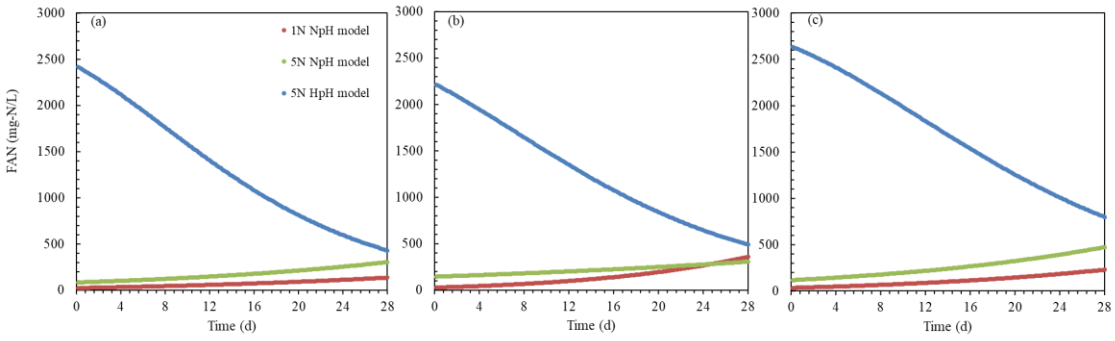

Figure E1. Model simulation results for FAN concentration: (a) without addition acetate; (b) with 20 g-COD/L acetate; (c) with 40 g-COD/L acetate.

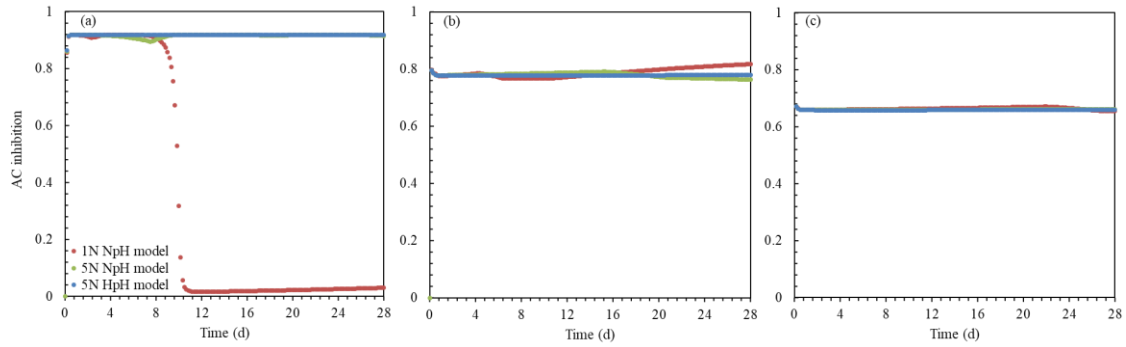

Figure E2. Model simulation results for AC (substrate) inhibition: (a) without addition acetate; (b) with 20 g-COD/L acetate; (c) with 40 g-COD/L acetate.

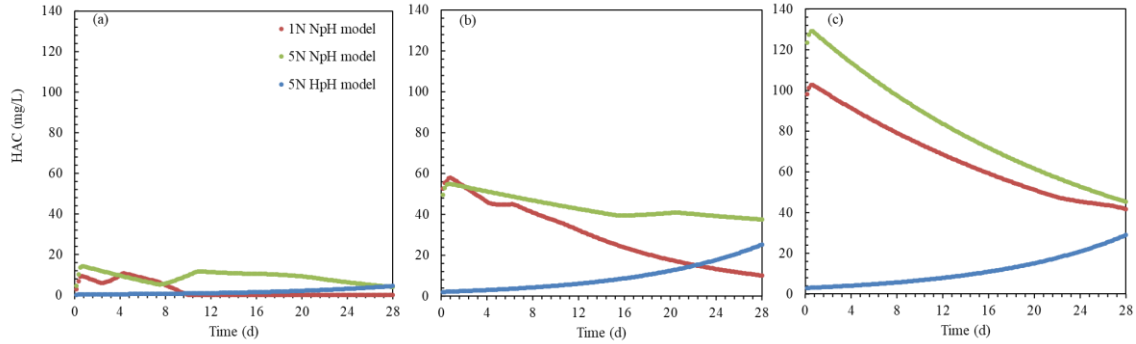

Figure E3. Model simulation results for HAC concentration: (a) without addition acetate; (b) with 20 g-COD/L acetate; (c) with 40 g-COD/L acetate.

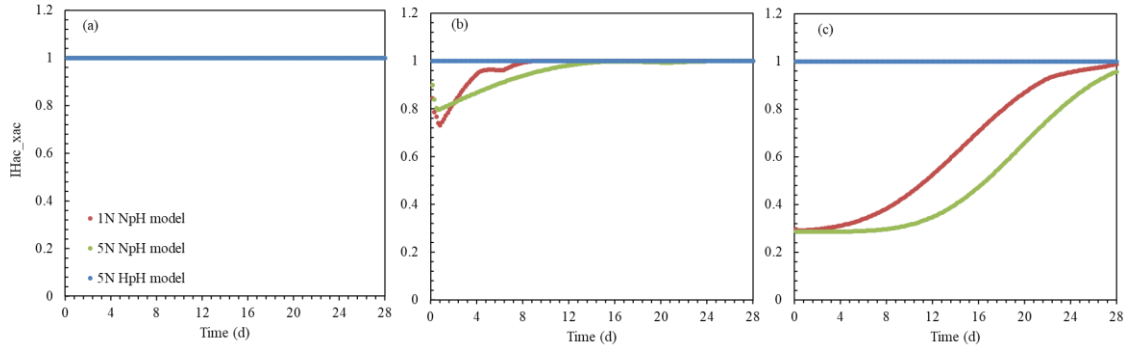

Figure E4. Model simulation results for HAC inhibition on acetoclastic methanogenesis: (a) without addition acetate; (b) with 20 g-COD/L acetate; (c) with 40 g-COD/L acetate.

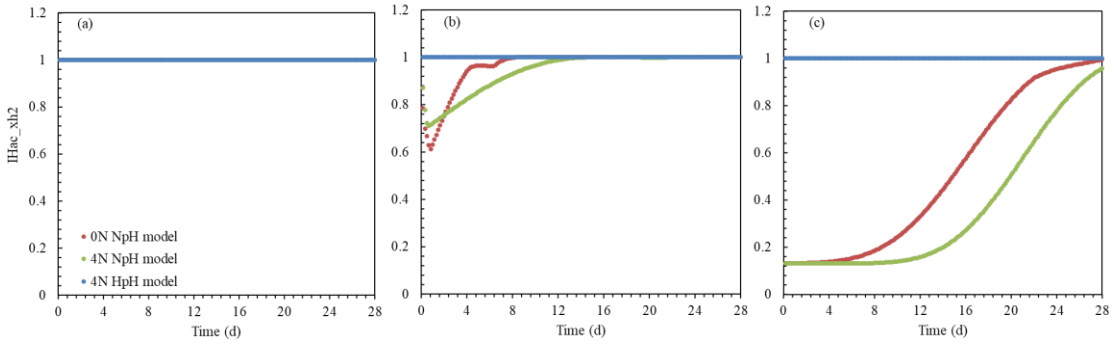

Figure E5. Model simulation results for HAC inhibition on hydrogenotrophic methanogenesis: (a) without addition acetate; (b) with 20 g-COD/L acetate; (c) with 40 g-COD/L acetate.

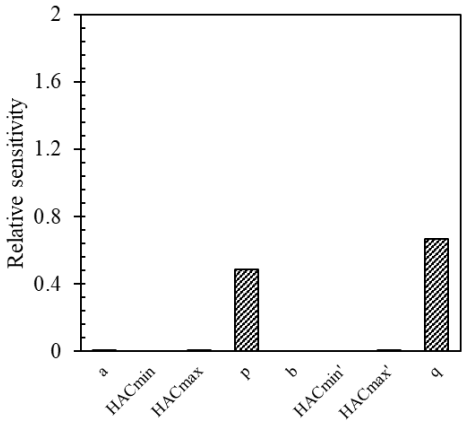

Figure E6. The relative sensitivity of parameters in acetic acid inhibition functions at pH of 7 with 4 g-N/L of TAN and 40 g-COD/L of acetate.